Identification and Characterization of Importin 13 Substrates

Dissertation

for the award of the degree

“Doctor rerum naturalium”

of the Georg-August-Universität Göttingen

within the doctoral program *Molecular Biology of Cells*

of the Georg-August University School of Science (GAUSS)

submitted by

Imke Baade

from Dachau

Göttingen 2017

Thesis Committee/ Examination Board

Prof. Dr. Ralph H. Kehlenbach (referee)

Department of Molecular Biology

Georg-August-Universität Göttingen

Prof. Dr. Heike Krebber (2nd referee)

Department of Molecular Genetics

Georg-August-Universität Göttingen

Prof. Dr. Jörg Großhans

Department of Developmental Biochemistry

Georg-August-Universität Göttingen

Further Members of the Examination Board

Prof. Dr. Michael Meinecke

European Neuroscience Institute Göttingen

Dr. Nuno Raimundo

Department of Cellular Biochemistry

Georg-August-Universität Göttingen

Dr. Hans Dieter Schmitt

Department of Neurobiology

Max Planck Institute for Biophysical Chemistry

Date of oral examination: 7th September 2017

Affidavit

I hereby declare that I have written this PhD thesis independently and with no other aids or sources than quoted.

……

Imke Baade

June 2017

Göttingen

Contents

Abstract

Nuclear pore complexes embedded in the nuclear envelope regulate the bidirectional transport of macromolecules between the nucleus and the cytoplasm. Small molecules can rapidly move through the permeability barrier of the nuclear pore complex, whereas larger macromolecules typically require nuclear transport receptors to facilitate their diffusion. With more than 20 different transport receptors identified, only three have been reported to mediate both nuclear import and export, namely human exportin 4, yeast Msn5 and human importin 13. The latter was characterized as a bidirectional transport receptor in 2001 and since then several importin 13 import cargoes have been identified. For a long time, however, the translation initiation factor eIF1A remained the only established export cargo. For a better understanding of the physiological significance of nuclear transport receptors and their diverse transport competencies, more cargoes need to be identified.

The central aim of this study was to expand the range of known importin 13 substrates using an importin 13 overexpression screen and a quantitative proteomics approach based on stable isotope labeling with amino acids in cell culture (SILAC). This approach should allow for the identification of proteins that bind to importin 13 in pull-down experiments under conditions that promote the formation of either import or export complexes.

In the overexpression screen, DBC-1, DMAP1, DDX43 and DDX59 were found to be redistributed to the cytoplasm upon importin 13 coexpression, identifying them as possible importin 13 substrates. Interestingly, transport of these proteins has previously been shown to be Nup358-dependent, suggesting a functional link between importin 13 and Nup358, possibly by Nup358 serving as an assembly or disassembly platform for importin 13 transport complexes. Detailed analysis of DBC-1 showed that its coiled-coil domain is required for interaction with importin 13.

In the SILAC based screen, more than 200 proteins were identified as potential importin 13 substrates, greatly expanding the repertoire of known cargoes for this transport receptor. Using importin 13 overexpression experiments, RTCA, FEN1, APEX1, SRP14, NSUN2, HNRNPD, XRCC5, BTF3, EIF2D, XRCC6 and SET were validated as potential importin 13 export cargoes, while ERI1 and NELFCD were identified as potential importin 13 import cargoes. In addition, importin 13 seems to function as an exportin for M9 signal sequence containing proteins.

Ultimately, the larger spectrum of importin 13 cargoes should give new insights into the physiological significance of importin 13, its bidirectional transport competence, its unique mechanisms of cargo recognition and cargo release and, eventually, the identification of one or possibly even several conserved nuclear localization signals in cargo proteins.

1. Introduction

1.1 Intracellular Compartments

The eukaryotic cell is subdivided into membrane-enclosed compartments or organelles, each containing their own functionally distinct subset of proteins and other molecules. One of the most prominent organelles is the nucleus, which contains the genome and is the principal site of DNA and RNA synthesis. The nucleus is encapsulated by the double membrane of the nuclear envelope, which physically separates the nucleus from the cytosol, the site of protein synthesis. This spatial separation of transcription and translation allows for more complex levels of gene expression as compared to prokaryotes that lack a membrane bound nucleus (1).

As the majority of proteins are synthesized in the cytosol, specific intracellular sorting signals and transport mechanisms are required that direct the proteins to their cellular compartments and allow for translocation of proteins across the organelle membranes. Proteins with functions in the nucleus such as histones, DNA and RNA polymerases, gene regulatory proteins and RNA processing proteins need to be selectively imported into the nuclear compartment, while at the same time tRNAs and mRNAs that are synthesized in the nucleus as well as ribosomal subunits need to be exported into the cytosol. Similarly, a resegregation of nuclear and cytoplasmic content is required upon nuclear envelope reassembly at the end of mitosis in mammalian cells (1).

There are three distinct mechanisms of protein trafficking between organelles, namely transmembrane transport, vesicular transport and gated transport. One example of gated transport, which will be further detailed in the following chapters, is the transport of RNA and proteins between the nucleus and the cytosol across the nuclear envelope through large macromolecular complexes, termed nuclear pore complexes (NPCs). NPCs serve as selective gates that allow active transport of specific macromolecules and macromolecular assemblies and free diffusion of smaller molecules (1).

1.2 The Nuclear Pore Complex

NPCs were initially observed by electron microscopy as pores within the nuclear envelope that later were shown to contain cylindrical formations (2, 3). The term “pore complex” was first assigned in 1959 (2) and since then advances in electron microscopy and other structural methods such as X-ray crystallography, mass spectroscopy and NMR spectroscopy have contributed significantly to the elucidation of the atomic structure of the

NPC. Only recently, the first predictive structural model of the nuclear pore scaffold was presented by docking crystal structures of nucleoporins (proteins of the NPC) and nucleoporin complexes into a cryo-electron tomographic reconstruction of the intact human NPC (4–7). The core scaffold of the NPC is formed by three ring-like structures, the cytoplasmic ring, the central spoke ring and the nuclear ring, which surround the aqueous transport channel with a diameter of ~60 nm (4–8) (Figure 1A). The central spoke ring is anchored in the nuclear envelope and connects the nuclear ring with the cytoplasmic ring. The cytoplasmic ring is decorated with eight cytoplasmic filaments, while a basket-like structure is connected to the nuclear ring where eight rod-like structures unite into a distal ring. Surrounding the central transport channel are eight smaller peripheral channels with a diameter of ~9 nm at the narrowest point that have been suggested to allow diffusion of integral membrane proteins from the outer nuclear membrane to the inner nuclear membrane (9–11).

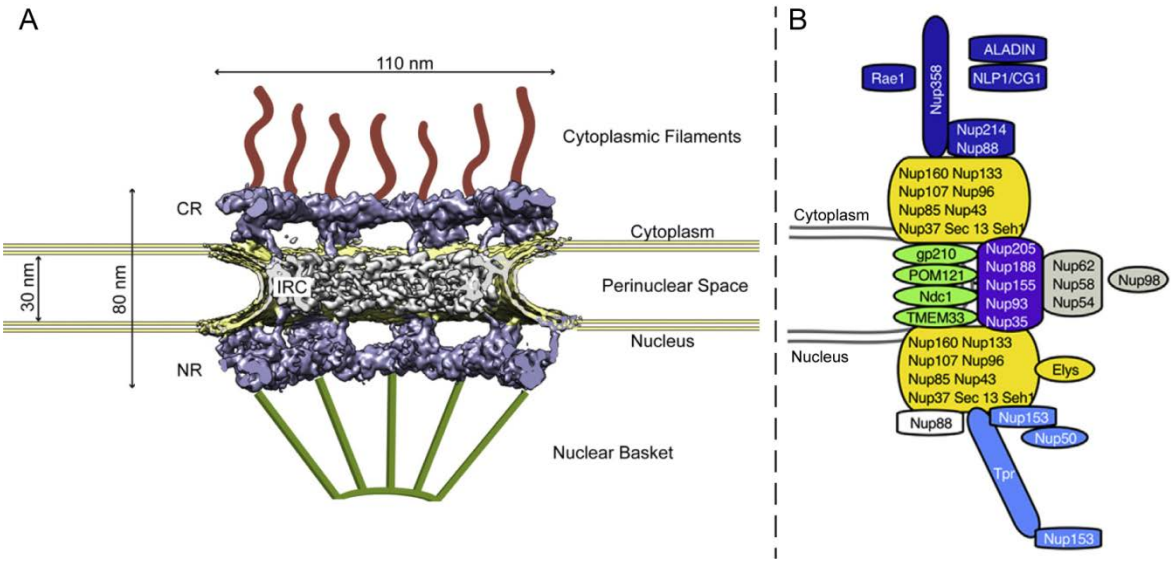

Figure 1: Structure of the nuclear pore complex. (A) Cryo-electron tomographic structure of the human NPC embedded in the nuclear envelope, decorated with schematic cytoplasmic filaments and the nuclear basket. CR: cytoplasmic ring; IRC: inner ring complex; NR: nucleoplasmic ring (modified from Schwartz 2016 (12)). (B) Structural organization and position of individual nucleoporins within the NPC (modified from Dickmanns *et al.*, 2015 (13)).

NPCs show an eightfold rotational symmetry (14) along the nucleocytoplasmic axis and have a molecular mass of ~112 MDa (15), a diameter of ~110 nm and a height of ~80 nm (excluding cytoplasmic filaments and nuclear basket) in vertebrates (16). Structural

features of the NPC are conserved between species even though its size ranges from ~66 MDa in yeast (17, 18) to ~112 MDa in vertebrates (15). Furthermore, the density of NPCs in the nuclear envelope varies between different species with a typical mammalian cell containing 2,000-5,000 NPCs (19). Kinetic analysis of translocation through nuclear pore complexes suggests that up to 1,000 translocation events can occur per second per NPC, allowing a mass flow of nearly 100 MDa/s (20). Despite its gigantic dimensions, the NPC is composed of only ~30 different proteins, termed nucleoporins (21, 22). As nucleoporins occur in multiple copies, the fully assembled NPC consists of ~500-1,000 protein molecules (3).

1.3 Nucleoporins

Of the approximately thirty different nucleoporins (Nups) (Figure 1B) that constitute the NPC ~20 nucleoporins are conserved among all eukaryotes, while the remaining ~10 nucleoporins appear to be more specific to the different species (12). Historically, nucleoporins are named after their molecular weight but as this varies between different species no uniform nomenclature for nucleoporins exists (12). Instead, nucleoporins are classified into three different groups based on their amino acid sequence and predicted structural motifs, termed peripheral nucleoporins, scaffold nucleoporins and transmembrane nucleoporins (13). The transmembrane nucleoporins anchor the NPC to the nuclear envelope, the scaffold nucleoporins form a major part of the cytoplasmic and nuclear scaffold rings and the channel nucleoporins contain extensive natively unfolded phenylalanine-glycine repeats (FG-repeats) and form the permeability barrier of the NPC (13). Nucleoporins have been shown to organize into stable subcomplexes that include the Nup107 complex (also called Y complex), Nup93 complex, Nup62 complex and the Nup214 complex (3, 13). Further associated with the cytoplasmic ring is the Nup358-RanGAP1-SUMO1-Ubc9 complex that is implicated in the assembly and disassembly of transport complexes (6, 23–25).

Approximately a third of the nucleoporins contain intrinsically disordered FG-repeat regions that are believed to form the permeability barrier of the NPC and facilitate the selective transport of cargo through the pore by interacting with nuclear transport receptors (16). FG-nucleoporins contain FG stretches in multiples of 4 to 48 that are separated by spacer sequences of around 20, mainly polar, amino acids (19, 13). FG-domains are hydrophobic and characterized by an extreme depletion of charged residues. They can form either cohesive or non-cohesive interactions (16, 26). FG-nucleoporins both interact

with constituents of the NPC scaffold and form homo- and heterotypical interactions with other FG-domains (26). The most common FG-repeat motifs are FG-, GLFG-, or FxFG-repeats (13, 26). The repetitive FG motifs mediate facilitated diffusion through the NPC by providing multiple low-affinity, high-specificity interactions with nuclear transport receptors (27). Even though much progress has been made in understanding the transport selectivity of NPCs, the exact gating mechanism remains unclear. Several transport models have been proposed that attempt to explain the selective barrier of NPCs (see section 1.4).

Apart from nucleocytoplasmic transport, nucleoporins are also involved in other cellular processes such as regulation of transcription, transcriptional memory, chromatin organization and DNA repair (19, 28, 29). Dysregulation of nucleoporins can lead to the development of human diseases, such as cancer and certain genetic disorders (13, 30, 31).

1.4 NPC Selectivity and Directionality of Transport

The NPC is freely permeable for small molecules, while larger molecules with a diameter of more than ~5 nm or ~30 kDa in mass either take longer to cross the NPC or require nuclear transport receptors to facilitate their passage (13, 16). However, the permeability barrier of the NPC is not assumed to be perfect, also allowing the passage of proteins whose functions are purely cytoplasmic or nucleoplasmic (32). To avoid any harmful effects on cellular processes in the wrong cellular compartment, these proteins would either need to be inhibited or transported back into their designated compartment.

Several lines of evidence suggest that FG domains constitute the permeability barrier of the NPC (reviewed in (16)). In *Saccharomyces cerevisiae*, a reduced permeability barrier was observed upon genetic depletion of FG domains (26). Similarly, non-selective NPCs were observed upon nuclear assembly in *Xenopus* egg extracts depleted of specific FG-domains (33). Furthermore, purified FG domains have been shown to form FG-hydrogels with NPC-like properties that allow an influx of nuclear transport receptor-cargo complexes but prevent entry of large inert cargoes (34, 35). Despite the well-established requirement of FG-domains to confer transport selectivity, the precise composition of the FG-permeability barrier and translocation of nuclear transport receptors through the NPC is unknown. Various models have been proposed to explain the transport selectivity of NPCs, including the selective phase model (20), the virtual gate model (36), the reversible collapse model (37), the Kap-centric model (38), the forest-model (39) and

the ring cycle model (40, 41). The models vary in the arrangement of FG-nucleoporins to confer a selective barrier and have been extensively discussed in several review papers (16, 42, 43).

The virtual gate model (36) assumes that the central transport channel is densely covered by bristling, non-interacting FG-filaments that form an entropic barrier. Nuclear transport receptors can compensate for a loss in entropy with a change in enthalpy upon binding to the FG-domains of nucleoporins. The release of binding energy can then facilitate the entry of molecules into the crowded volume of the NPC, while inert molecules are excluded. The selective phase model (20) assumes that the FG-domains form intra- and intermolecular interactions resulting in a three-dimensional meshwork with sieve-like properties. Small molecules can diffuse through the meshwork, whereas molecules larger than the mesh-size would be excluded. Nuclear transport receptors can antagonize the cohesive inter-FG interactions by directly interacting with the hydrophobic FG-repeats, thereby partitioning the FG hydrogel, allowing the nuclear transport receptors to pass through the NPC. The forest model (39) is based on FG domains forming collapsed-coil and extended-coil conformations that can form cohesive or non-cohesive interactions, respectively. This results in two separate transport zones, a central route for macromolecules and a lateral route for small molecules.

The above transport models only consider the permeability barrier of the nuclear pore complex but do not address determinants of transport directionality. A well-established factor for directionality is the coupling of facilitated diffusion to the RanGTP gradient, with nuclear RanGTP concentrations being at least 200-fold higher than cytoplasmic concentrations (44, 45). The RanGTP gradient is established by the RanGTPase system and is discussed extensively in section 1.5. Further, peripheral nucleoporins often show high-affinity, RanGTP-sensitive binding of transport receptors that are believed to function as assembly or disassembly sites for transport complexes (for reviews see (13, 42)). This observation is also part of the affinity gradient model that suggests that transport receptors show an increase in affinity for nucleoporins along the translocation pathway (46). A requirement for nucleoporins in the assembly of transport complexes has been shown, among others, for Nup358. Depletion of Nup358 in human cells resulted in a clear reduction of importin α/β and transportin-dependent transport that could only partially be restored by the addition of other transport factors (47, 48). This suggests that Nup358 is not absolutely required for nuclear import but facilitates the formation of transport complexes at the NPC by increasing the local concentration of transport receptors. Moreover, Nup358 was shown to interact directly with some cargoes such as DBC-1

(deleted in breast cancer 1) and DMAP1 (DNA methyltransferase 1 associated protein 1), which might assist their interaction with nuclear import receptors and subsequent nuclear translocation (49).

1.5 Nucleocytoplasmic Transport

Transport between the nucleus and the cytoplasm across the nuclear envelope is mediated by transport machinery consisting of NPCs and the RanGTPase system as well as nuclear transport receptors that continuously shuttle between the nucleus and the cytoplasm (Figure 2). Nuclear transport receptors, which are divided into importins and exportins, bind their cargoes on one side of the nuclear envelope, cross the central channel of the NPC through interaction with FG-nucleoporins and release their cargo on the other side (16). To allow for an accumulation of the substrates against their chemical potential, an energy input is required that is usually derived from the RanGTPase system through GTP hydrolysis (50, 51). The RanGTPase system consists of the chromatin-bound guanine nucleotide exchange factor RCC1 (regulator of chromosome condensation 1) (52), the cytoplasmic filament-bound RanGTP activating protein (RanGAP) (53) and the small GTP-binding protein Ran (52). Due to the compartmentalization of RanGAP to the cytoplasm and of RCC1 to the nucleus, a steep RanGTP gradient is generated, with high nuclear RanGTP levels and low cytoplasmic levels (50, 51). RanGTP in turn actively regulates substrate binding and release by switching nuclear transport receptors between low- and high-affinity cargo-binding states (16, 54). RanGTP hydrolysis is not required for NPC translocation *per se* but for disassembly of transport complexes and consequently directionality of transport (43).

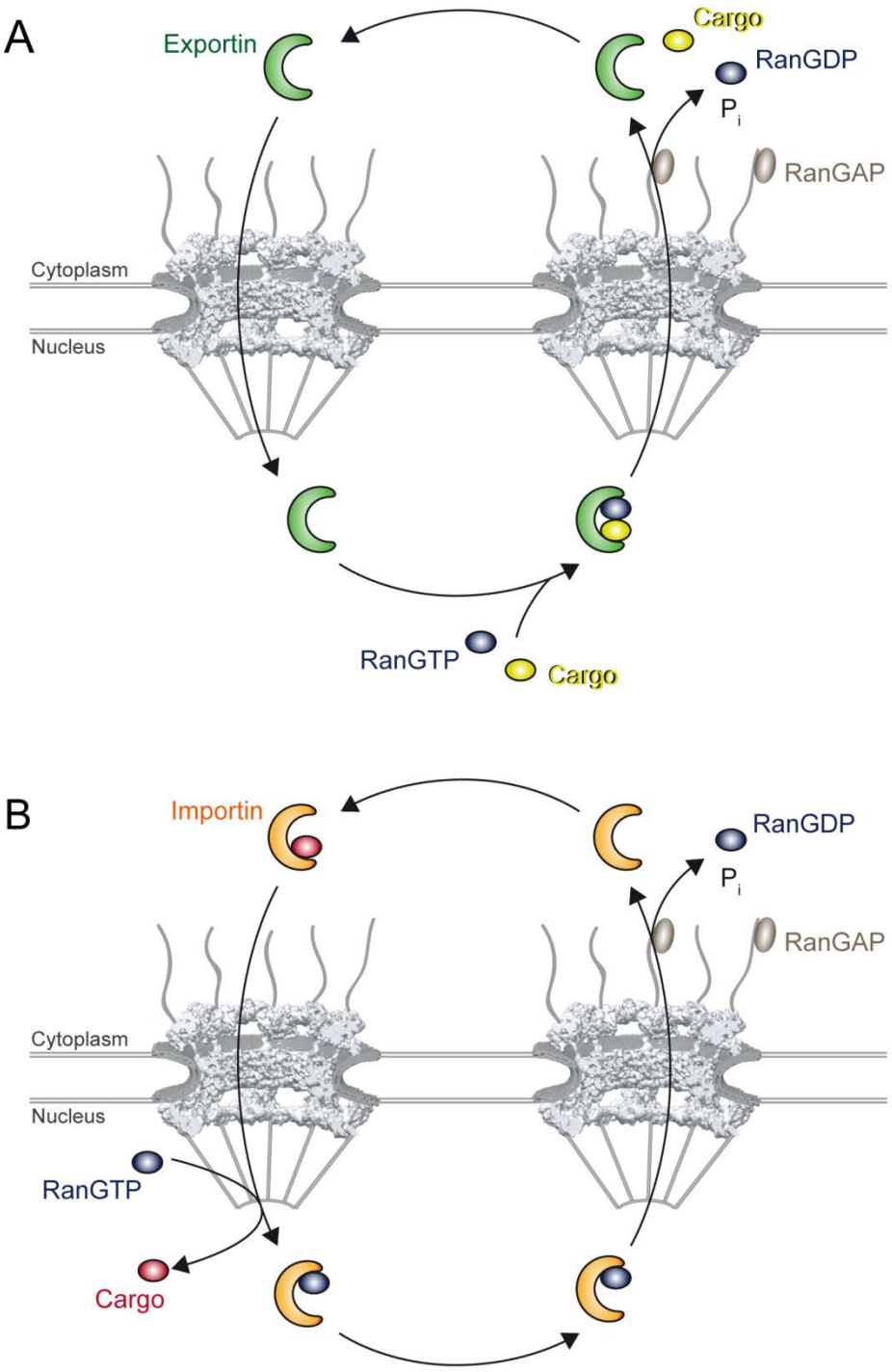

Figure 2: Nucleocytoplasmic transport. (A) Nuclear export. Exportins form a trimeric export complex with RanGTP and export cargo in the nucleus, shuttle through the nuclear pore complex and are disassembled in the cytoplasm by RanGAP mediated hydrolysis of GTP-bound Ran. Free exportins are recycled back to the nucleus for the next transport round. (B) Nuclear import. Importins bind their cargo in the cytoplasm, translocate across the nuclear pore complex and release the cargo in the nucleus upon RanGTP binding. Free importin bound to RanGTP is recycled back to the cytoplasm for the next transport round. The cryo-electron tomographic structure of the human NPC was taken from Appen *et al*., 2015 (6).

Importins either directly bind their cargoes in the cytoplasm at low RanGTP concentrations or indirectly with the help of adaptor proteins. The import complex shuttles across the NPC via interactions with FG-nucleoporins and the cargo is released into the nucleus upon RanGTP binding (54, 55). The importin-RanGTP complex is then recycled back to the cytoplasm for subsequent transport rounds. In contrast, facilitated export in most cases requires the binding of exportins to both export cargo and RanGTP in a cooperative manner to form stable trimeric export complexes in the nucleus (56, 57). Export complexes can then translocate through the NPC into the cytoplasm, where they are disassembled upon GTP-hydrolysis on Ran. The intrinsic GTPase activity of Ran is promoted by RanGAP, assisted by soluble RanBP1 and NPC-bound Nup358 (also known as RanBP2) (25, 53, 58, 59). Following hydrolysis, free exportin and RanGDP in complex with its dedicated transport receptor, the nuclear transport factor 2 (NTF2), return to the nucleus (60–63), where RanGDP is converted back to RanGTP by the action of RCC1 (52, 64).

1.6 Nuclear Transport Receptors

In 1990, a study by Adam *et al*. (65) provided the first evidence that soluble transport factors are required for nuclear protein import. Through selective permeabilization of mammalian cells with digitonin, a reagent that permeabilizes the plasma membrane but leaves the nuclear envelope intact, they could show that nuclear accumulation of the SV40 large T antigen nuclear localization sequence fused to a fluorescent protein depends on the addition of exogenous cytosol. In subsequent studies, this assay allowed for the identification of several cytosolic proteins required for nuclear transport through fractionation of cytosol and testing the different fractions for nuclear import activity into the nuclei of digitonin permeabilized cells. The cytosolic transport proteins identified included importin α, importin β, Ran and NTF2 (61, 60, 66–69).

Since these early studies, more than 20 different nuclear transport receptors have been identified that all share the ability to interact directly with FG-nucleoporins (43). Individual FG-nucleoporins bind to the convex outer surface of nuclear transport receptors through an interaction of FG-repeat domains with multiple hydrophobic patches on the nuclear transport receptor (13, 70). The interactions are transient and of low affinity, allowing for movement through the NPC (20, 54). Transport receptors are categorized into different classes based on conserved structural domains, including the importin β protein family, the Mex67/TAP family and the NTF2 family (13, 43). By far the largest class is the superfamily of importin β-related proteins also known as β-karyopherins, named after the first transport

receptor identified (43). This family of transport receptors recognizes nuclear localization signals and is responsible for most nucleocytoplasmic transport of proteins through the NPC (71). Even though β-karyopherins share a weak sequence homology of only 15-20%, they show a similar overall structural organization containing ~20 HEAT-repeats that arrange into a superhelical or ring-like structure (72). The HEAT repeat, which consists of two antiparallel α-helices connected by a short loop, is named after the proteins Huntingtin, elongation factor 3 (EF3), protein phosphatase 2A (PP2A) and the yeast PI3 kinase TOR1 where the structural motif was first identified (73, 74). This modular architecture gives β-karyopherins an intrinsic flexibility and allows for recognition of a wide range of different cargoes. Apart from the overall structural conservation, further unifying features of β-karyopherins are the similar molecular weights (90-150 kDa), an acidic isoelectric point (pI=4.0-5.0) and the presence of an N-terminal RanGTP binding site at the inner concave surface (75).

β-karyopherins can be further divided into importins that shuttle proteins into the nucleus, exportins that shuttle proteins out of the nucleus and bidirectional transport receptors that mediate both nuclear import and export. In humans, ten β-karyopherins have been classified as importins (Impβ, Trn1, Trn2, Trn-SR3, Imp4, Imp5, Imp7, Imp8, Imp9 and Imp11), seven as exportins (Crm1, CAS, Exp5, Exp6, Exp7, Expt and RanBP17) and two as bidirectional (Imp13 and Exp4) (76). In yeast, all nuclear transport receptors have been reported to sum up to a cellular concentration of >10 µM (77).

Until recently, only a limited number of cargoes had been identified for many nuclear transport receptors. Major advancements in mass spectrometry coupled with the use of stable isotope labeling with amino acids in cell culture (SILAC) (78, 79) allowed for identification of numerous transportin (80), importin β (81), importin α/β (81) and Crm1 cargoes (32, 82), as well as cargoes of twelve import receptors in a study published this year (76). Only for some of these cargoes a consensus structure of the nuclear transport receptor binding site has been established.

As nucleoporins, nuclear transport receptors are not only involved in nucleocytoplasmic transport but also play a role in a range of other cellular processes such as mitosis and nuclear envelope assembly (71, 83–87), and are functionally regulated by protein modifications, inhibitory factors and specific anchorings (reviewed in (88)).

1.7 Cargo Recognition of Karyopherins

Current crystal structures of transport complexes suggest that each β-karyopherin has multiple cargo binding sites. Nevertheless, the majority of importins seem to bind their cargoes at the concave inner surface of their C-terminus (89–100), whereas the major export receptor Crm1 appears to bind its cargoes at the convex outer surface of its C-terminus (101–104). For other exportins, only a limited number of crystal structures are available, making the identification of a potentially preferred binding site difficult (105–108). While most β-karyopherins associate directly with their cargoes, some also use adaptor proteins that bridge between the transport receptor and the targeting signal. One example is importin β, which uses one of the seven species of the importin α family (109, 110) as well as snurportin as an adapter for cargo binding (111), but also directly interacts with cargo (112). In addition to this, importin β can also form a heterodimer with importin 7 and drive the nuclear import of the linker histone H1 (113, 114).

Some cargoes bind to several β-karyopherins, suggesting a certain redundancy in cargo transport (76, 115–118). However, this finding is mainly based on *in vitro* studies and a preference for one particular transport receptor *in vivo* has been hypothesized (43). Nevertheless, some cargoes, especially larger cargoes, have been reported to require the simultaneous binding of multiple transport receptors to facilitate their transport (119).

Nuclear transport receptors are thought to bind their cargoes through nuclear localization signals, but consensus targeting signals have only been established for a few nuclear transport receptors (reviewed in (71, 120)). The first targeting signal characterized was the ‘classical’ basic nuclear localization signal (cNLS) rich in lysines or arginines (121–123) that binds to importin α and is imported via the importin β/importin α heterodimer (66, 124, 125). Prototypic nuclear localization signals (NLSs) are the monopartite NLS in the SV40 T antigen and the bipartite NLS in nucleoplasmin, which contain one or two clusters of positively charged amino acids (121, 123, 122). The PY-NLS represent another class of NLSs that is recognized by transportin (91). The PY-NLS has an $RX_{2\text{-}5}PY$ motif at its C-terminus and either hydrophobic or basic motif at its N-terminus (91). Transportin-SR1 and its splice variant transportin-SR2 bind to RS domains that are rich in arginine-serine dipeptide repeats (126). The main export receptor Crm1 recognizes a short leucine-rich or hydrophobic nuclear export signal (NES) that was initially identified in HIV-1 Rev and protein kinase inhibitor A (127–130). For the other nuclear transport receptors, no consensus NLS has been described and their binding sites are not believed to be defined by a specific consensus sequence. Instead, they are ascribed by a number of physical properties such as intrinsic structural disorder, length, charge, hydrophobicity and spacing

of key residues as well as three-dimensional conformations (71, 120). Ultimately, atomic structures of the transport complexes will be required to define more complicated and potentially three-dimensional binding sites.

As already discussed in section 1.5, cargo binding and release can occur via direct binding or through an allosteric mechanism and is often regulated by RanGTP binding. Cargo recognition is further regulated by the masking of the binding site through other proteins or nucleic acids, conformational changes in the binding site region or posttranslational modifications such as phosphorylation (131, 132).

1.8 Importin 13

The coding sequence of importin 13 was identified by Nagase *et al.* (133) in 1998 in a screen for cDNA clones from human brain coding for proteins larger than 50 kDa. The open reading frame of the importin 13 gene (IPO13), which they called KIAA0724, was mapped to chromosome 1 by radiation hybrid analysis. Sequence homology and motif searches against existing databases disclosed that importin 13 showed a sequence identity of less than 20% to known gene products at that time. A study in 2000 by Zhang *et al.* (134), identified KIAA0724 (termed LGL2) as a member of the β-karyopherin family, with the greatest homology to the transportin-SR subgroup. Nagase *et al.* in 1998 (133) had analyzed the expression pattern of importin 13 mRNA in ten different human tissues using reverse transcription-polymerase chain reaction coupled with an enzyme-linked immunosorbent assay (RT-PCR ELISA). Importin 13 mRNA was present in all tissues tested with the highest expression levels present in the brain, followed by testis, heart, skeletal muscle, lung and kidney. Lower expression levels were detected in spleen, pancreas, liver and ovary.

The human protein encoded by KIAA0724 was analyzed in detail by Mingot *et al.* (135) in 2001. By searching Expressed Sequence Tags (EST) databases for sequences with significant homology to known members of the importin β superfamily, they identified KIAA0724, which they termed importin 13 (IPO13 gene) and which codes for a human protein with 963 amino acids and a molecular weight of 108 kDa. Sequence homology analysis showed that importin 13 has putative orthologues in *Arabidopsis thaliana*, *Drosophila melanogaster*, *Caenorhabditis elegans* and *Schizosaccharomyces pombe*. In *Schizosaccharomyces cerevisiae*, no protein with a significant sequence homology is present, the closest orthologue being Pdr6p (also known as Kap122p).

As a first confirmation that importin 13 might function as a nuclear transport receptor, Mingot *et al.*, 2001 (135) showed that recombinant human importin 13 specifically interacts with RanGTP. By mass spectrometry they then identified several potential importin 13 substrates that bound to immobilized importin 13 from a HeLa cell extract in a RanGTP-dependent manner. Interestingly, most of the proteins identified, including 60S ribosomal protein L5, RNA-binding protein Y14 (referred to as RBM8,) protein mago nashi homolog (Mago, referred to as MGN), nuclear transcription factor Y subunit beta (referred to as NF-YB) and SUMO-conjugating enzyme Ubc9, bound in the absence of RanGTP. Nup50 (referred to as NPAP), however, and eukaryotic translation initiation factor 1A (eIF1A) bound efficiently only in the presence of RanGTP. Using binding assays and transport assays in digitonin permeabilized cells, Ubc9 and the Mago-Y14 protein complex were confirmed to be importin 13 cargoes, whereas eIF1A was verified to be an export cargo, confirming the bidirectional transport capacity of importin 13.

Since the characterization of importin 13 in 2001, several importin 13 import cargoes have been identified in various studies (see Table 1). Only recently, two larger screens expanded the list of potential importin 13 substrates, using a stable isotope labeling with amino acids in cell culture (SILAC) based *in vitro* transport (SILAC-Tp) system, a method that employs nuclear import assays in digitonin permeabilized cells coupled with SILAC (76), and a yeast two-hybrid screen to identify interactors of the testis-specific form of importin 13, which lacks the N-terminus of importin 13 (amino acids 526-963) (136). However, for a long time, eIF1A remained the only identified export cargo. Only at the end of 2016, eukaryotic translation initiation factor 4γ2 (eIF4G2) and high mobility group protein 20A (HMG20A) were also reported to be importin 13 export cargoes, underlining the bidirectional transport capacity of importin 13 (136).

Table 1: Importin 13 import and export cargoes.

Cargo	Function	Experiment	Position targeting signal	Karyopherins	Reference
Importin 13 import cargoes					
Ubc9	SUMO E2-conjugating enzyme	binding assay, transport assay	folded domain		(93, 135)
Mago/ Y14 (RBM8A)	core components of the exon junction complex	binding assay, transport assay	folded domain		(92, 135)
Pax6	paired homeodomain transcription factors	yeast two hybrid, binding assay, transport assay	paired-type homeodomain (aa 208-288)		(137)
Pax3	paired homeodomain transcription factor	binding assay, transport assay	paired-type homeodomain	Impα2	(137)
Crx	paired homeodomain transcription factor	binding assay, transport assay	paired-type homeodomain		(137)
Arx	paired homeodomain transcription factor	yeast-two-hybrid, binding assay, transport assay	paired homeodomain	Impβ, Imp9	(138, 139)
Nkx2-2	transcriptional activator	binding assay, transport assay	homeodomain	Impβ	(140)
NFYB/ NFYC	component of transcriptional activator NFY	binding assay, transport assay	histone fold domain		(141)
c-Jun	part of the transcriptional complex AP-1	binding assay, siIPO13	basic region preceding leucine zipper	Impβ, transportin, Imp7, Imp9	(117, 142)
GRL	member of the nuclear receptor superfamily of transcriptional regulators	overexpression experiment, binding assay, siIPO13		Impα/β, Imp7	(143)
CAR	member of the nuclear receptor superfamily of transcriptional regulators	binding assay	ligand-binding domain		(144)
DBC-1	multiple cellular functions	binding assay		Impα/β, Imp7, Imp9, transportin	(49)
CTCF	transcriptional repressor	binding assay; overexpression experiment, siIPO13	middle region		(145)
NC2α (Drap1)/ NC2β (Dr1)	transcriptional regulator	overexpression experiment, binding assay	histone-fold domain	Impα/β	(146)
CHRAC15 (CHRAC1)/ CHRAC17	component of the chromatin accessibility complex	overexpression experiment, transport assay	histone-fold domain		(135, 147)
p12/CHRAC17	component of polymerase ε	overexpression experiment, transport assay	histone-fold domain		(135, 147)
Myopodin	actin-bundling protein	yeast-two hybrid, binding assay, siIPO13	C-terminal portion	Impα	(148)
ARH1	tumor suppressor	binding assay		Impα, Imp7, Imp9	(149)
Importin 13 export cargoes					
eIF1A	translation initiation factor	binding assay, transport assay	folded domain		(107, 135)
EIF4G2	translation initiation factor	binding assay, IPO13 knock-out,			(136)
HMG20A	transcriptional regulator	binding assay, IPO13 knock-out, overexpression experiment, FRAP			(136)

Apart from importin 13, the only nuclear transport receptors that have been characterized as bidirectional transport receptors are exportin 4 and yeast Msn5 (150, 151). Yeast Msn5 was shown to export the inhibitor of G1 cyclin-Cdk complex Far1p and transcription factors Swi5p, Swi6p, Msn2p and Pho4p while also importing the trimeric replication protein A (RPA), which is required for multiple aspects of DNA metabolism, including DNA replication, DNA repair and recombination (151–156). Human exportin 4 exports the translation initiation factor eIF5A, the intracellular signal transducer and transcriptional modulator Smad3 and the thyroid hormone receptor but was also shown to import the sex-determining region Y protein (SRY) (157, 158) and the transcription factor Sox2 (150, 157–159). Both SRY and Sox2 are Sox family members and are imported through their high-mobility group (HMG), which is hypothesized to be recognized as a three-dimensional structure and not as a linear signal sequence (150). Interestingly, exportin 4 has also been reported to interact with the transcription factor Sox9 via its high-mobility group domain in the absence of RanGTP and to modulate its DNA binding activity but not to affect its intracellular localization (160).

In contrast to other karyopherins, bidirectional nuclear transport receptors can shuttle not only one, but two cargoes per hydrolysis of one GTP molecule through the NPC (135). However, this lesser expenditure of energy is suggested to limit the extent of cargo accumulation and therefore bidirectionality is not believed to be a universal transport mechanism of karyopherins (135). Instead, several karyopherins transport some of their cargoes as homodimers, heterodimers or even larger complexes. One example is importin 13, which was shown to shuttle the heterodimers Mago-Y14 (core components of the exon junction complex), NC2α/NC2β (transcriptional regulation), CHRAC15/CHRAC17 (part of a chromatin remodeling complex), p12/CHRAC17 (integral component of DNA-polymerase ε) and NFYB/NFYC (part of the transcriptional activator NFY) across the nuclear envelope (135, 141, 146, 147). Importin 13 is not only distinctive in its ability to mediate both nuclear import and export but also appears to be differentially regulated compared to other nuclear transport receptors in terms of cargo recognition and transport complex disassembly.

1.8.1 Importin 13 Cargo Recognition and Release

Similar to other β-karyopherins, importin 13 folds into 20 consecutive HEAT repeats, a motif that consists of two antiparallel α-helices (three parallel α-helices for the last repeat) with inter-repeat and intra-repeat loops protruding to opposite sides (92, 93, 107). The

superhelical structure of importin 13 is highly flexible, allowing for a whole range of importin 13 conformations, from a tight ring-like structure to a wide, open superhelix (92, 93, 107). Apo-importin 13 and importin 13 when bound to the import cargoes Mago/Y14 and Ubc9 have a more extended conformation, while importin 13 bound to Ran and the export cargo eIF1A, or Ran alone, has a more compact conformation (92, 93, 107).

Crystal structures of importin 13 in complex with Ubc9, the heterodimer Mago/Y14 and eIF1A/Ran (Figure 3) as well as binding assays suggest that importin 13 recognizes and also releases its cargoes via different mechanisms (92, 93, 107, 135). Importin 13 does not bind its cargoes through a linear sequence or through a small portion of its cargoes, as reported for importin β, transportin and Crm1, but instead seems to recognize its cargoes via folded domains and several conserved charged and polar residues distributed over the entire protein (92, 93, 107). An example are the homeodomain containing cargo proteins, such as Pax6 and Crx, which require cooperativity between two basic clusters located at the N-terminus and the C-terminus of their homeodomain, in order to be imported by importin 13 (137, 161, 140).

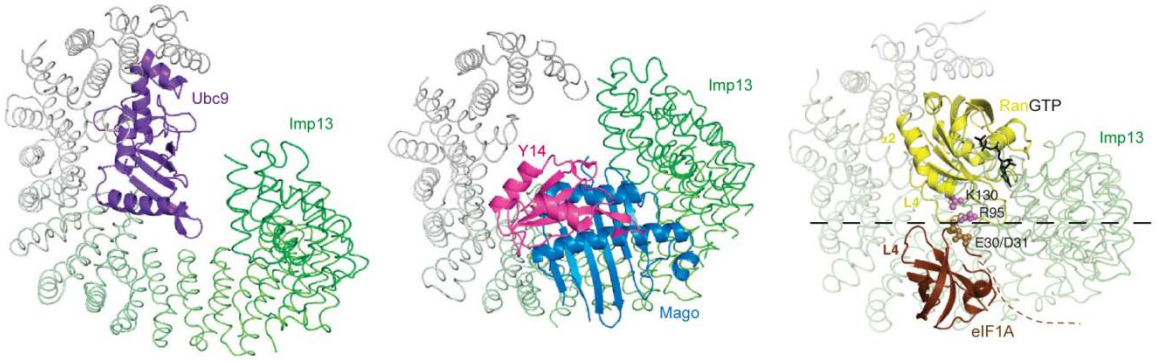

Figure 3: Structures of importin 13 import and export complexes. Importin 13 is shown as a ribbon trace, with a color gradient from grey (N-terminus) to green (C-terminus). Bound molecules are shown as cartoons, with Ubc9 in purple, Mago in blue, Y14 in magenta, Ran in yellow, GTP in black and eIF1A in brown (modified from Grünwald *et al.*, 2011 (93) and 2013 (107)).

Importin 13 binds its import cargoes Ubc9 and Mago/Y14 at its inner concave surface at non-overlapping sites, with Mago/Y14 binding to the C-terminal arch of importin 13 shifted

towards the inter-repeat loops rather than the intra-repeat loops of the HEAT motif, and Ubc9 binding to the N-terminal half of importin 13 shifted towards the intra-repeat loops (93, 107). This binding mode of Ubc9 is rather unusual as most importin structures solved to date suggest that importins bind their cargoes primarily through their C-terminal arch (89, 91, 94–100, 111). An exception is the parathyroid hormone-related protein (PTHrP), which binds in a highly extended conformation to the HEAT repeats 2-11 of importin β, largely overlapping its RanGTP binding site (90).

Comparable to other karyopherins, Ran in its GTP-bound form binds to the inner concave surface of importin 13 shifted towards the intra-repeat loops of the HEAT motif and contacts two highly conserved sites at an N-terminal (HEAT 1-3) and a central region of importin 13 (HEAT 8-9) as well as a less conserved region at its C-terminus (HEAT 16-19) (92). While RanGTP contacts HEAT 14 and 15 in importin β and yeast Cse1 (human orthologue is CAS), it contacts HEAT 16-19 in importin 13 and Crm1, resulting in a more closed conformation of the later karyopherins (92).

In contrast to other karyopherins, importin 13 likely does not bind its export cargo eIF1A through cooperative binding with RanGTP. Instead, RanGTP binding seems to facilitate the formation of the export complex by displacing bound import cargo (107, 135). However, it should be noted that eIF1A has been suggested to engage in a stabilizing contact with RanGTP when bound to importin 13 (107). Importin 13 recognizes eIF1A at its inner surface, shifted towards the inter-repeat loops of the HEAT motif, through two major binding sites that spatially overlap with the Mago/Y14 binding site (107). The larger interaction surface can be found in the middle region of importin 13, while the smaller interaction surface is located to its very C-terminus (107). Although the crystal structures suggest that a concomitant binding of eIF1A and Ubc9 as well as Mago/Y14 and Ubc9 would theoretically be possible, binding experiments show that simultaneous binding does not occur (93, 107).

As a consequence of the different cargo binding sites, importin 13 has different mechanisms for cargo release. In contrast to other karyopherins, importin 13 lacks the acidic loop that is utilized by importin β (HEAT 8), transportin (HEAT 8) and Crm1 (HEAT 9) for cargo release (92). Instead, importin 13 cargo release into the nucleus is mediated by RanGTP binding through both a steric hindrance mechanism and a direct competition mechanism for the same binding surface (92, 93). The direct competition mechanism is employed by the import cargo Ubc9, as RanGTP binds to the same binding site as Ubc9 (93), while Mago/Y14, which docks to a binding site adjacent to RanGTP, is released due to steric clashes of the two proteins (92). High nuclear concentrations of

RanGTP as well as its higher affinity for importin 13 compared to the import cargoes, efficiently facilitates import cargo release into the nucleus (107). *In vitro*, however, efficient Mago/Y14 release depends not only on RanGTP binding but also requires the presence of the importin 13 export cargo eIF1A, suggesting that eIF1A locks importin 13 in an export complex and prevents reassociation of Mago/Y14. Interestingly, similar to Mago/Y14, hydrolysis of RanGTP is likely not sufficient to disassemble the eIF1A export complex *in vitro*. Additionally, the loading of a tightly binding import cargo is required to fully displace the export cargo eIF1A from importin 13 (107, 135).

1.8.2 Biological Function of Importin 13

Importin 13 has been reported to be expressed in various tissues in a cell type- and differentiation stage-specific manner, and to play a role in the embryonic development of lung, brain and heart, while its deregulation has been linked to human diseases. Importin 13 regulates its own expression via a positive feedback mechanism, mediating nuclear import of CCCTC-binding factor (CTCF), a multivalent zinc-finger protein that binds to the IPO13 promoter and induces expression of importin 13 (145).

The expression of importin 13 is developmentally regulated in rat fetal lung, human limbal epithelial basal cells and mouse fetal brain. In rat fetal lung, importin 13 expression is hormonally regulated by glucocorticoids and importin 13 is enriched in epithelium relative to the mesenchyme (134). Importin 13 mRNA levels are most abundant during the pseudoglandular stage of lung development (Days 14-16) and decrease during the canalicular (Day 18) and saccular (Day 20) stages (134). Interestingly, not only the expression level of importin 13 is developmentally regulated in rat fetal lung but also its nucleocytoplasmic shuttling, with importin 13 entering the nucleus much more rapidly at fetal Day 18 than at Day 21 (162). This suggests a role of importin 13 in normal lung embryogenesis by possibly mediating nuclear import of transcription factors (162). Indeed, it could be shown that importin 13 regulates nuclear import of the glucocorticoid receptor in airway epithelial cells, which regulates the transcription of genes involved in development, metabolism and immune response (143). This could be of relevance for anti-inflammatory asthma therapy, as glucocorticoids are critical to the treatment of asthma and other airway inflammations (143). Genetic variations of importin 13 have been shown to be associated with improved airway responsiveness in childhood asthma (163).

Importin 13 is solely expressed in human limbal epithelial cells, not in other cell layers of the limbus (border of the cornea and the white of the eye) and was shown to play an

important role in maintaining the undifferentiated phenotype and high proliferation potential of corneal epithelial progenitor cells (164). Increased importin 13 activity is associated with the pathogenesis of pterygium, a triangular wing-shaped overgrowth of abnormal conjunctiva onto the cornea (142). Overexpression or knock-down of importin 13 increased or decreased pterygium epithelial cell proliferation, respectively (142).

Expression and subcellular distribution of importin 13 are also regulated during brain development in mice, with the highest expression levels in fetal brain tissues at mouse embryonic day 13.5 (E13.5) and then gradually decreasing, with the lowest expression in adult mouse brain tissues (165). In the telencephalon (embryonic structure from which the cerebrum develops prenatally) tissue at stage E11.5 endogenous importin 13 is mainly localized in the cytoplasm, while at later stages from E15.5 to P0, importin 13 is mainly located in the nucleus (165). Further support for a potential role of importin 13 in neural development comes from a study (166) showing that importin 13 regulates neurotransmitter release at the *Drosophila* neuromuscular junction and that some of the identified importin 13 substrates are important in embryonic neural development. Pax6, for example, is a master control for eye morphogenesis (137, 167, 168) and Arx is necessary for development of the forebrain (138, 169, 170).

During mouse development, importin 13 expression increases significantly from fertilized egg to blastocysts (171). Furthermore, meiotic differentiation of mouse germ cells is influenced by the stage-specific activity of importin 13 (172). Importin 13 is expressed in the primordial germ cells in the mouse embryo and is later expressed predominantly at the pachytene phase of meiosis in both male and female germ cells (172). Knock-down of importin 13 in fetal oocytes impedes the progression of meiosis through the pachytene phase of prophase I (172). In the same study, the authors identified a shorter transcript of mouse importin 13, which is encoded by the IPO13 gene but utilizes a different transcription start site (172). This shorter transcript is identical to the C-terminal fragment of importin 13 but lacks the N-terminal RanGTP-binding site and was shown to be only expressed in the germ cells in the adult testis (172). Expression of this shorter importin 13 testis-specific transcript prevented nuclear localization of Ubc9 in GC1 cells derived from spermatogenic cells, whereas expression of full-length importin 13 resulted in a primarily nuclear localization of Ubc9. The authors suggest that this short importin 13 transcript may act as a dominant negative regulator of importin 13 mediated nuclear import (172). This function was further confirmed in a study (136), where they identified the interactome of the testis-specific form of importin 13. In the same study, the authors also demonstrated

that the short importin 13 transcript may not only play a role in the germ cells of the testis, but also in mature spermatozoa (136).

Differential expression of importin 13 has also been linked to cancer, with increased importin 13 expression in endometrial carcinoma compared to secretory endometrium (173).

Even though many of the cargoes known to be regulated by importin 13 have been linked to cellular functions, much remains to be investigated to understand how importin 13 affects specific cellular states. For this, not only will more cargoes need to be identified, but also importin 13 expression regulation, its effect on cargo subcellular localization and consequently specific cellular pathways will need to be analyzed in detail and ultimately linked. Another aim will be to understand how deregulation of any of these individual processes can lead to pathogenic alterations of cellular states.

1.9 Aim of Work

Importin 13 is one of the few transport receptors known to function both in nuclear import and export. While comprehensive lists of potential transportin, importin α/β and Crm1 cargoes were available (80–82), only a few importin 13 cargoes had been reported when this work was started. The aim of this thesis was therefore to expand the range of importin 13 substrates using three different approaches.

The first approach focused on the specific identification of importin 13 export cargoes. For this, nuclear proteins derived from the 'LIFE database' (174, 175), were expressed in HeLa cells and their subcellular localization was analyzed upon coexpression of importin 13. In the second approach, potential substrates from a HeLa cell extract, which interact specifically with immobilized importin 13, were identified by mass spectrometry. The third approach was similar to the second approach but was designed to allow the distinction between import and export cargoes using quantitative proteomics. To this end, stable isotope labeling of amino acids in cell culture (SILAC) was applied, to identify proteins that specifically interact with immobilized importin 13 from a HeLa cell extract. Finally, identified cargo candidates should be validated in binding assays and importin 13 overexpression experiments.

Together, these approaches should lead to a better understanding of importin 13-dependent nuclear transport.

2. Materials and Methods

2.1 Material

2.1.1 Software

Adobe Illustrator CS7	Adobe
AxioVision LE64 4.9.1.0	Zeiss
CellProfiler 2.1.1	Broad Institute
Citavi 5	Swiss Academic Software
DAVID Bioinformatics Resources 6.8	NIH
GraphPad Prism 5.01	GraphPad Software Inc.
Image Reader LAS-3000	Fujifilm
ImageJ/Fiji	NIH
Lasergene 10.1.1 (3)	DNASTAR
LSM 510 Release Version 4.0 SP2	Zeiss
LSM Image Browser	Zeiss
MaxQuant 1.5.1.0	Max Planck Institute of Biochemistry
Microsoft Office 2010	Microsoft
NanoDrop 2000 Software	Thermo Scientific
Perseus 1.5.0.15	Max Planck Institute of Biochemistry
PPT Drawing Toolkits	Motifolio Inc.
Proteome Discoverer 1.4	Thermo Scientific
SnapGene Viewer 3.1.4	GSL Biotech LLC
STRING 10.0	STRING Consortium
Tm Calculator	Thermo Scientific
Venny 2.1.0	Centro Nacional de Biotecnología

2.1.2 Equipment

Agarose gel documentation GelSTICK touch	INTAS Science Imaging Instruments
Agarose gel running chamber	Home-made, Workshop, UMG
Acclaim™ PepMap™ 100 pre-column	Thermo Scientific

ÄKTA column HiLoad 26/60 Superdex 200 prep grade	GE Healthcare
ÄKTA column HiLoad 26/60 Superdex 75 prep grade	GE Healthcare
ÄKTA column MonoS 5/50 GL	GE Healthcare
ÄKTA column Superdex 200 10/300 GL	GE Healthcare
ÄKTA column Superdex 75 10/300 GL	GE Healthcare
ÄKTApurifier	Amersham Biosciences
Autoclave DX-200	Systec
BioPhotometer	Eppendorf
CASY 1	Schärfe System
Cell culture hood Herasafe™ KS	Thermo Scientific
Cell culture incubator Heracell™ 150i	Thermo Scientific
Cell culture incubator Cytoperm 2	Heraeus Instruments
Centrifuge 5415R	Eppendorf
Centrifuge 5424	Eppendorf
Centrifuge Sigma 1-15	Sigma-Aldrich
Centrifuge Allegra® X-15R with rotor SX4750	Beckman Coulter
Centrifuge Allegra® X 22 with rotor SX4250	Beckman Coulter
Centrifuge Avanti™ J-30I with rotor JA30.50Ti	Beckman Coulter
Centrifuge J6-MI with rotor JS 4.2	Beckman Coulter
Centrifuge Optima MAX-XP with rotor TLA100.3	Beckman Coulter
Confocal microscope LSM 510 META	Zeiss
Decon FS-100 ultrasonic bath	Decon Laboratories
Developer machine CURIX60	Agfa
Dual Gel Caster for Mini Vertical Units	Hoefer
EmulsiFlex-C3	Avestin
Fluorescence microscope Axioskop 2	Zeiss
Incubator Heraeus function line	Heraeus
Incubator Shaker INNOVA 4430	New Brunswick Scientific
Incubation/Inactivation Water Bath Model 1003	GFL
Mini Trans-Blot® Cell	Bio-Rad
Olympus CK40 Culture Microscope	Olympus
Orbitrap Velos Pro™ Nano ESI Mass Spectrometer	Thermo Scientific
SE250 Mighty Small II Mini Vertical Electrophoresis Unit	Hoefer
SDS gel documentation LAS-3000	Fujifilm

Spectrophotometer NanoDrop 2000c	Thermo Scientific
SpeedVac Concentrator	Savant
Thermocycler FlexCycler2	Analytik Jena AG
Thermocycler PTC-200 DNA Engine	MJ Research
Thermocycler Tprofessional	Biometra
Thermomixer comfort	Eppendorf
Thermomixer compact	Eppendorf
UltiMate™ 3000 RSLCnano System	Thermo Scientific
UV sterilizer	Biometra
UV transilluminator	Uvitec
Vacuum Christ Alpha 1-4	W. Krannich
Vortexer MS2 Minishaker	IKA
XCell SureLock® Mini-Cell	Life technologies

2.1.3 Consumables

5 mL Polystyrene Round-Bottom Tubes	BD Biosciences
Amersham Hybond ECL Nitrocellulose Blotting Membrane	GE Healthcare
Amersham Hyperfilm™ ECL	GE Healthcare
Amersham Protran 0.45 µm NC Nitrocellulose Blotting Membrane	GE Healthcare
Cell culture consumables	Sarstedt, Greiner bio-one
Cell culture plastic ware	Sarstedt, Greiner bio-one, Nagle Nunc International
Centrifuge Bottle Assembly, Polycarbonate 50 mL	Beckman Coulter
Centrifuge tube, thickwall, Polycarbonate 500 µL	Beckman Coulter
Casy cups with lids	Roche Diagnostics (Fisher Scientific)
Empore™ C18 47 mm Extraction Disc, Model 2215	3M Company
LC-MS Screw Neck Vial, 1.5 mL	Grace
LC-MS vial insert, 250 µL	Agilent Technologies
Medix XBU medical x-ray film	FOMA Bohemia
Microscope cover slips (10 mm, 12 mm Ø)	Marienfeld
Microscope slides	Thermo Scientific
Mini-Protean® TGX Gels	Bio-Rad

Minisart RC 15, single use syringe filters (0.45 µm, 0.20 µm)	Sartorius Stedim Biotech
Minisart single use filter units (0.45 µm, 0.20 µm)	Sartorius Stedim Biotech
NuPAGE® Novex® 4-12% Bis-Tris Protein Gels	Thermo Scientific
Parafilm "M"	Bemis Company, Inc.
PD-10 columns	GE Healthcare
pH indicator strips	Macherey-Nagel
Protein LoBind Tubes	Eppendorf
Reaction tubes (1.5, 2 mL)	Sarstedt, greiner bio-one
Spectra/Por® Dialysis Membrane	Spectrum Laboratories
Spin-X® UF Concentrator	Corning
Syringes and needles	B. Braun, Servoprax
Whatman gel blotting paper	GE Healthcare

2.1.4 Kits

CloneJET PCR Cloning Kit	Thermo Scientific
Duolink® In Situ Detection Reagents Red	Sigma-Aldrich
Duolink® In Situ Kit	Sigma-Aldrich
NucleoBond™ Xtra Midi	Macherey-Nagel
NucleoSpin® Gel and PCR Clean-up	Macherey-Nagel
NucleoSpin® Plasmid	Macherey-Nagel
Pierce® BCA Protein Assay Kit	Thermo Scientific
Pierce® Silver Stain Kit	Thermo Scientific
RNeasy Mini Kit	Qiagen

2.1.5 Chemicals and Reagents

All standard chemicals and solvents not listed here were obtained from AppliChem GmbH (Darmstadt), Carl Roth GmbH + Co. KG (Karlsruhe), Serva Electrophoresis GmbH (Heidelberg), Sigma-Aldrich (Taufkirchen) or Merck (Darmstadt).

Arg-6:HCl	Silantes
Arg-10:HCl	Silantes
Lys-4D:2HCl	Silantes
Lys-8:HCl	Silantes
β-Mercaptoethanol	Roth

Acetonitrile, Optima™ LC/MS Grade	Fisher Scientific
Acrylamide 4K Solution (30%)	AppliChem
Adenosine 5’-triphosphate disodium salt hydrate (order number A3377)	Sigma-Aldrich
Ammonium hydrogen carbonate	Roth
Bovine Serum Albumin (BSA) (20 mg/mL)	Thermo Scientific
BSA, fraction V	AppliChem
Coomassie Plus™ Protein Assay Reagent	Thermo Scientific
Coulter ISOTON® II Diluent	Beckman Coulter
Cyanogen bromide-activated Sepharose 4B	Sigma-Aldrich
Dako Fluorescence Mounting Medium	Dako
DAPI (D9542)	Sigma-Aldrich
DEAE-Sepharose	Sigma-Aldrich
Digitonin	Calbiochem
dNTP Set, 100 mM solutions	Thermo Scientific
FBS Superior	Biochrom
Formaldehyde solution min. 37%	Millipore
Formic Acid, 99.5+%, Optima™ LC/MS Grade	Fisher Scientific
Gelatin from cold water fish	Sigma-Aldrich
GeneRuler 100bp DNA Ladder	Thermo Scientific
GeneRuler 1kb DNA Ladder	Thermo Scientific
Gibco® DMEM (1x)	Thermo Scientific
Gibco® DMEM (1x) no glutamine, lysine & arginine	Thermo Scientific
Gibco® L-Glutamine	Thermo Scientific
Gibco® Opti-MEM® (1x)	Thermo Scientific
Gibco® Penicillin Streptomycin (Pen Strep)	Thermo Scientific
Glutathione Sepharose 4 Fast Flow	GE Healthcare
Glutathione Sepharose High Performance	GE Healthcare
Guanosine 5’-diphosphate sodium salt (G7127)	Sigma-Aldrich
Guanosine 5’-triphosphate sodium salt hydrate (51120)	Sigma-Aldrich
IgG-Sepharose 6 Fast Flow	GE Healthcare
Immobilon™ Western Chemiluminescent HRP Substrate	Millipore
Iodoacetamide, BioUltra	Sigma-Aldrich
Isopropyl β-D-1-thiogalactopyranoside	Thermo Scientific

Lectin from *Triticum vulgaris*	Sigma-Aldrich
Leptomycin B Enzo	Life Sciences
L-Glutathione reduced	AppliChem
Lipofectamine® 2000	Thermo Scientific
Methanol, Optima™ LC/MS Grade	Fisher Scientific
MOWIOL® 4-88	Calbiochem
Ni-NTA Agarose	Qiagen
NuPAGE® MES SDS Running Buffer (20x)	Thermo Scientific
NuPAGE® MOPS SDS Running Buffer (20x)	Thermo Scientific
Oligofectamine™ Reagent	Thermo Scientific
Oligonucleotides	Sigma-Aldrich
ortho-Phosphoric acid 85% p.A.	AppliChem
PageRuler Prestained Protein Ladder	Thermo Scientific
PageRuler Unstained Protein Ladder	Thermo Scientific
Poly-L-Lysine solution 0.1% (w/v)	Sigma-Aldrich
SafeView™ Classic (DNA stain)	Applied Biological Materials Inc.
SP-Sepharose Fast Flow	Roth
Water, Optima™ LC/MS Grade	Fisher Scientific

2.1.6 Enzymes

Creatine phosphokinase, Rabbit Skeletal Muscle	Calbiochem
DNaseI	Roth
Fast alkaline phosphatase (FastAP)	Thermo Scientific
Phusion® High-Fidelity DNA Polymerase	Thermo Scientific
Restriction enzymes	Thermo Scientific
RiboLock RNase Inhibitor	Thermo Scientific
SuperScript® III Reverse Transcriptase	Thermo Scientific
T4 DNA ligase	Thermo Scientific
Gibco® Trypsin/ EDTA 0.25% (1x)	Thermo Scientific
Trypsin NB Sequencing Grade (peptide digestion)	Serva

2.1.7 Stock Solutions

1,4-Dithiothreitol (DTT)	1 M in H_2O
Ammonium persulfate (APS)	10% APS (Sigma) in H_2O

Ampicillin	100 mg/mL in H_2O
Aprotinin	1 mg/mL in 20 mM HEPES pH 7.4
Adenosine triphosphate (ATP)	100 mM ATP in 100 mM $Mg(OAc)_2$, 20 mM HEPES (pH 7.4)
Calcium chloride buffer	250 mM $CaCl_2$ H_2O
Chloramphenicol	34 mg/mL in EtOH
Creatine phosphokinase	2000 U/mL in 50% glycerol, 20 mM HEPES pH 7.4
Creatine phosphate	80 mg/mL in H_2O
Cytosol (9 mg/mL)	prepared as described in Kehlenbach *et al*., 1998
Digitonin	10% (w/v) in DMSO
FITC-Phalloidin	0.2 mg/mL in methanol
Hoechst 33258	10 mg/mL in H_2O
Isopropyl b-D-1-thiogalactopyranoside (IPTG)	1 M in H_2O
Kanamycin	50 mg/mL in H_2O
Leupeptin/Pepstatin	1 mg/mL each, in DMSO
Phenylmethylsulfonyl fluoride (PMSF)	100 mM in 2-propanol
WGA (wheat germ agglutinine/lectin)	2 mg/mL in TPB

2.1.8 Buffers and Solutions

2YT-medium	1.6% (w/v) tryptone, 1% (w/v) yeast extract, 0.5% (w/v) NaCl, pH 7.0
Carbonate buffer	0.2 M $NaHCO_3/Na_2CO_3$, pH 8.9
Coomassie destaining solution	10% acetic acid
Coomassie fixation solution	40% ethanol, 10% acetic acid
Coomassie staining solution	5% aluminum sulfate-(14-18)-hydrate, 10% ethanol, 2% ortho-phosphoric acid, 0.02% CBB-G250
DNA loading buffer (6x)	0.2% bromophenol blue, 0.2% xylene cyanole, 60% glycerol, 60 mM EDTA
GST buffer	50 mM Tris pH 6.8, 300 mM NaCl, 1 mM $MgCl_2$, 2 mM DTT, 0.1 mM PMSF, 1 µg/mL of each AP and LP

HBS (2x) buffer	50 mM HEPES, 250 mM NaCl, 1.5 mM Na_2HPO_4, pH 6.98
His buffer	50 mM Tris pH 7.5, 500 mM NaCl, 10 mM MgAc, 5% glycerol, 10 mM β-mercaptoethanol, 0.1 mM PMSF, 1 µg/mL of each AP and LP
Laemmli running buffer (10x)	250 mM Tris, 1.92 M glycine, 0.5% SDS
LB-medium	1% (w/v) bacto-tryptone, 0.5% (w/v) yeast extract, 1% (w/v) NaCl, pH 7.0
LB agar plates	LB supplemented with 1.5% (w/v) bacto-agar
Mowiol mounting medium	13.3% (w/v) Mowiol 4-88, 33.3% (w/v) glycerol, 133 mM Tris-HCl, pH 8.5, 1 µg/mL DAPI
PBS (10x)	1.37 M NaCl, 27 mM KCl, 100 mM Na_2HPO_4, 18 mM KH_2PO_4, pH 7.5
PBS-T	1x PBS + 0.1% Tween-20
PLA Wash Buffer A	0.01 M Tris pH 8.0, 0.15 M NaCl, 0.05% Tween 20
PLA Wash Buffer B	0.2 M Tris pH 7.5, 0.1 M NaCl
PonceauS staining solution	0.5% PonceauS in 1% acetic acid
Pulldown buffer	50 mM Tris pH 7.4, 200 mM NaCl, 5% glycerol, 2 mM DTT
Ran buffer	50 mM Tris pH 8.0, 75 mM NaCl, 1 mM $MgCl_2$, 100 µM PMSF, 1 µg/mL of each AP and LP
SDS sample buffer (4x)	125 mM Tris pH 6.8, 4% SDS, 0.02% Bromophenol blue, 10% glycerol
SOC-medium	2% (w/v) tryptone, 0.5% (w/v) yeast extract, 10 mM NaCl, 2.5 mM KaCl, 10 mM $MgCl_2$, 10 mM $MgSO_4$, 0.36% (w/v) glucose, pH 7.0
STOP buffer	7% charcoal, 10% ethanol, 0.1 M HCl, 10 mM NaH_2PO_4
TAE buffer (50x)	2 M Tris, 0.05 M EDTA, 5.71% acetic acid
Transport buffer (10x)	200 mM HEPES, 1.1 M KOAc, 20 mM $Mg(OAc)_2$, 10 mM EGTA, pH 7.3
Ubc9 buffer	50 mM Na-phosphate pH 6.5, 50 mM NaCl, 0.1 mM PMSF, 1 µg/mL of each AP and LP, 1mM DTT

Western blot transfer buffer (10x)	250 mM Tris, 1.93 M glycine, 0.2% SDS
Western blot transfer buffer (1x)	10% Western blot transfer buffer (10x), 20% MeOH

2.1.9 Mammalian Cell Lines

Cell line	Specification	Origin
HeLa P4 (P4 MAGI CCR5+ Cells)	Human adenocarcinoma cell line that expresses CD4; derived from cervix of a 31-year-old woman	NIH AIDS Reagent Program; (176)
U2-OS (U2OS)	Human osteosarcoma cell line; derived from a moderately differentiated sarcoma of the tibia of a 15-year-old girl	ATCC® HTB96
293T HEK	Human embryonic kidney cell line transformed with adenovirus 5 DNA; derived from fetus	ATCC, CRL-2828
COS-7	Monkey African green kidney cell line transformed with SV40	Sigma-Aldrich, 87021302

2.1.10 Bacterial Strains

Bacterial strain	Specification and Genotype
BL21 (DE3) codon+	F- ompT hsdS(rB- mB-) dcm+ Tetr gal l (DE3) endA Hte [argU proL Camr] LEMO21 (DE3) fhuA2 [lon] ompT gal (lDE3) [dcm] hsdS/ pLemo(CamR)
DH5α	F- Φ80lacZΔM15 Δ (lacZYA-argF) U169 recA1 endA1 hsdR17 (rK-,mK+) phoA supE44 λ- thi-1 gyrA96 relA1
JM109	endA1 glnV44 thi-1 relA1 gyrA96 recA1 mcrB+ Δ(lac-proAB) e14- [F' traD36 proAB + lacIq lacZΔM15] hsdR17(rK- mK+)

2.1.11 Antibodies

Table 2: Primary antibodies

Number	Name	Species	Origin	IF Dilution	WB Dilution	PLA Dilution
Ab013	α-FLAG (M2)	mouse	Sigma	1:3,000	1:1,000	
Ab029	α-IPO13	rabbit	Proteintech	1:300	1:2,000	
Ab051	α-Ran	mouse	BD	1:2,000	1:5,000	
Ab121	α-FLAG (M2)	rabbit	SIGMA	1:1,000	1:1,000	
Ab132	α-HA	mouse	hybridoma supernatant	1:5,000	1:5,000	
Ab181	α-Transportin	mouse	BD	unspecific	1:1,000	
Ab186	α-HA	mouse	Convance	1:1,000	1:1,000	
Ab208a	α-Imp β	rabbit	A. Nath		1:1,000	
Ab219	α-eIF1A	rabbit	Abcam	1:500	1:200,000	1:2,000
Ab227	α-IPO13	rabbit	this work*	1:300	1:1,000	1:500
Ab228	α-IPO13	rabbit	this work*	1:300	1:1,000	
Ab234	α-STRAP	rabbit	Proteintech	-	1:300	
Ab235	α-NCAPG	rabbit	Proteintech	1:100	1:1,000	
Ab236	α-NSUN2	rabbit	Proteintech	1:500	1:5,000	
Ab237	α-WDR77	rabbit	Proteintech	-	1:100	
Ab238	α-OLA1	rabbit	Proteintech	1:50	1:300	
Ab239	α-SRP14	rabbit	Proteintech	1:300	1:1,000	
Ab240	α-ERI1	rabbit	Proteintech	1:100	1:1,000	
Ab241	α-EDC3	rabbit	Proteintech	1:50	1:1,000	
Ab242	α-WDR61	rabbit	Proteintech	1:300	1:1,000	
Ab243	α-EIF3G	rabbit	Proteintech	1:50	1:100	
Ab244	α-APEX	rabbit	Proteintech	1:50	1:500	
Ab245	α-FEN1	rabbit	Proteintech	1:500	1:1,000	
Ab250	α-RTCD1	rabbit	Proteintech	1:50	1:500	
Ab309	α-Ubc9	mouse	Santa Cruz	1:100	1:5,000	1:500

IF: immunofluorescence, WB: immunoblotting, PLA: *in situ* proximity ligation assay

*: for details see section 2.3.9

Table 3: Secondary antibodies

Name	Species	Origin	Application	Dilution
anti-mouse HRP	goat	Jackson ImmunoResearch	WB	1:10,000
anti-rabbit HRP	goat	Jackson ImmunoResearch	WB	1:10,000
anti-mouse AlexaFluor® 488 conjugated	donkey	Molecular Probes	IF	1:1,000
anti-mouse AlexaFluor® 594 conjugated	donkey	Molecular Probes	IF	1:1,000
anti-rabbit AlexaFluor® 488 conjugated	donkey	Molecular Probes	IF	1:1,000
anti-rabbit AlexaFluor® 594 conjugated	donkey	Molecular Probes	IF	1:1,000

Name	Species	Origin	Application	Dilution
Duolink® In Situ PLA® Probe Anti-Rabbit MINUS	donkey	Sigma-Aldrich	PLA	1:5
Duolink® In Situ PLA® Probe Anti-Mouse PLUS	donkey	Sigma-Aldrich	PLA	1:5
FITC-Phalloidin	Amanita phalloides	Sigma-Aldrich	IF	1:600

2.1.12 siRNAs

siRNA	Sequence (5' → 3')	Target	Company
siIPO13_1	AACAAUAUCAGGAUGAUCCct	IPO13	Ambion
siRNA non-targeting (nt)	Silencer Negative Control #1 siRNA (Cat. # AM4635)	scrambled sequence	Ambion

2.1.13 Oligonucleotides

Oligonucleotides were obtained from Sigma-Aldrich with a concentration of 100 µM, a synthesis scale of 0.025 µmol and the purification grade desalted. For cloning, restriction sites were added to the 5'-end of the oligonucleotides, as well as, a 5'-end overhang to ensure high cleavage efficiency of the restriction enzymes as specified by the manufacturer (Thermo Scientific). Oligonucleotides were designed to have a melting temperature close to 58°C for a three-step PCR protocol or between 69-72°C for a two-step protocol using the Phusion DNA polymerase. The melting temperature of oligonucleotides was calculated using the Tm Calculator from Thermo Scientific.

Table 4: Oligonucleotides for cloning

Number	Name	Sequence (5' → 3')
G1435	Ubc9_EcoRI_fwd	TTTGAATTCATGTCGGGGATCGCCCTCA
G1436	Ubc9_SalI_rev	AATGTCGACTTATGAGGGCGCAAACTTCTTG
G1437	eIF1A_EcoRI_fwd (HPLC)	TTTGAATTCATGCCCAAGAATAAAGGTAAAGG
G1438	eIF1A_SalI_rev (HPLC)	TTTGTCGACTTAGATGTCATCAATATCTTCATCATC
G1437	eIF1A_EcoRI_fwd (HPLC)	TTTGAATTCATGCCCAAGAATAAAGGTAAAGG
G1438	eIF1A_SalI_rev (HPLC)	TTTGTCGACTTAGATGTCATCAATATCTTCATCATC
G1448	eIF1A_EcoRI_fwd+spacer+ext	TTTTTTTTTGAATTCTATGCCCAAGAATAAAGGTAAAGG
G1449	eIF1A_SalI_rev+ext	TTTTTTTTTGTCGACTTAGATGTCATCAATATCTTCATCATC
G1478	Ubc9_EcoRI_fwd+spacer	TTTTGAATTCTATGTCGGGGATCGCCCTC
G1479	Ubc9_SalI_rev_mouse	AAATGTCGACTTATGAGGGGGCAAACTTCTTCGC
G1483	IPO13_AgeI_fwd	TTTTACCGGTATGGAGCGGCGGGAGG
G1484	IPO13_XhoI_rev	TTTTCTCGAGTCAGTAGTCAGCTGTGTAATCTGTGCCA
G1601	01_AIFM2_KpnI_fwd	TTTTGGTACCATGGGGTCCCAGGTCTCGGT
G1602	01_AIFM2_BamHI_rev	TTTTGGATCCTTAGGTGGAGACTGCCTCATGGTTTTC

Number	Name	Sequence (5' → 3')
G1603	02_PP1B_KpnI_fwd	TTTTGGTACCATGGCGGACGGGGAGCT
G1604	02_PP1B_BamHI_rev	TTTTGGATCCTTCCTTTTCTTCGGCGGATTAGCTG
G1605	03_ZRAB2_KpnI_fwd	TTTTGGTACCATGTCGACCAAGAATTTCCGAGTCAG
G1606	03_ZRAB2_BamHI_rev	TTTGGATCCTTGGGTTGTTTAGTGTTTTCACCAATCACCT
G1607	04_PRMT1_KpnI_fwd	TTTTGGTACCATGGCGGCAGCCGAGG
G1608	04_PRMT1_BamHI_rev	TTTTGGATCCTTGCGCATCCGGTAGTCGGTG
G1609	05_RAE1L_KpnI_fwd	TTTGGTACCATGAGCCTGTTTGGAACAACCTCAG
G1610	05_RAE1L_BamHI_rev	TTTGGATCCTTCTTCTTATTCCTGGGCTTTAGCTCTTCG
G1611	07_CELF1_HindIII_fwd	TTTTAAGCTTTTATGAACGGCACCCTGGACC
G1612	07_CELF1L_EcoRI_rev	TTTTGAATTCTGTAGGGCTTGCTGTCATTCTTCGA
G1613	08_HAT1_KpnI_fwd	TTTTGGTACCATGGCGGGATTTGGTGCTATG
G1614	08_HAT1_BamHI_rev	TTTGGATCCTTCTCTTGAGCAAGTCGTTCAATAACACG
G1615	09_IF4A1_HindIII_fwd	TTTTAAGCTTTTATGTCTGCGAGCCAGGATTCC
G1616	09_IF4A1_EcoRI_rev	TTTTGAATTCTGATGAGGTCAGCAACATTGAGGG
G1617	10_RUVB1_KpnI_fwd	TTTGGTACCATGAAGATTGAGGAGGTGAAGAGCACT
G1618	10_RUVB1_BamHI_rev	TTTGGATCCTTCTTCATGTACTTATCCTGCTGGTCAGCC
G1619	KPNB1_linker_SacI_fwd	TTTTGAGCTCTTGGTGGAGGTGGATCTGGAGGTGGAGGTTCT ATGGAGCTGATCACCATTCTC
G1620	TPNO1_linker_XhoI_fwd	TTTTCTCGAGTTGGTGGAGGTGGATCTGGAGGTGGAGGTTCT ATGGAGTATGAGTGGAAACCTGACG
G1621	IPO13_linker_XhoI_fwd	TTTTCTCGAGTTGGTGGAGGTGGATCTGGAGGTGGAGGTTCT ATGGAGCGGCGGGAGGA
G1635	01_RTCA_KpnI_fwd	TTTGGTACCATGGCGGGGCCGC
G1636	01_RTCA_BamHI_rev	TTTGGATCCTTTAGATTTGGATTTGTCATCCCAATTCC
G1637	02_APEX1_KpnI_fwd	TTTGGTACCATGCCGAAGCGTGGG
G1638	02_APEX1_BamHI_rev	TTTGGATCCTTCAGTGCTAGGTATAGGGTGATAGG
G1639	03_SRP14_KpnI_fwd	TTTGGTACCATGGTGTTGTTGGAGAGCGAGC
G1640	03_SRP14_BamHI_rev	TTTGGATCCTTCTGTGCTGCTGTTGCTGCTGT
G1641	04_NSUN2_EcoRI_fwd	TTTGAATTCAATGGGGCGGCGGTCG
G1642	04_NSUN2_EcoRI_rev	TTTGAATTCTCCGGGGTGGATGGACCC
G1643	05_TYW3_KpnI_fwd	TTTGGTACCATGGATCGCAGCGC
G1644	05_TYW3_BamHI_rev	TTTGGATCCTTGTAATCTTCAGGGAAGATGGTAAC
G1645	06_FEN1_HindIII_fwd	TTTTAAGCTTTTATGGGAATTCACGGCCTTGC
G1646	06_FEN1_KpnI_rev	TTTGGTACCTTTTTTCCCCTTCGGAACTTCCC
G1647	07_ HNRNPD_KpnI_fwd	TTTGGTACCATGTCGGAGGAGCAGTTC
G1648	07_ HNRNPD_BamHI_rev	TTTGGATCCTTGTATGGTTTGTAGCTATTTTGATG
G1649	08_XRCC5_KpnI_fwd	TTTGGTACCATGGTGCGGTCGGGGA
G1650	08_XRCC5_BamHI_rev	TTTGGATCCTTTATCATGTCCAATAAATCGTCCACATCA
G1651	09_XRCC6_BamHI_fwd	TTTGGATCCATGTCAGGGTGGGAGTCATATTAC
G1652	09_XRCC6_BamHI_rev	TTTGGATCCTTGTCCTGGAAGTGCTTGGTG
G1653	10_MCM3_HindIII_fwd	TTTTAAGCTTTTATGGCGGGTACCGTGGTG
G1654	10_MCM3_EcoRI_rev	TTTGAATTCTGATGAGGAAGATGATGCCCTCAGAC
G1655	11_DBR1_KpnI_fwd	TTTGGTACCATGCGGGTGGCTGTGGC
G1656	11_DBR1_BamHI_rev	TTTGGATCCTTAGCTGCATCGTCATCATCATCATC
G1657	12_SET_KpnI_fwd	TTTGGTACCATGTCGGCGCCGGC
G1658	12_SET_BamHI_rev	TTTGGATCCTTGTCATCTTCTCCTTCATCCTCCTCTCC
G1659	13_EIF2AK2_KpnI_fwd	TTTGGTACCATGGCTGGTGATCTTTCAG
G1660	13_EIF2AK2_BamHI_rev	TTTGGATCCTTACATGTGTGTCGTTCATTTTT
G1661	14_DDX1_HindIII_fwd	TTTAAGCTTTTATGGCGGCCTTCTCC
G1662	14_DDX1_HindIII_rev	TTTGGATCCTTGAAGGTTCTGAACAGCTGG

Number	Name	Sequence (5' → 3')
G1663	15_PRMT5_EcoRI_fwd	TTTGAATTCAATGGCGGCGATGGCG
G1664	15_PRMT5_EcoRI_rev	TTTGAATTCTGAGGCCAATGGTATATGAGCGGC
G1665	16_BTF3_KpnI_fwd	TTTGGTACCATGCGACGGACAGGCGC
G1666	16_BTF3_BamHI_rev	TTTGGATCCTTGTTTGCCTCATTCTTGGAAGCCTC
G1667	17_EIF2D_EcoRI_fwd	TTTGAATTCAATGTTTGCCAAGGCCTTTCGG
G1668	17_EIF2D_EcoRI_rev	TTTGAATTCTCTTCTTCTTGCCAGGTTTGAGGG
G1669	18_STRAP_KpnI_fwd	TTTGGTACCATGGCAATGAGACAGACGCCG
G1670	18_STRAP_BamHI_rev	TTTGGATCCTTGGCCTTAACATCAGGAGCTGAAGG
G1673	19_TFCP2_KpnI_fwd	TTTGGTACCATGGCCTGGGCTCTG
G1674	19_TFCP2_BamHI_rev	TTTGGATCCTTCTTCAGTATGATATGATAGCTATCATTG
G1675	20_TRIM28_HindIII_fwd	TTTTAAGCTTTTATGGCGGCCTCCGCG
G1676	20_TRIM28_EcoRI_rev	TTTGAATTCTGGGGCCATCACCAGGGC
G1677	21_TNIP1_KpnI_fwd	TTTGGTACCATGGAAGGGAGAGGACCGTACCG
G1678	21_TNIP1_BamHI_rev	TTTGGATCCTTCTGAGGCCCCTCACGGTCA
G1679	22_ERI1_KpnI_fwd	TTTGGTACCATGGAGGATCCACAGAGTAA
G1680	22_ERI1_KpnI_rev	TTTGGTACCAACTTTCTAAAATGTGGCATTTG
G1681	23_BYSL_HindIII_fwd	TTTTAAGCTTTTATGCCCAAATTCAAGGC
G1682	23_BYSL_EcoRI_rev	TTTGAATTCTCTCCACGGTGATGGG
G1683	24_EIF3F_HindIII_fwd	TTTTAAGCTTTTATGGCCACACCGG
G1684	24_EIF3F_EcoRI_rev	TTTGAATTCTCAGGTTTACAAGTTTTTCATTG
G1685	25_EIF3G_HindIII_fwd	TTTTAAGCTTTTATGCCTACTGGAGACTTTGA
G1686	25_EIF3G_EcoRI_rev	TTTGAATTCTGTTGGTGGACGGCTT
G1687	26_PDCD4_KpnI_fwd	TTTGGTACCATGGATGTAGAAAATGAGCAG
G1688	26_PDCD4_BamHI_rev	TTTGGATCCTTGTAGCTCTCTGGTTTAAGACG
G1689	27_GTF2F2_HindIII_fwd	TTTTAAGCTTTTATGGCCGAGCGC
G1690	27_GTF2F2_EcoRI_rev	TTTGAATTCTGTCACTCTTTTCTTCTCCTTG
G1691	28_PPP1CA_KpnI_fwd	TTTGGTACCATGTCCGACAGCGAGAAGCTCA
G1692	28_PPP1CA_BamHI_rev	TTTGGATCCTTTTTCTTGGCTTTGGCGGAATTG
G1693	29_CDK1_HindIII_fwd	TTTTAAGCTTTTATGGAAGATTATACCAAAATAGAG
G1694	29_CDK1_EcoRI_rev	TTTGAATTCTCATCTTCTTAATCTGATTGTCC
G1695	30_DDX3_KpnI_fwd	TTTGGTACCATGAGTCATGTGGCAGTG
G1696	30_DDX3_BamHI_rev	TTTGGATCCTTGTTACCCCACCAGTCAAC
G1697	31_XPA_KpnI_fwd	TTTGGTACCATGGCGGCGGCCG
G1698	31_XPA_BamHI_rev	TTTGGATCCTTCATTTTTTCATATGTCAGTTCATGGCCAC
G1699	32_GPN1_HindIII_fwd	TTTTAAGCTTTTATGCGGTGTCTCTATGGTC
G1700	32_GPN1_EcoRI_rev	TTTGAATTCTTTTATTGTTTCTCTTCCAGTATTG
G1701	33_SQSTM1_HindIII_fwd	TTTTAAGCTTTTATGGCGTCGCTCACCGTG
G1702	33_SQSTM1_EcoRI_rev	TTTGAATTCTCAACGGCGGGGGATGC
G1703	34_RBM22_KpnI_fwd	TTTGGTACCATGGCGACCTCTCTGGGTTCC
G1704	34_RBM22_BamHI_rev	TTTGGATCCTTGGGGCTGCTGTGTTTTCCAG
G1705	35_NELFA_KpnI_fwd	TTTGGTACCATGGCGTCCATGCGGG
G1706	35_NELFA_BamHI_rev	TTTGGATCCTTGGACACATTGGTCATGGGCTTG
G1707	36_NELFB_KpnI_fwd	TTTGGTACCATGTTCGCGGGGCTGCA
G1708	36_NELFB_BamHI_rev	TTTGGATCCTTGAGCGGGGCAGGGGC
G1709	37_NELFCD_EcoRI_fwd	TTTGAATTCAATGCGCCGCGCTCG
G1710	37_NELFCD_EcoRI_rev	TTTGAATTCTGTTCACCATGATGAAGTTAGATTTGCAGTG
G1739	tIPO13_EcoRI_fwd	TTTGAATTCAATGATCAACAGTGTTCTGCCC
G1740	tIPO13_XhoI_rev	TTTCTCGAGTCAGTAGTCAGCTGTGTAATCTGTG
G1765	40_OLA1_HindIII_fwd	TTTAAGCTTTTATGCCCCCTAAAAAGGGAGGTG

Number	Name	Sequence (5' → 3')
G1766	40_OLA1_EcoRI_rev	TTTGAATTCTTTTCTTCTTCGGTTGTTGAGGTGTG
G1767	41_WDR77_HindIII_fwd	TTTAAGCTTTTATGCGGAAGGAAACCCCACC
G1768	41_WDR77_EcoRI_rev	TTTGAATTCTCTCAGTAACACTTGCAGGTCCAGGG
G1769	38_EDC3_HindIII_fwd	TTTAAGCTTTTATGGCTACAGATTGGCTGGGAAG
G1770	38_EDC3_EcoRI_rev	TTTGAATTCTAGCAGAGTGCAGTGGGATAACAAACTTG
G1771	39_WDR61_HindIII_fwd	TTTAAGCTTTTATGACCAACCAGTACGGTATTCTCTTCAAAC
G1772	39_WDR61_EcoRI_rev	TTTGAATTCTAATTGGACAATCATAGATGTGAATTTCCTGG

Table 5: Oligonucleotides for sequencing

Number	Name	Sequence (5' → 3')
G828	Importin13 Bp 1102 for	CAGGATGATATTCTATCC
GATC	pcDNA3.1-FP	CTCTGGCTAACTAGAGAAC
GATC	pcDNA3.1-RP/1	CAAACAACAGATGGCTGGC
GATC	pEGFP_C2-RP	TTTAAAGCAAGTAAAACCTC
GATC	pGEX5-FP	AACGTATTGAAGCTATCCC
GATC	SP6	ATTTAGGTGACACTATAGAA
GATC	T3	ATTAACCCTCACTAAAGGGA
GATC	T7	TAATACGACTCACTATAGGG

Table 6: Oligonucleotide for cDNA synthesis

Name	Sequence (5' → 3')	Origin
Oligo(dT)	TTTTTTTTTTTTTTTTTTTTTTTTVN (V is any nucleotide apart from T; N is any nucleotide)	Prof. Markus Bohnsack, Department of Molecular Biology, Göttingen

2.1.14 Vectors

Table 7: Vectors

Number	Name	Tag	Resistance	Application	Origin
4	pET-28a	His (N-terminal)	kanamycin	expression	Novagen
30	pEGFP-C1	EGFP (N-terminal)	kanamycin	transfection	Clontech
46	pGex-6P-1	GST (N-terminal)	ampicillin	expression	Amersham
51	pcDNA 3.1(+)	none	ampicillin	transfection	Invitrogen
52	pcDNA3.1(+)-HA	HA-Tag (C-terminal)	ampicillin	transfection	S. Wälde
82	pGEX-6P-1-MCS2	GST (N-terminal)	ampicillin	expression	this work, MCS from #290 in vector #46 (EcoNI, BamHI)

2.1.15 Plasmids

Table 8: Available plasmids

Number	Name	Origin
2	pET3d-RanQ69L	
186	pCMV-HA-DDX3	K.T. Jeang
249	pCMV-HA-DDX1	R.J. Pomerantz
290	pEGFP-GST	D. Doenecke
294	pdEGFP-C1	
297	pdEGFP-GST-NLS (Xenopus)	D. Doenecke
299	pEYFP-Fos	M. Duterque
300	pECFP-Jun	M. Duterque
320	pdGFP-GST-RevNLS	M. Nassiri
328	pEF-HA-Snurportin1	S. Hutten
330	pEF-HA-DDX43	C. Spillner
333	pEF-HA-DMAP1	C. Spillner
335	pEF-HA-DBC1	C. Spillner
396	pdEGFP-Jun	I. Waldmann
403	pdEGFP-M9	S. Hutten
467	pdEGFP-Fos	S. Roloff
510	pcDNA3.1-HA-Ubc9	Melchior
545	pcDNA3.1-TERT-HA	S. Wälde
553	pcDNA-HA-p53	EM
651	pcDNA4-HA-ER alpha	S. Johnson
687	pCS2plus-FLAG-importin 13	D. Doenecke
731	pEGFP-C1-DBC1	S. Wälde
731	pEGFP-C1-DBC1	S. Wälde
755	pECFP-C1-DDX 43	S. Wälde
757	pECFP-C1-DDX 59	S. Wälde
767	pmCherry-C1-Sirt1	S. Wälde
789	pdEGFP-cNLS-DBC-1 (aa 793-923)	S. Wälde
813	pCS2plus-FLAG-importin13 (aa 1-410)	D. Doenecke
814	pCS2plus-FLAG-importin13 (aa 1-669)	D. Doenecke
815	pCS2plus-FLAG-importin13 (aa 1-784)	D. Doenecke
816	pCS2plus-FLAG-importin13 (aa 153-963)	D. Doenecke
817	pCS2plus-FLAG-importin13 (aa 153-784)	D. Doenecke
833	pEGFP-N1-TERT	C. Frohnert
834	pEGFP-C1-DMAP	A. Nath
1102	pEGFP-C1-SQSTM1	T. Johansen
1112	GFP-Bystin-like	K. Thakar
1165	pEGFP-C1-HA-importin 13 (no GFP)	A. Nath
1166	pEGFP-C1-HA-importin 13-E436R/D481R (no GFP)	A. Nath
1167	pEGFP-N3-eIF1A	A. Nath
1168	pEGFP-N3-eIF1A-R46E	A. Nath
1239	pET328-His-zz-tev	F. Vilardi
1511	pQE80-His-importin 13	D. Doenecke
1514	pET23-Ubc9	R. Geiss-Friedländer
1576	pET-MCN-GST-importin 13	F. Bono

Number	Name	Origin
1577	pcDNA4-SET-myc-His	C. Kaether
1689	pCAGGS-HA-NELFA	Y. Yamaguchi
LIFEdb	pEYFP-N-Hsp22	LIFEdb, DKFZ
LIFEdb	pEYFP-N-CPF	LIFEdb, DKFZ
LIFEdb	pEYFP-N-Lim6	LIFEdb, DKFZ
LIFEdb	pEYFP-N-Tmp29	LIFEdb, DKFZ
LIFEdb	pEYFP-N-Nip30	LIFEdb, DKFZ
LIFEdb	pEYFP-N-Zinc313	LIFEdb, DKFZ
LIFEdb	pEYFP-N-KIAA1826	LIFEdb, DKFZ
LIFEdb	pEYFP-N-DNAPTP6	LIFEdb, DKFZ
LIFEdb	pEYFP-N-H3.3B	LIFEdb, DKFZ

Table 9: Generated plasmids

Number	Name	Cloning	Generated by*
1513	pCS2plus-FLAG-importin 13-E436R/D481R	mutant part of IPO13 transferred from #1166 to #687 (SmaI/EcoRV)	J. M. Reyes del Castillo
1515	pGEX-6P-1-Ubc9	Ubc9 from #1514 (G1435, G1436) in vector #46 (EcoRI/SalI)	
1516	pGEX-6P-1-eIF1A	eIF1A from #1167 in vector #46 (EcoRI/SalI)	
1518	pET28a-His-eIF1A	eIF1A from #1167 (G1437, G1438) in vector #4 (EcoRI/SalI)	
1522	pdEGFP-eIF1A	eIF1A from #1167 (G1448, G1449) in # 294 (EcoRI/SalI)	
1547	pEGFP-GST-Ubc9	Ubc9 from #1514 (G1478, G1479) in #290 (EcoRI/SalI)	
1569	pET328-Hzz-importin 13	IPO13 from #1511 (G1483, G1484) in #1239 (AgeI/XhoI)	
1643	pEGFP-GST-eIF1A	eIF1A from #1522 in #290 (EcoRI/SalI)	
1660	pcDNA3.1-AIFM2-HA	Insert from cDNA (G1601, G1602) in vector #52 (KpnI/BamHI)	C. Spillner
1661	pEGFP-GST-AIFM2	Insert from cDNA (G1601, G1602) in #290 (KpnI/BamHI)	C. Spillner
1662	pcDNA3.1-PPP1CB-HA	Insert from cDNA (G1603, G1604) in vector #52 (KpnI/BamHI)	C. Spillner
1663	pEGFP-GST-PPP1CB	Insert from cDNA (G1603, G1604) in #290 (KpnI/BamHI)	C. Spillner
1664	pcDNA3.1-ZRAB2-HA	Insert from cDNA (G1605, G1606) in vector #52 (KpnI/BamHI)	C. Spillner
1665	pEGFP-GST-ZRAB2	Insert from cDNA (G1605, G1606) in #290 (KpnI/BamHI)	C. Spillner
1666	pcDNA3.1-PRMT1-HA	Insert from cDNA (G1607, G1608) in vector #52 (KpnI/BamHI)	C. Spillner
1667	pEGFP-GST-PRMT1	Insert from cDNA (G1607, G1608) in #290 (KpnI/BamHI)	C. Spillner

Number	Name	Cloning	Generated by*
1671	pcDNA3.1-CELF1-HA	Insert from cDNA (G1611, G1612) in vector #52 (HindIII/EcoRI)	C. Spillner
1672	pEGFP-GST-CELF1	Insert from cDNA (G1611, G1612) in #290 (HindIII/EcoRI)	C. Spillner
1674	pcDNA3.1-IF4A1-HA	Insert from cDNA (G1615, G1616) in vector #52 (HindIII/EcoRI)	C. Spillner
1675	pEGFP-GST-IF4A1	Insert from cDNA (G1615, G1616) in #290 (HindIII/EcoRI)	C. Spillner
1676	pcDNA3.1-RUVB1-HA	Insert from cDNA (G1617, G1618) in vector #52 (KpnI/BamHI)	C. Spillner
1677	pEGFP-GST-RUVB1	Insert from cDNA (G1617, G1618) in #290 (KpnI/BamHI)	C. Spillner
1690	pcDNA3.1-RTCA-HA	Insert from cDNA (G1635, G1636) in vector #52 (KpnI/BamHI)	
1691	pcDNA3.1-APEX1-HA	Insert from cDNA (G1637, G1638) in vector #52 (KpnI/BamHI)	
1692	pcDNA3.1-SRP14-HA	Insert from cDNA (G1639, G1640) in vector #52 (KpnI/BamHI)	
1693	pcDNA3.1-NSUN2-HA	Insert from cDNA (G1641, G1642) in vector #52 (EcoRI)	
1694	pcDNA3.1-TYW3-HA	Insert from cDNA (G1643, G1644) in vector #52 (KpnI/BamHI)	
1695	pcDNA3.1-HNRNPD-HA	Insert from cDNA (G1647, G1648) in vector #52 (KpnI/BamHI)	
1696	pcDNA3.1-XRCC6-HA	Insert from cDNA (G1651, G1652) in vector #52 (BamHI)	
1697	pcDNA3.1-MCM3-HA	Insert from cDNA (G1653, G1654) in vector #52 (HindIII/EcoRI)	
1698	pcDNA3.1-DBR1-HA	Insert from cDNA (G1655, G1656) in vector #52 (KpnI/BamHI)	
1699	pcDNA3.1-SET-HA	Insert from #1577 (G1657, G1658) in vector #52 (KpnI/BamHI)	
1700	pcDNA3.1-PRMT5-HA	Insert from cDNA (G1663, G1664) in vector #52 (EcoRI)	
1701	pcDNA3.1-BTF3-HA	Insert from cDNA (G1665, G1666) in vector #52 (KpnI/BamHI)	
1702	pcDNA3.1-STRAP-HA	Insert from cDNA (G1669, G1670) in vector #52 (KpnI/BamHI)	
1703	pcDNA3.1-TFCP2-HA	Insert from cDNA (G1673, G1674) in vector #52 (KpnI/BamHI)	
1704	pcDNA3.1-ERI1-HA	Insert from cDNA (G1679, G1680) in vector #52 (KpnI)	
1705	pcDNA3.1-BYSL-HA	Insert from #1112 (G1681, G1682) in vector #52 (HindIII/EcoRI)	
1706	pcDNA3.1-EIF3F-HA	Insert from cDNA (G1683, G1684) in vector #52 (HindIII/EcoRI)	
1707	pcDNA3.1-EIF3G-HA	Insert from cDNA (G1685, G1686) in vector #52 (HindIII/EcoRI)	
1708	pcDNA3.1-PPP1CA-HA	Insert from cDNA (G1691, G1692)	

Number	Name	Cloning	Generated by*
		in vector #52 (KpnI/BamHI)	
1709	pcDNA3.1-GPN1-HA	Insert from cDNA (G1699, G1700) in vector #52 (HindIII/EcoRI)	
1710	pcDNA3.1-RBM22-HA	Insert from cDNA (G1703, G1704) in vector #52 (KpnI/BamHI)	
1711	pcDNA3.1-NELFA-HA	Insert from #1689 (G1705, G1706) in vector #52 (KpnI/BamHI)	
1712	pcDNA3.1-NELFB-HA	Insert from cDNA (G1707, G1708) in vector #52 (KpnI/BamHI)	
1713	pcDNA3.1-NELFCD-HA	Insert from cDNA (G1709, G1710) in vector #52 (EcoRI)	
1725	pcDNA3.1-XRCC5-HA	Insert from cDNA (G1649, G1650) in vector #52 (KpnI/BamHI)	C. Spillner
1726	pcDNA3.1-CDK1-HA	Insert from cDNA (G1693, G1694) in vector #52 (HindIII/EcoRI)	C. Spillner
1727	pcDNA3.1-EIF2AK2-HA	Insert from cDNA (G1659, G1660) in vector #52 (KpnI/BamHI)	C. Spillner
1728	pcDNA3.1-DDX1-HA	Insert from #249 (G1661, G1662) in vector #52 (HindIII/EcoRI)	C. Spillner
1729	pcDNA3.1-DDX3-HA	Insert from #186 (G1695, G1696) in vector #52 (KpnI/BamHI)	C. Spillner
1730	pcDNA3.1-SQSTM1-HA	Insert from #1102 (G1701, G1702) in vector #52 (HindIII/EcoRI)	C. Spillner
1731	pcDNA3.1-XPA-HA	Insert from cDNA (G1697, G1698) in vector #52 (KpnI/BamHI)	C. Spillner
1732	pEGFP-GST-BTF3	Insert from #1701 in #290 (KpnI/BamHI)	
1733	pEGFP-GST-DBR1	Insert from #1698 in #290 (KpnI/BamHI)	
1734	pEGFP-GST-TFCP2	Insert from #1703 in #290 (KpnI/BamHI)	
1735	pEGFP-GST-XRCC5	Insert from #1725 in #290 (KpnI/BamHI)	C. Spillner
1736	pEGFP-GST-NSUN2	Insert from #1693 in #290 (EcoRI)	C. Spillner
1737	pEGFP-GST-DDX1	Insert from #1728 in #290 (HindIII/BamHI)	C. Spillner
1738	pEGFP-GST-XPA	Insert from #1731 in #290 (KpnI/BamHI)	C. Spillner
1739	pEGFP-GST-SQSTM1	Insert from #1730 in #290 (HindIII/EcoRI)	C. Spillner
1740	pEGFP-GST-EIF2AK2	Insert from #1727 in #290 (KpnI/BamHI)	C. Spillner
1741	pEGFP-GST-FEN1	Insert from cDNA (G1645, G1646) in #290 (HindIII/KpnI)	C. Spillner
1745	pcDNA3.1-EIF2D-HA	Insert from cDNA (G1667, G1668) in vector #52 (EcoRI)	
1746	pcDNA3.1-GTF2F2-HA	Insert from cDNA (G1689, G1690) in vector #52 (HindIII/EcoRI)	
1747	pEGFP-GST-RTCA	Insert from #1690 in #290	

Number	Name	Cloning	Generated by*
		(KpnI/BamHI)	
1748	pEGFP-GST-APEX1	Insert from #1691 in #290 (KpnI/BamHI)	
1749	pEGFP-GST-SRP14	Insert from #1692 in #290 (KpnI/BamHI)	
1750	pEGFP-GST-TYW3	Insert from #1694 in #290 (KpnI/BamHI)	
1751	pEGFP-GST-HNRNPD	Insert from #1695 in #290 (KpnI/BamHI)	
1752	pEGFP-GST-MCM3	Insert from #1697 in #290 (HindIII/EcoRI)	
1753	pEGFP-GST-SET	Insert from #1699 in #290 (KpnI/BamHI)	
1754	pEGFP-GST-EIF2D	Insert from #1745 in #290 (EcoRI)	
1755	pEGFP-GST-STRAP	Insert from #1702 in #290 (KpnI/BamHI)	
1756	pEGFP-GST-BYSL	Insert from #1705 in #290 (HindIII/EcoRI)	
1757	pEGFP-GST-EIF3F	Insert from #1706 in #290 (HindIII/EcoRI)	
1758	pEGFP-GST-EIF3G	Insert from #1707 in #290 (HindIII/EcoRI)	
1759	pEGFP-GST-PPP1CA	Insert from #1708 in #290 (KpnI/BamHI)	
1760	pEGFP-GST-GPN1	Insert from #1709 in #290 (HindIII/EcoRI)	
1761	pEGFP-GST-NELFA	Insert from #1711 in #290 (KpnI/BamHI)	
1762	pEGFP-GST-NELFB	Insert from #1712 in #290 (KpnI/BamHI)	
1807	pEGFP-GST-PRMT5	Insert from #1700 in #290 (EcoRI)	
1808	pcDNA3.1-PDCD4-HA	Insert from cDNA (G1687, G1688) in vector #52 (KpnI/BamHI)	C. Spillner
1809	pcDNA3.1-importin 13	Insert from #687 in vector #52 (EcoRI/XhoI)	C. Spillner
1810	pcDNA3.1-importin 13-E436R/D481R	Insert from #1513 in vector #51 (EcoRI/XhoI)	C. Spillner
1812	pCS2+MT-FLAG-impotin13 (aa 526-963)	Insert from #687 (G1739, G1740) in #687 (EcoRI/XhoI)	C. Spillner
1814	pEGFP-GST-ERI1	Insert from #1704 in #290 (KpnI)	
1815	pEGFP-GST-GTF2F2	Insert from #1746 in #290 (HindIII/EcoRI)	C. Spillner
1827	pEGFP-GST-NELFCD	Insert from #1713 in #290 (EcoRI)	
1829	pEGFP-GST-XRCC6	Insert from #1696 in #290 (BamHI)	
1843	pEGFP-GST-PDCD4	Insert from #1808 in #290 (KpnI/BamHI)	C. Spillner
1849	pEGFP-GST-WDR61	Insert from #1868 in #290 (HindIII/EcoRI)	C. Spillner
1853	pEGFP-GST-OLA1	Insert from #1860 in #290	C. Spillner

Number	Name	Cloning	Generated by*
		(HindIII/EcoRI)	
1859	pCDNA3.1-WDR77-HA	Insert from cDNA (G1767, G1768) in vector #52 (HindIII/EcoRI)	C. Spillner
1860	pCDNA3.1-OLA1-HA	Insert from cDNA (G1765, G1766) in vector #52 (HindIII/EcoRI	C. Spillner
1861	pEGFP-GST-DDX3	Insert from #1729 in #290 (KpnI/BamHI)	C. Spillner
1862	pEGFP-GST-WDR77	Insert from #1859 in #290 (HindIII/EcoRI)	C. Spillner
1868	pcDNA3.1-WDR61-HA	Insert from cDNA (G1771,G1772) in vector #52 (HindIII/EcoRI)	C. Spillner
1871	pcDNA3.1-EDC3-HA	Insert from cDNA (G1769, G1770) in vector #52(HindIII/EcoRI)	C. Spillner
1872	pEGFP-GST-EDC3	Insert from #1871 in #290 (HindIII/EcoRI)	C. Spillner

*if not indicated otherwise, plasmids were generated by Imke Baade

2.2 Molecular Biology Methods

2.2.1 RNA Isolation from Cellular Extracts

Total RNA was purified from HeLa P4 cell pellet using the RNeasy Mini Kit (Qiagen), following the protocol 'Purification of Total RNA from Animal Cells using Spin Technology'. RNA was eluted with two times 30 µL RNase-free water and stored at -20°C. Purity of the RNA was confirmed by measuring the A_{260}/A_{280} ratio with the NanoDrop 2000c. Samples with a ratio of 1.7-1.9 were considered as pure RNA.

2.2.2 cDNA Synthesis

For the synthesis of complementary DNA (cDNA) from total RNA, the SuperScript® III reverse transcriptase (Thermo Scientific) was used according to the manufacturer's instructions. Reactions of 13 µL were set up with 2 µg total RNA, 1 µL of 50 µM oligo(dT) and 1 µL of 10 mM dNTPs in RNase-free water. The reaction mix was incubated at 65°C for 5 minutes, followed by incubation on ice for 1 minute. Synthesis of cDNA was initiated by addition of 4 µL 5x First-Strand Buffer, 1 µL 0.1 M DTT, 1 µL RiboLockRNase Inhibitor (40 U/µL) as well as 1 µL SuperScript® III RT (200 U/µL) and incubation at 50°C for 1 hour. Reactions were inactivated at 70°C for 15 minutes and cDNA was stored at -20°C.

2.2.3 Polymerase Chain Reaction (PCR)

For amplification of specific DNA segments from genomic or plasmid DNA, the polymerase chain reaction (PCR) was used. PCR reactions were performed with Phusion® High-Fidelity DNA Polymerase (Thermo Scientific) according to the manufacturer's recommendations. In brief, 50 µL reactions were set up with 1x HF Phusion Buffer, 200 µM dNTPs, 5 µM forward and reverse primer (see section 2.1.13 for primers), 0.02 U/µL Phusion® High-Fidelity DNA Polymerase and 1 pg -10 ng template DNA. In the case of amplification of a gene from cDNA, 1-2 µL of cDNA was used in the PCR reaction. DNA segments were amplified for 30-35 cycles in a thermocycler using either the 3-step or 2-step (combined annealing and extension step at 72°C) protocol according to the manufacturer's instructions. Annealing temperatures of oligonucleotides were calculated using the 'Tm calculator' from Thermo Scientific (www.thermoscientific.com/pcrwebtools). The extension time was adjusted to the size of the PCR product.

PCR reactions were analyzed by agarose gel electrophoresis (2.2.4). PCR products were excised from the gel and purified using the NucleoSpin® Gel and PCR Clean-up kit from Macherey-Nagel (2.2.5).

2.2.4 Agarose Gel Electrophoresis

DNA fragments were separated according to their size by agarose gel electrophoresis. Depending on the size of the DNA fragments 0.5-2.0% agarose gels were prepared. The agarose powder was dissolved in 1x TAE buffer by heating in a microwave and regular agitation. After the melted agarose had cooled sufficiently, the SafeView™ Classic DNA stain was added to a 1:20,000 dilution and the gel was poured. The solidified gel was placed in a running chamber with 1x TAE buffer. Samples prepared with 6x DNA loading buffer together with a molecular weight marker (GeneRuler 100bp DNA Ladder or GeneRuler 1kb DNA Ladder) were loaded onto the gel and separated at 120 V.

Agarose gels were documented with the GelSTICK 'touch' system. DNA fragments used for further cloning were excised from the agarose gel on a UV transilluminator.

2.2.5 Purification of DNA Fragments from Agarose Gel

DNA fragments were isolated from agarose gels using the NucleoSpin® Gel and PCR Clean-up kit, following the manufacturer's protocol 'DNA extraction from agarose gels'. DNA fragments were eluted with 25-30 µL elution buffer and the plasmid DNA concentration was determined with the NanoDrop 2000c.

2.2.6 DNA Restriction Digestion

DNA was digested at 37°C for 1-2 h using the restriction enzyme ratio and buffer recommended by the 'DoubleDigest Calculator' tool from Thermo Scientific (www.thermoscientific.com/doubledigest). For preparative digestion, 25 µL of the PCR product and 2-5 µg plasmid DNA was cut with not more than 1 µL of enzyme (10 U/µL) per one µg of DNA in a 20-50 µL reaction volume. For restriction analysis of plasmid DNA from small scale DNA preparations, 5 µL of the eluted plasmid DNA was digested with not more than 0.2 µL of enzyme (10 U/µL) in a 10 µL reaction volume. Alternatively, digestion was also performed with FastDigest enzymes from Thermo Scientific following the manufacturer's instructions.

Digested DNA was analyzed by agarose gel electrophoresis (2.2.4).

2.2.7 Dephosphorylation of Linearized Vectors

Cut vector DNA was dephosphorylated with FastAP Thermosensitive Alkaline Phosphatase (Thermo Scientific) to remove the 5' phosphate from the DNA to prevent recircularization of the vector. The digested vector was incubated with 1 U Alkaline Phosphatase per 1µg DNA in 1x FastAP reaction buffer for 10 minutes at room temperature. The enzyme was inactivated for 5 minutes at 75°C.

2.2.8 Ligation of DNA Fragments

DNA fragments were ligated into linearized vectors using the T4 DNA ligase (Thermo Scientific). Ligation was performed with 100 ng linear vector DNA, a 3:1 molar ratio of insert DNA to vector DNA, 1x T4 DNA ligase buffer and 1 U of T4 DNA ligase in a total reaction volume of 10 µL. The reaction mix was incubated for 1 hour at room temperature and transformed into *Escherichia coli* (*E. coli*) DH5α (2.2.9).

2.2.9 Transformation of *E. coli* with Plasmid DNA

For transformation, 10 µL of ligation mixture or 0.1 µg of plasmid-DNA was added to 50 µL of chemically competent cells. *E. coli* DH5α cells were used for cloning. The transformation mix was incubated on ice for 15 minutes, before the cells were heat shocked for 90 seconds at 42°C. The cells were recovered on ice for 2 minutes, resuspended in 300 µL SOC-medium and incubated at 37°C for 1 hour at 850 rpm. Half of the transformation mix was spread on a selective LB agar plate and incubated overnight at 37°C.

2.2.10 Small Scale Plasmid DNA Isolation

Plasmid DNA was isolated from 2-4 mL *E. coli* overnight culture using the NuceloSpin® Plasmid kit following the 'Isolation of high-copy plasmid DNA from *E.coli*' protocol. For the overnight culture, 3-5 mL of LB medium containing the respective antibiotics were inoculated with a single colony picked from a selective LB agar plate. The culture was incubated overnight at 37°C, 180 rpm. The purified DNA was eluted with 50 µL elution buffer. The correctness of the plasmid DNA was confirmed by restriction analysis and sequencing.

2.2.11 Large Scale Plasmid DNA Isolation

For large scale preparation of plasmid DNA, the NucleoBond™ Xtra Midi kit was used following the supplied protocols 'High-copy plasmid purification' or 'Low-copy plasmid purification'. For the overnight culture, 100-200 mL of LB medium supplemented with the appropriate antibiotics was inoculated with a single colony. The culture was incubated overnight at 37°C, 180 rpm. The plasmid DNA was eluted with desalted water and the concentration was adjusted to 1 mg/mL using the Nanodrop 2000c.

2.2.12 Sequencing

To verify the success of ligation and ascertain that no frame-shifts or mutations were introduced, the isolated ligation product was sent for sequencing to the company GATC Biotech. Sequencing primers were selected from the GATC PrimerScout tool (www.gatc-biotech.com) or custom-made primers were used (2.1.13).

2.3 Biochemical Methods

2.3.1 SDS-PAGE

To separate proteins according to their electrophoretic mobility an SDS-PAGE was performed. Depending on the size of the target protein SDS gels with separation gels of 6-15% acrylamide were prepared and overlaid with a 4% stacking gel. Protein samples or cell lysates were mixed with reducing SDS sample buffer and heated for 5-10 minutes at 95°C. The prepared samples, as well as a protein ladder (PageRuler Prestained, PageRuler Unstained), were loaded onto the polyacrylamide gel. Gel electrophoresis was performed with 1x Laemmli buffer in Mighty Small II Mini Vertical Electrophoresis Units

(Hoefer) with 25-30 mA per gel until the bromophenol blue dye had completely passed through the gel.

Proteins were either visualized by Coomassie staining (2.3.2), silver staining (2.3.3) or by targeting the protein of interest with a specific antibody in a Western blot (2.3.4).

Additionally to the self-made gels, two types of precast gradient gels were used. The 4-20% Mini-PROTEAN^{R} TGX™ Precast Protein Gels (BioRad) were run with 1x Laemmli buffer in SE250 Mighty Small II Mini Vertical Electrophoresis Units (Hoefer) at 100 V until the samples had passed through the separation gel and then at 300 V for ~30 minutes. The NuPAGE^{R} Novex^{R} 4-12% Bis-Tris gradient gels (Invitrogen) were run with 1x NuPAGE^{R} MES SDS running buffer in XCell SureLock^{R} Mini-Cells at 200 V for ~45 minutes.

2.3.2 Coomassie Staining

Polyacrylamide gels were rinsed with water, fixed for 10 minutes to one hour with Coomassie fixation solution and stained for one hour to overnight in Coomassie staining solution on a shaker. Gels were destained with deionized water, or if the background signal was too high, with Coomassie destaining solution. Coomassie-stained gels were documented with the LAS-3000 and imported into the Fiji software for editing and quantification.

2.3.3 Silver Staining

Compared to Coomassie staining of polyacrylamide gels, silver staining is more sensitive and allows detection of low amounts of proteins. Silver staining was performed with the Pierce® Silver Stain kit following the manufacturer's instructions. Silver-stained gels were documented with the LAS-3000 and edited with Fiji software.

2.3.4 Western Blotting

For the immunological detection of specific proteins, Western Blots were performed. Proteins separated by SDS-PAGE were transferred to a Amersham Protran 0.45 µm NC Nitrocellulose Blotting Membrane (GE Healthcare) using a Mini Trans-Blot® Cell (Bio-Rad). The transfer was performed in Western blot transfer buffer (25 mM Tris, 193 mM glycine, 0.02% SDS, 20% methanol) at 100 V and 350 mA. Transfer times were adjusted depending on the protein size and percentage of the resolving gel.

The 4–20% Mini-PROTEAN^{R} TGX™ Precast Protein Gels from BioRad were pre-incubated for 30 minutes in 1x Western blot transfer buffer prior to transfer. The

NuPAGE^R Novex^R 4-12% Bis-Tris gradient gels from Invitrogen were blotted at 60 V for 90 minutes.

The quality of protein transfer was tested by staining the membrane with PonceauS staining solution for 2 minutes and visualization of the protein bands by rinsing several times with 0.1% acetic acid. Stained membranes were documented with the LAS-3000 (Fujifilm) and destained with PBS-T (137 mM NaCl, 2.7 mM KCl, 10 mM Na_2HPO_4, 1.8 mM KH_2PO_4, 0.1% Tween-20) for further processing.

The Nitrocellulose membrane was blocked with 4% milk powder in PBS-T for 45 minutes at room temperature to prevent unspecific binding of antibodies, followed by incubation with the primary antibody (2.1.11) diluted in 4% milk powder/PBS-T overnight at 4°C. The membrane was washed three times with PBS-T for 10 minutes and incubated with the secondary HRP-coupled antibody (2.1.11) diluted 1:10,000 in 4% milk powder/PBS-T for 1 hour at room temperature. Unbound antibody was removed by washing three times for 10 minutes with PBS-T and bound antibodies were detected by chemiluminescence using the Immobilon™ Western Chemiluminescent HRP Substrate (Millipore) kit and exposure to Amersham Hyperfilm™ ECL (GE Healthcare) or Medix XBU medical x-ray films (FOMA Bohemia). Film exposure times depended on the strength of the signal and exposed films were developed with the developer machine CURIX60 (Agfa).

2.3.5 Protein Purification

His-importin 13

His-importin 13 was purified as described before (Mingot *et al.,* 2001). For protein expression, the plasmid coding for His-importin 13 was transformed (2.2.9) into JM109 *E. coli* bacteria and plated on an LB agar plate supplemented with ampicillin. The next day several colonies were picked and used for inoculation of 100 mL 2x YT-medium supplemented with 2% glycerol, 30 mM K_2HPO_4 and 100 µg/mL ampicillin. The 100 mL starter culture was grown overnight at 37°C, 150 rpm and was used to inoculate 700 mL of 2x YT-medium supplemented with 2% glycerol, 30 mM K_2HPO_4 and 100 µg/mL ampicillin. The culture was grown at 37°C, 110 rpm to an OD_{600} of 0.6 before 1.2 L of cold 2x YT-medium supplemented with 2% glycerol, 30 mM K_2HPO_4 and 100 µg/mL ampicillin were added. The temperature was shifted to 16°C and the culture was grown to an OD_{600} of 0.75 prior to induction of protein expression with 0.1 mM IPTG overnight at 16°C. Bacterial cells were collected by centrifugation for 20 minutes at 4,200 rpm (Centrifuge J6-MI with rotor JS 4.2, Beckman Coulter), washed with PBS and stored at -80°C for protein purification.

Each bacterial pellet from 1.5 L of culture was resuspended in 35 mL His buffer (50 mM Tris pH 7.5, 500 mM NaCl, 10 mM MgAc, 5% glycerol, 10 mM β-mercaptoethanol, 0.1 mM PMSF, 1 µg/mL of each AP and LP) and disrupted with three to four cycles using an EmulsiFlex-C3 (Avestin). Lysates were cleared by centrifugation at 100,000 x g, 4°C for 30 minutes. The supernatant was collected and incubated with 0.25 mL equilibrated Ni-NTA Sepharose and 10 mM imidazole rotating for 1 hour at 4°C. The Ni-beads were washed two times with His buffer containing 10 mM imidazole and once with 20 mM imidazole. Beads were transferred to an empty column and proteins were eluted with His buffer containing 300 mM imidazole. The eluate was filtered with a Minisart RC 15 single use syringe filter and further purified over a HiLoad 26/60 Superdex 200 prep grade column connected to a ÄKTApurifier system (Amersham Biosciences) using pulldown buffer (50 mM Tris pH 7.4, 200 mM NaCl, 5% glycerol, 2 mM DTT). Peak fractions containing the protein of interest were pooled and concentrated using a Spin-X UF concentrator (His-importin 13: MWCO=50 kDa; His-eIF1A: MWCO=10kDa). The protein was aliquoted, flash frozen and stored at -80°C.

Other His-tagged proteins

All His-tagged proteins were purified using the same protocol as for His-importin 13 but different expression strains and expression conditions were used. Plasmids coding for Hzz-importin 13 (contains His- and zz-tag) and the Hzz-tag were transformed into BL21 CodonPlus (DE3) and plasmids coding for His-eIF1A were transformed into BL21 (DE3) *E. coli* bacteria.

For protein expression, 200 mL LB medium was inoculated with several colonies from a selective LB agar plate and incubated overnight at 37°C, 150 rpm. For large scale protein expression, 1.5 L of LB medium was inoculated 1:100 with the overnight culture and grown at 37°C, 110 rpm to an OD_{600} of 0.5-0.8. Protein expression was induced with 0.1 mM Isopropyl β-D-1-thiogalactopyranoside (IPTG) for His-importin 13 and 1 mM IPTG for His-eIF1A and cultures were grown overnight at 16°C, 110 rpm. Bacterial cells were harvested by centrifugation for 20 minutes at 4,200 rpm (Centrifuge J6-MI with rotor JS 4.2, Beckman Coulter) and washed once with PBS. Cell pellets were either flash frozen and stored at -80°C or were used directly for protein purification. The His-tagged proteins were purified as described for His-importin 13.

GST-tagged proteins

Plasmids coding for GST-tagged proteins were transformed into BL21 CodonPlus (DE3), grown overnight at 37°C and several colonies were used for inoculation of 200 mL LB-medium supplemented with 100 µg/mL ampicillin. Overnight cultures grown at 37°C, 150 rpm were used to inoculate 1.5 L cultures to a 1:100 dilution. Cultures were grown at 37°C, 110 rpm to an OD600=0.5-0.8 before protein expression was induced with 1 mM IPTG. Protein expression was allowed to occur overnight at 16°C, 110 rpm. Cells were harvested at 4,200 rpm (Centrifuge J6-MI with rotor JS 4.2, Beckman Coulter) for 20 minutes and either flash frozen and stored at -80°C or were directly used for protein purification.

Cell pellets were resuspended in 35 mL GST buffer (50 mM Tris pH 6.8, 300 mM NaCl, 1 mM $MgCl_2$, 2 mM DTT, 0.1 mM PMSF, 1 µg/mL of each AP and LP) and disrupted with three to four cycles using an EmulsiFlex-C3 (Avestin). Lysates were cleared by centrifugation at 100,000 x g, 4°C for 30 minutes and supernatants were transferred to 0.25 mL GST beads equilibrated in GST-buffer. After incubation for 1 hour with rotation at 4°C, beads were washed three times with GST buffer and transferred to an empty column. Bound protein was eluted with GST-buffer containing 15 mM reduced glutathione, pH 8. GST-importin 13 was filtered with a Minisart RC 15 single use syringe filter and further purified over a HiLoad 26/60 Superdex 200 prep grade column attached to a ÄKTApurifier system (Amersham Biosciences) using pulldown buffer (50 mM Tris pH 7.4, 200 mM NaCl, 5% glycerol, 2 mM DTT) and concentrated with a Spin-X UF concentrator (MWCO=50 kDa). GST-eIF1A and GST-Ubc9 were dialyzed against pulldown buffer using a dialysis membrane with a molecular weight cut-off of 12-14 kDa. To remove any residual glutathione, the buffer was changed after 1 hour, overnight and then again after 1 hour. Proteins were aliquoted, flash frozen and stored at -80°C.

Ubc9 (no tag)

Ubc9 without a tag was purified as described in Pichler *et al.*, 2002 (177). Several colonies from a selective LB agar plate transformed with plasmid DNA coding for Ubc9 were used for inoculation of 200 mL LB medium supplemented with 100 µg/mL ampicillin. The culture was grown overnight at 37°C, 110 rpm and used for inoculation of a 1.5 L culture to a 1:100 dilution. Cells were grown at 37°C, 110 rpm to an OD_{600}=0.5-0.6 before protein expression was induced with 1 mM IPTG for 4 hours at 37°C, 110 rpm. Cells were harvested at 4,200 rpm (Centrifuge J6-MI with rotor JS 4.2, Beckman Coulter), resuspended in 60 mL Ubc9 buffer (50 mM Na-phosphate pH 6.5, 50 mM NaCl, 0.1 mM

PMSF, 1 µg/mL of each AP and LP, 1mM DTT), flash frozen and stored at -80°C at least until the next day. Freezing of bacterial cells at -80°C overnight and rapid thawing was sufficient for cell lysis and release of Ubc9.

Cell lysates were thawed, supplemented with 0.1 mM PMSF, 1 µg/mL of each AP and LP and 1 mM DTT and cleared by centrifugation at 100,000 x g, 4°C for 30 minutes. Cleared supernatants were run over 7.5 mL of SP-Sepharose (Roth) equilibrated in Ubc9 buffer. The flow-through was discarded and the SP-Sepharose was washed with two column volumes of Ubc9 buffer. Bound Ubc9 was eluted with 2-3 column volumes of Ubc9 buffer containing 300 mM NaCl and protein containing fractions were pooled, concentrated with a Spin-X UF concentrator (MWCO=5 kDa), filtered with a Minisart RC 15 single use syringe filter and further purified over a HiLoad 26/60 Superdex 75 prep grade column connected to a ÄKTApurifier system (Amersham Biosciences) using transport buffer (20 mM HEPES, 110 mM KOAc, 2 mM $Mg(OAc)_2$, 1 mM EGTA, pH 7.3, 2 mM DTT). Peak fractions containing Ubc9 were pooled, concentrated with a Spin-X UF concentrator (MWCO=5 kDa), aliquoted, flash frozen and stored at -80°C.

RanQ69L

RanQ69L was expressed and purified as described in Melchior *et al*., 1995 (178). For the SILAC experiments, a RanQ69L protein stock prepared by Christiane Spillner that was purified over DEAE-Sepharose and a HiLoad 26/60 Superdex 75 prep grade column was used. For all other experiments, a self-made RanQ69L protein stock was used that was also purified over DEAE-Sepharose and a HiLoad 26/60 Superdex 75 prep grade column but additionally was further purified over a MonoS 5/50 GL column.

2.3.6 Protein Concentration Determination by Densitometry

To determine the protein concentration by densitometry, 0.5, 1.0 and 1.5 µg BSA as well as 1, 2 and 3 µL of the protein sample were applied on a polyacrylamide gel, separated by SDS-PAGE (2.3.1), Coomassie stained (2.3.2) and imaged using the LAS-3000. Protein concentrations were determined with Fiji using BSA as a standard protein to generate a standard curve.

2.3.7 Loading of RanQ69L with GTP

The RanQ69L mutant, which can bind but not hydrolyze GTP was loaded with GTP following a protocol adapted from Kehlenbach *et al.*, 1999 (58). Purified RanQ69L was incubated with 2.5 mM GTP and 15 mM EDTA in transport buffer for 30 minutes at room

temperature. The loading reaction was stopped by the addition of 40 mM $MgCl_2$ for 15 minutes on ice. GTP-loaded RanQ69L was aliquoted, snap frozen and stored at -80°C.

2.3.8 Binding Assays

Binding Assay with Purified Proteins

To analyze the interaction between importin 13 and potential substrates, binding assays were performed. For this, either GST-tagged proteins were immobilized to Glutathione Sepharose High-Performance beads (GE Healthcare) or Hzz-tagged proteins were immobilized to IgG-Sepharose 6 Fast Flow (GE Healthcare). Beads (20 µL) were incubated with 5 mg/mL BSA in PBS (137 mM NaCl, 2.7 mM KCl, 10 mM Na_2HPO_4, 1.8 mM KH_2PO_4, pH 7.5) as a blocking reagent with rotation for 30 minutes at 4°C, followed by immobilization of 5-20 µg GST- or Hzz-bound fusion proteins rotating for one hour at 4°C in the same buffer. The beads were washed three times with 1 mL PBS containing 2 mg/mL BSA and incubated with an equimolar or excess amount of the protein of interest in a total volume of 500 µL, rotating for one hour at 4°C. Unbound proteins were removed by washing three times with 1 mL PBS. Proteins bound to Glutathione Sepharose were eluted with 4x SDS sample buffer and proteins bound to IgG-Sepharose were eluted with either glycine or magnesium chloride. Glycine elution was done with 40 µL 0.1 M glycine, pH 3 for 1 minute with constant mixing, followed by neutralization with 5 µL 1 M Tris, pH 10.4. The beads were pellet by centrifugation and the supernatant was collected and mixed 1:1 with 4x SDS sample buffer. Magnesium chloride elution was done with 150 µL 1.5 M $MgCl_2$ in 50 mM Tris, pH 7.4, vortexing and incubation for 10 minutes on ice. The supernatant was collected and precipitated with 1,350 µL 100% isopropanol, vortexing and incubation for 10 minutes on ice, followed by centrifugation for 20 minutes at 14,000 x g. The supernatant was carefully removed and the protein pellet air evaporated prior to reconstitution of the pellet in 60 µL 4x SDS-sample buffer. To analyze the efficiency of the first protein elution, a second elution step was performed by washing the beads two times with transport buffer and eluting with 60 µL 4x SDS-sample buffer. All eluates were boiled for 10 minutes at 95°C and analyzed by SDS-PAGE (2.3.1) and optionally Western blotting (2.3.4).

Binding Assay with Cell Lysate

The binding assay with cell lysate was performed similarly to the binding assay with recombinantly purified proteins. The only differences were that transport buffer (20 mM HEPES, 110 mM KOAc, 2 mM $Mg(OAc)_2$, 1 mM EGTA, pH 7.3, 2 mM DTT, 1 µg/ml of

each AP and LP and 1x Roche complete protease inhibitor cocktail) instead of PBS was used as a buffer and that as a source of the protein of interest a cell lysate was used instead of a purified protein. The cells lysate was prepared by trypsinizing two HeLa P4 15-cm plates and collecting the cells in transport buffer containing 10% fetal calf serum. The fetal calf serum was removed by washing three times with transport buffer and the cells were adjusted to a concentration of $1x10^8$ cells/mL. Cells were permeabilized with three freeze/thaw cycles in liquid nitrogen or with 0.07% digitonin on ice for 3-5 minutes. Digitonin permeabilization efficiency was checked under the microscope by mixing 1 µL of cell suspension with Trypan blue. The lysate was cleared by centrifugation at 1,500 x g for 15 minutes, 4°C to remove nuclei and cell debris, followed by ultracentrifugation at 100,000 x g for 30 minutes, 4°C. The supernatant was collected and added to the prepared affinity matrix as described above.

2.3.9 Antibody Purification

For the production of rabbit polyclonal antibodies against importin 13, two rabbits were immunized with His-importin 13 (2.3.5) by the company Seramun Diagnostica GmbH. To allow for the purification of anti-importin 13 antibodies from the raised hyperimmune serum, an affinity matrix was generated. For this, 0.5 mg GST-importin 13 was dialyzed overnight against carbonate buffer (0.2 M $NaHCO_3/Na_2CO_3$, pH 8.9) at 4°C with three buffer changes, after minimum one hour, overnight and one hour to remove any free amine groups. The dialyzed GST-importin 13 was immobilized to 0.8 g Cyanogen bromide-activated Sepharose 4B (swelled in 1 mM cold HCl for 30 minutes, followed by two washes with deionized water and one wash with 0.2 M $NaHCO_3/Na_2CO_3$, pH 8.9) for one hour at room temperature, followed by overnight incubation at 4°C. The affinity matrix was washed two times with carbonate buffer and remaining coupling sites were blocked with 100 mM ethanolamine in carbonate buffer for one hour at room temperature. After three more washes with carbonate buffer, the affinity matrix was equilibrated with PBS containing 500 mM NaCl, split into two parts and incubated with half of the serum from each rabbit (rabbit 83/14 = 12.5 mL and rabbit 85/14 = 11.5 mL) at 4°C, overnight and slow rotation. Beads were harvested by pulse centrifugation at 1,000 rpm, washed two times with PBS containing 500 mM NaCl and transferred to a column. Beads were washed with PBS containing 500 mM NaCl until no more proteins came down in the flow-through. Antibodies were eluted with 0.2 M acetic acid, pH 2.7 containing 500 mM NaCl and 0.5 mL fractions were collected. Each fraction was immediately neutralized with 100 µL 1 M Tris/Base. To check for the presence of antibodies, 1 µL of each fraction was spotted onto

a nitrocellulose membrane, followed by staining with PonceauS. Protein containing fractions were combined and concentrated using a Spin-X UF concentrator (MWCO=30 kDa) to ~0.5 mL. The buffer was changed to PBS by repeated dilution with PBS and concentrating with the Spin-X UF concentrator. The concentrated antibody was mixed with one volume of 87% glycerol and stored at -20°C. The purified antibody was tested by Western blot (2.3.4) and indirect immunofluorescence (2.4.9).

2.4 Cell Biology Techniques

2.4.1 Requirements for Sterile Working

To prevent fungal or bacterial contaminations all cell culture work was performed under a laminar flow cabinet. Necessary tools and materials were either autoclaved and/or sterilized with 70% ethanol.

2.4.2 Maintaining Cell Culture

All cell lines were cultivated in Dulbecco's Modified Eagle Medium (DMEM) supplemented with 10% fetal bovine serum (FCS), 2 mM L-glutamine, 100 U/mL penicillin and 100 µg/mL streptomycin at 37°C and 5% CO_2 in a humidified cell incubator. To guarantee optimal cell growth the medium was changed twice a week, often accompanied by cell sub-culturing.

2.4.3 Sub-culturing of Adherent Cells

To maintain cell proliferation, cells were sub-cultured upon reaching a confluency of ~80%. The overlying medium was aspirated, cells were washed once with 1x PBS and incubated with 1 mL trypsin at 37°C for optimal trypsin activity. Trypsin was inactivated by the addition of 9 mL of serum containing medium (Dulbecco's Modified Eagle Medium (DMEM) containing 10% fetal bovine serum (FBS), 2 mM L-glutamine and optionally 100 U/mL penicillin and 100 µg/mL streptomycin – in the following sections referred to as DMEM-10). For cell resuspension and dispersion of cell clumps, the cell suspension was rinsed several times over the bottom of the culture dish. Depending on the passage number of the cells and desired splitting ratio, a defined volume of the obtained cell suspension was transferred to a new culture dish and supplemented with DMEM-10 to a total volume of 10 mL. The culture dish was pivoted gently to obtain an even distribution of cells and placed in a humidified cell incubator at 37°C and 5% CO_2. HeLa P4 cells were typically sub-cultivated two times per week and diluted in a ratio of 1:10 - 1:20.

2.4.4 Determination of Cell Concentration

Cell numbers were determined by diluting 100 µL of cell suspension in 10 mL of Coulter ISOTON II Diluent and counting with the CASY 1 system (Schärfe System).

2.4.5 Coating of Cover Clips with Poly-L-Lysine

Cover slips were treated with Poly-L-lysine to enhance the attachment of cells, due to the electrostatic interaction between negatively charged ions of the cell membrane and the positively charged Poly-L-Lysine. Cover slips were washed with 2-propanol, dried and coated with 0.01 % (v/v) Poly-L-Lysine followed by incubation for 30 minutes at room temperature. Unbound Poly-L-lysine was removed by washing two times with sterile water and dried cover slips were sterilized with UV light for 3 minutes at 0.12 J/ cm^2.

2.4.6 Calcium Phosphate Transfection of Mammalian Cells

For transfection of mammalian cells with plasmid DNA using the calcium phosphate method, cells were seeded at 50,000 cells per well on cover slips in 500 µL DMEM-10 into a 24-well plate format so that the cells had a confluence of ~50% on the day of transfection. The next day 20 µL $CaCl_2$ (250 mM) was added to 0.8 µg of total plasmid DNA, mixed by vortexing at medium speed for 10 seconds, followed by a dropwise addition of 20 µL 2x HBS buffer (50 mM HEPES, 250 mM NaCl, 1.5 mM Na_2HPO_4, pH 6.98) and vortexing at maximum speed for 10 seconds. The mix was incubated for 20 minutes at room temperature to allow for the formation of calcium phosphate-DNA complexes prior addition to the cells. The cells were grown overnight in a humidified incubator at 37°C and 5% CO_2.

2.4.7 Lipofectamine Transfection

For transfection of mammalian cells with plasmid DNA using the Lipofectamine method, cells were seeded at 100,000 cells per well on a CS in 500 µL DMEM-10 medium into a 24-well plate formats so that the cells had a confluence of ~70-90% on the day of transfection. Prior to transfection, the medium was changed to DMEM-10 medium without antibiotics. For transfection, 0.8 µg of total plasmid DNA as well as 1 µL of Lipofectamine® 2000 were diluted into 25 µL Opti-MEM medium each. Both mixes were gently mixed and incubated for 5 minutes at room temperature. The diluted DNA was combined with the diluted Lipofectamine® 2000, gently mixed and incubated for 20 minutes at room temperature to allow for the formation of nucleic acid-Lipofectamine complexes. The transfection mix was added dropwise to the cells and incubated for 4-5 hours in a

humidified incubator at 37°C and 5% CO_2. The transfection medium was replaced with DMEM-10 containing antibiotics and incubated overnight in a humidified incubator at 37°C and 5% CO_2. For longer transfection times, the cells were sub-cultivated after 24 hours.

2.4.8 RNA Interference (RNAi)

For Lipofectamine transfection of siRNA, HeLa P4 cells were seeded at a density of 100,000 cells per 24-well so that the cells had a density of 70-90% on the day of transfection. Prior to transfection, the medium was changed to 250 µL DMEM-10 medium without antibiotics. For transfection, 2 µL of Lipofectamine® 2000 was added to 48 µL of Opti-MEM and 1.75 µL of siRNA (20 µM) was added to 48.25 µL of Opti-MEM medium and gently mixed. The Lipofectamine mix was incubated for 5 minutes at room temperature prior to addition to the siRNA mix. The transfection mix was gently mixed, incubated for 20 minutes at room temperature and added dropwise to the cells to a final siRNA concentration of 100 nM. The cells were incubated for 4 hours in a humidified incubator at 37°C and 5% CO_2 before the medium was changed to 500 µL DMEM-10 containing antibiotics. After 24 hours cells were sub-cultivated on Poly-L-lysine coated cover slips and assayed for gene knock-down after 48-72 hours.

2.4.9 Indirect Immunofluorescence

For the detection of endogenous or tagged proteins transfected into mammalian cells, proteins were labeled by indirect immunofluorescence. Cells grown on cover slips were washed with PBS and fixed for 10 minutes with 3.7% formaldehyde. For optional Hoechst staining of nuclei, the Hoechst dye (10 mg/mL) was diluted 1:10,000 into the fixation solution. The fixation solution was removed by washing two times with PBS, followed by permeabilization with 0.5% Triton X-100 on ice for 5 minutes. To reduce unspecific antibody staining, cells were blocked with 1% BSA, 10% FCS or 0.2% fish gelatin for 10 minutes. For the detection of the target protein, cover slips were transferred to a dark humidity chamber and incubated with the primary antibody (2.1.11) diluted in the respective blocking reagent for 1 hour, followed by three washes with PBS for 5-10 minutes each and addition of the secondary antibody (2.1.11) diluted in the blocking reagent for 1 hour. Unbound antibodies were washed away by three washes with PBS for 5-10 minutes each, followed by a final quick wash with water. Cover slips were dried and mounted with Dako Fluorescent Mounting Medium or with Mowiol mounting medium containing 1 µg/mL DAPI for staining of the cell nuclei.

2.4.10 Proximity Ligation Assays (PLA)

The Duolink® *in situ* Proximity Ligation Assay kit was used to detect proteins in close proximity in single cells with a maximum theoretical distance of 40 nm. HeLa P4 cells were seeded on poly-L-lysine coated cover slips (2.4.5) in a 24-well plate at a concentration of 45,000 cells/well. Cells were allowed to attach to the cover slips for a minimum of 48 hours prior to fixation. Cells were washed three times with PBS, fixed with 3.7% formalin for 30 minutes, washed three times with PBS and were permeabilized with 0.5% Triton X-100 for 5 minutes at room temperature. After washing three more times with PBS, the cells were blocked with Duolink® blocking solution for 30 minutes in a humidity chamber preheated to 37°C. Primary antibodies (2.1.11) of two different species that bind to the proteins to be detected were diluted in 50 µL Duolink® antibody diluent and were added to each sample for one hour at room temperature. The slides were washed two times with 120 µL PLA Wash Buffer A for 5 minutes with gentle agitation and the secondary antibodies conjugated with oligonucleotides (PLA probe MINUS and PLA probe PLUS) were diluted 1:5 in Duolink® antibody diluent. Cells were incubation with the secondary antibodies in a pre-heated humidity chamber for 1 hour at 37°C. Unbound secondary antibodies were removed by washing two times with 120 µL PLA Wash Buffer A for 5 minutes with gentle agitation. The PLA probe oligonucleotides were linked in a ligation reaction by addition of a ligation solution consisting of ligase and two oligonucleotides that can hybridize to the two PLA probes and join them to form a closed circle if they are in close proximity. Ligation was done in a humidity chamber for 30 minutes at 37°C, followed by two wash steps with 120 µL PLA Wash Buffer A for 2 minutes with gentle agitation and incubation with the amplification solution for 100 minutes at 37°C. The amplification solution consists of a polymerase, nucleotides and fluorescently labeled oligonucleotides and allows for rolling circle amplification of the ligated circle template, generating a concatemeric product. By hybridization of fluorescently labeled oligonucleotides to the concatemer, proteins in close proximity are visualized as distinct fluorescent spots. Slides were washed two times with 120 µL PLA Wash Buffer B for 10 minutes to remove the amplification solution. If required, a counterstaining step (see below) was included after this step to detect the proteins of interest or an indirect immunofluorescence (2.4.9) was performed starting from the blocking step. If no counterstaining or indirect immunofluorescence staining was done, the slides were washed with 120 µL 0.01x PLA Wash Buffer B for 1 minute. Coverslips were mounted with Duolink® *in situ* mounting medium (contains DAPI), sealed with nail polish and stored at -20°C. Cover slips were

imaged with the Confocal microscope LSM 510 META and PLA dots were quantified with CellProfiler (2.4.13).

Counterstaining Method

After removal of the amplification-polymerase solution, the cover slips were washed two times with Wash Buffer B for 10 minutes, followed by one wash step with Wash Buffer A for 1 minute. The samples were incubated with the primary antibody (50 µL/well) diluted in Duolink® antibody diluent for 40 minutes. Optionally, a FITC-Phalloidin antibody (0.2 mg/mL) was added at a 1:600 dilution to delineate the entire cell by staining for filamentous actin. After washing for 1 minute with Wash Buffer A, the cells were incubated with the secondary antibody diluted in Duolink® antibody diluent for 30 minutes. The cover slips were washed two times with Wash Buffer A for 2 minutes and once with 0.01x Wash Buffer B for 1 minute prior to mounting as described above. All steps were performed at room temperature.

2.4.11 Transport Assay

The transport assay is based on a method developed by Adam *et al*., 1990 (65). HeLa P4 cells were grown on Poly-L-lysine coated cover slips to 60-80% confluence. Cells were washed twice with ice-cold transport buffer (20 mM HEPES, 110 mM KOAc, 2 mM $Mg(OAc)_2$, 1 mM EGTA, pH 7.3, 2 mM DTT, 1 µg/mL of each AP and LP) and permeabilized with 0.007% digitonin on ice for 3-5 minutes. At low concentrations, digitonin selectively permeabilizes the cholesterol-rich plasma membrane and leaves other membranes lower in cholesterol such as the nuclear envelope intact (179, 180). Permeabilization efficiency was checked by Trypan blue staining. Cytosolic proteins were washed out by washing three times for 3 minutes with TPB and the permeabilized cells were incubated with 20 µL import reaction for 30 minutes at 30°C in a humidity chamber or at 4°C on ice. The import mix consisted of 500 nM import substrate, 500 nM import receptor, 4 µM Ran, 0.5 µL ATP regenerating system (1 mM ATP, 5 mM creatine phosphate, 20 U/mL creatine phosphokinase), 2 mg/mL BSA in transport buffer and optionally 8 µL cytosol (9 mg/mL). The import reaction was stopped by washing three times for 3 minutes with TPB and fixation with 3.7% formaldehyde in PBS for 10 minutes. Proteins were detected by indirect immunofluorescence (2.4.9).

2.4.12 Confocal Microscopy

Fluorescent samples were analyzed with an Axiovert 200 M inverted microscope with a 63x Plan-Neofluar 1.3 NA water-corrected objective using the water-based Immersol W 2010 immersion oil and the X-cite 120 mercury lamp as a light source. Confocal images were acquired with the Zeiss LSM 510 META confocal imaging system. The confocal imaging system is equipped with five different laser lines that allow for excitation of various fluorophores. The Diode laser 405 nm was used for excitation of Hoechst 33258 or DAPI, the tunable Argon 458/477/488/514 nm laser for GFP, CFP and the AlexaFluor488 dye, the HeNe 543 nm laser for YFP, the HeNe 594 nm laser for mCherry and AlexaFluor594 dye and the HeNe 633 nm laser for AlexaFluor633 or AlexaFluor647 dye. To reduce cross-talk between different channels, the Multi Track image acquisition mode was used in the LSM 5 software. Laser transmission was adjusted depending on the fluorescence signal intensity and to minimize bleaching effects. Typically the pinhole was set to a diameter of 1 airy unit, but if required, was changed to 0.8-2.0 airy units to increase signal intensity or to have the same optical slice thickness for co-localization studies. Image intensity and background level gains were controlled with the Detector Gain and the Amplifier Offset, respectively, and adjusted with the help of the range indicator function in the palette tool. To increase the signal to noise ratio, four images were averaged at a data depth of 8 bit and a scan speed of 1.28-3.2 µs/pixel was used. Acquired images were edited with the Fiji software. If necessary, the brightness and contrast were linearly enhanced for printing.

2.4.13 CellProfiler

The CellProfiler software (version 2.1.1) was used for the quantification of *in situ* proximity ligation assay (PLA) interactions. A pipeline was generated to count the number of PLA interactions in the whole cell, the cytoplasm and the nucleus. Cell nuclei were identified with the “IdentifyPrimaryObject” module using DAPI images. The typical diameter of the objects was set to 80-150 pixels and two-class Otsu adaptive thresholding was applied. Clumped objects were distinguished based on intensity values and the smoothing filter for declumping and the minimum allowed distance between local maxima was set to be calculated automatically. The cellular area was demarcated with the “IdentifySecondaryObjects” module using the Distance - N method by expanding the identified nuclear area by 80 pixels. Using the “IdentifyTertiaryObjects” the nuclear area was then subtracted from the cell area to obtain the cytoplasm. Cells touching the border of an image were excluded from further analysis. PLA fluorescent dots were identified with the “IdentifyPrimaryObjects” module using PLA images. The typical diameter of the PLA

objects was set to 2-10 pixels for the PLA objects and two-class Otsu adaptive thresholding was used with a minimum threshold of 0.15. Clumped objects were separated as described for the identification of cell nuclei. PLA dots in the nucleus and the cytoplasm were distinguished with the help of the “MaskImage” module. With the “RelateObjects” module the identified PLA objects in the cell, the nucleus and the cytoplasm were related back to the previously identified cell, nuclear and cytoplasmic area, respectively. Data was exported with the “ExportToSpreadsheet” module and visualized with the GraphPad Prism software (version 5.01).

2.5 SILAC and Mass Spectrometry

2.5.1 Dialyzed FCS

FCS was dialyzed against PBS using a dialysis membrane (Spectra/Por® Dialysis Membrane) with a molecular weight cut-off of 8 kDa. PBS was changed three times after 1 hour, overnight and again after 1 hour incubation at 4°C under constant stirring. The dialyzed FCS was sterile aliquoted and frozen at -20°C.

2.5.2 Metabolic Labeling of HeLa P4 Cells

For SILAC experiments, HeLa P4 cells were grown in DMEM, high glucose, no glutamine, no lysine, no arginine supplemented with 10% dialyzed FCS, 6 mM L-glutamine, 100 U/mL penicillin, 100 µg/mL streptomycin and labeled or unlabeled L-lysine and L-arginine at final concentrations of 73 mg/L and 42 mg/L, respectively. For light SILAC media, DMEM, high glucose, no glutamine, no lysine, no arginine was mixed in a 1:1 ratio with DMEM, high glucose, which contains light L-lysine (Lys0) and L-arginine (Arg0) at final concentrations of 146 mg/L and 84 mg/L, respectively. The medium SILAC media was supplemented with 4,4,5,5-D4-L-Lysine 2HCl (Lys4) and $^{13}C_6$-L-arginine HCl (Arg6) and the heavy SILAC media with $^{13}C_6{}^{15}N_2$-L-lysine HCl (Lys8) and $^{13}C_6{}^{15}N_4$-L-arginine HCl (Arg10). To achieve labeling efficiency of more than 95% cells were allowed to undergo at least five doublings. Typically, cells were subcultivated every 2-3 days with the appropriate SILAC media for a total of five passages at 37°C and 5% CO_2 in a humidified cell incubator prior to harvesting.

2.5.3 Binding Assay with Labeled HeLa P4 Cells

Preparation of Phenyl-Sepharose

Phenyl-Sepharose (80 µL/reaction) was washed once each with deionized water and transport buffer (20 mM HEPES, 110 mM KOAc, 2 mM $Mg(OAc)_2$, 1 mM EGTA, pH 7.3, 2 mM DTT, 1 µg/mL of each AP and LP) containing 10 mg/mL BSA. After blocking in the same buffer with rotation for 30 minutes at 4°C, the beads were washed once with transport buffer containing 10 mg/mL BSA and used for pre-clearing of cell lysates.

Preparation of Affinity Matrix

IgG-Sepharose (20 µL/reaction) was washed once each with deionized water and transport buffer (20 mM HEPES, 110 mM KOAc, 2 mM Na_2CO_3, 1 mM EGTA, pH 7.3, 2 mM DTT, 1 µg/mL of each AP and LP) containing 10 mg/mL BSA, followed by blocking in the same buffer with rotation for 30 minutes at 4°C. The beads were washed once in the same buffer and 0.5 nmol Hzz-importin 13 was immobilized to 20 µL blocked IgG-Sepharose rotating for one hour at 4°C in a total volume of 500 µL in transport buffer containing 10 mg/mL BSA. The beads were pelleted by centrifugation at 300 x g for 2 minutes and washed three times with 1 mL transport buffer. The Hzz-importin 13 affinity was pre-incubated with either 10 µM $RanGTP_{Q69L}$, 5 µM Ubc9 or transport buffer alone in a total volume of 500 µL rotating for one hour at 4°C. The beads were washed three times with 1 mL transport buffer prior to assembly of the binding reactions.

Preparation of Cell Lysate

For SILAC binding experiments, two 15-cm HeLa P4 cell plates per labeling condition were washed two times with PBS and coated with 2 mL trypsin. The trypsin was aspirated and the plates were incubated at 37°C until the cells started to detach. The labeled cells were collected separately in PBS containing 10% dialyzed FCS to neutralize the trypsin and washed three times with transport buffer to remove any residual FCS and trypsin. The cells were counted with the CASY 1 system (Schärfe System), adjusted to $1x10^8$ cells/mL in transport buffer (20 mM HEPES, 110 mM KOAc, 2 mM $Mg(OAc)_2$, 1 mM EGTA, pH 7.3, 2 mM DTT, 1 µg/mL of each AP and LP and 1x Roche complete protease inhibitor cocktail) and transferred to a 1.5 mL Protein LoBind Tube. The cells were permeabilized with 0.07% digitonin on ice for 3-5 minutes by adding 7 µL of 10% digitonin per $1x10^8$ cells. Permeabilization efficiency was checked under the microscope by mixing 1 µL of lysate with 10 µL Trypan blue. If necessary, the digitonin concentration was slightly increased

until more than 95% of the cells were permeabilized. Cell lysates were cleared by centrifugation at 1,500 x g for 15 minutes to remove nuclei and cell debris, followed by ultracentrifugation in the Centrifuge Optima MAX-XP with the rotor TLA100.3 at 100,000 x g, 4°C for 30 minutes. Two reduce unspecific binding to the affinity matrix, each cell lysate from 2x 15-cm plates was pre-incubated with 60 µg Hzz immobilized to 20 µL blocked IgG-Sepharose, as well as, 80 µL blocked Phenyl-Sepharose to deplete the cell extract of nuclear transport receptors, with rotation for two hours at 4°C. The beads were pelleted by centrifugation for 2 minutes at 300 x g and the supernatant was collected for the binding reaction. A sample of both the uncleared and cleared lysate was taken for later analysis.

Binding Reaction

For binding reactions, 20 µL of Hzz-importin 13 affinity matrix was incubated with 350 µL HeLa P4 lysate from two 15-cm plates (precleared with IgG-Hzz and Phenyl-Sepharose) and either 10 µM $RanGTP_{Q69L}$, 5 µM Ubc9 or transport buffer alone in a final volume of 500 µL rotating for two hours at 4°C. Beads were pelleted at 800 x g for 2 minutes, an unbound sample was collected for later analysis and the beads were washed with one quick wash and one 5 minute wash with transport buffer. After this step, all beads were combined for the last washing step and bound proteins were eluted together with 150 µL 1.5 M $MgCl_2$ in 50 mM Tris, pH 7.4, vortexing and incubation for 10 minutes on ice. Beads were pelleted by centrifugation and the supernatant was collected and transferred to a new tube. Proteins were precipitated by addition of 1350 µL 100% isopropanol, vortexing and incubation for 10 minutes on ice, followed by centrifugation for 20 minutes at 14,000 x g. The supernatant was removed and the protein pellet was dried prior to reconstitution in 60 µL 4x SDS-sample buffer. The magnesium chloride eluted beads were washed two times with transport buffer and a second elution was done with 60 µL 4x SDS-sample buffer to identify remaining proteins bound to the affinity matrix. All eluates were boiled at 95°C for 10 minutes and analyzed by SDS-PAGE, followed by Coomassie staining (2.3.2), silver staining (2.3.3) or Western blotting (2.3.4).

2.5.4 In-Gel Tryptic Digestion of Proteins

One-third of the magnesium chloride eluate from the importin 13 binding reaction was loaded onto a 12% SDS gel. The SDS-PAGE (2.3.1) was stopped after the samples had entered one-quarter of the stacking gel. The gel was washed with deionized water, fixed for one hour with fixation solution (40% ethanol, 10% acetic acid) and washed two times

for 10 minutes with deionized water. Each sample lane was split into 6 parts, cut into 2 mm sized pieces and transferred to low-bind Eppendorf cups. In-gel digestion was performed based on a protocol provided by Dr. Oliver Valerius (Universität Göttingen), which in turn was adapted from Shevchenko *et al.*, 1996 (181). All solutions were prepared with LC/MS Grade Optima™ Water. In brief, gel pieces were dehydrated with 50 µL acetonitrile and dried in a SpeedVac Concentrator (Vacuum Christ Alpha 1-4, W. Krannich) for 10 minutes after removal of the acetonitrile. Gel pieces were rehydrated in 150 µL 10 mM DTT, 100 mM NH_4CO_3 to reduce disulfide bonds for 1 hour at 56°C. The DTT solution was removed and resulting free cysteine thiol groups were alkylated with 150 µL 55 mM iodoacetamide, 100 mM NH_4CO_3 for 45 minutes at room temperature in the dark. Gel pieces were washed with 150 µL 100 mM NH_4CO_3 and then dehydrated with 150 µL acetonitrile both times shaking at 1,000 rpm for 10 minutes at room temperature. The washing (rehydration of gel) and dehydration steps were repeated once and then the gel pieces were dried for 10 minutes in a SpeedVac after removal of the acetonitrile. Gel pieces were rehydrated in 50 µL trypsin digestion buffer (20 µg/mL trypsin (Serva), prepared according to the manufacturer's instructions) for 45 minutes on ice. The digestion buffer was discarded and gel pieces were completely covered with 50 µL 25 mM NH_4CO_3. Tryptic peptide digestion was allowed to occur overnight at 37°C.

2.5.5 Extraction of Peptides

Following trypsin digestion, supernatants were collected by centrifugation for 1 minute at 13,000 rpm (Centrifuge 5415R, Eppendorf) and transferred to new tubes. Residual acidic peptides were extracted from the gel pieces by incubation with 50 µL 20 mM NH_4CO_3 shaking at 1,000 rpm for 10 minutes at room temperature. Residual basic peptides were extracted three times by incubation with 50 µL 50% acetonitrile, 5% formic acid shaking at 1,000 rpm for 20 minutes at room temperature. All supernatants were collected by centrifugation for 1 minute at 13,000 rpm, pooled and completely dried by vacuum evaporation in a SpeedVac. Samples were either stored at -20°C or directly desalted over C18 stage tips (2.5.6). Peptide extraction was performed based on a protocol provided by Dr. Oliver Valerius (Universität Göttingen), which in turn was adapted from Shevchenko *et al.*, 1996 (181).

2.5.6 Desalting of Peptides

Peptides were desalted by purification over C18 stage tips following a protocol provided by Dr. Oliver Valerius (Universität Göttingen), which in turn is based on a tutorial provided by

the group of Prof. Dr. Matthias Mann (http://www.biochem.mpg.de/226863/Tutorials). In brief, C18 stage tips were assembled by cutting out small circles of C18 material (Empore™ C18 47 mm Extraction Disc, 3M Company) and placing two on top of each other into the tip of a 200 µL pipette tip. C18 stage tips were activated with 100 µL 100% methanol, 0.1% formic acid and washed with 100 µL 70% acetonitrile, 0.1% formic acid, followed by two wash steps with 100 µL H_2O, 0.1% formic acid by centrifugation for 2 minutes at maximum speed. Simultaneously, dried peptide pellets were resuspended in 20 µL fresh sample buffer (98% H_2O, 2% acetonitrile, 0.1% formic acid) by shaking for 10 minutes at 1,000 rpm and incubation in a Decon FS-100 ultrasonic bath at maximum power for 3 minutes. Samples were loaded onto the C18 stage tips and brought in contact with the C18 material by brief centrifugation for 5 seconds at 1,000 rpm (Centrifuge 5415R, Eppendorf). After incubation for 5 minutes, samples were centrifuged for 5 minutes at 4,000 rpm. To increase the peptide yield samples were reloaded and centrifuged again for 5 minutes at 4,000 rpm. At this step, all peptides should be bound to the C18 material, therefore the flow-through was discarded. The C18 column was washed twice with 100 µL H_2O, 0.1% formic acid by centrifugation for 2 minutes at 10,000 rpm. For peptide elution, the C18 stage tip was transferred to a 1.5 mL low-bind Eppendorf cup and bound peptides were eluted with 60 µL 70% acetonitrile, 0.1% formic acid by centrifugation for 5 minutes at 4,000 rpm. Peptide eluates were dried completely in the SpeedVac and peptide pellets were stored at -20°C until liquid chromatography-coupled-mass spectrometry (LC-MS) analysis of peptides.

2.5.7 Liquid Chromatography-Coupled-Mass Spectrometry (LC-MS) Analysis of Peptides

Prior to the analysis of peptides with nanoflow liquid chromatography (UltiMate™ 3000 RSLCnano System, Thermo Scientific) coupled to nano electrospray ionization (nESI) mass spectrometry, dried peptide pellets were solved in 20 µL sample buffer (98% H_2O, 2% acetonitrile, 0.1% formic acid) by shaking for 10 minutes at 1,000 rpm. Samples were incubated for 3 minutes at maximum power in an ultrasonic bath and transferred to LC-MS vials (Grace). Sample solutions of 1 to 2 µL were loaded and washed on an Acclaim™ PepMap™ 100 pre-column (100 µm x 2 cm, C18, 5 µm, 100 Å, Thermo Scientific) in 100% solvent A (98% water, 2% acetonitrile, 0.07% trifluoroacetic acid) at a flow rate of 25 µL/min for 6 minutes. Peptides were separated by reverse phase chromatography, on an Acclaim™ PepMap™ RSLC column (75 µm x 50 cm, C18, 2 µm, 100 Å, Thermo Scientific). A first gradient was run from 98% solvent A (water, 0.1% formic acid) and 2%

solvent B (80% acetonitrile, 20% water, 0.1% formic acid) to 32% solvent B within 110 minutes, followed by a second gradient from 32% to 65% solvent B within 16 minutes at a flow rate of 300 nL/min (solvents and acids from Fisher Chemicals). Peptides eluting from the chromatography were on-line ionized by nESI using the Nanospray Flex Ion Source (Thermo Scientific) at 2.4 kV and continuously transferred into the Orbitrap Velos Pro™ Nano ESI Mass Spectrometer, (Thermo Scientific). Full scans were acquired with the Orbitrap-FT analyzer in the mass range of 300-1,850 m/z and with a resolution of 60,000. The LTQ Velos Pro linear ion trap (CID) was used for parallel data-dependent top 10 fragmentation. Programming of LC-MS methods and data acquisition was done with the XCalibur 2.2 software (Thermo Scientific). All LC-MS analyses of peptides were performed by the Service Unit LCMS Protein Analytics (Dr. Oliver Valerius and Dr. Kerstin Schmitt), Georg-August-Universität Göttingen.

2.5.8 Analysis of Mass Spectrometry Data

Raw mass spectrometry files were analyzed with the MaxQuant 1.5.1.0 software in the case of quantitative SILAC data or the Proteome Discoverer Software version 1.4 in the case of all other mass spectrometry analyses. In the case of the Proteome Discoverer, mass spectrometry data was searched against the NCBI-derived 'homo sapiens' protein database including gb, ref, dbj, emb, and pdb entries (status 09/14/2016, 124176 sequences). Search parameters were set as follows: trypsin digestion mode with the maximum of two missed cleavage sites, oxidation of methionine and N-terminal protein acetylation were set as variable modifications and carbamidomethylation of cysteine as fixed modification. The mass tolerance for the peptide precursors was 10 ppm and 0.6 Da for fragment ions. False discovery rates were calculated with Proteome Discoverer, using the reverse-decoy mode, and the filter for valid peptide sequence matches was set to high confidence (FDR ≤ 0.01). The Proteome Discoverer search was performed by the Service Unit LCMS Protein Analytics (Dr. Oliver Valerius and Dr. Kerstin Schmitt), Georg-August-Universität Göttingen.

In the case of quantitative data analysis with the MaxQuant software, mass spectrometry data was analyzed against the human protein database derived from Uniprot (Proteome ID: UP000005640, 71,913 entries, download 2016). Search parameters were set as follows: trypsin/P digestion mode (tryptic specificity with no proline restriction) with maximum of two missed cleavages, oxidation of methionine and N-terminal protein acetylation were set as variable modifications and carbamidomethylation of cysteine was set as a fixed modification. Arg6 and Lys4 were defined as medium peptide labels and

Arg10 and Lys8 as heavy peptide labels. The mass tolerance for peptide precursors was 4.5 ppm and for fragment ions 0.5 Da. Fourier transform-based mass spectrometer (FTMS) requantification and FTMS recalibration were enabled. Protein quantification was performed with a minimum ratio count of two and unique plus razor peptides were considered. False discovery rates were calculated by MaxQuant, using the revert-decoy mode and the filter for valid peptide sequence matches was set to 0.01. MaxQuant output data was further processed using Perseus software 1.5.0.15. Gene Ontology (GO) analysis was done using DAVID Bioinformatics Resources 6.8 (182, 183). Only GO terms for biological processes were considered (GOTERM_BP_ALL).

3. Results

Until recently, only a limited number of importin 13 cargoes had been identified. To expand the range of known importin 13 import and specifically export cargoes, three different approaches were applied. These included an importin 13 overexpression screen using a library of nuclear proteins, an importin binding experiment followed by mass spectrometry and a SILAC based proteomics approach coupled to an importin 13 binding assay that allowed for the distinction of importin 13 import and export cargoes. Further, various cellular and biochemical assays were established with known importin 13 cargoes, to allow for analysis of newly identified importin 13 substrate candidates.

3.1 Characterization of Importin 13 and Established Cargoes

3.1.1 Importin 13 Expression Levels Are Low in Different Human Cancer Cell Lines

To define the endogenous importin 13 expression levels in different cancer cell lines and determine whether importin 13 may be a limiting factor in nucleocytoplasmic transport, the cellular concentration of importin 13 in three different human cancer cell lines was determined. For this, the cell lysates of a defined number of HeLa P4, U2OS and 293T HEK cells were loaded onto an SDS gel together with known amounts of purified His-importin 13 and analyzed by Western blot (Figure 4).

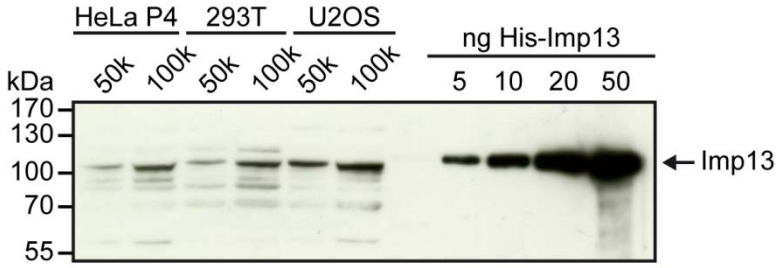

Figure 4: Endogenous importin 13 concentrations in cancer cell lines. Defined amounts of HeLa P4, 293T HEK and U2OS cells (50,000 and 100,000 cells) were lysed in SDS sample buffer and analyzed by SDS-PAGE together with 5, 10, 20 and 50 ng of purified His-tagged importin 13, followed by immunoblotting with an anti-importin 13 antibody. Assuming a cell volume of ~2,500 μm^3 an importin 13 concentration in the range of 110-310 nM was determined for all three cancer cell lines.

Based on the assumption that these cells have a volume of ~2,500 µm^3 (184), a cellular importin 13 concentration of ~110 nM was determined for HeLa P4 cells, ~120 nM for 293T HEK cells and ~310 nM for U2OS cells. In comparison, other transport receptors have been estimated to have cellular concentrations between 1-4 µM (77, 185). This shows that at least in the analyzed cell lines importin 13 is not an abundant protein and therefore could be rate limiting for transport.

3.1.2 Importin 13 Is Rate Limiting in HeLa P4 Cells

To test whether endogenous importin 13 is indeed rate limiting in HeLa P4 cells, the effect of importin 13 overexpression on the subcellular localization of the endogenous export cargo eIF1A was analyzed. Cells transfected with plasmids coding for FLAG-importin 13 or mock transfected cells were immunostained for endogenous eIF1A with an anti-eIF1A antibody (Figure 5). In mock transfected cells, eIF1A showed a predominantly nuclear localization and a weak cytoplasmic signal, while in cells overexpressing FLAG-importin 13 most of the nuclear signal was lost. Thus, importin 13 is rate limiting for eIF1A export in HeLa P4 cells.

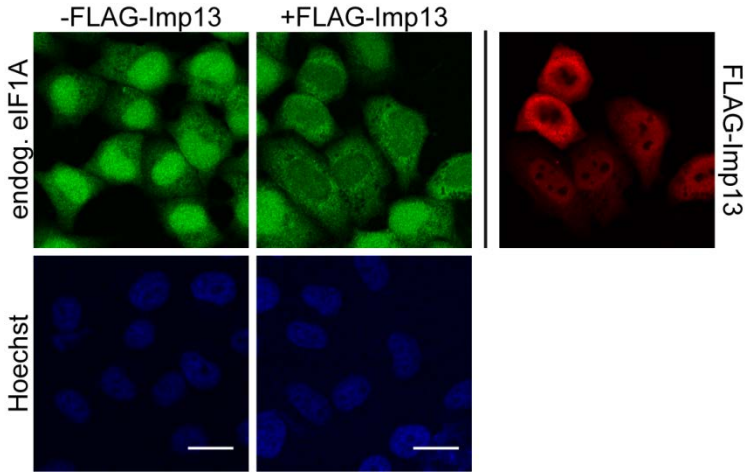

Figure 5: Importin 13 is rate limiting for export of endogenous eIF1A. HeLa P4 cells were transiently transfected with plasmids coding for FLAG-importin 13 or mock transfected using the calcium phosphate method and immunostained with an anti-eIF1A antibody and anti-FLAG antibody. The scale bars correspond to 20 µm.

3.1.3 Importin 13 Affects the Subcellular Localization of eIF1A and Ubc9

Grünwald *et al.*, 2013 (107) demonstrated that only cells expressing importin 13 wild type, but not the importin 13 mutant Glu436Arg/Asp481Arg, can export eIF1A-GFP *in vivo*. To test whether these findings can be repeated and to establish eIF1A as a positive control for importin 13 mediated nuclear export, importin 13 overexpression experiments were performed. In addition, the effect of importin 13 on the known importin 13 import cargo Ubc9 was analyzed, to establish Ubc9 as a positive control for importin 13 mediated nuclear import. In order to do this, HeLa P4 cells were co-transfected with plasmids coding for Ubc9 or eIF1A and importin 13 or an empty control vector and analyzed for any changes in subcellular distribution (Figure 6). As previously reported (107), GFP-tagged eIF1A was mainly localized in the nucleus and showed strong nucleoli enrichment but was strongly depleted from these sites upon importin 13 coexpression. In contrast, mutant importin 13-E436R/D481R did not affect the subcellular localization of eIF1A-GFP.

Further, to determine whether the size of eIF1A affects its subcellular localization, eIF1A was fused to an N-terminal GFP-GST-tag. This fusion construct (72 kDa) should be well above the diffusion limit of the NPC and as a consequence GFP-GST-eIF1A should only be able to enter the nucleus with the help of β-karyopherins, but not by diffusion. Indeed, GFP-GST-eIF1A showed a cytoplasmic localization in the absence of importin 13, supporting the hypothesis that eIF1A enters the nucleus by passive diffusion due to its small size (16.5 kDa) (135). However, it cannot be entirely excluded that nuclear import of GFP-GST-eIF1A is impeded due the fusion-tag. Note that the GFP-GST-tag was fused to the N-terminus, while the GFP-tag was fused to the C-terminus of eIF1A. In summary, the above observations are in agreement with the previous reports (107, 135) that eIF1A enters the nucleus by passive diffusion and is exported back out of the nucleus by importin 13, while the importin 13 mutant Glu436Arg/Asp481Arg is impaired in eIF1A export.

To establish a positive control for importin 13 mediated nuclear import, the subcellular localization of Ubc9 fused to both a GFP-GST- and a HA-tag was analyzed. While HA-Ubc9 by itself already showed a nuclear localization and consequently was not affected by importin 13 coexpression, GFP-GST-Ubc9 was too large to efficiently enter the nucleus on its own and required coexpression of FLAG-importin 13 to localize to the nucleus. This suggests that HA-Ubc9 (~19 kDa) as eIF1A can enter the nucleus by passive diffusion due to its small size. Further, importin 13 has been shown to bind its cargoes Ubc9 and eIF1A at non-overlapping binding sites (107) and indeed the importin 13 mutant impaired in eIF1A export was still fully functional in mediating import of GFP-GST-Ubc9 (107).

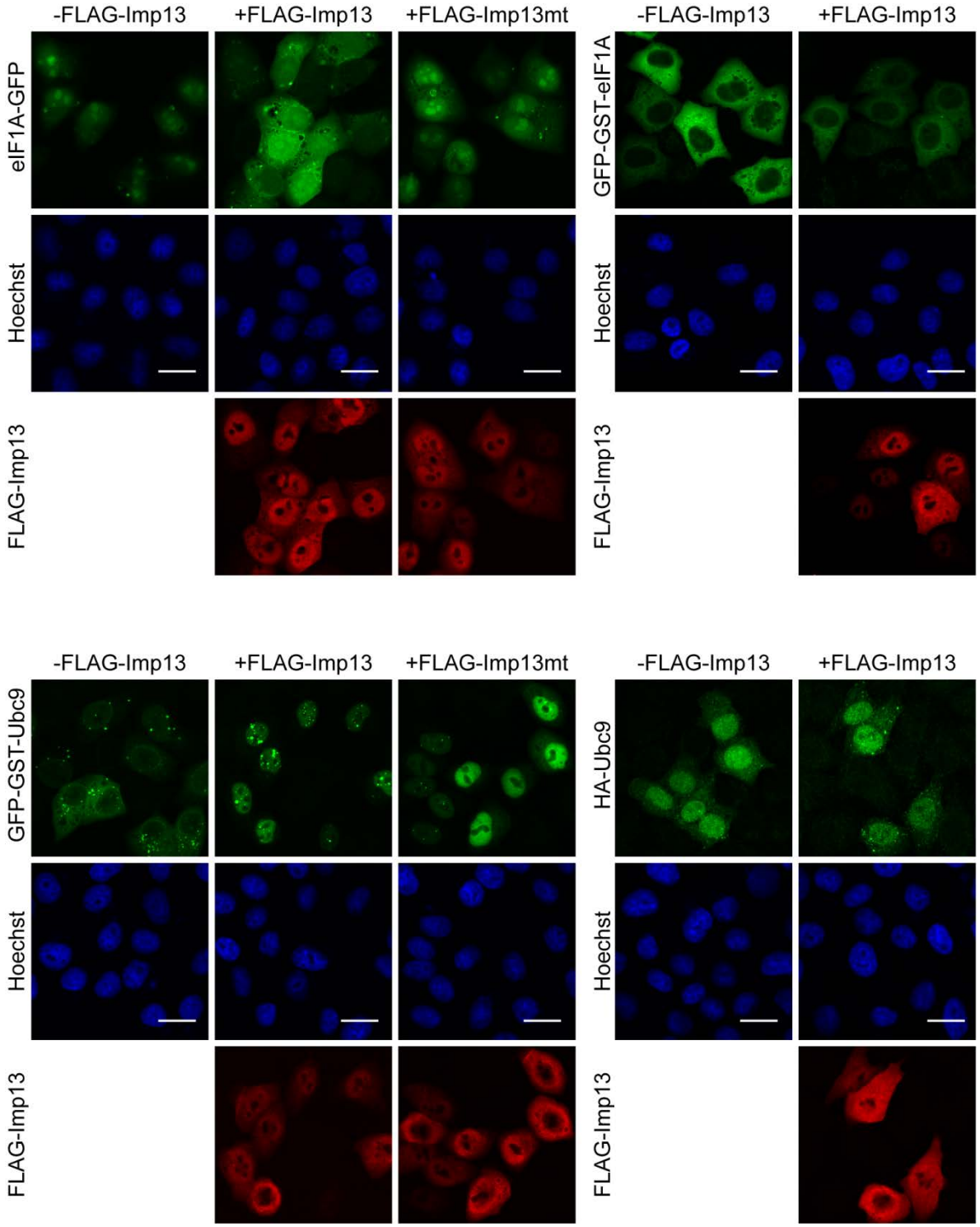

Figure 6: Importin 13 promotes nuclear import of Ubc9 and nuclear export of eIF1A. HeLa P4 cells were transiently transfected using the calcium phosphate method with plasmids coding for Ubc9 or eIF1A and importin 13 wild-type (+FLAG-Imp13), importin 13-E436R/D481R (+FLAG-Imp13mt; mutant impaired in eIF1A export) or an empty control vector. HA-Ubc9 and FLAG-importin 13 were visualized by indirect immunofluorescence with an anti-HA and anti-FLAG antibody, respectively. The scale bars correspond to 20 µm.

In summary, importin 13 can promote the import and export of overexpressed GFP-GST-Ubc9 and eIF1A-GFP, respectively, while the importin 13 mutant Glu436Arg/Asp481Arg cannot export eIF1A but is still capable of importing Ubc9. Consequently, eIF1A-GFP and GFP-GST-Ubc9 are effective controls for importin 13 mediated transport in importin 13 overexpression experiments.

3.1.4 Importin 13 Mediates Nuclear Import of Ubc9 *In Vitro*

Mingot *et al.,* 2001 (135) showed that fluorescently labeled GST-Ubc9 is specifically imported by importin 13 into the nuclei of digitonin permeabilized HeLa cells and that the import efficiency is stimulated in the presence of Ran and an energy-regenerating system. To test whether these findings can be reproduced and to ascertain that the recombinant purified GST-Ubc9 and His-importin 13 are functional, transport assays were performed. HeLa P4 cells were permeabilized with digitonin, which selectively permeabilizes the plasma membrane but leaves the nuclear envelope intact, washed to remove soluble transport factors and incubated with defined transport mixes to analyze the import of GST-Ubc9 (Figure 7).

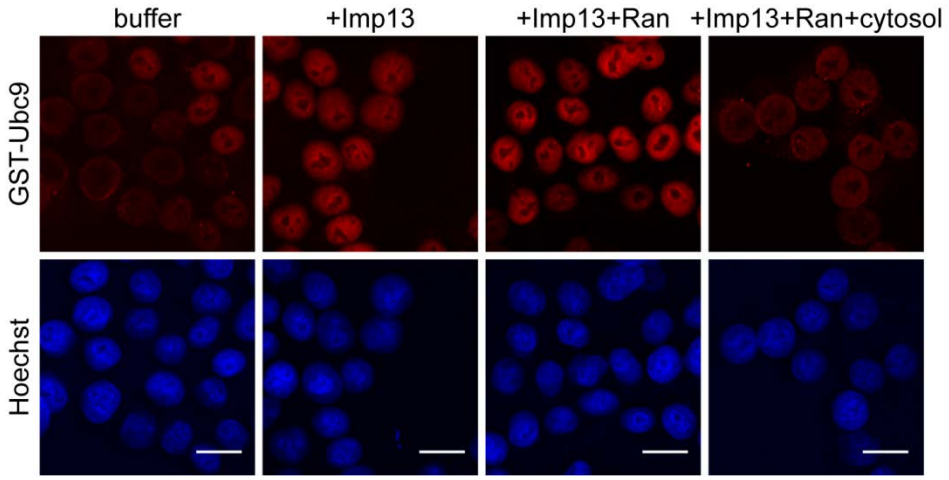

Figure 7: Importin 13 mediates import of GST-Ubc9. Digitonin permeabilized HeLa P4 cells were incubated with GST-Ubc9, an energy-regenerating system and buffer or His-importin 13 in the absence or presence of Ran and cytosol, as indicated. GST-Ubc9 was visualized by indirect immunofluorescence with an anti-GST antibody. The detector gain was decreased for GST-Ubc9+Imp13+Ran from 666 to 621 as the signal intensity was too strong. The scale bars correspond to 20 µm.

In the absence of importin 13, only a minimal import of GST-Ubc9 was detected. Addition of importin 13 resulted in a clear accumulation of GST-Ubc9 in the cell nuclei and import was further enhanced in the presence of Ran, confirming the results from Mingot *et al.,* 2001 (135). Interestingly, addition of cytosol strongly reduced nuclear import of GST-Ubc9, suggesting that some factor present in the cytosol prevents nuclear localization of Ubc9, either by inhibiting import or by promoting export of Ubc9. These results confirm that Ubc9 is imported into cell nuclei by importin 13 and that import is enhanced in the presence of Ran.

3.1.5 Importin 13 Directly Interacts with Ubc9

Mingot *et al.,* 2001 (135) not only demonstrated that nuclear import of Ubc9 depends on importin 13 but also showed that Ubc9 as well as the export cargo eIF1A directly interact with importin 13 in a RanGTP-dependent manner. As ultimately binding assays are to be used for the identification of importin 13 substrates, it was tested if the reported results are reproducible and whether our recombinantly purified proteins are fully functional. GST-tagged Ubc9 and eIF1A were immobilized on beads and incubated with either His- or Hzz (His- and zz-tag)-tagged importin 13 in the absence or presence of Ran_{Q69L} loaded with GTP (Figure 8A). $RanGTP_{Q69L}$ is a mutant deficient in hydrolysis of Ran bound GTP and therefore is predominantly found in the GTP-bound form (186). This Ran mutant promotes binding of export cargoes to their nuclear transport receptor and strongly inhibits binding of import cargoes. As expected both His-importin 13 and Hzz-importin 13 bound efficiently to the import cargo GST-Ubc9 and binding was significantly reduced in the presence of $RanGTP_{Q69L}$. Equimolar amounts of $RanGTP_{Q69L}$ were not sufficient to completely abolish importin 13 binding to GST-Ubc9, suggesting that an excess of RanGTP is required to fully prevent the formation of importin 13 import complexes. In comparison to GST-Ubc9, binding of the export cargo GST-eIF1A was much less efficient and was dependent on the presence of $RanGTP_{Q69L}$. Only binding of Hzz-importin 13 but not His-importin 13 to GST-eIF1A could be observed.

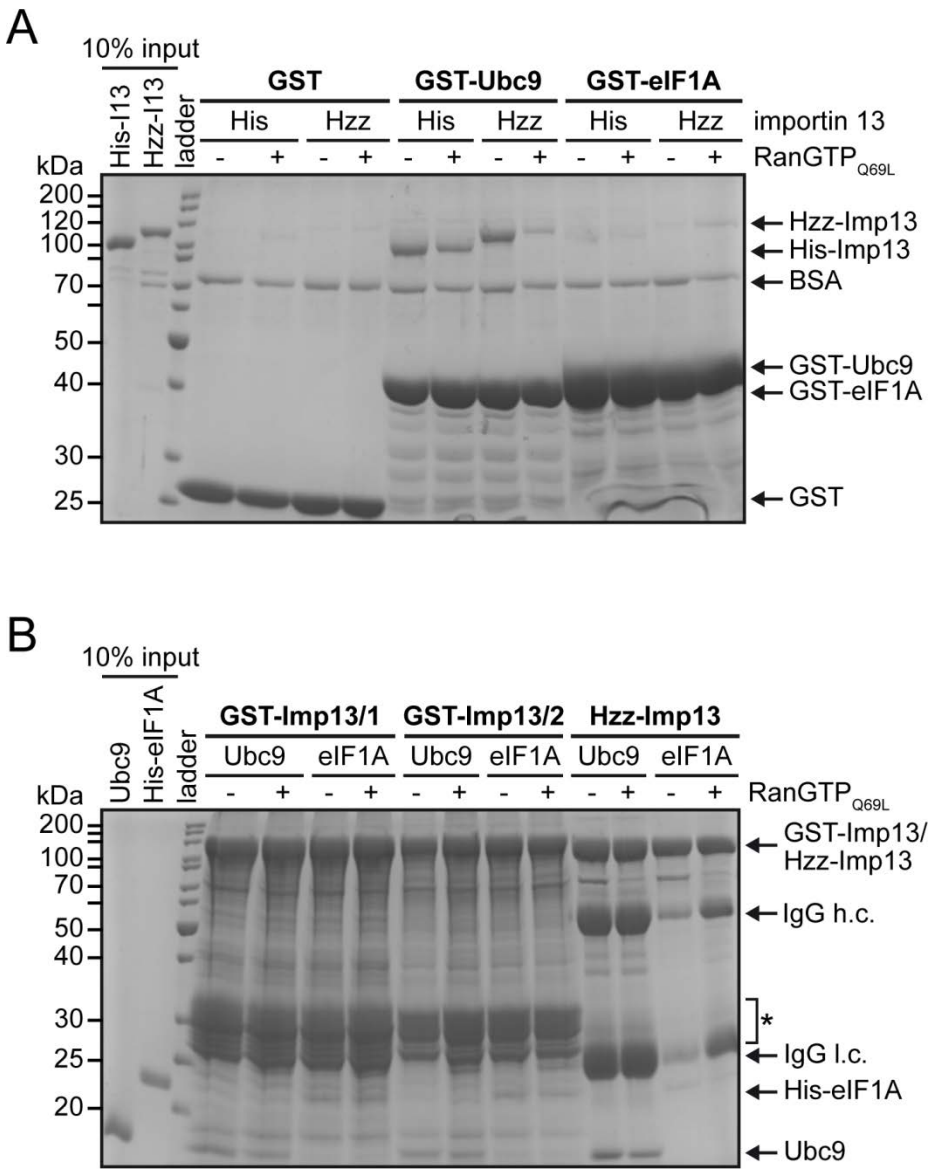

Figure 8: Importin 13 directly interacts with Ubc9 and eIF1A. In (A) GST-tagged Ubc9 and eIF1A (20 µg) were immobilized on glutathione-Sepharose beads and incubated with 5 µg His- or Hzz-tagged importin 13. In (B) GST- and Hzz-tagged importin 13 (20 µg) was immobilized on glutathione-Sepharose and IgG-Sepharose, respectively, and incubated with 5 µg untagged Ubc9 or 7 µg His-eIF1A. All reactions were performed in the absence or presence of 5 µg RanGTP$_{Q69L}$ in PBS supplemented with 2 mg/mL BSA. Proteins bound to GST-tagged proteins were eluted with 4x SDS-sample buffer and proteins bound to Hzz-importin 13 were eluted by glycine elution. Interacting proteins were analyzed by SDS-PAGE, followed by Coomassie staining. Asterisk in (B) marks contaminants visible between 25-35 kDa that likely correspond to GST-importin 13 degradation products. GST-importin 13/1: expressed from plasmid #1576 with a linker of 13 amino acids; GST-importin 13/2: expressed from plasmid #887 with a linker of 17 amino acids; l.c.: light chain; h.c.: heavy chain; ladder: PageRuler Unstained Protein Ladder.

To test whether the cargoes can also bind to immobilized importin 13, reverse binding experiments were performed using three differently tagged importin 13 proteins. Binding experiments were done with two GST-importin 13 variants that differed in the size of their linker and one Hzz-tagged importin 13 variant. The Hzz-tag consists of a His-tag and two IgG-binding domains of protein A from *Staphylococcus aureus* (zz-tag). The three importin 13 variants were immobilized on beads and incubated with untagged Ubc9 or His-eIF1A in the absence or presence of $RanGTP_{Q69L}$ (Figure 8B). Both Ubc9 and His-eIF1A bound efficiently to all three importin 13 fusion proteins in a RanGTP-dependent manner, with Ubc9 showing a slightly higher affinity for Hzz-importin 13 and His-eIF1A showing a slightly higher affinity for GST-importin 13. As in the previous binding experiment, binding of Ubc9 to importin 13 was stronger than for His-eIF1A. The identity of the bound proteins was confirmed by immunoblotting with an anti-Ubc9 and anti-eIF1A antibody (data not shown).

In summary, the reported direct interaction between importin 13 and its cargoes Ubc9 and eIF1A could be confirmed using proteins with various tags. Binding of importin 13 cargoes to the two GST-importin 13 variants was comparable but in the case of Ubc9 less efficient than binding to Hzz-importin 13. Further, GST-importin 13 was more prone to degradation than Hzz-importin 13. Thus, Hzz-importin 13 was used in subsequent binding experiments and ultimately also in the pull-down experiment coupled to mass spectrometry for the identification of importin 13 substrates.

3.1.6 Importin 13 Binds Endogenous Ubc9 from HeLa P4 Cell Extracts

One central aim of this study was to identify importin 13 cargoes that bind to immobilized importin 13 from a HeLa P4 cell extract. Previously, binding of endogenous Ubc9 and eIF1A from a HeLa lysate to immobilized importin 13 has been demonstrated by mass spectrometry (135). Binding conditions were established with immobilized importin 13 using the known importin 13 cargoes Ubc9 and eIF1A. Hzz-tagged importin 13 was immobilized on beads and incubated with a digitonin or freeze/thaw HeLa P4 lysate in the presence or absence of recombinant cargoes and $RanGTP_{Q69L}$ (Figure 9). Both endogenous and recombinant Ubc9 bound efficiently to Hzz-importin 13 from both HeLa P4 cell extracts with slightly more Ubc9 binding from the digitonin HeLa P4 cell lysate. Ubc9 binding was not affected by equimolar amounts of $RanGTP_{Q69L}$ showing that RanGTP becomes limiting in the presence of cell lysate, which contains high concentrations of other nuclear transport receptors that compete for RanGTP binding.

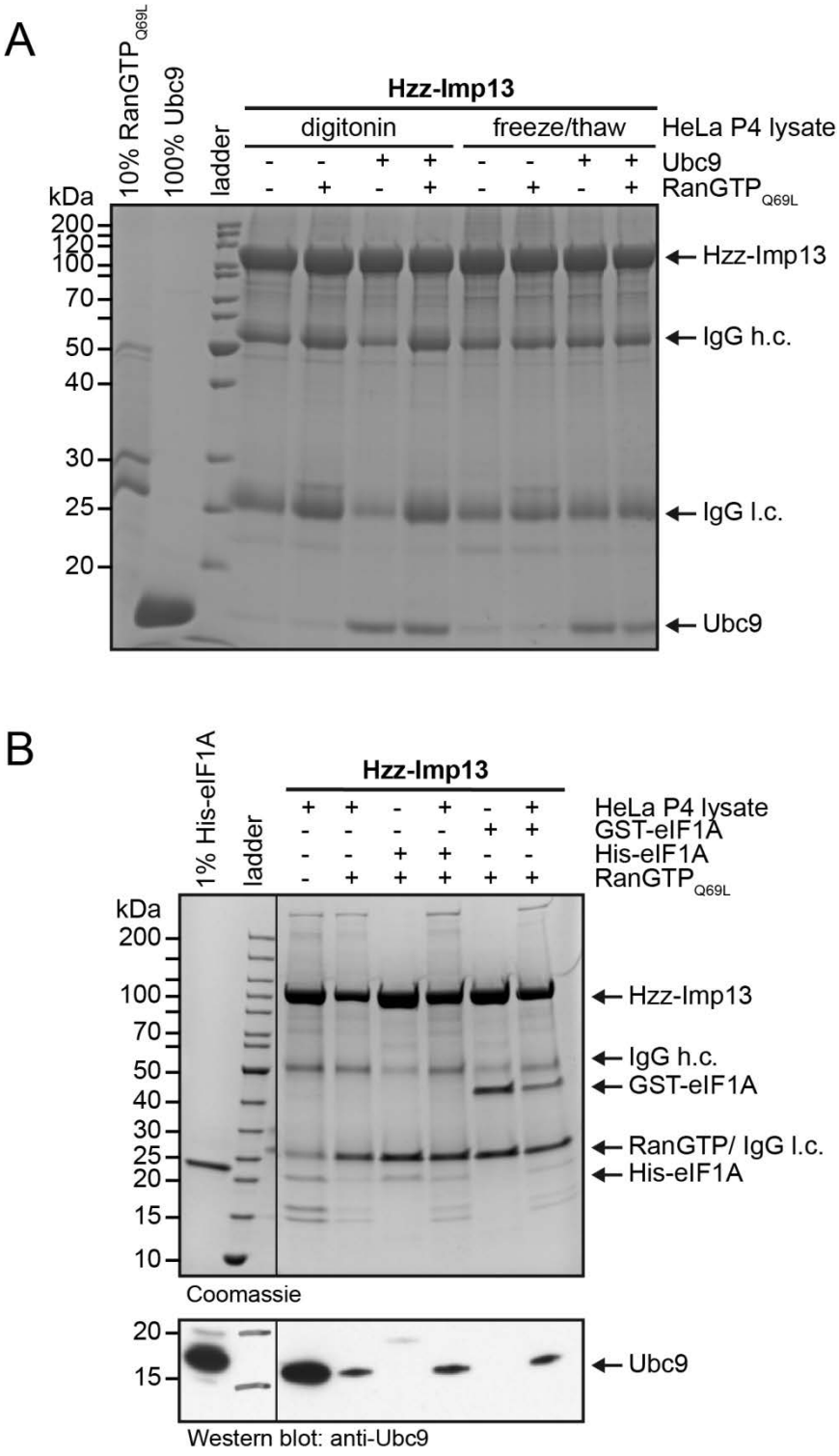

Figure 9: Importin 13 binds endogenous Ubc9 and recombinant eIF1A from HeLa P4 cell extract. Hzz-importin 13 (20 µg) was immobilized on IgG-Sepharose and incubated with a digitonin or freeze/thaw HeLa P4 cell extract in the absence or presence of (A) 5 µg Ubc9 or 5 µg $RanGTP_{Q69L}$ and (B) 7 µg His-eIF1A, 7 µg GST-eIF1A or 15 µg $RanGTP_{Q69L}$ in PBS supplemented with 2 mg/mL BSA. Bound proteins were eluted and analyzed as in (Figure 8). In (B) a freeze/thaw

HeLa P4 cell lysate was used and binding of endogenous Ubc9 was detected by immunoblotting with an anti-Ubc9 antibody. l.c.: light chain; h.c.: heavy chain; ladder: PageRuler Unstained Protein Ladder.

For the export cargo eIF1A, only binding of recombinant His-eIF1A and GST-eIF1A but not endogenous eIF1A to Hzz-importin 13 could be detected (Figure 9), which was further confirmed by immunoblotting (data not shown). Binding of recombinant GST-eIF1A to Hzz-importin 13 was more efficient than binding of His-eIF1A and both interactions were significantly reduced in the presence of HeLa P4 cell extract suggesting competition of other cargoes with eIF1A for importin 13 binding. Indeed, concomitant binding of Ubc9 could be confirmed by immunoblot analysis in binding reactions performed with HeLa P4 cell extract. The immunoblot also showed that binding of endogenous Ubc9 was reduced if exogenous $RanGTP_{Q69L}$ was present in the binding reaction.

An interaction between importin 13 and Ubc9 or eIF1A could further be confirmed using *in situ* proximity ligation assays (Figure S1). Endogenous proteins were targeted with antibodies and *in situ* interactions were visualized as single fluorescent dots using the proximity ligation assay. Knock-down of importin 13 reduced the number of fluorescent dots (one fluorescent dot corresponds to one single protein-protein interaction), confirming the specificity of the observed interactions. Interestingly, *in situ* interactions of importin 13 with Ubc9 were mainly observed in the nucleus, while interactions of importin 13 with eIF1A were mainly observed in the cytoplasm. This suggests that the importin 13 import complexes are more transient in the cytoplasm than in the nucleus and vice versa for export complexes.

The results demonstrate that importin 13 binding experiments with HeLa P4 cell lysate could be an effective approach to identify new importin 13 cargoes. However, the results also show that the efficiency of cargo identification will depend strongly on the affinity of importin 13 for its cargoes. As demonstrated above, Ubc9, which has a reported eightfold lower dissociation constant than eIF1A (107), also showed stronger binding to importin 13 than eIF1A. Furthermore, binding of endogenous Ubc9 to Hzz-importin 13 was found to be slightly more efficient from a HeLa P4 cell extract generated by digitonin treatment, suggesting that a digitonin cell lysate might be more effective for the identification of importin 13 substrates than a freeze/thaw cell lysate.

3.2 Identification of Potential Importin 13 Export Cargoes Using an Importin 13 Overexpression Screen

3.2.1 Importin 13 Overexpression Screen Using a Library of Nuclear Proteins

When this thesis was started several importin 13 import cargoes had been identified but only one export cargo, the translation initiation factor eIF1A was known. To specifically screen for potential importin 13 export cargoes, labeled proteins from a library of proteins with known nuclear localization were transiently expressed in HeLa P4 cells and monitored for any changes in subcellular localization upon coexpression of importin 13. The plasmid clones coding for the tagged nuclear proteins were derived from the 'LIFE database' (174, 175).

The initial overexpression screen to identify potential importin 13 export cargoes was performed by Annegret Nath, a former member of our group (data not shown). While the majority of ~200 tested proteins was not affected (>60%), several proteins changed their subcellular localization upon importin 13 coexpression. Clear effects were observed for about 10-15% of the proteins.

Candidate proteins that were affected as well as proteins that were not affected by importin 13 overexpression in the initial screen were reanalyzed for effects of importin 13 coexpression on their subcellular localization (Table S1). As in the initial overexpression screen, plasmids coding for tagged proteins were transiently transfected into HeLa P4 cells and changes in subcellular distribution upon coexpression of importin 13 were analyzed (Figure 10 and Figure S2). The known importin 13 cargoes eIF1A-GFP and GFP-GST-Ubc9 were included in the screen as positive controls and both confirmed that the coexpressed FLAG-importin 13 was fully functional. Additionally, several negative controls were included such as different fusion tags, known artificial cargoes of other nuclear transport receptors as well as randomly selected proteins.

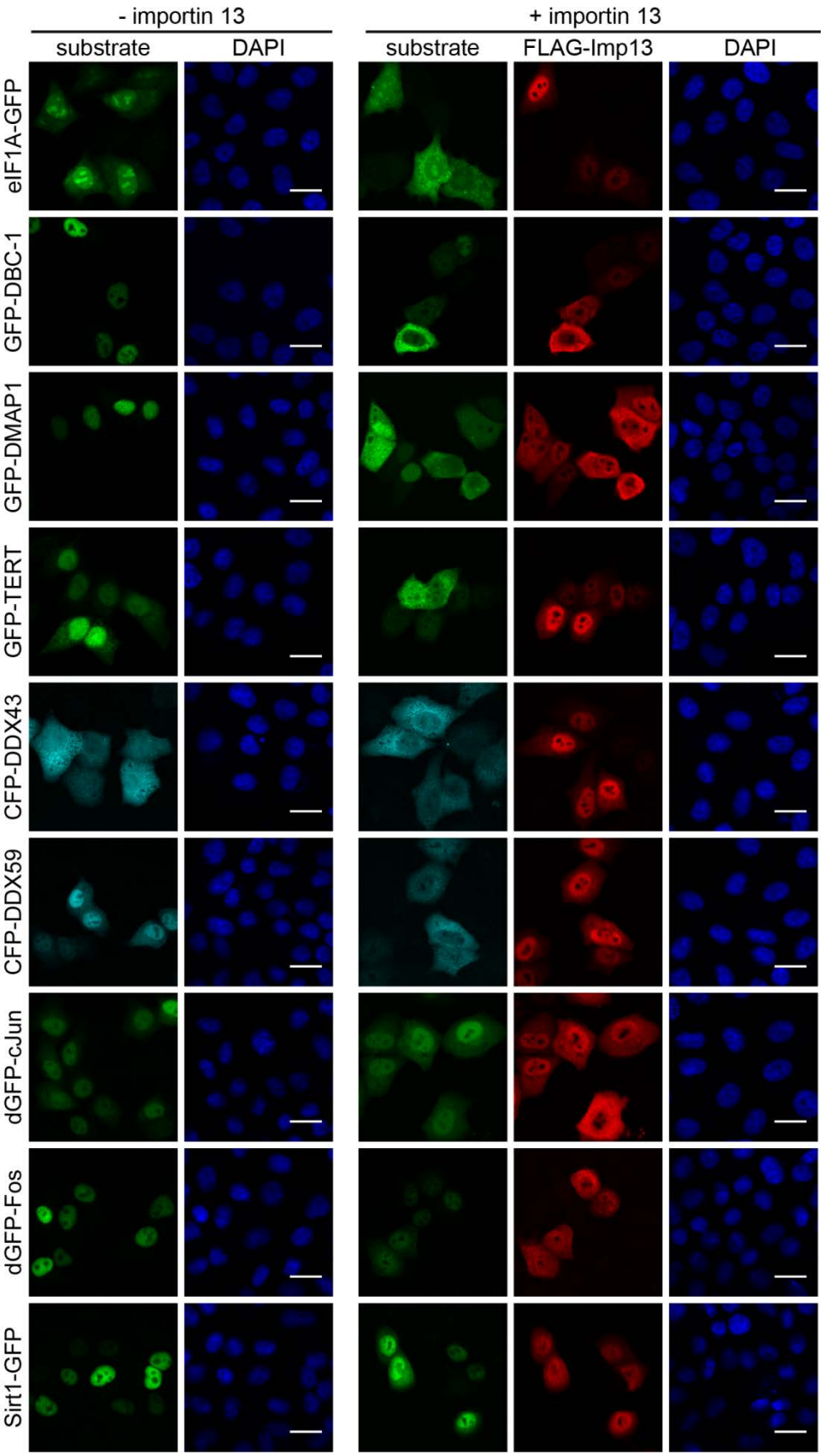
- importin 13
+ importin 13
substrate
DAPI
substrate
FLAG-Imp13
DAPI
eIF1A-GFP
GFP-DBC-1
GFP-DMAP1
GFP-TERT
CFP-DDX43
CFP-DDX59
dGFP-cJun
dGFP-Fos
Sirt1-GFP

Figure 10: Importin 13 affects the subcellular localization of DBC-1, DMAP1, TERT, DDX43, DDX59, cJun, Fos and Sirt1. HeLa P4 cells were transiently cotransfected with plasmids coding for fluorescently tagged DBC-1, DMAP1, TERT, DDX43, DDX59, cJun, Fos or Sirt1 and FLAG-importin 13 or an empty control vector using the calcium phosphate method. FLAG-importin 13 was visualized by indirect immunofluorescence with an anti-FLAG antibody. For controls and further proteins tested see supplemental Figure S2 and Table S1. The scale bars correspond to 20 µm.

Similar to the findings of the initial screen, coexpression of importin 13 had strong effects on the nuclear proteins DBC-1, DMAP1, TERT, DDX43, DDX59 and c-Jun, promoting their cytoplasmic localization (see Table S1 for full protein names). The effect of importin 13 on DBC-1 and c-Jun is not entirely surprising, as both proteins have previously been reported to bind to importin 13 (49, 117). However, the binding was reduced in the presence of $RanGTP_{Q69L}$, implicating them rather as importin 13 import than export cargoes (49, 117). Proteins that were slightly affected by importin 13 overexpression included Fos, Tmp29, Nip30 and Sirt1. Surprisingly, the M9 nuclear import signal (PY-NLS found in hnRNPA1 and A2), which is recognized by transportin, was also slightly affected by importin 13 overexpression, resulting in a more cytoplasmic localization (Figure S2).

The other artificial cargoes, including dGFP-GST-cNLS (Xenopus), which is imported by importin α/β and dGFP-GST-RevNLS (from HIV-1 Rev), which is imported by transportin and potentially several other karyopherins (48, 116), as well as the Crm1 cargo protein snurportin 1 (187), were not affected by importin 13 coexpression. These GFP-fusion constructs also demonstrate that the importin 13 mediated redistribution of the identified proteins is not an unspecific effect of the GFP-tag. However, to fully exclude that the tag might affect the subcellular localization, other fusion tags for both importin 13 and the potential importin 13 cargoes were also tested (Figure S2 or data not shown). Irrespective of the tag used, importin 13 coexpression always resulted in a shift towards the cytoplasm of DBC-1, DMAP1, TERT, DDX43 and DDX59. However, with all HA-tagged constructs the observed effects were less strong.

For yet unidentified reasons, the importin 13 effect varied not only between different experiments but also between individual cells, with some cells showing a strong redistribution of DBC-1 and DMAP1 and others only a weak or even no redistribution upon importin 13 coexpression. Although a trend could be observed that cells with high importin 13 expression levels had a more cytoplasmic localization of DBC-1 and DMAP1, the same could also be observed in cells with low importin 13 expression levels, albeit less frequently. Interestingly, importin 13 induced relocalization of DBC-1 and DMAP1 was

strongest in cells sub-cultivated for only one to three passages after thawing from liquid nitrogen (data not shown). This suggests that HeLa P4 cells thawed from liquid nitrogen take longer to recover or that a stress response is induced in these cells that affects importin 13 nucleocytoplasmic transport. However, heat shock did not influence the observed importin 13 effect (data not shown). The importin 13 mediated relocalization also is not cell specific, as similar effects were also observed in 293T HEK, U2OS and COS-7 cells (data not shown). Interestingly, with some of the identified proteins not only the candidate protein but also importin 13 showed relocalization to the cytoplasm and a very similar distribution pattern, suggesting that they form stable complexes in the cytoplasm.

In summary, DBC-1, DMAP1, TERT, DDX43, DDX59 and c-Jun were significantly affected by importin 13 overexpression, while the effect on Fos, Tmp29, Nip30 and Sirt1 was less strong. Even though these proteins showed a clear shift towards the cytoplasm upon importin 13 overexpression, one cannot conclude with certainty that these proteins are importin 13 export cargoes. Importin 13 could also indirectly enhance the cytoplasmic localization of these proteins or function as a negative regulator of nuclear import.

3.2.2 DBC-1, DMAP1, DDX43 and DDX59 Bind Importin 13 Differently to eIF1A

The importin 13 mutant Glu436Arg/Asp481Arg is deficient in eIF1A export (107). To test whether the putative importin 13 export cargoes DBC-1, DMAP1, DDX43 and DDX59 bind to the same key residues on importin 13 as eIF1A, plasmids coding for these cargoes were transfected in HeLa P4 cells and the effect of FLAG-importin 13-E436R/D481R cotransfection was analyzed (Figure 11). While eIF1A only changed its subcellular localization upon coexpression of wild type but not mutant importin 13, the putative importin 13 export cargoes showed relocalization to the cytoplasm with both wild type and mutant importin 13. Thus, these proteins either have a different binding site on importin 13 or more residues need to be mutated to abolish the interaction. As in the previous experiment (3.2.1), importin 13 showed a more cytoplasmic localization in some cells if co-expressed with DBC-1 or DMAP1.

The results indicate that DBC-1, DMAP1, DDX43 and DDX59 bind importin 13 differently than the established export cargo eIF1A.

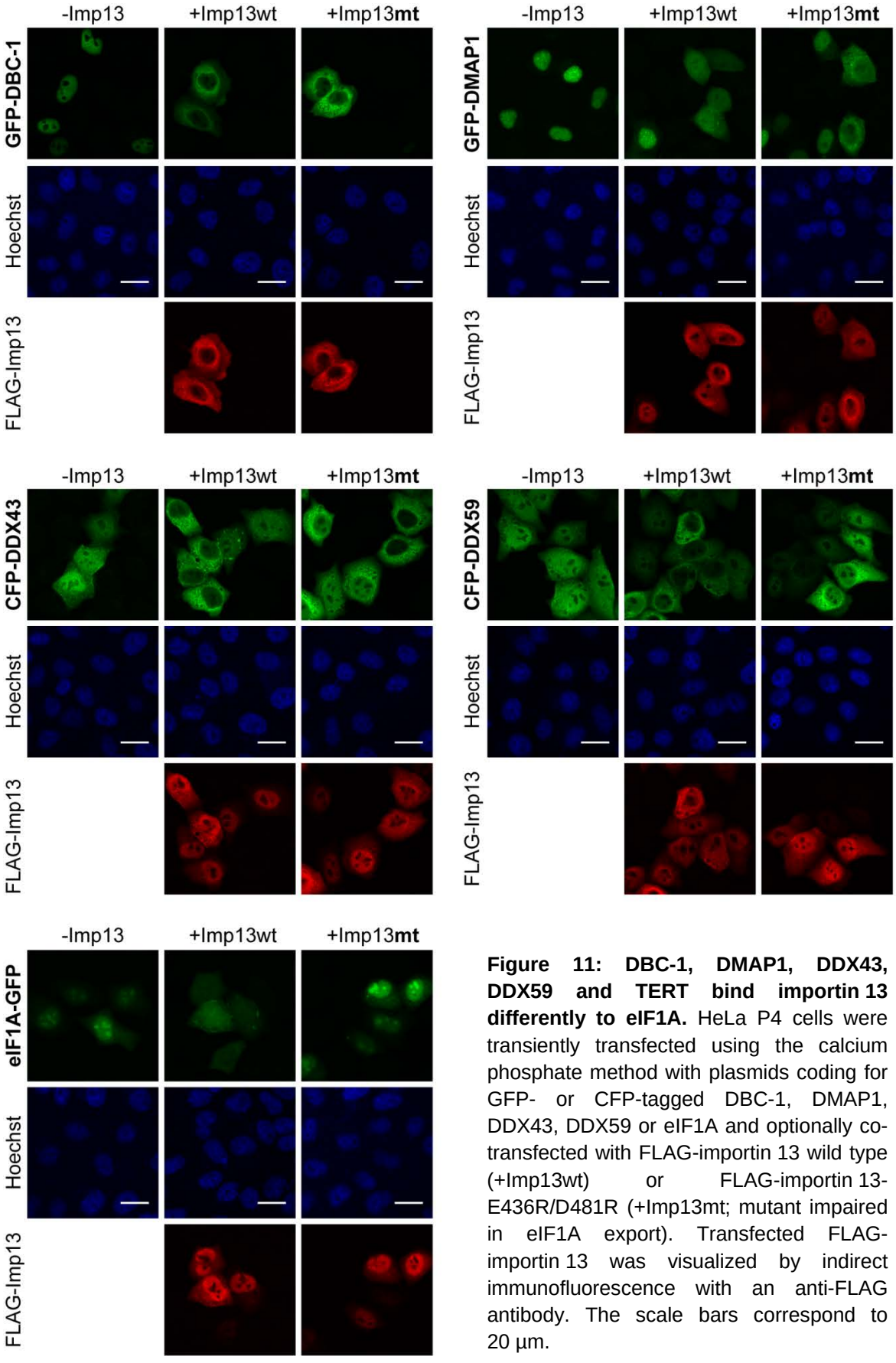

Figure 11: DBC-1, DMAP1, DDX43, DDX59 and TERT bind importin 13 differently to eIF1A. HeLa P4 cells were transiently transfected using the calcium phosphate method with plasmids coding for GFP- or CFP-tagged DBC-1, DMAP1, DDX43, DDX59 or eIF1A and optionally co-transfected with FLAG-importin 13 wild type (+Imp13wt) or FLAG-importin 13-E436R/D481R (+Imp13mt; mutant impaired in eIF1A export). Transfected FLAG-importin 13 was visualized by indirect immunofluorescence with an anti-FLAG antibody. The scale bars correspond to 20 µm.

3.2.3 Characterization of DBC-1 Interaction with Importin 13

3.2.3.1 Importin 13 Interacts with the Coiled-coil Domain of DBC-1

Previous experiments in the lab suggested that the coiled-coil domain of DBC-1 (amino acids 793-923) is required for the importin 13 mediated cytoplasmic localization. To test whether this is indeed the case, HeLa P4 cells were transiently transfected with plasmids coding for the coiled coil domain of DBC-1 fused to a cNLS, to localize it to the nucleus, and analyzed for changes in nucleocytoplasmic distribution upon importin 13 coexpression (Figure 12). In the absence of importin 13, the coiled-coil domain of DBC-1 fused to a cNLS was mainly nuclear but in the presence of importin 13, a shift to the cytoplasm could be observed. As shown for full-length DBC-1, the importin 13 mutant impaired in eIF1A binding (importin 13-E436R/D481R), was still capable of relocalizing the coiled-coil domain of DBC-1 to the cytoplasm. This confirms that the coiled-coil domain of DBC-1 is required for interaction with importin 13. However, binding assays will need to be performed to show that the interaction is direct rather than indirect.

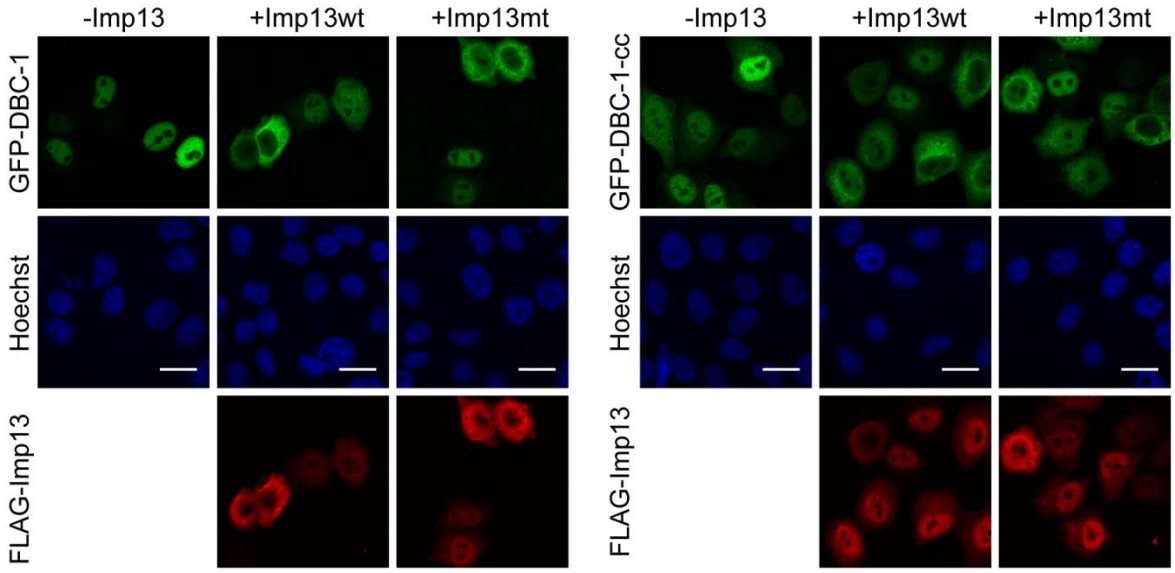

Figure 12: Importin 13 interacts with the coiled-coil domain of DBC-1. HeLa P4 cells were transiently transfected with plasmids coding for full length DBC-1 or the coiled-coil domain of DBC-1 (aa793-923, DBC-1-cc) using the calcium phosphate method. Optionally cells were cotransfected with plasmids coding for either wild type FLAG-importin 13 (+Imp13wt) or FLAG-importin 13-E436R/D481R (+Imp13mt). FLAG-tagged importin 13 was visualized by indirect immunofluorescence using anti-FLAG antibody. The scale bars correspond to 20 µm.

3.2.3.2 The N-terminal Domain of Importin 13 Is Required for Recognition of DBC-1

To get an idea as to where DBC-1 might bind to importin 13, the effect of different importin 13 fragments on the subcellular localization of DBC-1 was analyzed. A physiologically relevant N-terminally truncated importin 13 isoform has previously been reported to function as a negative regulator of nuclear import in testis (136, 172), a function that could also be relevant for DBC-1. HeLa P4 cells were cotransfected with plasmids coding for GFP-DBC-1 and different N-terminal and C-terminal fragments of FLAG-tagged importin 13 (Figure 13).

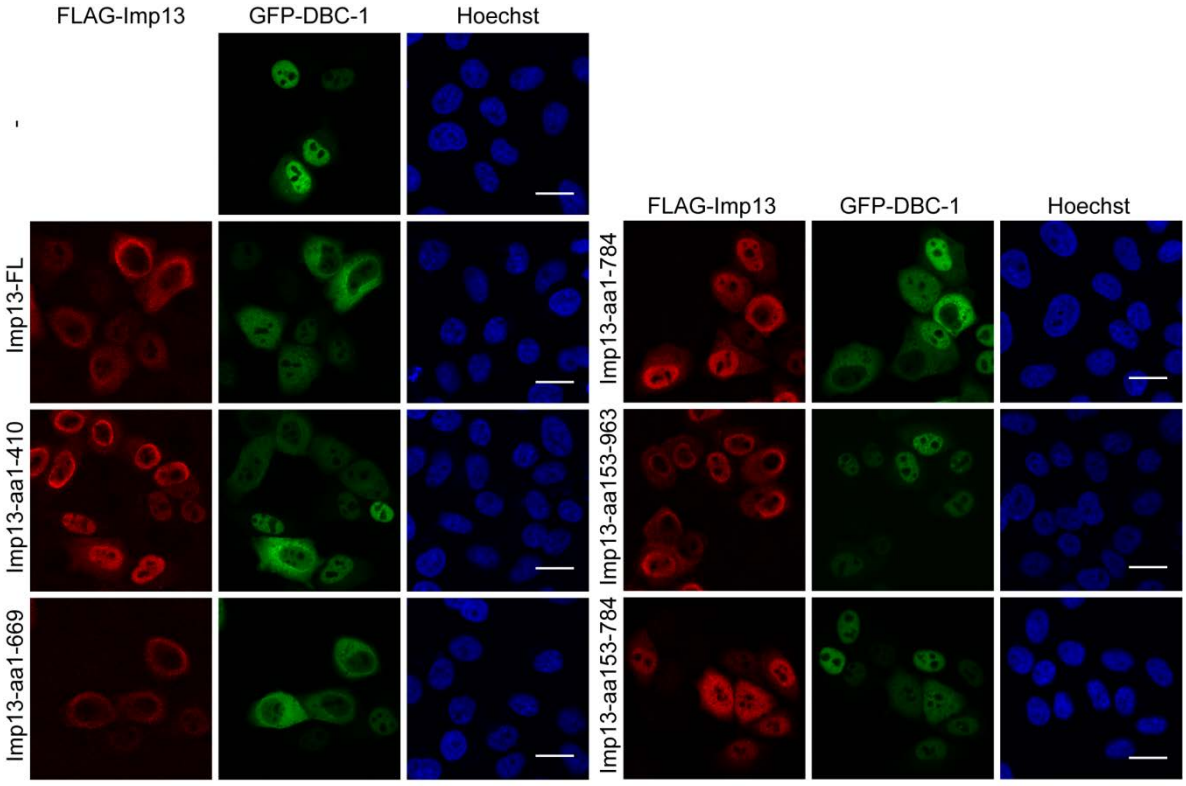

Figure 13: The C-terminus of importin 13 is dispensable for recognition of DBC-1. HeLa P4 cells were transiently transfected with plasmid DNA coding for GFP-DBC-1 and wild type or truncated FLAG-importin 13. The different FLAG-importin 13 constructs were visualized by indirect immunofluorescence with an anti-FLAG antibody. The scale bars correspond to 20 µm.

The C-terminal fragments of importin 13 resulted only in a minor relocalization of DBC-1 to the cytoplasm, whereas the N-terminal fragments of importin 13 resulted in a clear shift towards the cytoplasm, similar to that seen with full-length importin 13. A weak shift

towards the cytoplasm was detected with amino acids 1-410 of FLAG-tagged importin 13, while the strongest shift was detected with amino acids 1-669. This indicates that several binding sites on importin 13 contribute to DBC-1 binding and that the major binding sites are present on the N-terminal arch of importin 13. However, binding to the C-terminal arch cannot be excluded, as the C-terminal fragments lack the N-terminal binding site for RanGTP, which is required for the formation of export complexes. Thus, even if binding would occur, the C-terminal importin 13 fragment would not be able to shuttle DBC-1 to the cytoplasm.

The other putative importin 13 export cargoes DMAP1, DDX43, DDX59 and TERT were also characterized for their interaction with importin 13 by cotransfection of different importin 13 fragments (data not shown). Similar to DBC-1, subcellular localization of these cargoes was not affected by C-terminal fragments but only by N-terminal fragments of importin 13. The longer the N-terminal fragment, the stronger the observed redistribution to the cytoplasm. As for DBC-1 this indicates that at least a part of the importin 13 N-terminus is involved in the interaction with these cargoes, while the far C-terminus appears to be dispensable.

3.3 Identification of Potential Importin 13 Cargoes by Mass Spectrometry

A major goal of this work was to significantly expand the number of known importin 13 cargoes. While the above importin 13 overexpression screen does allow for the identification of importin 13 interaction partners, it is limited in the number of available plasmids. Thus, two different mass spectrometry based approaches were established to allow for the large scale identification of importin 13 substrates. Both approaches focused on identifying proteins that bound to Hzz-importin 13 from a HeLa P4 cell lysate but differed in their strategy to reduce the number of false positive proteins. In the first approach, binding of proteins to both the Hzz-tag and Hzz-importin 13 from two different HeLa P4 cell extracts was compared, with the Hzz-tag reaction serving as a control for unspecific binding proteins. The second approach was based on quantitative mass spectrometry using stable isotope labeling with amino acids in cell culture (SILAC). To effectively distinguish between importin 13 import and export cargoes, binding reactions were performed in the absence or presence of Ubc9 and $RanGTP_{Q69L}$. $RanGTP_{Q69L}$ is expected to promote the formation of importin 13 export complexes as it has been reported to displace importin 13 import cargoes and facilitate the binding of export cargoes to importin 13 (93, 135). In contrast, Ubc9 is expected to prevent the formation of both

importin 13 import and export complexes as excess Ubc9 has been shown to compete with both RanGTP and other import cargoes for importin 13 binding (93, 135).

3.3.1 Mass Spectrometry Based Identification of Potential Importin 13 Substrates

To get an idea of the range of proteins that interact with importin 13, mass spectrometry analysis was performed to identify proteins that bind to immobilized Hzz-importin 13 from a HeLa P4 cell extract. Two different HeLa P4 cell extracts were compared, a freeze/thaw and a digitonin lysate to see whether cell lysate preparation affects the type of proteins identified. Digitonin is a reagent known to selectively permeabilize the plasma membrane and leave the nuclear envelope intact. In contrast, disruption by freeze/thaw is less selective potentially resulting in the release of harmful proteins from other cellular compartments such as proteases. To identify proteins that bind unspecifically to the Hzz-tag and the IgG-Sepharose, binding experiments were performed in parallel to Hzz-importin 13 with the Hzz-tag alone.

The Hzz-tag and Hzz-tagged importin 13 were immobilized on IgG-Sepharose and incubated with digitonin or freeze/thaw HeLa P4 cell extract. Bound proteins were eluted by magnesium chloride elution to prevent extensive co-elution of the IgG light and heavy chain. To assess the effectiveness of magnesium chloride elution, a second elution step was done with 4x SDS-sample buffer. Bound proteins eluted with magnesium chloride were separated by SDS-PAGE and protein peptides were extracted by in-gel tryptic digestion. Peptides were purified over C18 stage tips and given to our collaborators for mass spectrometry analysis. Raw data was analyzed with the Proteome Discoverer against a human protein database. Additionally, the magnesium chloride eluates were separated by SDS-PAGE and visualized by silver staining (Figure 14A). The silver stained gel showed that a lot of proteins bound unspecifically to the Hzz-tag and the IgG-Sepharose. However, more proteins were enriched with Hzz-importin 13 than with the Hzz-tag.

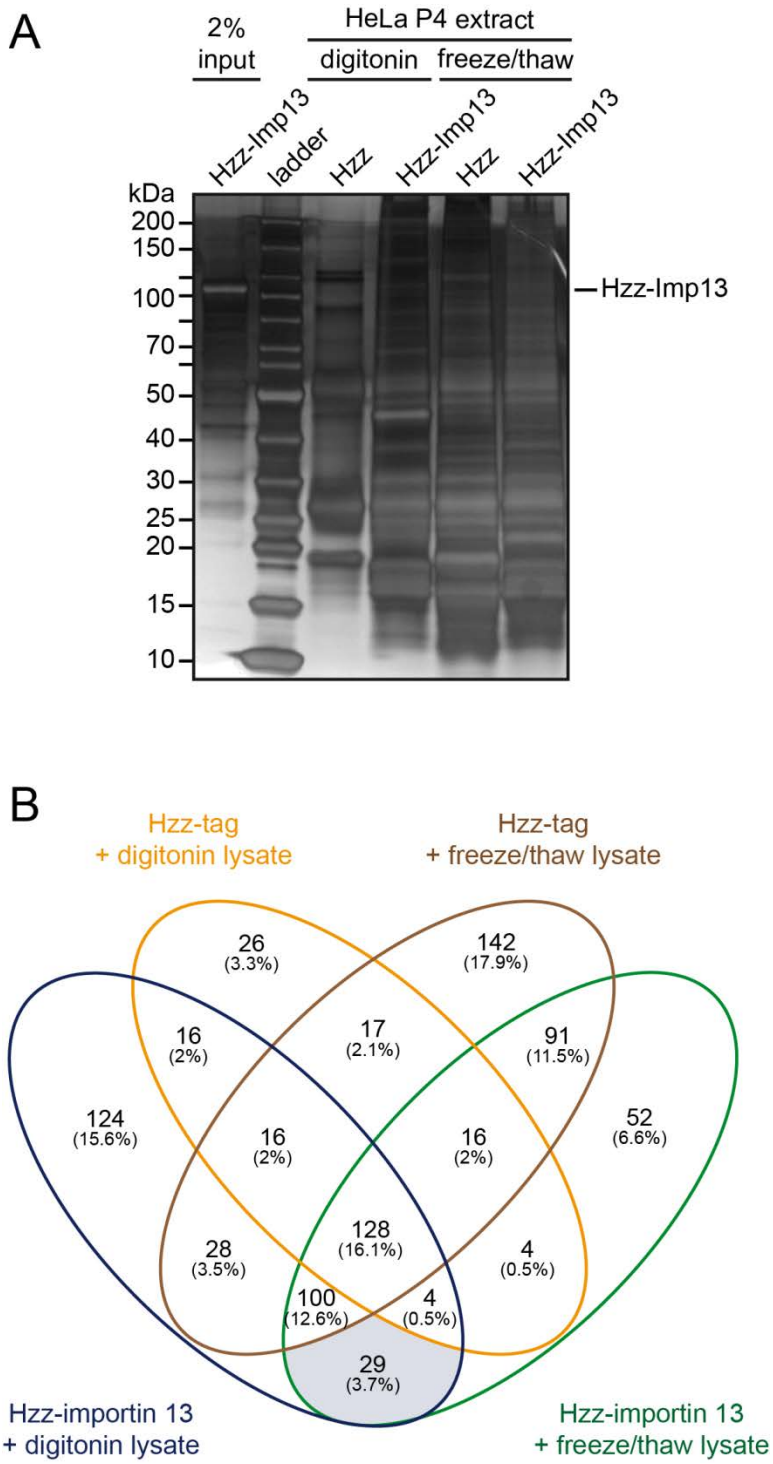

Figure 14: Proteins bound to Hzz-tag and Hzz-importin 13 from HeLa P4 cell extract. (A) Hzz-tag or Hzz-importin 13 was immobilized on IgG-Sepharose and incubated with digitonin or freeze/thaw HeLa P4 cell extract in transport buffer. Bound proteins were eluted with magnesium chloride and analyzed by SDS-PAGE, followed by silver staining. ladder: PageRuler Unstained Protein Ladder. (B) Venn diagram showing the overlap of proteins bound to Hzz-tag and Hzz-importin 13 from both digitonin and freeze/thaw HeLa P4 cell extract. See Table 10 for proteins that bound specifically to Hzz-importin 13 from both cell extracts (area shaded in light blue).

Using a threshold of minimum 10 peptide spectrum matches (PSMs, total number of identified peptide spectra matched to a protein), a total of 445 proteins were identified by mass spectrometry that bound to Hzz-importin 13 from the digitonin HeLa P4 cell extract and 424 proteins that were bound from the freeze/thaw cell extract. Of these, only 29 proteins bound specifically to Hzz-importin 13 but not the Hzz-tag from both the digitonin and the freeze/thaw HeLa P4 cell lysate (Figure 14B, Table 10). Another 124 proteins were identified that specifically bound to importin 13 from the digitonin cell extract (Table S2) and 52 proteins that specifically bound to importin 13 from the freeze/thaw cell extract (Table S3).

Table 10: List of proteins that bound to Hzz-importin 13 from both a digitonin and a freeze/thaw HeLa P4 cell extract (see Table S2 and Table S3 for cell extract specific proteins)[#]

Uniprot ID	Protein	Gene	Reference
O94829	Importin-13	IPO13	
Q92538	Golgi-specific brefeldin A-resistance guanine nucleotide exchange factor 1	GBF1	
P63279	**SUMO-conjugating enzyme UBC9**	UBE2I	(135)
Q7Z3U7	Protein MON2 homolog	MON2	
Q9NRF9	**DNA polymerase epsilon subunit 3**	POLE3	(147)
E9PS17	N-terminal kinase-like protein	SCYL1	
P61326	**Protein mago nashi homolog**	MAGOH	(135)
Q9Y5S9	**RNA-binding protein 8A**	RBM8A	(135)
Q9H9A6	Leucine-rich repeat-containing protein 40	LRRC40	
O75420	PERQ amino acid-rich with GYF domain-containing protein 1	GIGYF1	
Q9NRG0	**Chromatin accessibility complex protein 1**	CHRAC1	(147)
Q9Y4H2	Insulin receptor substrate 2	IRS2	
Q8WUF5	RelA-associated inhibitor	PPP1R13L	
Q14160	Protein scribble homolog	SCRIB	
P27540	Aryl hydrocarbon receptor nuclear translocator	ARNT	
O43813	LanC-like protein 1	LANCL1	
E9PMS6	LIM domain only protein 7	LMO7	
J3KR24	Isoleucine--tRNA ligase	IARS	
Q7Z460	CLIP-associating protein 1	CLASP1	
P52655	Transcription initiation factor IIA subunit 1	GTF2A1	
F8W9S7	GTPase-activating protein and VPS9 domain-containing protein 1	GAPVD1	
Q16204	Coiled-coil domain-containing protein 6	CCDC6	
Q6P2H3	Centrosomal protein of 85 kDa	CEP85	
Q9BWH6	RNA polymerase II-associated protein 1	RPAP1	
B1ANR0	Polyadenylate-binding protein	PABPC4	
Q9P1Y5	Calmodulin-regulated spectrin-associated protein 3	CAMSAP3	
F8W726	Ubiquitin-associated protein 2-like	UBAP2L	
P35249	Replication factor C subunit 4	RFC4	
P26373	60S ribosomal protein L13	RPL13	

#: Proteins are sorted according to confidence from high to low. Proteins written in bold are known importin 13 cargoes.

Of the 29 proteins that bound to importin 13 from both cell lysates, five proteins (Ubc9, POLE3, MAGOH, RBM8A, CHRAC1) were known importin 13 cargoes demonstrating that the established importin 13 binding experiment as well as both cell extraction methods allow for the specific identification of importin 13 substrates. Another three known importin 13 cargoes (eIF1A, POLE4, NFYC) were specifically identified for the digitonin cell lysate (Table S2) and four (NFYC, NFYB, DRAP1, DR1) for the freeze/thaw cell lysate (Table S3), showing that both cell extraction methods can complement each other. The export cargo eIF1A was also identified in the mass spectrometry analysis to bind to Hzz-importin 13 from both the digitonin (24 PSMs) and the freeze/thaw cell lysate (5 PSMs), however, some unspecific binding to the Hzz-tag could also be detected.

Apart from the known importin 13 cargoes, several proteins were also found to interact with importin 13 that are involved in the regulation of the cytoskeleton (CLASP1, CCDC6, CAMSAP3) or the secretory pathway (GBF1, MON2). Nuclear transport receptors, such as Crm1, have previously been reported to actively sort cytoplasmic proteins from the nucleus (32, 157, 188–191).

The above experiment demonstrates that immobilization of importin 13 on beads and incubation with cell extract is an effective method to fish for importin 13 cargoes. In addition, the above findings suggest that a digitonin cell extract might be more effective in identifying importin 13 interaction partners than a freeze/thaw cell lysate, as with the digitonin cell lysate more proteins could be fished and less unspecific binding was detected. For this reason, the digitonin cell lysate was used in the SILAC based proteomics approach for the identification of importin 13 import and export cargoes (3.3.3). The newly identified proteins were not analyzed in further detail, as the SILAC experiments following in section 3.3.3 were expected to be more conclusive, allowing for the specific discrimination of importin 13 import and export cargoes. However, several of the proteins identified were also detected in the SILAC screen (Table S9), some of which were further characterized by overexpression experiments (3.3.3.4.3).

3.3.2 Identification of Single Importin 13 Bound Proteins Affected by Ubc9 or Enriched from HeLa P4 Cell Extract

A major limitation of the above mass spectrometry approach to identify proteins that bind to importin 13 from a HeLa P4 cell lysate (3.3.1) is that it does not allow for the distinction of importin 13 import and export cargoes. For this reason, binding experiments similar to the previous mass spectrometry experiment were established with the difference of

including Ubc9 (known import cargo) or $RanGTP_{Q69L}$ in the binding reactions. Presence of exogenous $RanGTP_{Q69L}$ was expected to promote the binding of importin 13 export cargoes to importin 13 from a cell extract, while exogenous Ubc9 was expected to compete with both endogenous importin 13 import and export cargoes for binding to importin 13.

Importin 13 binding experiments were optimized using the known export cargo eIF1A and the known import cargo Ubc9 as positive controls for binding of export and import cargoes, respectively. Various binding conditions were tested and optimized, including different binding buffers, protein concentrations, importin 13 fusion tags, cell extract preparation, cell extract amounts as well as different elution conditions. In these preliminary binding experiments, proteins could repeatedly be observed in Coomassie stained gels that were either significantly enriched from the cell lysate or whose binding to importin 13 was affected if Ubc9 or $RanGTP_{Q69L}$ were added to the binding reaction (an example is shown in Figure 15).

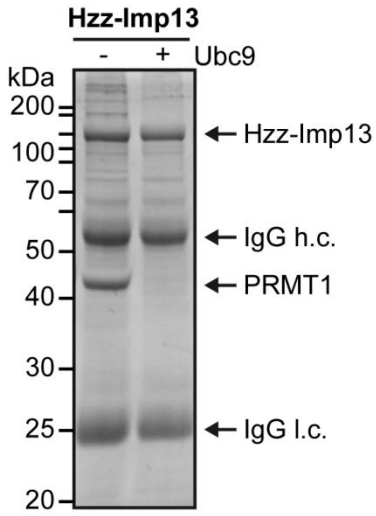

Figure 15: Example of importin 13 bound protein that is reduced in the presence of Ubc9. Hzz-importin 13 (20 µg) was immobilized on IgG-Sepharose and incubated with a digitonin HeLa P4 cell extract in the absence or presence of 5 µg Ubc9 in 20 mM HEPES, pH7.5, 50 mM NaCl, 10% glycerol, 0.01% NP-40 buffer supplemented with 2 mg/mL BSA. Bound proteins were eluted by glycine elution and analyzed by SDS-PAGE, followed by Coomassie staining. PRMT1 was detected in the protein band that was reduced in the presence of Ubc9. l.c.: light chain; h.c.: heavy chain.

Protein bands with altered protein amounts were excised, prepared for mass spectrometry and handed to our collaborators for mass spectrometry analysis. Raw data was analyzed with the Proteome Discoverer against a human protein database. However, in all of the analyzed protein bands, multiple proteins were identified by mass spectrometry, complicating the identification of a key protein. Nonetheless, seven proteins were selected (Table 11) that were in accordance with the expected molecular weight and analyzed in more detail.

Table 11: Importin 13 bound proteins enriched from a HeLa P4 cell extract or affected by exogenous Ubc9 addition[#]

Uniprot ID	Protein Name	Gene	MW [kDa]	Comment[a]	Imp13 co-expression[b]	SILAC[c]
Q9BRQ8	Apoptosis-inducing factor 2	AIFM2	40.5	reduced by Ubc9	-	-
P62140	**Serine/threonine-protein phosphatase PP1-beta catalytic subunit**	PPP1CB	37.2	reduced by Ubc9	++ (export)	import[d] export[d]
O95218	Zinc finger Ran-binding domain-containing protein 2	ZRAB2	37.4	reduced by Ubc9	-	-
E9PKG1	**Protein arginine N-methyltransferase 1**	PRMT1	37.7	reduced by Ubc9	++ (export)	export[e,*]
Q92879	CUGBP Elav-like family member 1	CELF1	52.0	enriched from lysate	++ (export)	-
P60842	**Eukaryotic initiation factor 4A-I**	EIF4A1	46.1	enriched from lysate	+ (import)	import[d]
Q9Y265	**RuvB-like 1**	RUVBL1	50.2	enriched from lysate	+ (import)	import[e]

#: single proteins detected in different binding experiments that were enriched upon HeLa P4 cell lysate addition or affected by Ubc9 addition were analyzed by mass spectrometry. Proteins of the expected size were selected for further analysis. Proteins highlighted in bold were also detected in the SILAC screen (3.3.3), where Ubc9 reduced binding of PPP1CB, PRMT1, RUVBL1 and $RanGTP_{Q69L}$ reduced binding of EIF4A1.

*: PRMT1 was detected in only one of the SILAC biological replicates.

a: single proteins whose binding to importin 13 was strongly enriched from cell lysate or whose binding was reduced in the presence of Ubc9; b: importin 13 effect in FLAG-importin 13 overexpression experiment; c: proteins that later also came up in the SILAC screen as import or export candidates; d: low confidence substrate; e: very low confidence substrate; -: no importin 13 effect; +: weak importin 13 effect; ++: importin 13 effect

For further analysis, proteins were cloned into different vector backbones and expressed as HA- and GFP-GST-fusion constructs in HeLa P4 cells and analyzed for any changes in subcellular localization upon importin 13 coexpression (Figure 16).

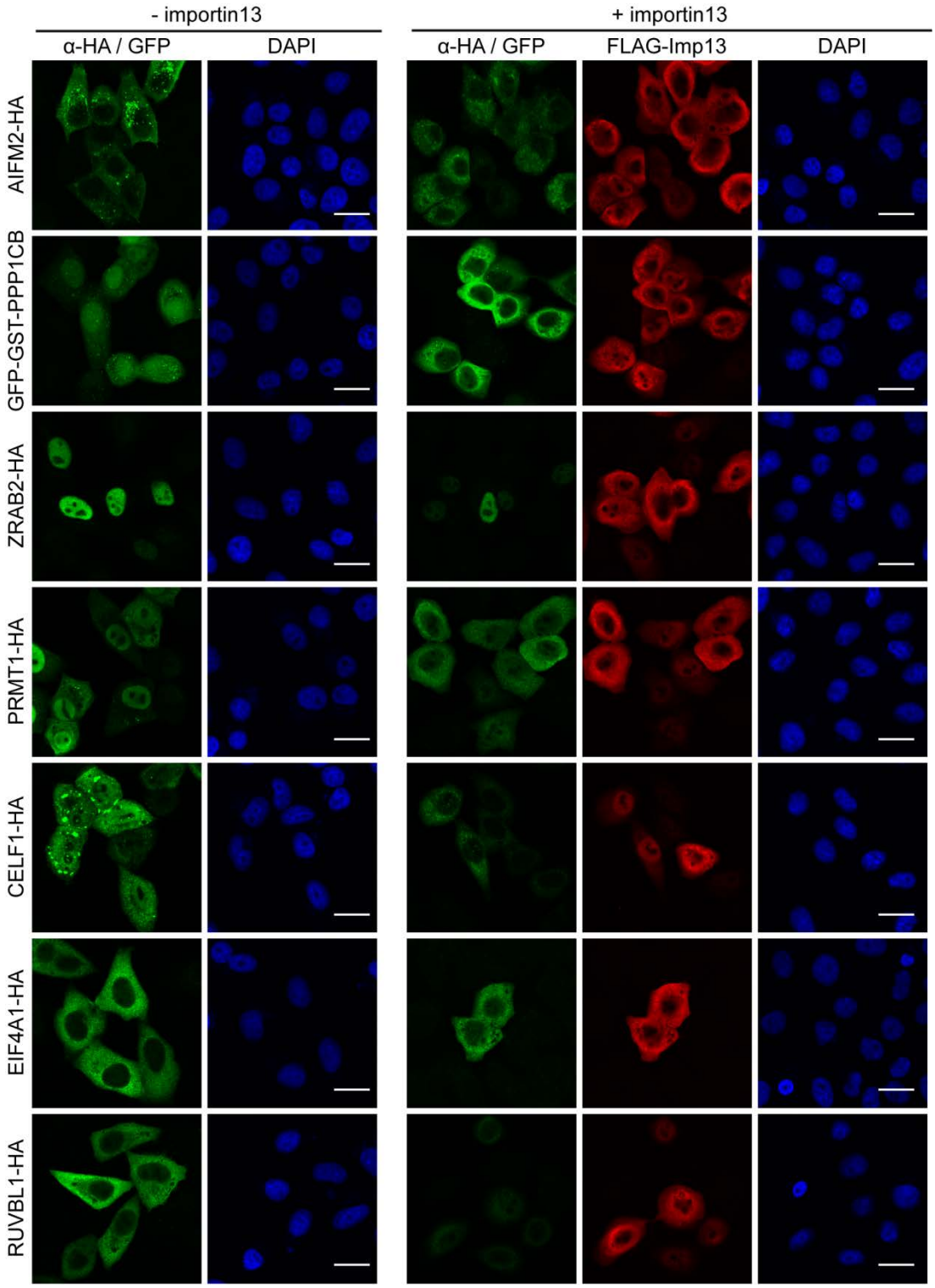

Figure 16: PPP1CB, PRMT1, CELF1, EIF4A1 and RUVBL1 change their subcellular localization upon importin 13 coexpression. HeLa P4 cells were transiently transfected with plasmids coding for HA- or GFP-GST-tagged proteins and optionally cotransfected with plasmids coding for FLAG-importin 13. Proteins were visualized by indirect immunofluorescence with an anti-HA and anti-FLAG antibody. See Table 11 for protein details. The scale bars correspond to 20 µm.

More than half of the proteins analyzed were affected by importin 13 coexpression. PRMT1 and CELF1 showed weak relocalization to the cytoplasm, while EIF4A1 and RUVBL1 showed weak relocalization to the nucleus, making them putative importin 13 export and import cargoes, respectively. Curiously, PPP1CA showed a relocalization to the nucleus if fused to an HA-tag and relocalization to the cytoplasm if fused to a GFP-GST-tag. However, with the exception of PPP1CB an importin 13 effect was only observed if the proteins were fused to a C-terminal HA-tag and not an N-terminal GFP-GST-tag (data not shown). The position and size of the GFP-GST-tag potentially prevent the proteins from interacting with importin 13. PPP1CB, EIF4A1 and RUVBL1 were later also identified as potential importin 13 import cargoes from a HeLa P4 cell lysate in the SILAC screen (3.3.3), albeit as low confidence cargoes.

In summary, PPP1CB, EIF4A1, RUVBL1, PRMT1 and CELF1 were affected by importin 13 overexpression, making them potential importin 13 cargoes. This demonstrates that pull-downs in the presence or absence of $RanGTP_{Q69L}$ or Ubc9 can allow for the specific identification of importin 13 interaction partners. To allow for comparative analysis of proteins bound to importin 13 from a HeLa P4 cell extract in the absence or presence of $RanGTP_{Q69L}$ or Ubc9, the binding experiments were coupled to a quantitative mass spectrometry approach using SILAC (3.3.3).

3.3.3 Quantitative Mass Spectrometry Based Identification of Importin 13 Import and Export Cargoes Using SILAC

As illustrated in section 3.3.1 and 3.3.2 mass spectrometry based importin 13 binding assays are effective methods for the identification of importin 13 interaction partners. However, analysis of HeLa P4 proteome binding to immobilized importin 13 alone does not yield a clear answer to the question of whether a bound protein is a potential importin 13 import or export cargo. As highlighted in section 3.3.2 addition of Ubc9 or $RanGTP_{Q69L}$ to the pull-down reaction can facilitate the specific identification of importin 13 import or export cargoes. To allow for the quantitative comparison of proteins bound to Hzz-importin 13 from a HeLa P4 cell extract in the absence of presence of Ubc9 or $RanGTP_{Q69L}$, triple stable isotope labeling with amino acids in cell culture (SILAC) experiments were performed.

3.3.3.1 Pull-down Based Identification of Potential Importin 13 Cargoes Using SILAC

To get a comprehensive list of importin 13 interaction partners and to allow for the specific distinction of importin 13 import and export cargoes, pull-down assays were performed in the absence or presence of excess $RanGTP_{Q69L}$ or Ubc9 using SILAC (illustrated in Figure 17).

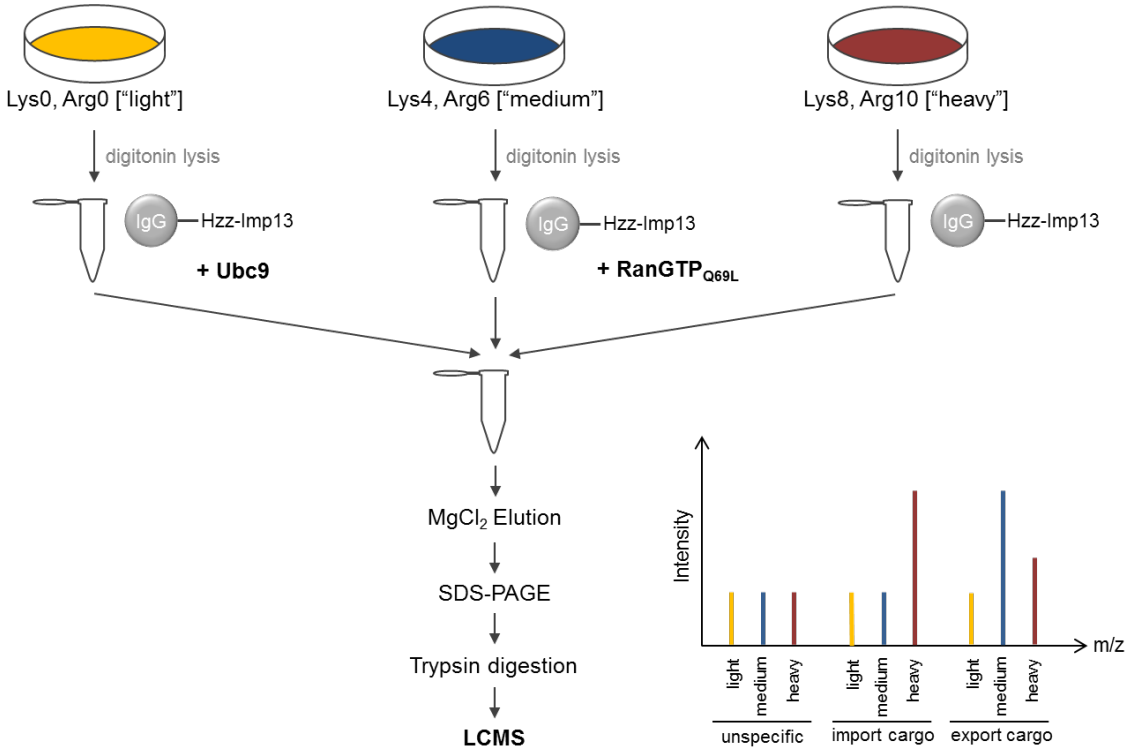

Figure 17: Experimental workflow of SILAC screen. Hzz-tagged importin 13 was immobilized on IgG-Sepharose and incubated with digitonin cell extracts of HeLa P4 cells grown in DMEM medium containing light (Lys0, Arg0), medium (Lys4, Arg6) or heavy (Lys8, Arg10) amino acids. One binding reaction was performed in the presence of cell extract alone, a second reaction was performed in the presence of $RanGTP_{Q69L}$ to favor the binding of importin 13 export cargoes and a third reaction was performed in the presence of Ubc9 to prevent the formation of importin 13 import and export complexes. After binding, all three reactions were pooled and bound proteins were eluted with magnesium chloride and separated by SDS-PAGE. Peptides were extracted by in-gel tryptic digestion, analyzed by liquid chromatography-mass spectrometry and raw data was processed using MaxQuant. The graph in the lower right corner depicts a schematic mass spectrometry output for the above exemplified labeling experiment with each peptide appearing as a triplet with distinct mass differences.

For all three binding reactions, Hzz-importin 13 was immobilized on IgG-Sepharose and incubated with differently labeled HeLa P4 cell extracts (Figure 18A). HeLa P4 cells were isotopically labeled by cultivating them in light, medium or heavy SILAC media that contained unlabeled L-lysine and L-arginine (Lys0, Arg0), 4,4,5,5-D4-L-Lysine and $^{13}C_6$-L-arginine (Lys4, Arg6) or $^{13}C_6{}^{15}N_2$-L-lysine and $^{13}C_6{}^{15}N_4$-L-arginine (Lys8, Arg10), respectively. Cells were lysed with digitonin and precleared with phenyl-Sepharose to selectively deplete endogenous nuclear transport receptors (27), as in previous mass spectrometry experiments (section 3.3.1 and data not shown) other nuclear transport receptors could be detected that likely were pulled out with importin 13 bound nucleoporins. As shown in Figure 18C (see Figure S3C, Figure S4C for label-swap experiments), importin 13, importin β and transportin were effectively removed from the cell extract by preincubation with phenyl-Sepharose. Depletion of these proteins had only minor effects on endogenous importin 13 cargo concentrations as tested for Ubc9 and eIF1A. In addition, the cell lysates were precleared with Hzz-IgG-Sepharose, to remove proteins binding unspecifically to the affinity matrix.

One binding reaction was performed in the presence of the known importin 13 import cargo Ubc9, as Ubc9 binding to importin 13 is expected to prevent the formation of other importin 13 import and export complexes. The importin 13 binding site for Ubc9 overlaps with the binding site for RanGTP, thus Ubc9 added in excess should compete with RanGTP for binding to importin 13 and prevent the formation of importin 13 export complexes. In addition, excess Ubc9 is expected to prevent the formation of importin 13 import complexes by either competing with other import cargoes for the same binding site or by preventing their binding to non-overlapping binding sites due to steric clashes. A second reaction was performed in the presence of $RanGTP_{Q69L}$, a Ran mutant that is impaired in RanGTP hydrolysis and is expected to facilitate the binding of export cargoes and trap them as stable complexes. In the third reaction, no exogenous Ubc9 or $RanGTP_{Q69L}$ but only cell lysate was added, to enrich for importin 13 import complexes. Export complexes are not expected to be enriched, as only RanGDP and not RanGTP should be present in the cell lysate, due to the activity of cytoplasmic RanGAP.

A

SILAC binding reactions:

1. Hzz-importin 13 + light HeLa P4 cell extract (l) + Ubc9
2. Hzz-importin 13 + medium HeLa P4 cell extract (m) + $RanGTP_{Q69L}$
3. Hzz-importin 13 + heavy HeLa P4 cell extract (h)

B

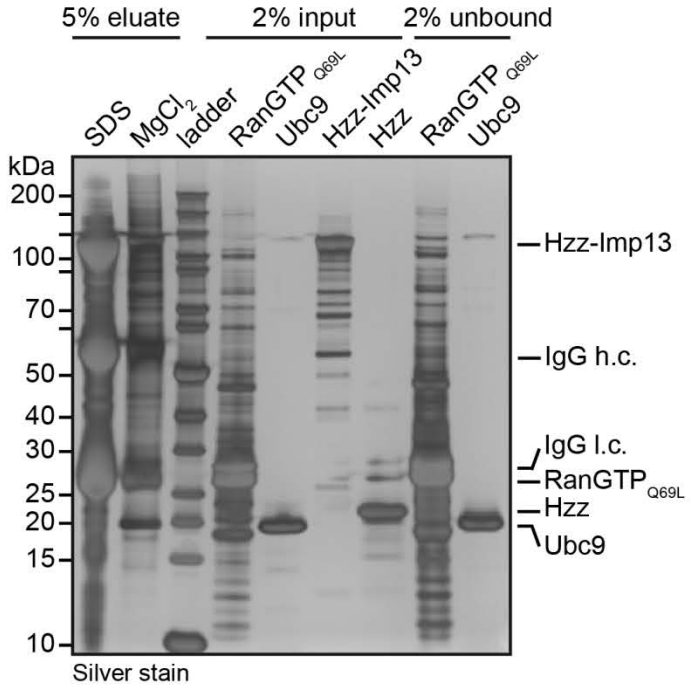

C

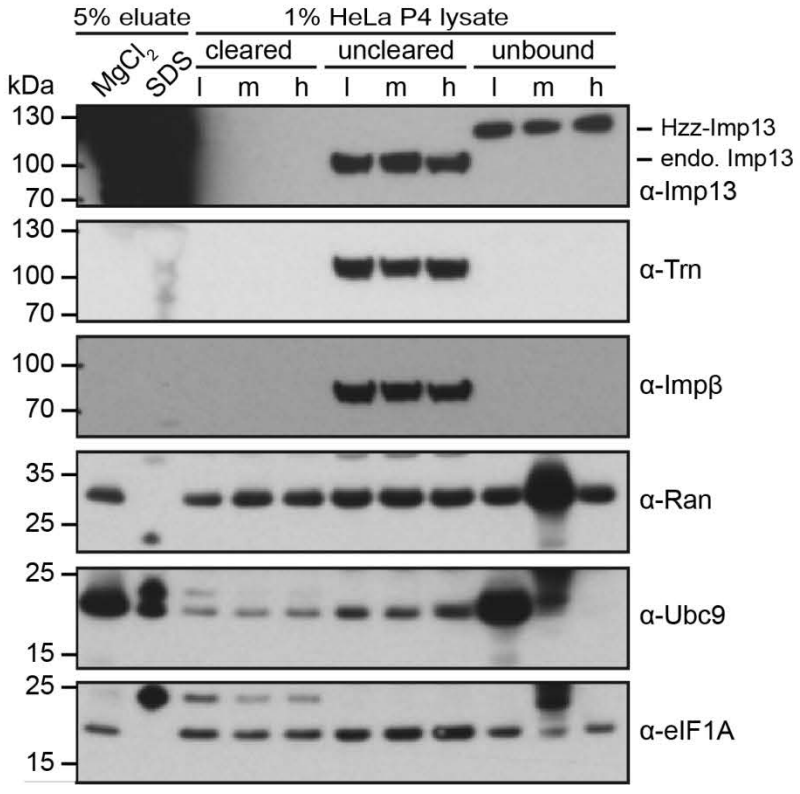

Figure 18: SILAC binding reactions and phenyl-Sepharose depletion of HeLa P4 cell extracts. (A) Schematic showing exemplary SILAC binding reactions. (B, C) Hzz-tagged importin 13 (0.5 nmol) was immobilized on IgG-Sepharose and incubated with cell extracts of HeLa P4 cells grown in DMEM medium containing light, medium or heavy amino acids in the absence or presence of 10 µM $RanGTP_{Q69L}$ or 5 µM Ubc9 in transport buffer. Cell extracts (uncleared) were precleared with Hzz/IgG-Sepharose and phenyl-Sepharose (cleared) to reduce unspecific interactions. Bound proteins were eluted in a first elution step with magnesium chloride, followed by a second elution step with 4x SDS sample buffer. Cell lysates and eluted proteins were separated by SDS-PAGE and analyzed by silver staining (B) or immunoblotting with an anti-importin 13, anti-transportin, anti-importin β, anti-Ran, anti-Ubc9 and anti-eIF1A antibody (C). Note that in the unbound samples free Hzz-importin 13 can be detected as well as exogenous $RanGTP_{Q69L}$ and Ubc9 that were added in excess to the binding reactions with medium and light isotopically labeled cell lysates, respectively. See Figure S3 and Figure S4 for replicate experiments. ladder: PageRuler Unstained Protein Ladder; $MgCl_2$: magnesium chloride eluate; SDS: 4x SDS sample buffer eluate; l: light; m: medium; h: heavy; endog.: endogenous.

To allow for quantitative comparison of the three binding reactions, a triple SILAC experiment was performed using light, medium and heavy isotopically labeled digitonin cell extracts. As the differential labeling of the cells allows for later distinction of each binding reaction by mass spectrometry, the IgG-Sepharose beads from all three binding reactions were pooled for protein elution to ensure homogenous elution of bound proteins with magnesium chloride. Rather mild elution conditions were essential to avoid extensive co-elution of the IgG light and heavy chain of the IgG-Sepharose. Eluted proteins were analyzed by SDS-PAGE, followed by silver staining, which confirmed that multiple proteins had bound to Hzz-importin 13 and that they were sufficiently eluted by magnesium chloride elution (Figure 18B, see Figure S3B and Figure S4B for replicates). Further, Ubc9 and $RanGTP_{Q69L}$ were significantly enriched in the eluate, showing that the recombinant proteins Ubc9 and $RanGTP_{Q69L}$ were functional and had bound efficiently to importin 13. For quantitative mass spectrometry, eluted proteins were separated by SDS-PAGE, followed by peptide extraction using in-gel tryptic digestion and analysis by liquid chromatography-mass spectrometry (LC-MS). LC-MS was performed by the Service Unit LCMS Protein Analytics (Dr. Oliver Valerius and Dr. Kerstin Schmitt), Georg-August-Universität Göttingen. Raw LC-MS data was searched against a human protein database using the MaxQuant software and the MaxQuant output data was analyzed with the Perseus software. For a detailed workflow of the Perseus analysis of importin 13 export and import cargoes see supplemental Table S4 and Table S5, respectively.

3.3.3.2 SILAC Based Importin 13 Pull-downs Selectively Identify Importin 13 Cargoes

Three biological replicates of the SILAC based binding assays were performed including label-swap experiments to increase the specificity of the identified proteins and to exclude experimental bias. In total, 1, 224 proteins were identified by mass spectrometry to bind to Hzz-importin 13 in the triple SILAC experiment. As SILAC is a quantitative approach, differences in protein amounts bound to Hzz-importin 13 in the absence or presence of $RanGTP_{Q69L}$ and Ubc9 can be detected by mass spectrometry. To assess how many proteins are enriched in their binding to importin 13 compared to binding reactions with importin 13 and excess $RanGTP_{Q69L}$ (Imp13/Imp13+Ran) or Ubc9 (Imp13/Imp13+Ubc9), normalized log2 SILAC ratios were calculated for each protein and visualized using scatter plots (Figure 19). The majority of the quantified proteins were distributed around logarithmic fold change values close to zero showing that the bulk part of the identified proteins were not affected by $RanGTP_{Q69L}$ or Ubc9 in their binding to importin 13. However, several proteins could be detected that were enriched several fold for the Imp13/Imp13+Ran ratio and even more for the Imp13/Imp13+Ubc9 ratio, identifying them as possible importin 13 substrates. Furthermore, enrichment was observed for binding reactions in the presence of $RanGTP_{Q69L}$, which is expected to facilitate the formation of importin 13 export complexes. Enrichment could also be observed in the presence of Ubc9, however, these proteins are likely unspecific binding proteins or possibly correspond to Ubc9 interaction partners.

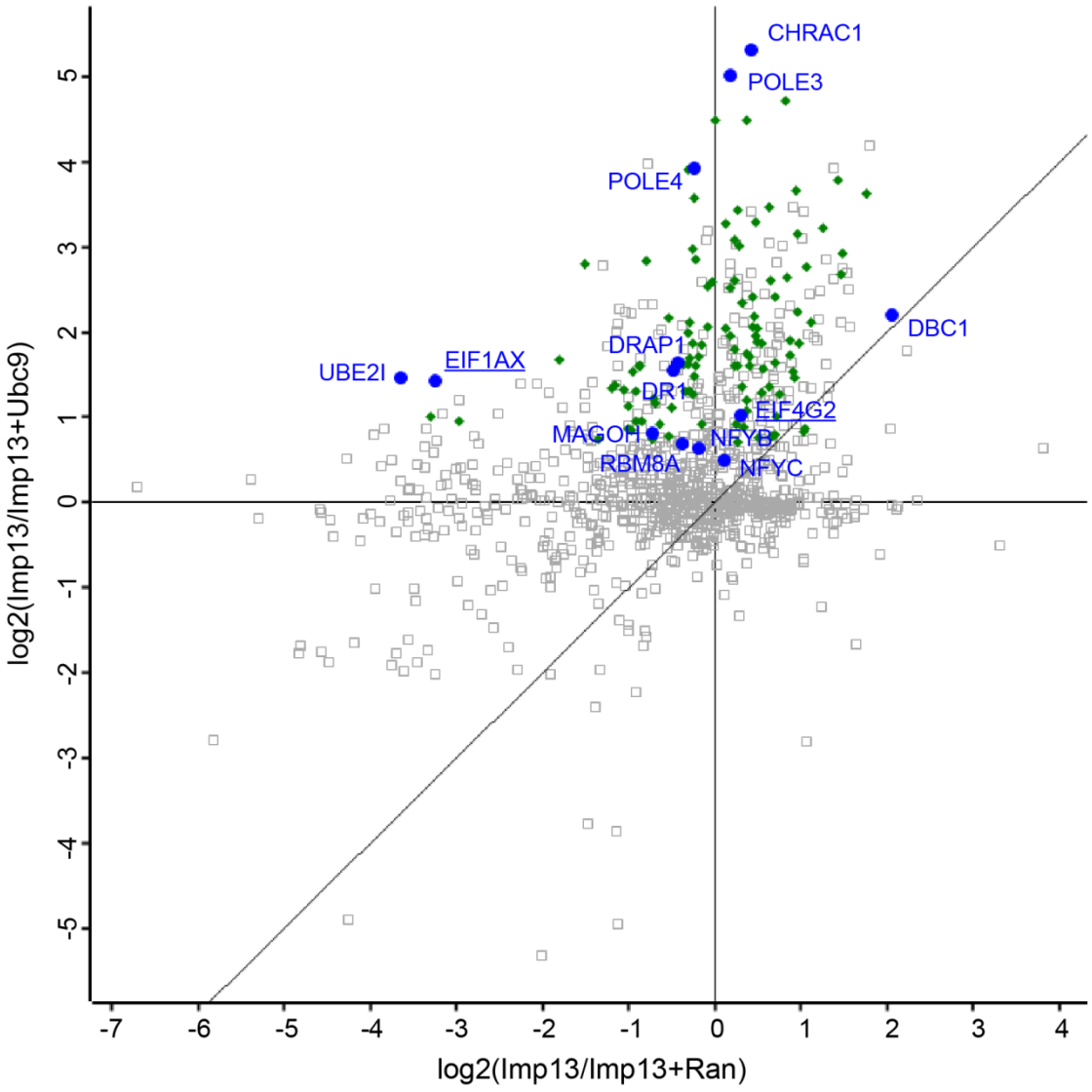

Figure 19: Putative and known importin 13 cargoes identified in SILAC screen (Imp13/Imp13+Ran vs. Imp13/Imp13+Ubc9). All proteins detected (grey squares) in the triple SILAC experiment by mass spectrometry (3.3.3.1) were plotted as log2(Imp13/Imp13+Ubc9) against log2(Imp13/Imp13+Ran) ratios. Ratios were averaged from three SILAC biological replicate experiments. Blue circles: known importin 13 substrates (underlined proteins are known export cargoes, the others are known import cargoes). Green diamonds: proteins detected by mass spectrometry with a log2(Imp13/Imp13+Ubc9) ≥ 0.5 for all three biological replicates. Proteins with an average log2(Imp13/Imp13+Ubc9) ≥ 0.5 that are not depicted in green were quantified with a lower SILAC ratio in at least one of the replicates. Note that the distribution of Ubc9 (UBE2I) is not representative as exogenous unlabeled Ubc9 was present in one of the binding reactions with unlabeled cell lysate and therefore was also quantified by mass spectrometry.

As a first validation of the SILAC based assay, proteins quantified by mass spectrometry were queried for known importin 13 cargoes (Table 1). More than half of the reported cargoes were detected in the SILAC screen (Table 12, Figure 19), proving the utility of the assay for the identification of novel importin 13 substrates. Known importin 13 import cargoes showed a significant enrichment for the Imp13/Imp13+Ubc9 ratio with average log2 SILAC ratios of 0.5 to 5.3 (Table 12, Figure 19). However, with the exception of DBC-1 (KIAA1967), which is only established as an importin 13 binding partner but not as a cargo, no or only minor enrichments for the Imp13/Imp13+Ran ratio could be detected, indicating that the Imp13/Imp13+Ubc9 ratio is more useful for the identification of novel import cargoes than the Imp13/Imp13+Ran ratio. Interestingly, the known heterodimeric importin 13 import cargoes MAGOH/RBM8A, CHRAC1/POLE3, POLE3/POLE4, DRAP1/DR1 and NFYB/NFYC (135, 141, 146, 147) showed a similar enrichment for both subunits of the heterodimer, confirming previous findings that these proteins are imported by importin 13 as heterodimers. While the NFYB/NFYC heterodimer was enriched 1.4-fold with a log2(Imp13/Imp13+Ubc9) ratio of ~0.5, the CHRAC1/POLE3 heterodimer had a log2(Imp13/Imp13+Ubc9) ratio of ~5.2, corresponding to a more than 35-fold enrichment. The subunits of the CHRAC1/POLE3 heterodimer were also the only proteins that showed enrichment for the Imp13/Imp13+Ran ratio with a log2 SILAC ratio of ~1.0. Note that the log2 SILAC ratios for Ubc9 are highly variable but this was to be expected as exogenous unlabeled Ubc9 was present in one of the reactions. In the first SILAC replicate (SILAC1), the unlabeled Ubc9 was added to the light HeLa P4 cell extract and therefore in this sample not only endogenous Ubc9 but also recombinant Ubc9 was measured, resulting in a negative log2(Imp13/Imp13+Ubc9) ratio. Apart from Ubc9 all other proteins showed similar log2 SILAC ratios for all three biological replicates, showing that there is only a low variability between the individual SILAC experiments.

Table 12: Known importin 13 cargoes that were identified in the SILAC screen

Export cargoes												
			log2(Imp13+Ran/Imp13)					log2(Imp13+Ran/Imp13+Ubc9)				
Uniprot_ID	Imp13 interactor	MW [kDa]	SILAC1	SILAC2	SILAC3	Average	-log(p value)*	SILAC1	SILAC2	SILAC3	Average	-log(p value)*
P47813	eIF1A (EIF1A)	16.5	3.26687	3.30372	3.18652	3.25237	4.24736	5.01948	4.67779	4.82963	4.8423	-
P78344	EIF4G2	102.4	-0.422233	-0.416948	-0.0333701	-0.29085	0.03442	-0.242226	0.513976	0.941697	0.404482	-

Import cargoes												
			log2(Imp13/Imp13+Ran)					log2(Imp13/Imp13+Ubc9)				
Uniprot_ID	Imp13 interactor	MW [kDa]	SILAC1	SILAC2	SILAC3	Average	-log(p value)*	SILAC1	SILAC2	SILAC3	Average	-log(p value)*
P63279	UBE2I (Ubc9)	18.0	0.0117819	-4.91737	-6.06226	-3.65595	0.0430585	-4.26446	3.72448	4.94542	1.46848	0.480393
P61326	MAGOH (Mago)	17.2	-1.08381	-0.378907	-0.711086	-0.724602	0.0156264	0.811224	0.665752	0.965643	0.814207	2.25492
F4I9J7	RBM8A (Y14)	19.9	-0.249994	-0.241612	-0.675765	-0.389124	0.0252879	0.773152	0.480539	0.831101	0.694931	1.92964
Q9NRG0	CHRAC1 (CHRAC15)	14.7	0.489029	0.683113	0.0801119	0.417418	1.14478	5.17273	5.3355	5.43066	5.31296	3.99816
Q9NRF9	POLE3 (CHRAC17)	16.9	0.207143	0.297602	0.00201835	0.168921	1.01523	4.47521	5.41648	5.16576	5.01915	2.80557
Q9NR33	POLE4 (p12)	12.2	-0.156965	-0.191327	-0.380935	-0.243075	0.0161895	3.4194	3.88773	4.45267	3.91994	2.54084
P25208	NFYB (NF-YB)	22.8	0.00733906	0.209391	-0.762314	-0.181861	0.155389	0.62938	0.385205	0.91937	0.644652	1.57798
Q13952	NFYC (NF-YC)	50.3	-0.185179	0.126841	0.385707	0.109123	0.540255	0.46069	0.285284	0.732332	0.492769	1.50084
Q14919	DRAP1 (NC2α)	22.4	-0.0442855	-0.266264	-0.993838	-0.434796	0.062666	1.27023	1.68302	1.99166	1.6483	2.10521
Q01658	DR1 (NC2β)	19.4	-0.118335	-0.285108	-1.03673	-0.480059	0.053382	1.21114	1.55211	1.87483	1.54603	2.12448
Q8N163	KIAA1967 (DBC-1)	102.9	2.05196	NaN	NaN	2.05196	0	2.20655	NaN	NaN	2.20655	0

*right sided, one sample t-test (p≤0.01), which tested the hypothesis that the log2 SILAC ratios were not equal to the value zero

As export cargoes are expected to be enriched in binding reactions with $RanGTP_{Q69L}$ (Imp13+Ran) compared to binding reactions without $RanGTP_{Q69L}$ (Imp13) or with Ubc9 (Imp13+Ubc9), the log2(Imp13+Ran/Imp13) ratio was plotted against the log2(Imp13+Ran/Imp13+Ubc9) ratio to also allow for an assessment of the Imp13+Ran/Imp13+Ubc9 ratio (Table 12, Figure 20). The first importin 13 export cargo to be reported was the translation initiation factor eIF1A, suggesting that it is one of the major importin 13 substrates and indeed eIF1A was identified as one of the top hits. It was enriched by more than 20-fold with an average log2 SILAC ratio for Imp13+Ran/Imp13 and Imp13+Ran/Imp13+Ubc9 of 4.2 and 4.8, respectively. Of the two other reported importin 13 export cargoes, EIF4G2 but not HMG20A was identified (Table 12). EIF4G2 was detected with a log2 SILAC ratio between 0.5 to 1.0 for the Imp13+Ran/Imp13+Ubc9 ratio for two of the replicates and a negative value for the third replicate, whereas for the Imp13+Ran/Imp13 ratio no enrichment could be detected. Similar to eIF1A, multiple of the newly identified proteins were enriched for both the Imp13+Ran/Imp13 and the Imp13+Ran/Imp13+Ubc9 ratio, making them promising importin 13 export candidates (Figure 20). Apart from the known export cargoes eIF1A and EIF4G2 also RanBP1 was identified as a high scoring export cargo. RanBP1 can directly bind to RanGTP and together with RanGAP initiates the disassembly of export complexes (58, 59). Consequently, RanBP1 was either indirectly identified through its binding to RanGTP or possibly it is an importin 13 export cargo. In this regard, it has been shown that RanBP1 can be exported by Crm1 (82, 191). This finding suggests that possibly apart from importin 13 export cargoes also RanGTP binding proteins might be identified in the SILAC screen.

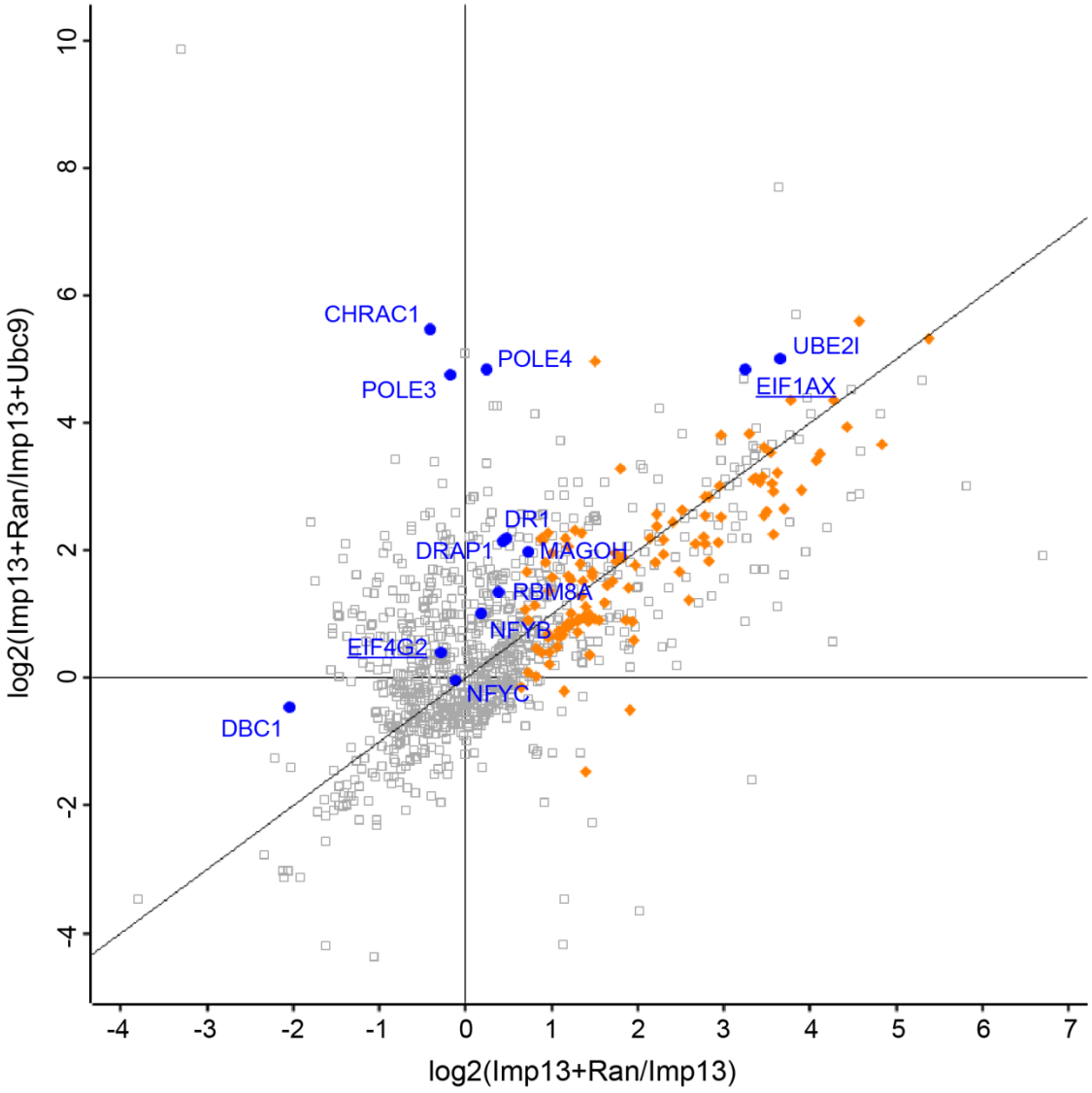

Figure 20: Putative and known importin 13 cargoes identified in SILAC screen (Imp13+Ran/Imp13 vs. Imp13+Ran/Imp13+Ubc9). All proteins detected (grey squares) in the triple SILAC experiment by mass spectrometry were plotted as log2(Imp13+Ran/Imp13+Ubc9) against log2(Imp13+Ran/Imp13) ratios. Ratios were averaged from three SILAC biological replicate experiments. Blue circles: known importin 13 substrates (underlined proteins are known export cargoes, the others are known import cargoes). Orange diamonds: proteins detected by mass spectrometry with a log2(Imp13+Ran/Imp13) ≥ 0.5 for all three biological replicates. Proteins with an average log2(Imp13+Ran/Imp13) ≥ 0.5 that are not depicted in orange were quantified with a lower SILAC ratio in at least one of the replicates. Note that the distribution of Ubc9 (UBE2I) is not representative as exogenous unlabeled Ubc9 was present in one of the binding reactions with unlabeled cell lysate and therefore was also quantified by mass spectrometry.

The above findings demonstrate that the SILAC based assay is an effective method to screen for novel importin 13 substrates, as several known importin 13 cargoes were confirmed to bind to importin 13 in a $RanGTP_{Q69L}$ or Ubc9 sensitive manner, with some even showing a more than 20-fold enrichment. While export cargoes appear to be effectively enriched for both the Imp13+Ran/Imp13 and the Imp13+Ran/Imp13+Ubc9 ratio, known import cargoes were only enriched for the Imp13/Imp13+Ubc9 but not the Imp13/Imp13+Ran ratio. Based on the findings for the known importin 13 cargoes, filtering criteria were generated to group proteins quantified in the SILAC screen into potential importin 13 import and export cargoes (see section 3.3.3.3 for details).

3.3.3.3 Filtering Criteria for the Identification of Importin 13 Import and Export Cargo Candidates

Several filtering criteria were applied on the SILAC data, to allow for the specific identification of importin 13 cargoes. Proteins were only considered to be significantly enriched if they had a normalized log2 SILAC ratio ≥ 0.5 in all three SILAC replicate experiments, which corresponds to an enrichment of minimum 1.4-fold. These filtering criteria were selected based on the previous observations that all known importin 13 cargoes showed a similar enrichment between all three biological replicates with log2 SILAC ratios of minimum 0.5. Additionally, a right-sided, one sample *t*-test with a threshold p-value of ≤ 0.01 was applied, which tested the hypothesis that the log2 SILAC ratios were not equal to the value zero.

All identified known importin 13 cargoes showed enrichment for binding reactions with importin 13 alone compared to binding reaction with importin 13 and excess Ubc9 (Imp13/Imp13+Ubc9) but not compared to binding reactions with excess $RanGTP_{Q69L}$ (Imp13/Imp13+Ran). Thus, quantified proteins were considered to be import cargoes if they showed enrichment for the Imp13/Imp13+Ubc9 ratio. For further validation, proteins were also selected that showed enrichment for Imp13/Imp13+Ran to ensure that potential importin 13 cargoes were not omitted. Using these filtering criteria, a total of 17 proteins were identified as potential importin 13 import cargoes for both ratios, another 22 proteins for Imp13/Imp13+Ran and 102 proteins for Imp13/Imp13+Ubc9 (Table S6). Of the 102 proteins identified for Imp13/Imp13+Ubc9, 16 proteins also showed enrichment for Imp13+Ran/Imp13 and consequently were considered to be ambiguous cargoes (Table S7). As importin 13 can bind its export cargo eIF1A also in the absence of RanGTP in a non-cooperative manner, some export cargoes are likely also enriched for the

Imp13/Imp13+Ubc9 ratio, qualifying the majority of the ambiguous proteins as potential export cargoes.

As the established importin 13 export cargo eIF1A showed strong enrichment for both the Imp13+Ran/Imp13 and the Imp13+Ran/Imp13+Ubc9 ratio, quantified proteins were considered to be potential export cargoes if enriched for either of these ratios. As the majority of the quantified proteins showed a similar enrichment for both ratios, the mass spectrometry data was analyzed by filtering for Imp13+Ran/Imp13. Using these filtering criteria a total of 113 proteins were identified as potential importin 13 export cargoes, 21 of which had a log2(Imp13+Ran/Imp13) ≥ 3.0 and 36 of which had a log2(Imp13+Ran/Imp13) ≥ 1.5 (Table S8).

Based on these filtering criteria, the identified cargo candidates were compared with proteins identified in the previous mass spectrometry experiment (3.3.1). In total 66 proteins were detected for both approaches, 19 of which were identified as potential export cargoes and 47 as potential import cargoes (Table S9). The proteins identified in the SILAC screen were also compared with the proteins identified in the importin 13 overexpression screen (see section 3.2). However, there was no overlap between the two screens, except for DBC-1 (KIAA1967), which was identified in one of the three SILAC experiments (Table 12). In this one replicate it was present with a high log2 SILAC ratio of more than two for both the Imp13/Imp13+Ran and the Imp13/Imp13+Ubc9 ratio, implicating it as an importin 13 import and not an export cargo as suggested by the overexpression screen. Finally, the identified proteins were also compared with previous screens for importin 13 cargoes. In a SILAC-based transport (SILAC-Tp) system (76), 309 proteins were identified as potential importin 13 cargoes (using their 2nd-Z-ranking filtering criteria), some of which were validated in bead halo assays but not all. Of these, 28 were also identified in the SILAC screen presented here (Table S10). In a yeast two-hybrid screen for interactors of the testis-specific form of importin 13 (136), 26 proteins were identified, two of which, EIF4G2 and CLASP1, were also identified in this study.

For additional validation of the SILAC screen, several of the quantified proteins were selected for further analysis based on the above filtering criteria and validated using pull-down experiments and importin 13 overexpression experiments (see section 3.3.3.4).

3.3.3.4 Validation of Importin 13 Cargo Candidates Identified in SILAC Screen

3.3.3.4.1 Selection of Importin 13 Cargo Candidates for Further Analysis

Having confirmed that the SILAC screen allowed for the effective identification of known importin 13 substrates, the next step was to verify other identified candidates as importin 13 cargoes. For this, proteins with varying levels of significance were selected, to get an idea with which filtering criteria high confidence importin 13 cargoes can be identified. Export cargoes were grouped into three categories based on their log2 (Imp13+Ran/Imp13) ratio, namely log2 ratios ≥ 0.5, ≥ 1.5 and ≥ 3.0 (Table 13, Figure 21). For importin 13 import cargoes, proteins were selected based on their Imp13/Imp13+Ran and Imp13/Imp13+Ubc9 ratio, as a high variability between these two groups could be observed (Table 14, Figure 22). Proteins enriched for both or only one of the two ratios and showing different log2 SILAC ratios were chosen. In addition, proteins were selected that showed a good enrichment for both ratios but were only detected in two out of three SILAC experimental replicates.

Additional selection criteria were the size of the proteins (<100 kDa) to facilitate cloning from cDNA as well as available information on function and subcellular location of these proteins. Further, proteins known to form heterodimers or larger complexes were selected, as importin 13 has been reported to mediate the transport of several heterodimers but not their individual subunits (135, 141, 146, 147).

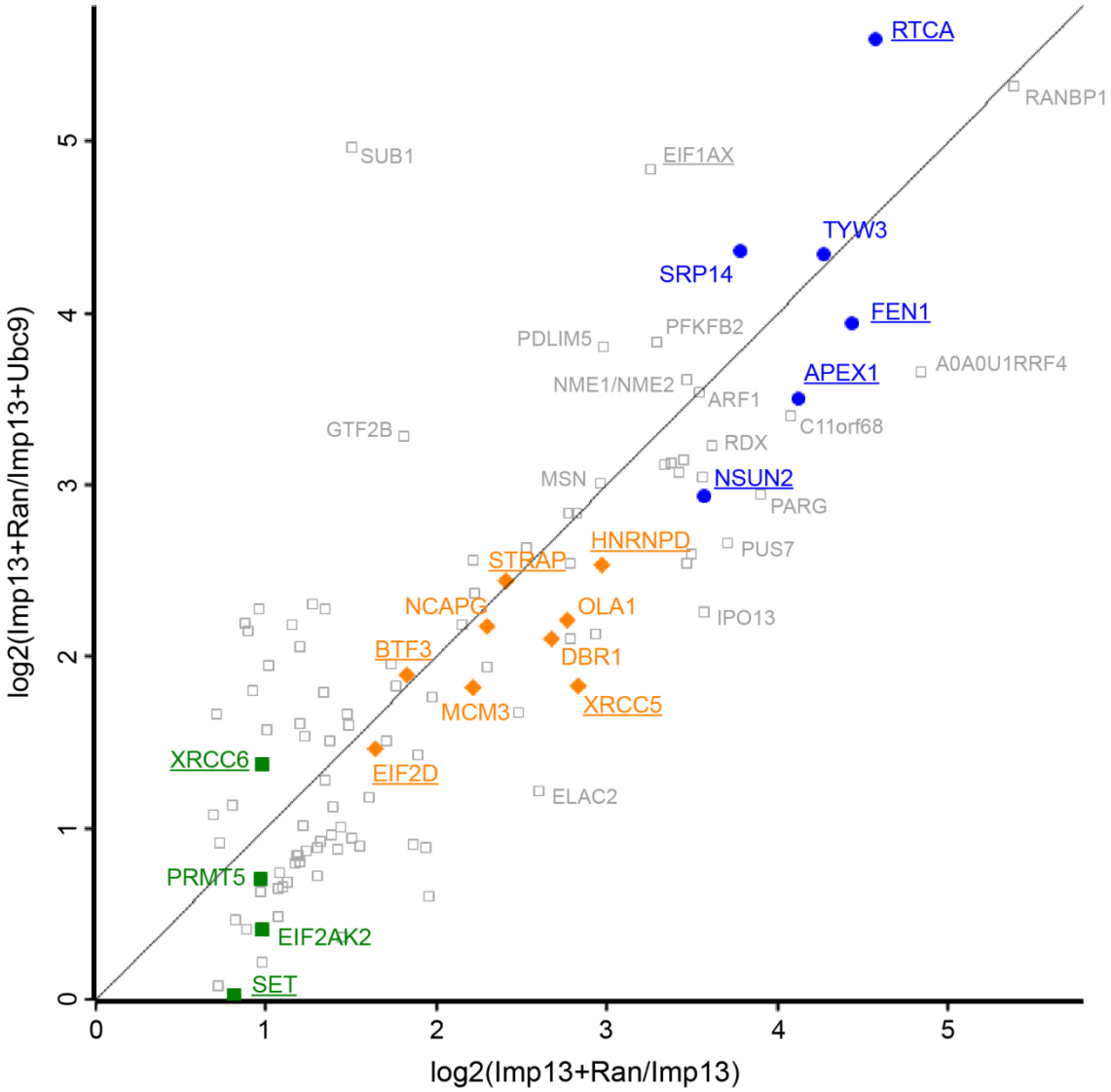

Figure 21: Importin 13 export candidates selected for further validation. All proteins detected by mass spectrometry with a log2(Imp13+Ran/Imp13) ≥ 0.5 (grey squares) for all three biological replicates (3.3.3.1) were plotted as log2(Imp13+Ran/Imp13+Ubc9) against log2(Imp13+Ran/Imp13) ratios. Proteins highlighted in color were selected for further analysis and underlined proteins were affected by importin 13 overexpression. Blue circles: proteins with an average log2(Imp13+Ran/Imp13) ≥ 3.0. Orange diamonds: proteins with an average log2(Imp13+Ran/Imp13) ≥ 1.5. Green squares: proteins with an average log2(Imp13+Ran/Imp13) ≥ 0.5. Grey squares: importin 13 export candidates that were not analyzed further, high scoring proteins were labeled with their gene name. Note that WDR77, which was selected for further testing is not shown as in two replicates it was present with a log2(Imp13+Ran/Imp13) < 0.5. See Table 13 for more details.

Table 13: List of potential importin 13 export cargoes identified in SILAC screen that were selected for further validation

Potential importin 13 export cargoes						
Uniprot ID	**Protein Name**	**Gene**	**log2(Imp13+Ran/Imp13)**	**log2(Imp13+Ran/Imp13+Ubc9)**	**-log(p value)**	**Imp13 pull-down[a]**
Proteins identified for Imp13+Ran/Imp13						
		log2(Imp13+Ran/Imp13) ≥ 3				
O00442	RNA 3-terminal phosphate cyclase	RTCA	4.57597	5.59694	2.50708	-
P39748	Flap endonuclease 1	FEN1	4.43566	3.9402	1.84603	-
Q6IPR3	tRNA wybutosine-synthesizing protein 3 homolog	TYW3	4.26835	4.34712	2.42506	
P27695	DNA-(apurinic or apyrimidinic site) lyase	APEX1	4.12269	3.50792	2.09237	-
P37108	Signal recognition particle 14 kDa protein	SRP14	3.77885	4.36023	3.05751	bound with RanGTP
Q08J23	tRNA (cytosine(34)-C(5))-methyltransferase	NSUN2	3.56745	2.93758	2.29027	-
		log2(Imp13+Ran/Imp13) ≥ 1.5				
H0YA96	Heterogeneous nuclear ribonucleoprotein D0	HNRNPD	2.96732	2.53505	2.24646	
P13010	X-ray repair cross-complementing protein 5	XRCC5	2.82663	1.82907	2.72781	
Q9NTK5	Obg-like ATPase 1	OLA1	2.76445	2.21738	3.92603	bound with RanGTP
Q9Y3F4	Serine-threonine kinase receptor-associated protein	STRAP	2.40696	2.44099	1.68925	-
Q9BPX3	Condensin complex subunit 3	NCAPG	2.29883	2.17429	2.48105	-
Q9UK59	Lariat debranching enzyme	DBR1	2.6774	2.10752	2.66408	
P25205	DNA replication licensing factor MCM3	MCM3	2.2095	1.8214	2.44116	
P20290	Transcription factor BTF3	BTF3	1.82755	1.8911	1.59095	
P41214	Eukaryotic translation initiation factor 2D	EIF2D	1.63737	1.46164	1.72077	
		log2(Imp13+Ran/Imp13) ≥ 0.5				
P12956	X-ray repair cross-complementing protein 6	XRCC6	0.977419	1.37652	1.40745	
P19525	Interferon-induced, double-stranded RNA-activated protein kinase	EIF2AK2	0.97668	0.410077	2.54683	
O14744	Protein arginine N-methyltransferase 5	PRMT5	0.967085	0.708434	1.96941	
Q9BQA1	Methylosome protein 50	WDR77	0.946335	0.381559	1.04849	bound with RanGTP
Q01105	Protein SET	SET	0.81555	0.0277848	2.56819	
Export control						
P47813	Eukaryotic translation initiation factor 1A	EIF1A	3.25237	4.8423	4.24736	bound with RanGTP

a: Protein binding from digitonin HeLa P4 cell lysate to Hzz-importin 13 immobilized on IgG-Sepharose

-: tested in importin13 pull-down but no binding detected

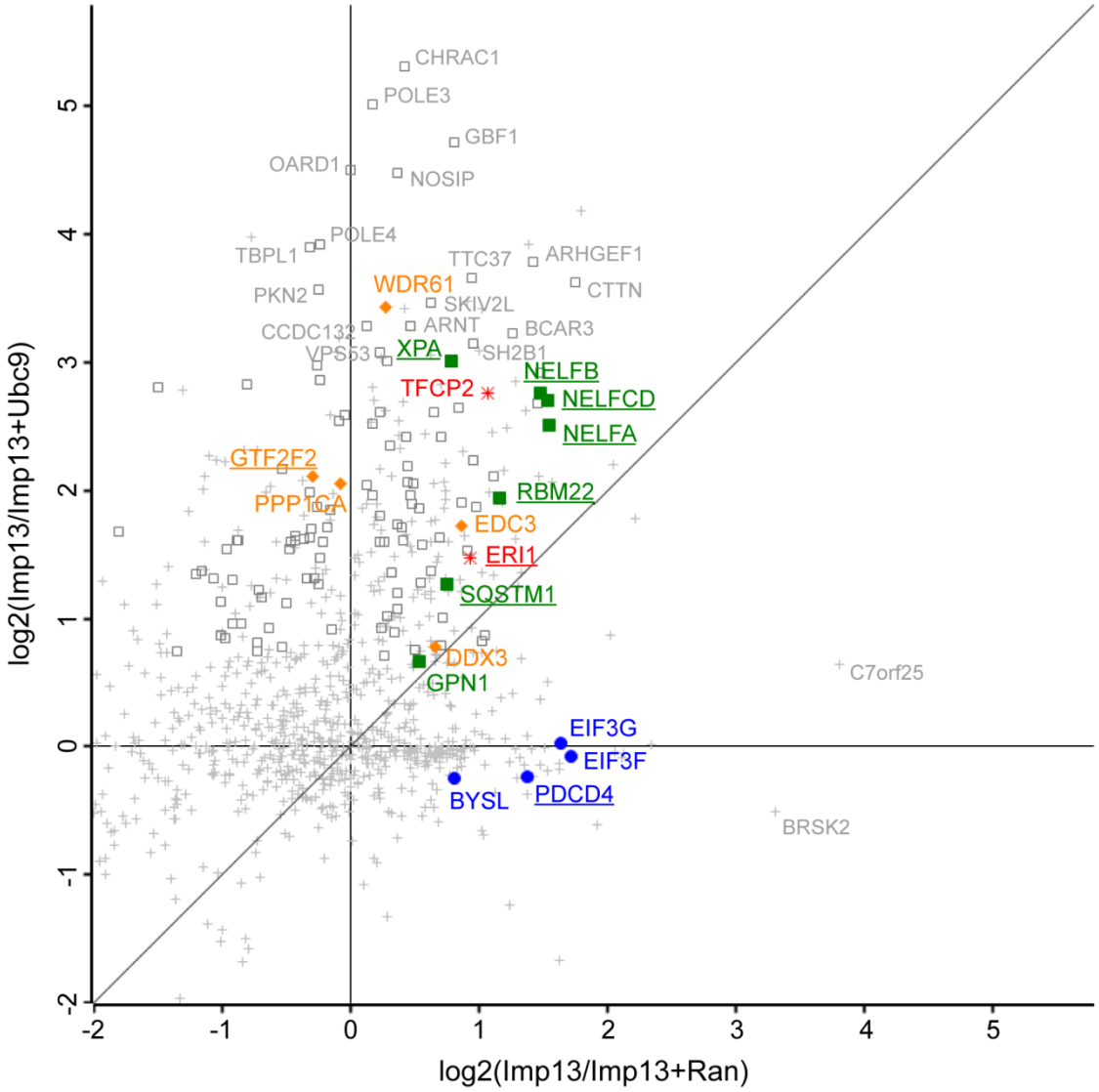

Figure 22: Importin 13 import candidates selected for further validation All proteins detected by mass spectrometry (grey cross) in the triple SILAC experiment (3.3.3.1) were plotted as log2(Imp13/Imp13+Ubc9) against log2(Imp13/Imp13+Ran) ratios. Ratios were averaged from three SILAC biological replicate experiments. Proteins highlighted in color were selected for further analysis and underlined proteins were affected by importin 13 overexpression. Red stars: proteins enriched for Imp13/Imp13+Ran and Imp13/Imp13+Ubc9. Blue circles: proteins enriched only for Imp13/Imp13+Ran. Orange diamonds: proteins enriched only for Imp13/Imp13+Ubc9. Green squares: proteins enriched for Imp13/Imp13+Ran and Imp13/Imp13+Ubc9 in two out of three SILAC replicates. Grey squares: proteins detected with a log2(Imp13/Imp13+Ubc9) ≥ 0.5 for all three SILAC biological replicates. See Table 14 for more details.

Table 14: List of potential importin 13 import cargoes identified in SILAC screen that were selected for further validation

Potential importin 13 import cargoes						
Uniprot ID	**Protein Name**	**Gene**	**log2(Imp13/Imp13+Ran)**	**log2(Imp13/Imp13+Ubc9)**	**-log(p value)**	**Imp13 pull-down[a]**
Proteins identified for Imp13/Imp13+Ran & Imp13/Imp13+Ubc9						
Q12800	Alpha-globin transcription factor CP2	TFCP2	1.06516	2.75921	2.5538	
Q8IV48	3-5 exoribonuclease 1	ERI1	0.93069	1.46739	3.46771	reduced by Ubc9 & RanGTP
Proteins identified for Imp13/Imp13+Ran						
O00303	Eukaryotic translation initiation factor 3 subunit F	EIF3F	1.71919	-0.0768488	1.84627	
O75821	Eukaryotic translation initiation factor 3 subunit G	EIF3G	1.63573	0.0269878	1.74379	
Q53EL6	Programmed cell death protein 4	PDCD4	1.38179	-0.239508	1.9684	
Q13895	Bystin	BYSL	0.812382	-0.246966	2.6437	
Proteins identified for Imp13/Imp13+Ubc9						
Q9GZS3	WD repeat-containing protein 61	WDR61	0.269134	3.43407	2.461	reduced by Ubc9 & RanGTP
P13984	General transcription factor IIF subunit 2	GTF2F2	-0.29533	2.1155	2.8392	
P62136	Serine/threonine-protein phosphatase PP1-alpha catalytic subunit	PPP1CA	-0.0792858	2.05476	2.28248	
Q96F86	Enhancer of mRNA-decapping protein 3	EDC3	0.867101	1.72773	2.35559	reduced by Ubc9 & RanGTP
O00571	ATP-dependent RNA helicase DDX3X/DDX3Y	DDX3	0.664858	0.780721	1.90872	
Proteins identified for Imp13/Imp13+Ran & Imp13/Imp13+Ubc9 for two out of three SILAC experiments						
F2Z2T2	DNA repair protein complementing XP-A cells	XPA	0.783184	3.01102	1.51456	
Q9HCN4	GPN-loop GTPase 1	GPN1	0.535254	0.668491	2.6656	
Q13501	Sequestosome-1	SQSTM1	0.755231	1.26888	2.83389	
Q9NW64	Pre-mRNA-splicing factor RBM22	RBM22	1.15759	1.93592	2.33561	
Q9H3P2	Negative elongation factor A	NELFA	1.54779	2.50404	2.54973	
Q8WX92	Negative elongation factor B	NELFB	1.47736	2.75735	2.2666	
Q8IXH7	Negative elongation factor C/D	NELFCD	1.54033	2.70383	2.29508	
Import control						
P63279	SUMO-conjugating enzyme UBC9	UBE2I	-3.65595*	1.46848*	0.480393*	reduced by RanGTP

a: Protein binding from digitonin HeLa P4 cell lysate to Hzz-importin 13 immobilized on IgG-Sepharose

*: recombinant unlabeled Ubc9 was added to the "light" cell extract, resulting in a not meaningful ratio

3.3.3.4.2 Validation of Importin 13 Cargo Candidates Using Pull-down Experiments

As the identified importin 13 cargo candidates were differently regulated by Ubc9 or $RanGTP_{Q69L}$, the binding experiments were repeated without SILAC and analyzed by immunoblotting using commercially available antibodies. To this end, Hzz-importin 13 was immobilized on IgG-Sepharose and incubated with unlabeled digitonin HeLa P4 cell lysate in the absence or presence of Ubc9 or $RanGTP_{Q69L}$. Beads were not pooled as in the SILAC experiment but instead bound proteins were eluted separately with magnesium chloride. Eluates were separated by SDS-PAGE and immunoblotted with antibodies targeted against the potential importin 13 substrates (Figure 23). The known importin 13 export cargo eIF1A was used as a control and indeed eIF1A bound in the presence of $RanGTP_{Q69L}$ but not Ubc9 and showed reduced binding in the absence of both.

Not for all proteins analyzed binding to immobilized importin 13 could be detected. This could be due to unspecific antibodies, low endogenous protein levels or proportionally less protein binding to importin 13 compared to the other proteins. Of seven export cargo candidates (APEX1, FEN1, STRAP, NSUN2, WDR77, OLA1, SRP14) tested, OLA1, WDR77 and SRP14 were bound to Hzz-importin 13 and as expected for *bona fide* export cargoes binding of OLA1 and WDR77 only occurred in the presence of $RanGTP_{Q69L}$. SRP14, similarly to eIF1A, showed binding to importin 13 both in the presence and absence of $RanGTP_{Q69L}$ but not in the presence of Ubc9. All import cargoes tested, namely ERI1, WDR61 and EDC3 bound to importin 13 and binding was abolished in the presence of Ubc9 or $RanGTP_{Q69L}$.

In summary, OLA1, WDR77 and SRP14 bound to importin 13 in the presence of RanGTP, validating them as potential export cargoes, while ERI1, WDR61 and EDC3 bound to importin 13 only in the absence of Ubc9 or $RanGTP_{Q69L}$, validating them as potential import cargoes.

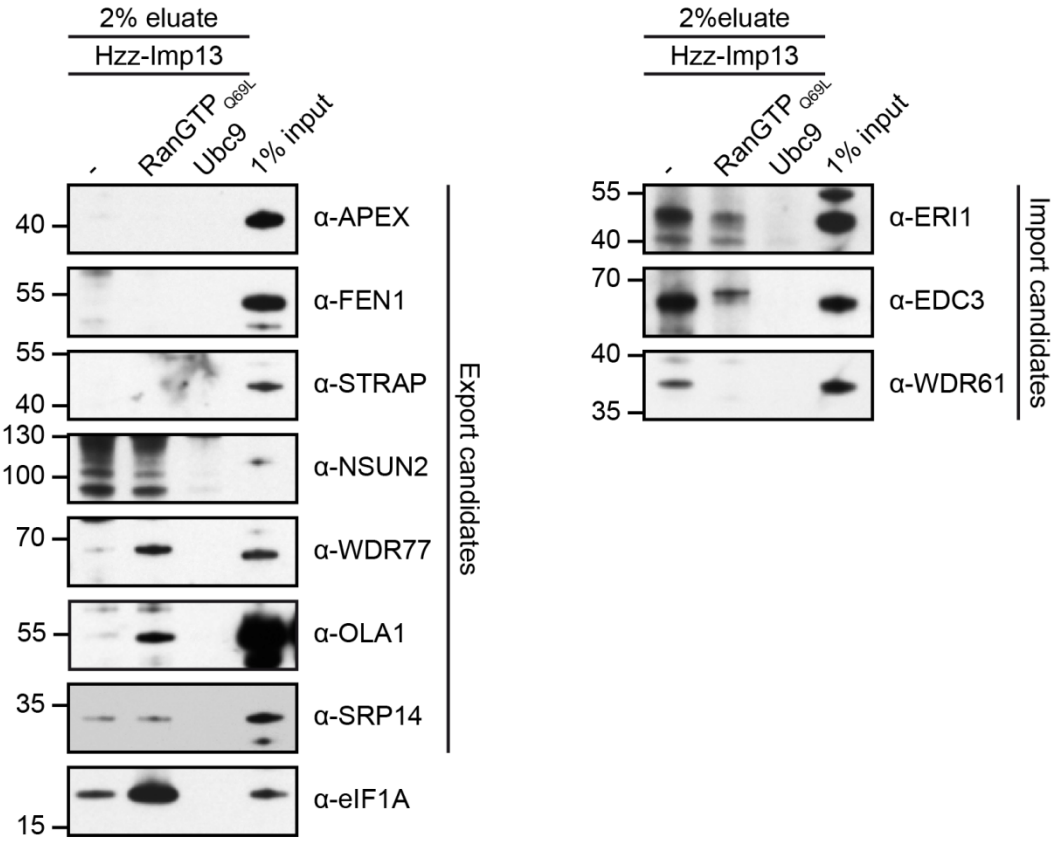

Figure 23: Endogenous SILAC candidate proteins that bind to importin 13 from HeLa P4 cell extract in a RanGTP$_{Q69L}$ or Ubc9 dependent manner. Hzz-tagged importin 13 (0.5 nmol) was immobilized on IgG-Sepharose and incubated with a digitonin HeLa P4 cell extract precleared with Hzz/IgG-Sepharose and phenyl-Sepharose in the absence or presence of 10 µM RanGTP$_{Q69L}$ or 5 µM Ubc9 in transport buffer. Bound proteins were eluted by magnesium chloride elution, separated by SDS-PAGE and analyzed by immunoblotting.

3.3.3.4.3 Validation of Importin 13 Cargo Candidates in Overexpression Experiments

For further validation of the SILAC screen, the identified importin 13 cargo candidates were tested in importin 13 overexpression experiments. For this, 36 cargo candidates were cloned as C-terminal HA-fusion constructs and 34 as N-terminal GFP-GST-fusion constructs. Cargoes were fused to a GFP-GST-tag to significantly increase their size and prevent their passive diffusion through the NPC. Generated plasmids were expressed in HeLa P4 cells and analyzed for any changes in subcellular localization upon coexpression of FLAG-importin 13. GFP-GST-Ubc9 and eIF1A-GFP were included as positive controls (see section 3.1.3), while dGFP-GST-cNLS was included as a negative control (see section 3.2.1) of importin 13 mediated transport.

Of 18 import cargo candidates tested (Figure 24 (HA-tagged), Figure 25 (GFP-GST-tagged), Table 15), 6 proteins, namely BYSL, PDCD4, GTF2F2, XPA, RBM22 and NELFA, fused to an HA-tag already exhibited a nuclear localization in the absence of importin 13, precluding the identification of an importin 13 mediated nuclear localization. Proteins from all four filtering groups (Imp13/Imp13+Ran, Imp13/Imp13+Ubc9, as well as both ratios with proteins identified in two or three of the SILAC experiments) were affected by importin 13 overexpression. ERI1 and NELFCD, which showed a strong enrichment for the Imp13/Imp13+Ran and the Imp13/Imp13+Ubc9 ratio, were both relocalized to the nucleus if importin 13 was coexpressed, validating them as import cargo candidates. Surprisingly, PDCD4, WDR61, GTF2F2, XPA, SQSTM1 (only in the presence of LMB, details follow below), RBM22 and NELFA were not relocalized to the nucleus upon importin 13 coexpression but instead to the cytoplasm. Of these, GTF2F2 showed a slight enrichment for the Imp13+Ran/Imp13 ratio designating it as a possible importin 13 export cargo. As mentioned earlier, the export cargo eIF1A has been demonstrated to bind effectively to importin 13 also in the absence of RanGTP, thus cargo candidates enriched for the Imp13/Imp13+Ubc9 ratio could also correspond to export cargo candidates. For the other proteins, importin 13 could function as a negative regulator of nuclear import, as reported for the testis-specific form of importin 13 (136), or an additional factor or modification is required to facilitate their importin 13-dependent nuclear import. Note that some of the proteins were only affected by importin 13 overexpression if fused to either the HA- or the GFP-GST-tag, suggesting that the fusion tag size and position can affect the interaction with importin 13. Observed importin 13 effects were independent of the FLAG-fusion tag, as untagged importin 13 had the same effect on the subcellular localization of both import and export cargo candidates as FLAG-tagged importin 13 (Figure S5).

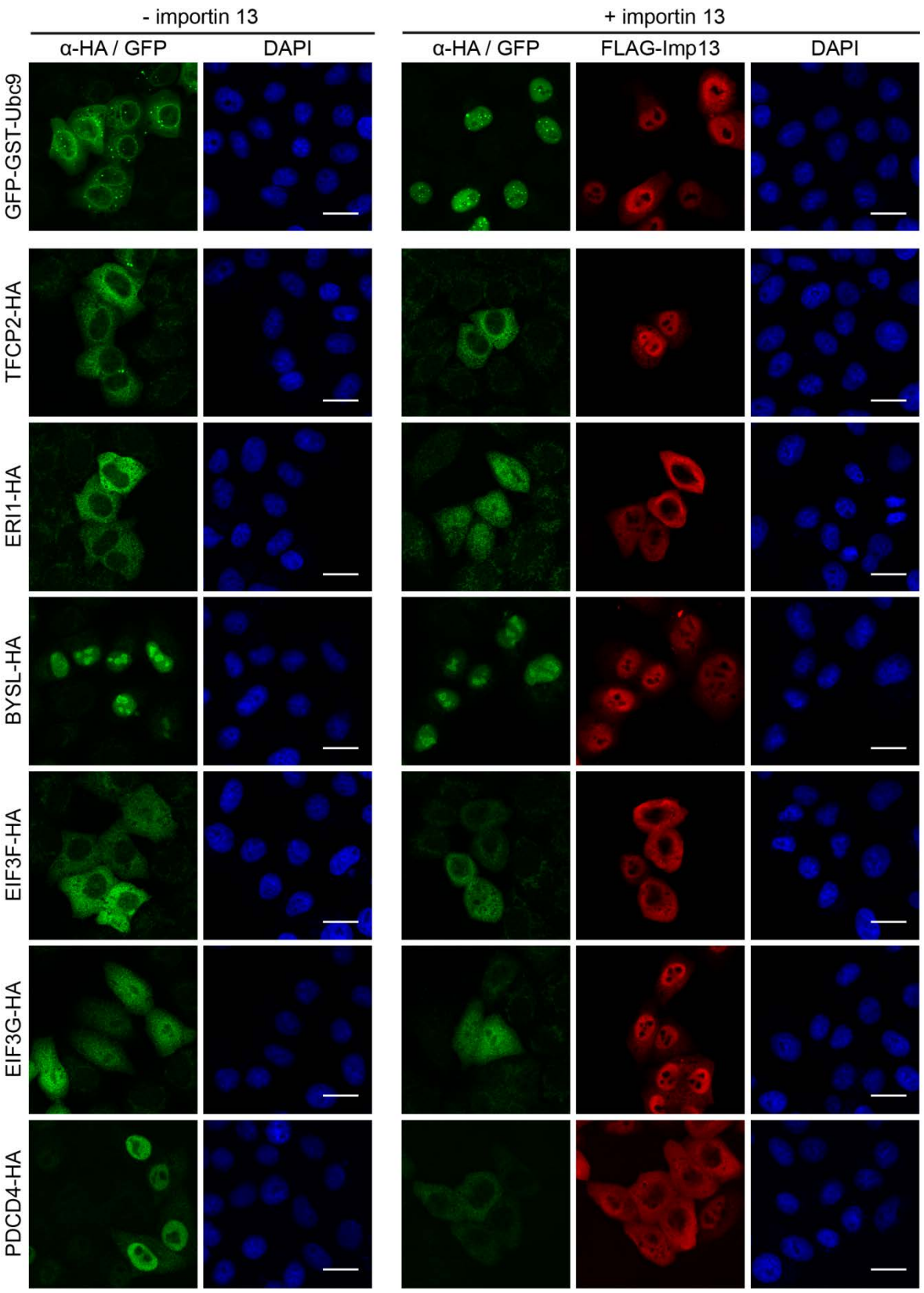
- importin 13
+ importin 13
α-HA / GFP
DAPI
α-HA / GFP
FLAG-Imp13
DAPI
GFP-GST-Ubc9
TFCP2-HA
ERI1-HA
BYSL-HA
EIF3F-HA
EIF3G-HA
PDCD4-HA

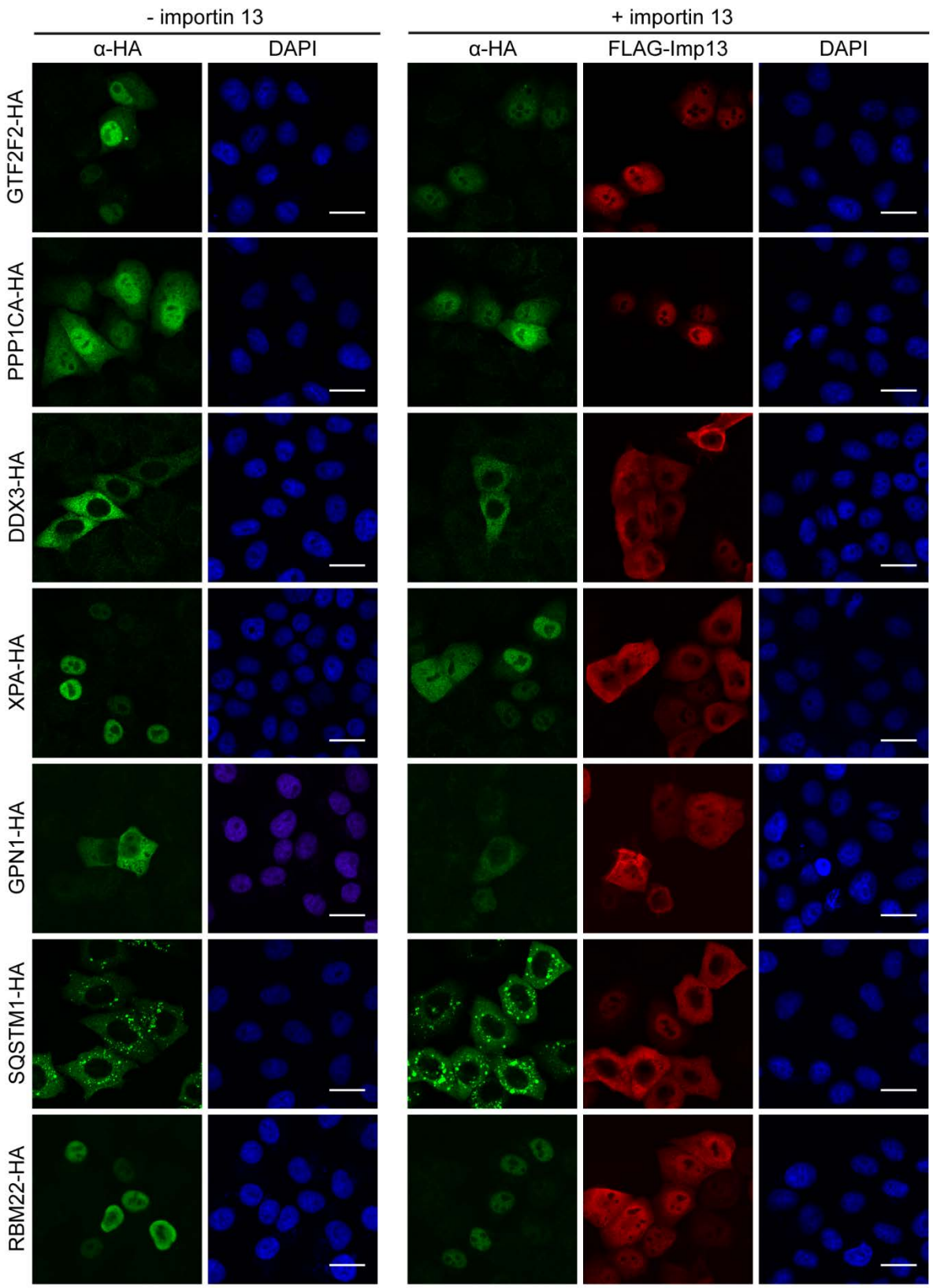
- importin 13
+ importin 13
α-HA
DAPI
α-HA
FLAG-Imp13
DAPI
GTF2F2-HA
PPP1CA-HA
DDX3-HA
XPA-HA
GPN1-HA
SQSTM1-HA
RBM22-HA

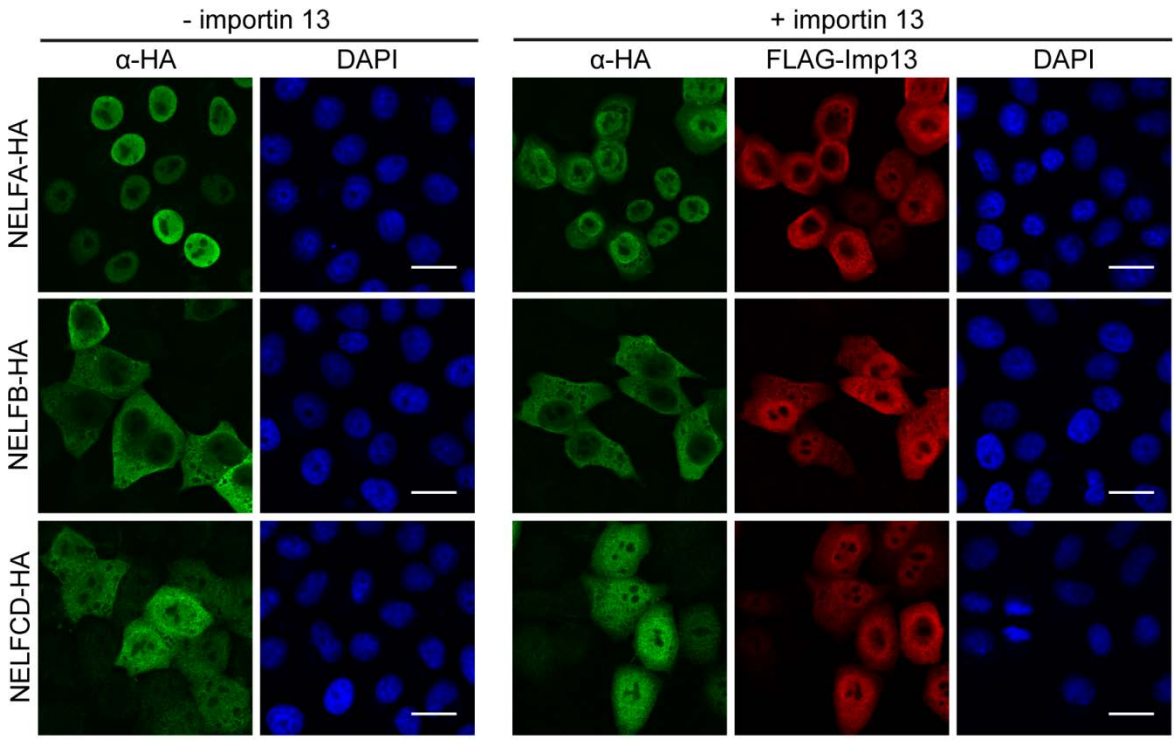

Figure 24: Effect of FLAG-importin 13 overexpression on subcellular localization of HA-tagged SILAC import cargo candidates. HeLa P4 cells were transiently cotransfected with plasmids coding for HA-tagged proteins form the SILAC screen and FLAG-importin 13 or an empty control vector (pcDNA3.1-HA) using the calcium phosphate method. FLAG-importin 13 and HA-substrates were visualized by indirect immunofluorescence with an anti-FLAG and anti-HA antibody, respectively. See Table 15 for summary of importin 13 effect. The scale bars correspond to 20 µm. DDX3, XPA and SQSTM1 were tested by Christiane Spillner.

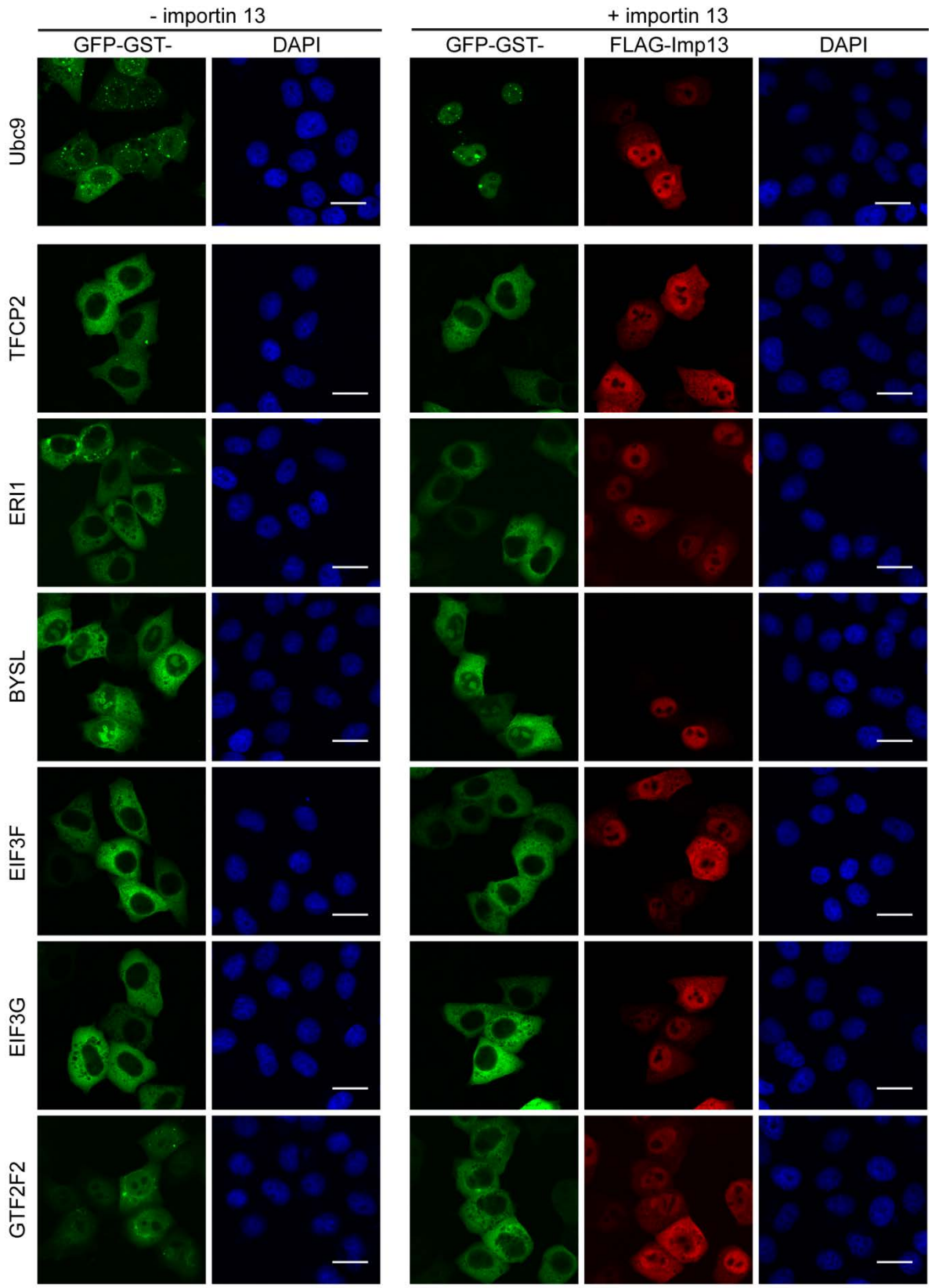
- importin 13
+ importin 13
GFP-GST-
DAPI
GFP-GST-
FLAG-Imp13
DAPI
Ubc9
TFCP2
ERI1
BYSL
EIF3F
EIF3G
GTF2F2

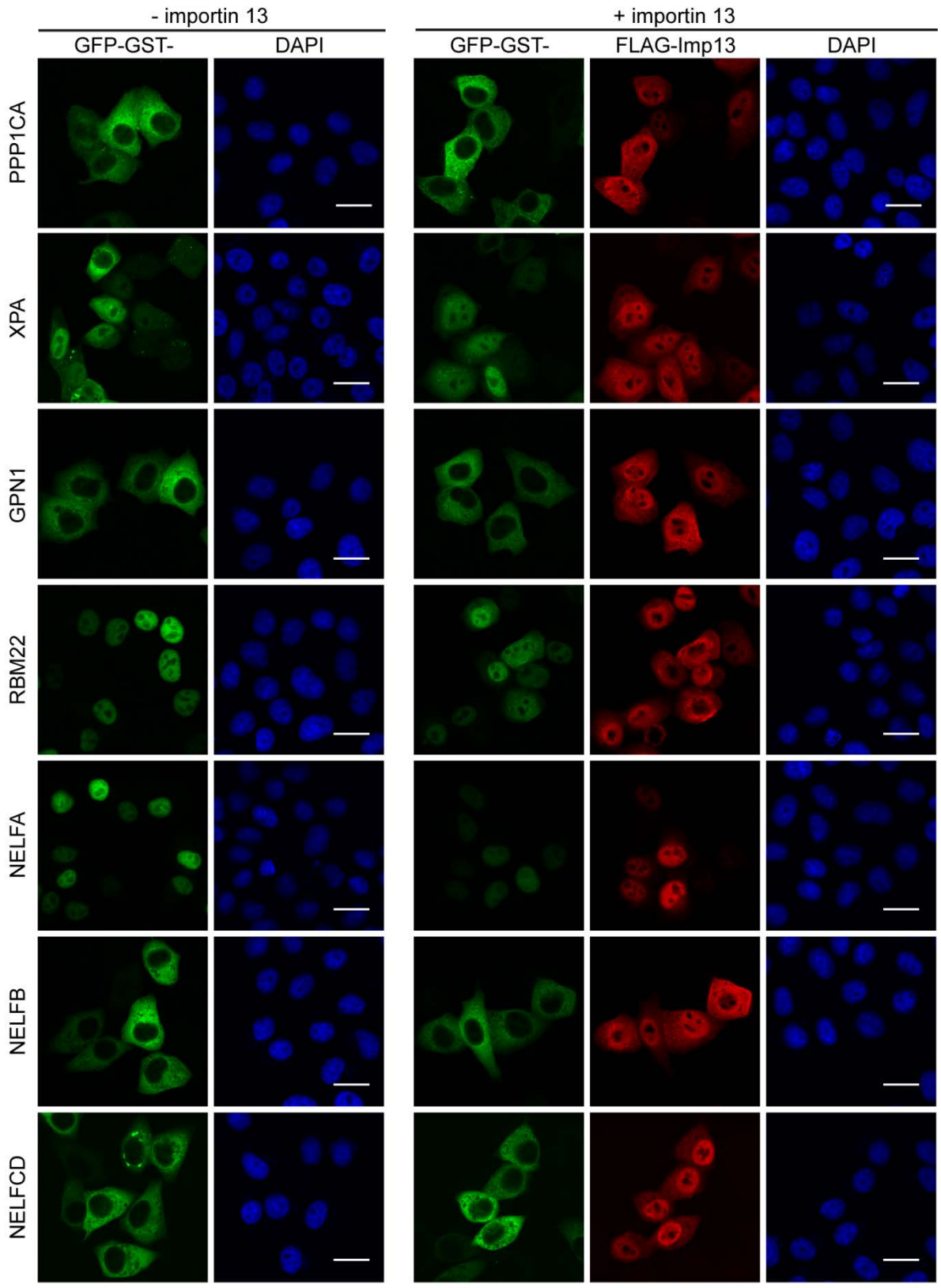
- importin 13
+ importin 13
GFP-GST-
DAPI
GFP-GST-
FLAG-Imp13
DAPI
PPP1CA
XPA
GPN1
RBM22
NELFA
NELFB
NELFCD

Figure 25: Effect of FLAG-importin 13 overexpression on subcellular localization of GFP-GST-tagged SILAC import cargo candidates. HeLa P4 cells were transiently cotransfected with plasmids coding for GFP-GST-tagged proteins form the SILAC screen and FLAG-importin 13 or an empty control vector (pEGFP-GST) using the calcium phosphate method. FLAG-importin 13 was visualized by indirect immunofluorescence with an anti-FLAG antibody. See Table 15 for summary of importin 13 effect. The scale bars correspond to 20 µm. XPA and RBM22 were tested by Christiane Spillner.

Table 15: Effect of importin 13 overexpression on importin 13 import cargo candidates identified in SILAC screen[#]

Potential importin 13 import cargoes						
Uniprot ID	**Protein Name**	**Gene**	**Cargo-HA**	**Cargo-HA + LMB****	**GFP-GST-cargo**	**Summary**
Proteins identified for Imp13/Imp13+Ran & Imp13/Imp13+Ubc9						
Q12800	Alpha-globin transcription factor CP2	TFCP2	✗		✗	✗
Q8IV48	3-5 exoribonuclease 1	ERI1	✓✓		✗	✓✓
Proteins identified for Imp13/Imp13+Ran						
O00303	Eukaryotic translation initiation factor 3 subunit F	EIF3F	✗		✗	✗
O75821	Eukaryotic translation initiation factor 3 subunit G	EIF3G	✗		✗	✗
Q53EL6	Programmed cell death protein 4	PDCD4	✓✓*			✓✓*
Q13895	Bystin	BYSL	✗		✗	✗
Proteins identified for Imp13/Imp13+Ubc9						
Q9GZS3	WD repeat-containing protein 61	WDR61	✓*		✗	✓*
P13984	General transcription factor IIF subunit 2	GTF2F2	✗		✓✓*	✓✓*
P62136	Serine/threonine-protein phosphatase PP1-alpha catalytic subunit	PPP1CA	✗		✗	✗
Q96F86	Enhancer of mRNA-decapping protein 3	EDC3	✗		✗	✗
O00571	ATP-dependent RNA helicase DDX3X/DDX3Y	DDX3	✗	✗		✗
Proteins identified for Imp13/Imp13+Ran & Imp13/Imp13+Ubc9 for two out of three SILAC experiments						
F2Z2T2	DNA repair protein complementing XP-A cells	XPA	✓*		✗	✓*
Q9HCN4	GPN-loop GTPase 1	GPN1	✗		✗	✗
Q13501	Sequestosome-1	SQSTM1	✗	✓✓*	✗	✓✓*
Q9NW64	Pre-mRNA-splicing factor RBM22	RBM22	✗		✓*	✓*
Q9H3P2	Negative elongation factor A	NELFA	✓		✗	✓*
Q8WX92	Negative elongation factor B	NELFB	✗		✗	✗
Q8IXH7	Negative elongation factor C/D	NELFCD	✓		✗	✓
Import control						
P63279	SUMO-conjugating enzyme UBC9	UBE2I	✗		✓✓	✓✓

#: two green ticks: strong importin 13 effect; one green tick: weak importin 13 effect; black cross: no importin13 effect

*: protein redistributed to cytoplasm not nucleus

**: cells were treated with 10 nM LMB for 2 hours, to shift the cytoplasmic protein to the nucleus

For the export cargo candidates, proteins from all three filtering criteria (log2(Imp13+Ran/Imp13) ≥ 3.0, ≥ 1.5 and ≥ 0.5) could be validated as importin 13 cargoes (Figure 26, Figure 27, Table 16). Of 19 proteins tested, 9 localized to the cytoplasm and WDR77 to the nucleus if importin 13 was coexpressed. For the filtering criterion log2(Imp13+Ran/Imp13) ≥ 0.5 ≤ 1.5, XRCC6 and SET were identified to be affected by importin 13 coexpression, whereas for the log2(Imp13+Ran/Imp13) ≥ 1.5 ≤ 3.0, HNRNPD, STRAP, BTF3 and EIF2D were affected (see Figure 28 for BTF3 and EIF2D). In contrast, all proteins validated as log2(Imp13+Ran/Imp13) ≥ 3.0, namely RTCA, FEN1, APEX1 and NSUN2, could be validated as importin 13 cargo candidates, with the exception of SRP14 and TYW3. However, as overexpressed TYW3 already has a cytoplasmic localization in the absence of importin 13 coexpression, an involvement of importin 13 in the subcellular localization of TYW3 cannot be confirmed with this assay. Similarly, EIF2AK2, BTF3, PRMT5 and EIF2D were also cytoplasmic and could not be analyzed for an importin 13 effect. The observed increased nuclear localization of WDR77 in the presence of overexpressed importin 13 was surprising, especially as in the previous binding experiment it was shown to bind exclusively in the presence of $RanGTP_{Q69L}$ (3.3.3.4.2). Possibly, WDR77 requires another factor apart from RanGTP to be exported by importin 13.

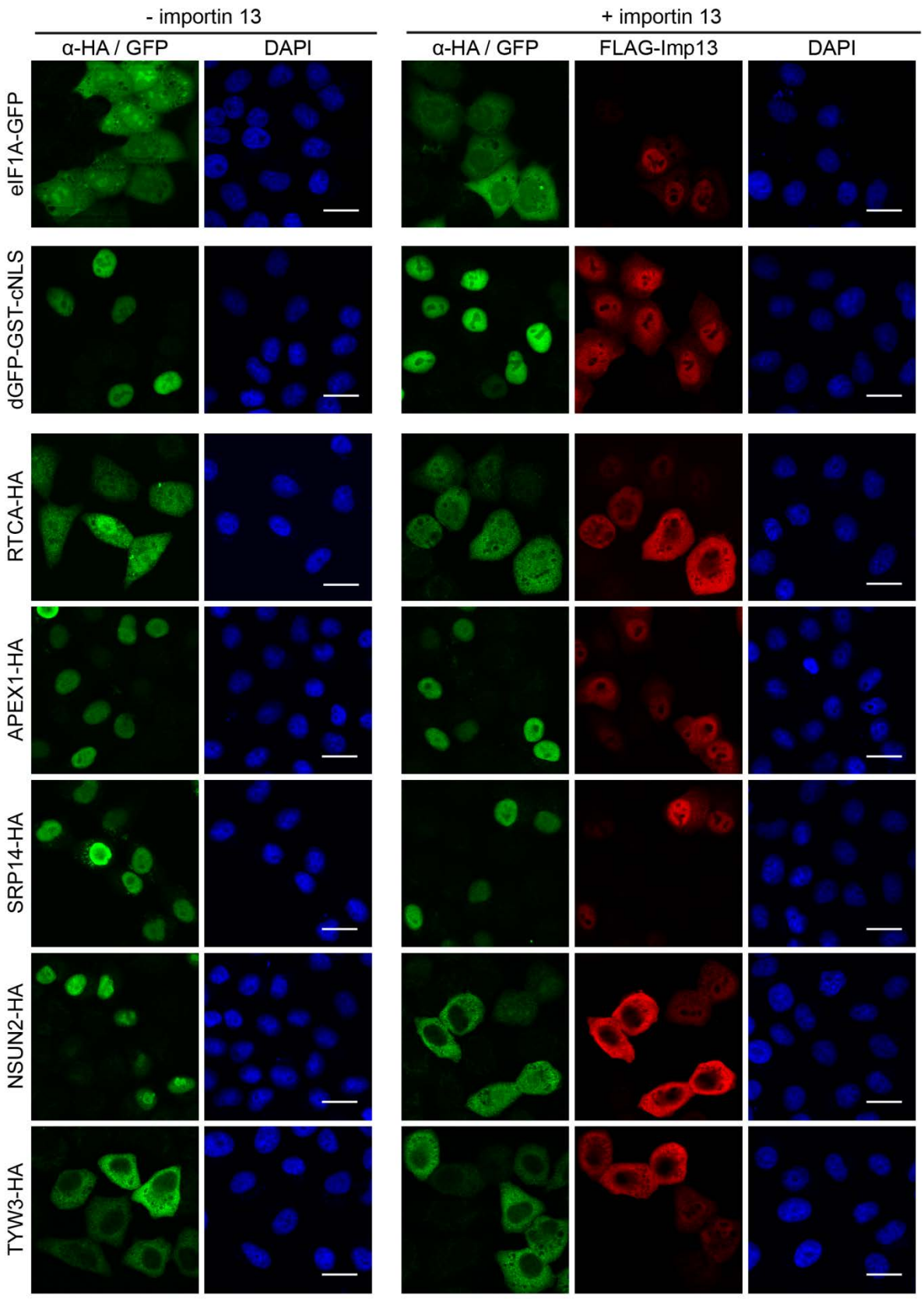
- importin 13
+ importin 13
α-HA / GFP
DAPI
α-HA / GFP
FLAG-Imp13
DAPI
eIF1A-GFP
dGFP-GST-cNLS
RTCA-HA
APEX1-HA
SRP14-HA
NSUN2-HA
TYW3-HA

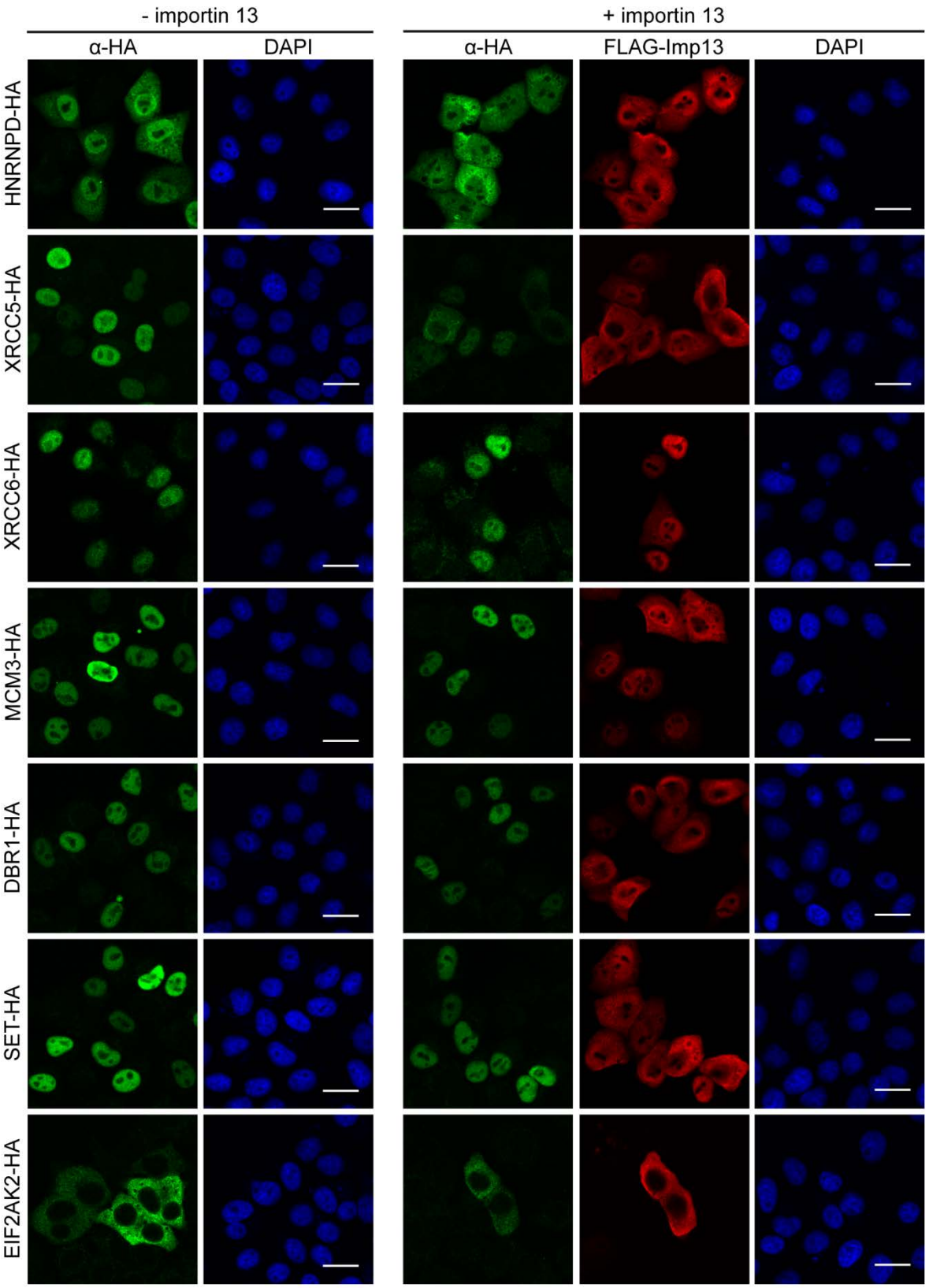
- importin 13
+ importin 13
α-HA
DAPI
α-HA
FLAG-Imp13
DAPI
HNRNPD-HA
XRCC5-HA
XRCC6-HA
MCM3-HA
DBR1-HA
SET-HA
EIF2AK2-HA

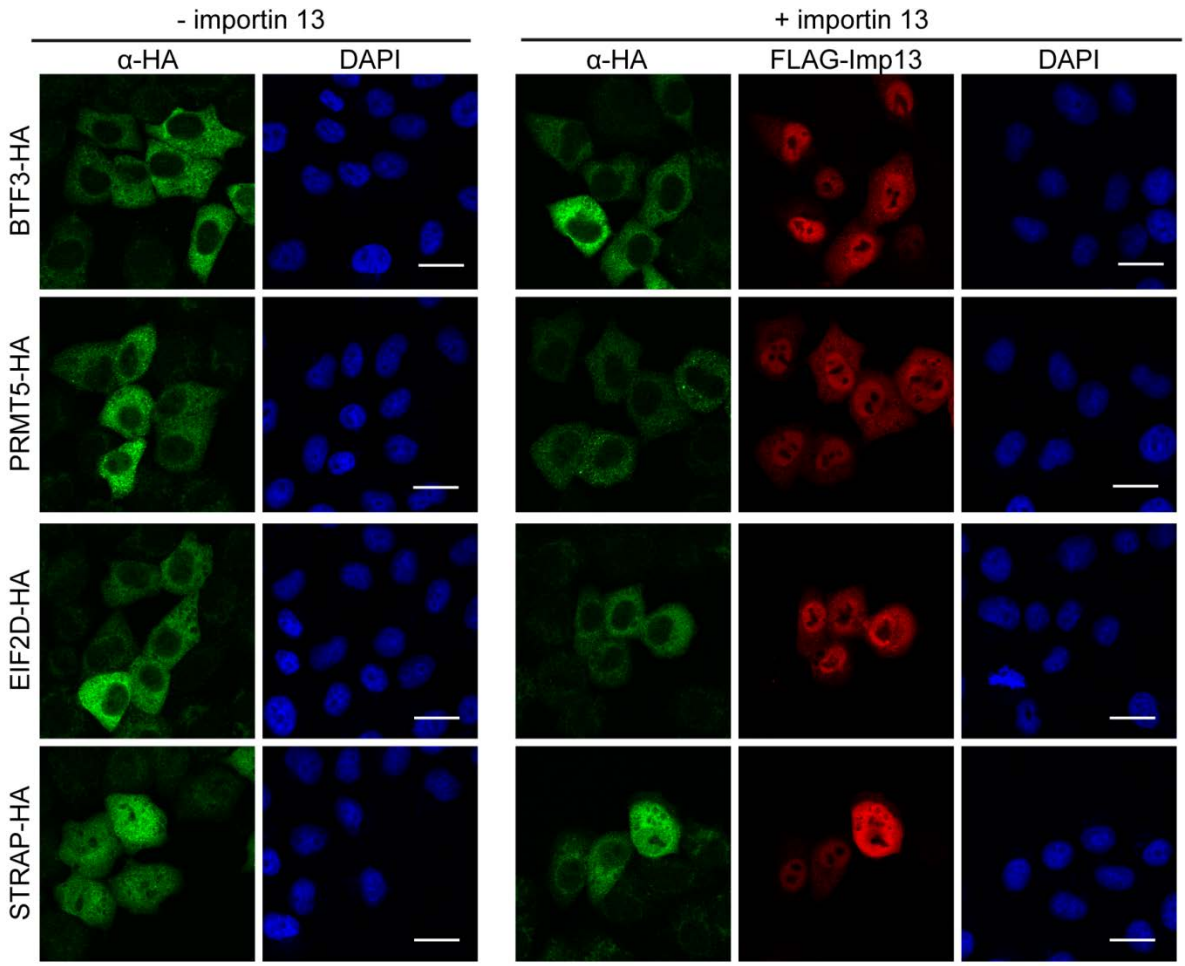

Figure 26: Effect of FLAG-importin 13 overexpression on subcellular localization of HA-tagged SILAC export cargo candidates. HeLa P4 cells were transiently cotransfected with plasmids coding for HA-tagged proteins from the SILAC screen and FLAG-importin 13 or an empty control vector (pcDNA3.1-HA) using the calcium phosphate method. FLAG-importin 13 and HA-substrates were visualized by indirect immunofluorescence with an anti-FLAG and anti-HA antibody, respectively. See Table 16 for summary of importin 13 effect. The scale bars correspond to 20 µm. XRCC5 and EIF2AK2 were tested by Christiane Spillner.

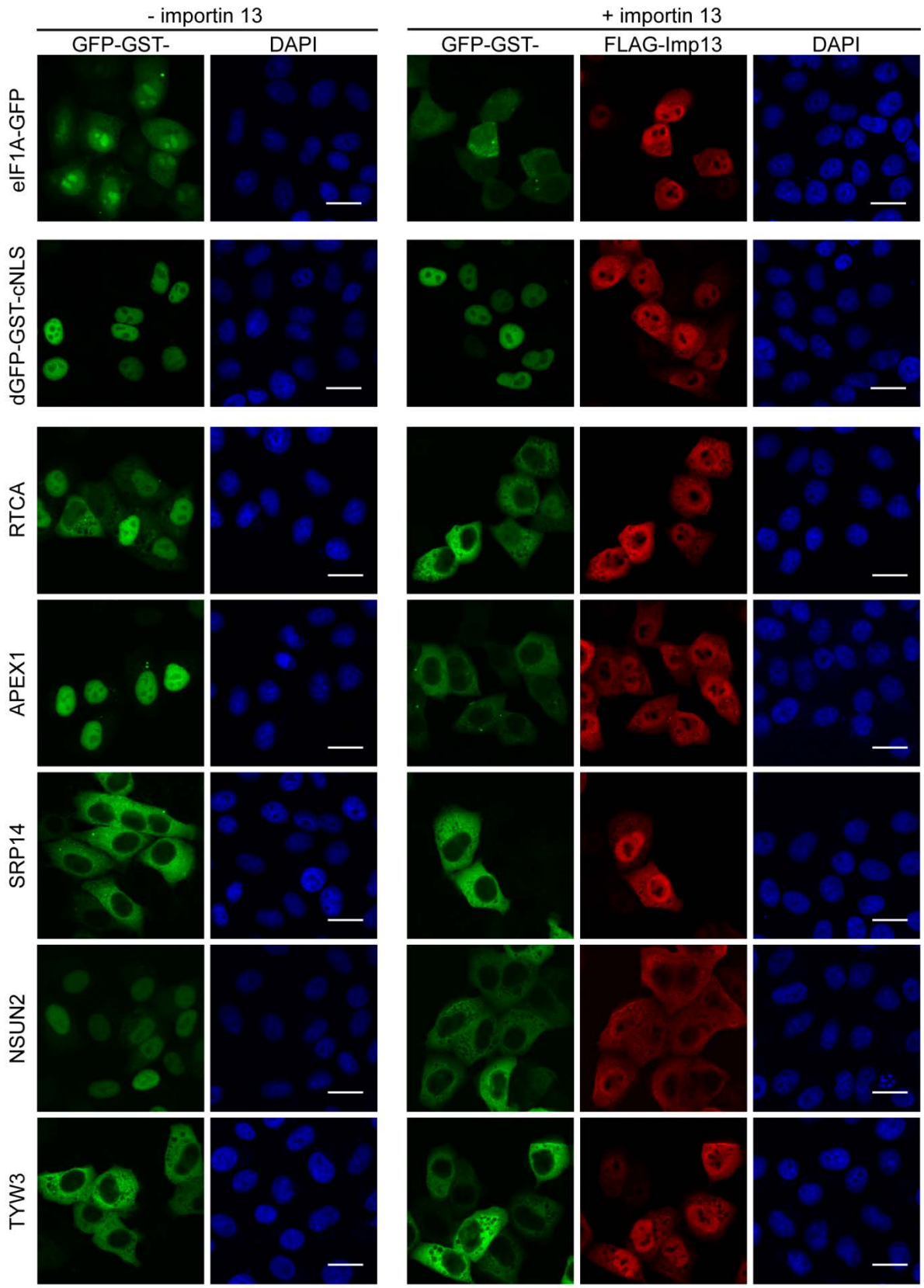
- importin 13
+ importin 13
GFP-GST-
DAPI
GFP-GST-
FLAG-Imp13
DAPI
eIF1A-GFP
dGFP-GST-cNLS
RTCA
APEX1
SRP14
NSUN2
TYW3

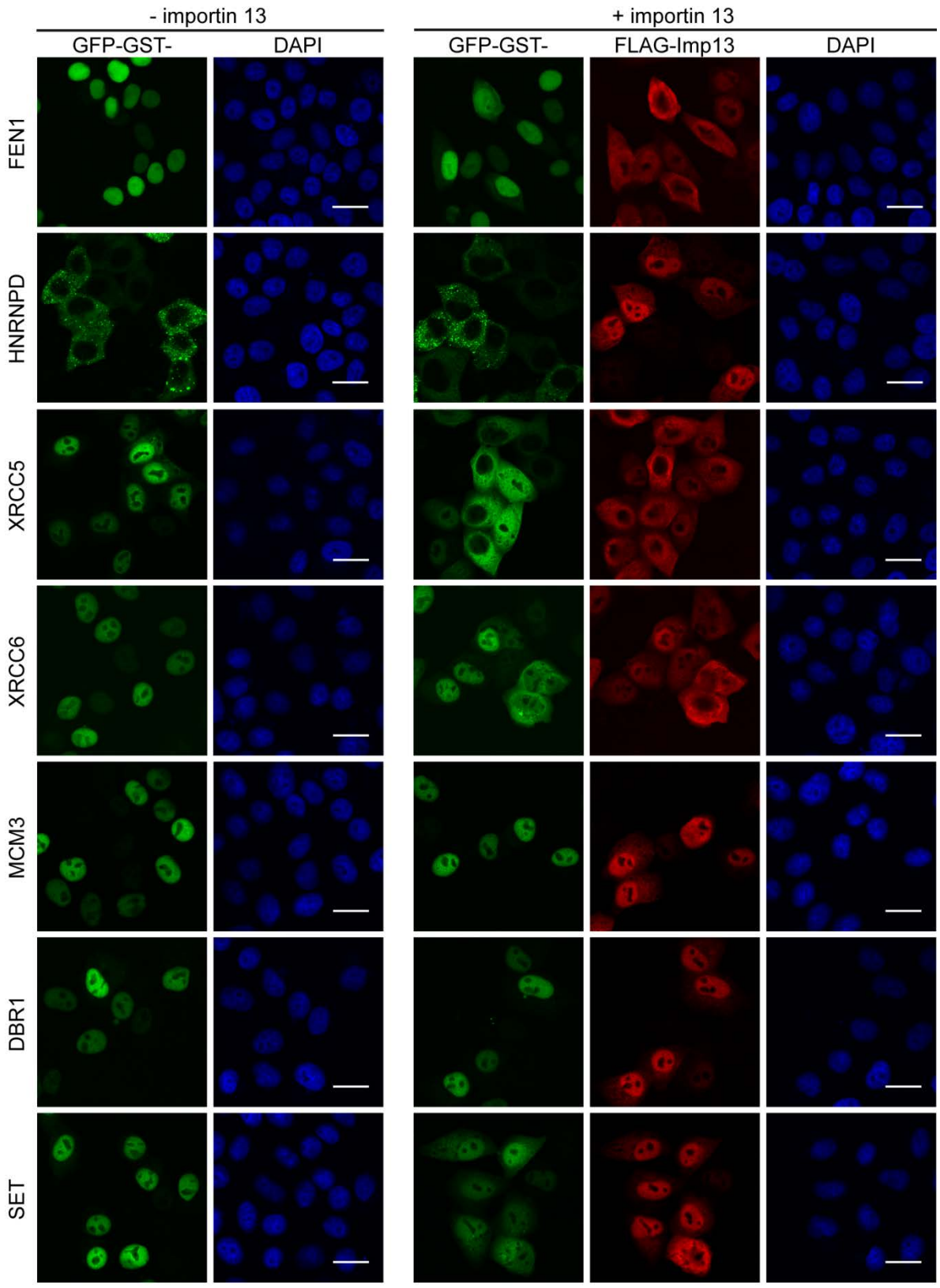
- importin 13
+ importin 13
GFP-GST-
DAPI
GFP-GST-
FLAG-Imp13
DAPI
FEN1
HNRNPD
XRCC5
XRCC6
MCM3
DBR1
SET

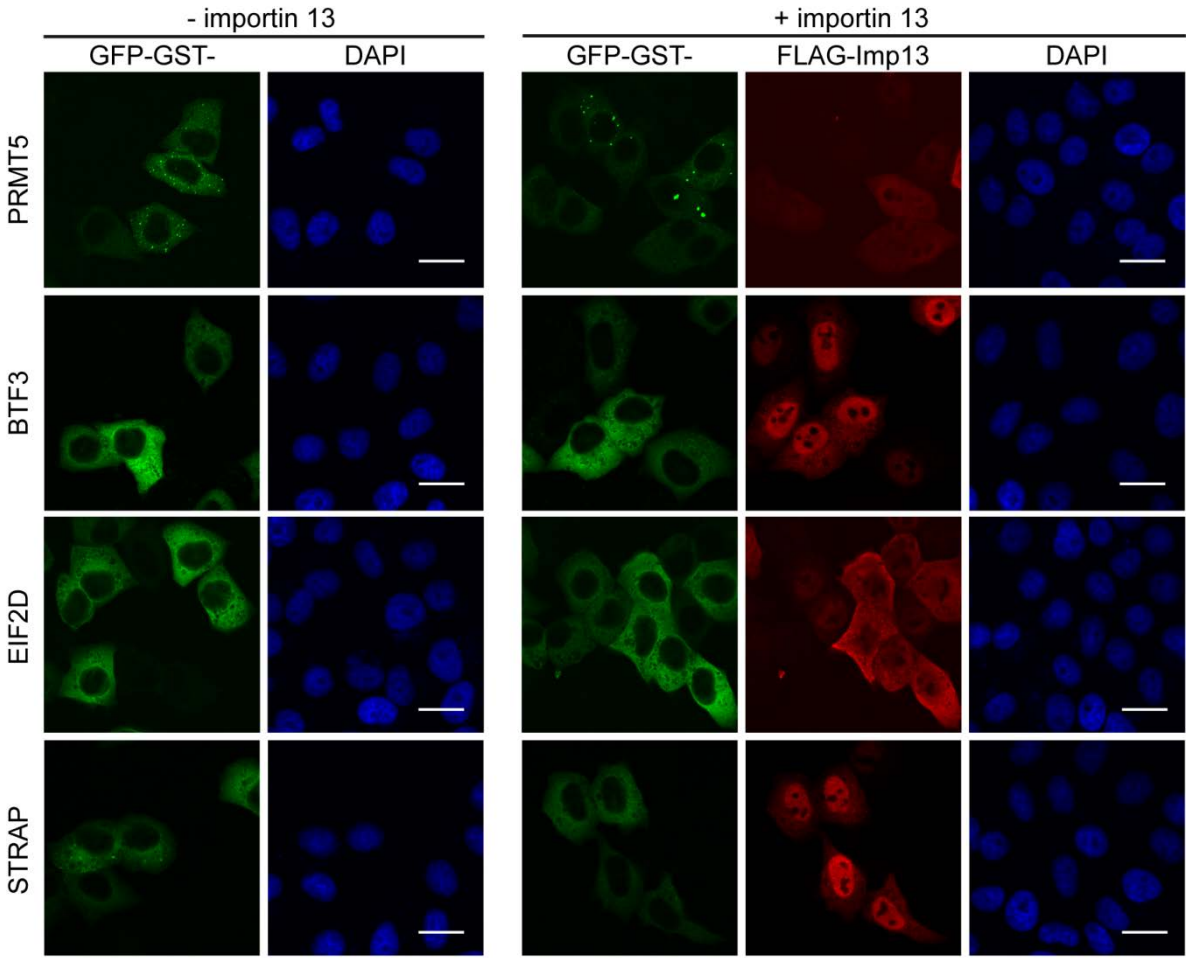

Figure 27: Effect of FLAG-importin 13 overexpression on subcellular localization of GFP-GST-tagged SILAC export cargo candidates. HeLa P4 cells were transiently cotransfected with plasmids coding for GFP-GST-tagged proteins from the SILAC screen and FLAG-importin 13 or an empty control vector (pEGFP-GST) using the calcium phosphate method. FLAG-importin 13 was visualized by indirect immunofluorescence with an anti-FLAG antibody. See Table 16 for summary of importin 13 effect. The scale bars correspond to 20 µm. FEN1, NSUN2 and XRCC5 were tested by Christiane Spillner.

Table 16: Effect of importin 13 overexpression on importin 13 export cargo candidates identified in SILAC screen[#]

Potential importin 13 export cargoes						
Uniprot ID	**Protein Name**	**Gene**	**Cargo-HA**	**Cargo-HA + LMB****	**GFP-GST-cargo**	**Summary**
Proteins identified for Imp13+Ran/Imp13						
log2(Imp13+Ran/Imp13) ≥ 3						
O00442	RNA 3-terminal phosphate cyclase	RTCA	✓		✓✓	✓✓
P39748	Flap endonuclease 1	FEN1			✓	✓
Q6IPR3	tRNA wybutosine-synthesizing protein 3 homolog	TYW3	×	×	×	×
P27695	DNA-(apurinic or apyrimidinic site) lyase	APEX1	×		✓✓	✓✓
P37108	Signal recognition particle 14 kDa protein	SRP14	×		×	×
Q08J23	tRNA (cytosine(34)-C(5))-methyltransferase	NSUN2	✓✓		✓✓	✓✓
log2(Imp13+Ran/Imp13) ≥ 1.5						
H0YA96	Heterogeneous nuclear ribonucleoprotein D0	HNRNPD	✓✓		×	✓✓
P13010	X-ray repair cross-complementing protein 5	XRCC5	✓✓		✓✓	✓✓
Q9NTK5	Obg-like ATPase 1	OLA1	×		×	×
Q9Y3F4	Serine-threonine kinase receptor-associated protein	STRAP	✓		×	✓
Q9UK59	Lariat debranching enzyme	DBR1	×		×	×
P25205	DNA replication licensing factor MCM3	MCM3	×		×	×
P20290	Transcription factor BTF3	BTF3	×	✓✓	×	✓✓
P41214	Eukaryotic translation initiation factor 2D	EIF2D	×	✓✓	×	✓✓
log2(Imp13+Ran/Imp13) ≥ 0.5						
P12956	X-ray repair cross-complementing protein 6	XRCC6	×		✓	✓
P19525	Interferon-induced, double-stranded RNA-activated protein kinase	EIF2AK2	×	×		×
O14744	Protein arginine N-methyltransferase 5	PRMT5	×	×	×	×
Q9BQA1	Methylosome protein 50	WDR77	✓*		×	✓*
Q01105	Protein SET	SET	×		✓✓	✓✓
Export control						
P47813	Eukaryotic translation initiation factor 1A	EIF1A			✓ (GFP-tag)	✓

#: two green ticks: strong importin 13 effect; one green tick: weak importin 13 effect; black cross: no importin13 effect

*: protein redistributed to nucleus not cytoplasm

**: cells were treated with 10 nM LMB for 2 hours, to shift the cytoplasmic protein to the nucleus

Previously, BTF3, PRMT5, EIF2D and SQSTM1 have been reported to be Crm1 export cargo candidates (82, 32), therefore it was tested whether these proteins as well as TYW3 and EIF2AK2 localize to the nucleus in cells treated with the Crm1 inhibitor leptomycin B (LMB) (Figure 28). Snurportin 1 was used as a control for the specificity of the LMB effect, as it is a well-established Crm1 cargo and was not identified as an importin 13 cargo candidate. Of the six proteins tested, BTF3, EIF2D and SQSTM1 were relocalized to the nucleus in LMB treated cells. Next it was analyzed whether importin 13 can reverse the LMB effect and indeed all three proteins were redistributed to the cytoplasm in cells expressing importin 13. Including the LMB sensitive cargoes, in total 12 out of 19 export cargo candidates were affected by importin 13 coexpression.

As several importin 13 cargo candidates were identified to be LMB sensitive, the redundancy of cargo candidates for importin 13 and Crm1 was compared. A total of 1,072 Crm1 cargo candidates were identified in a study to bind to immobilized Crm1 in a RanGTP-dependent manner (32), of these 56 proteins were identified as potential importin 13 cargoes in the SILAC screen (Table S11). The identified importin 13 cargo candidates were also compared with proteins identified in a study by Kimura *et al.*, 2017 (76) to interact with different importins. The largest overlap was found for importin 5, of 303 potential importin 5 cargoes identified, 32 were also detected in the SILAC screen as putative importin 13 cargoes (Table S12).

In summary, the SILAC based pull-down screen allows for the effective identification of potential importin 13 export cargoes. While proteins with a log2 SILAC ratio < 3 showed ambiguous results, proteins with a log2 SILAC ratio ≥ 3 can be classified as high confidence importin 13 export cargoes. Although the screen allowed for the effective identification of known importin 13 import cargoes (3.3.3.2), only few of the tested SILAC cargo candidates could be verified as potential importin 13 import cargoes by overexpression experiments. Based on this overexpression screen, RTCA, FEN1, APEX1, NSUN2, HNRNPD, XRCC5, STRAP, BTF3, EIF2D, XRCC6 and SET were validated as potential importin 13 export cargoes, while ERI1 and NELFCD were identified as potential import cargoes. Further, PDCD4, WDR61, GTF2F2, XPA, SQSTM1, RBM22 and NELFA were identified as potential importin 13 interaction partners.

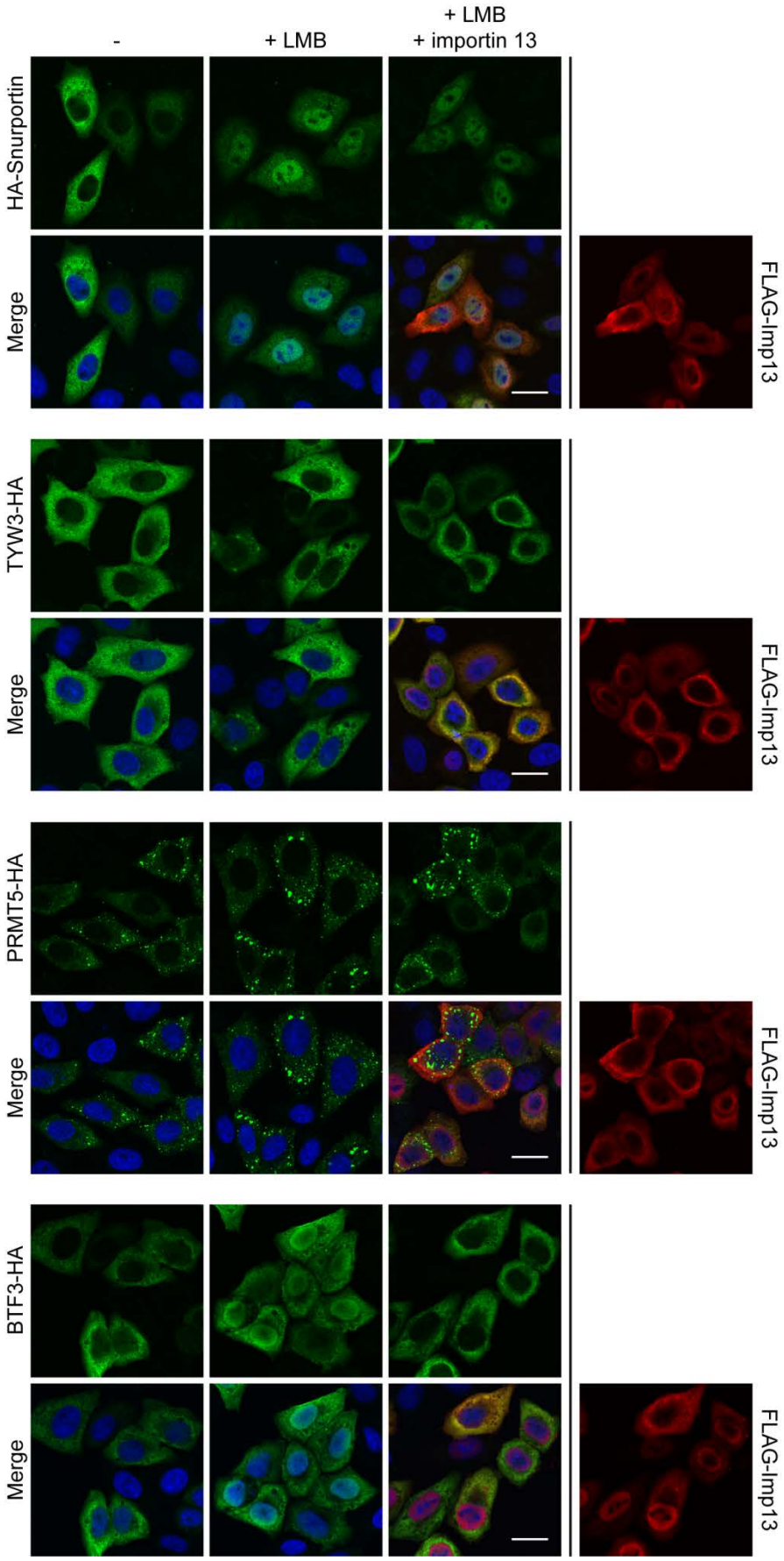
-
+ LMB
+ LMB
+ importin 13
HA-Snurportin
Merge
FLAG-Imp13
TYW3-HA
Merge
FLAG-Imp13
PRMT5-HA
Merge
FLAG-Imp13
BTF3-HA
Merge
FLAG-Imp13

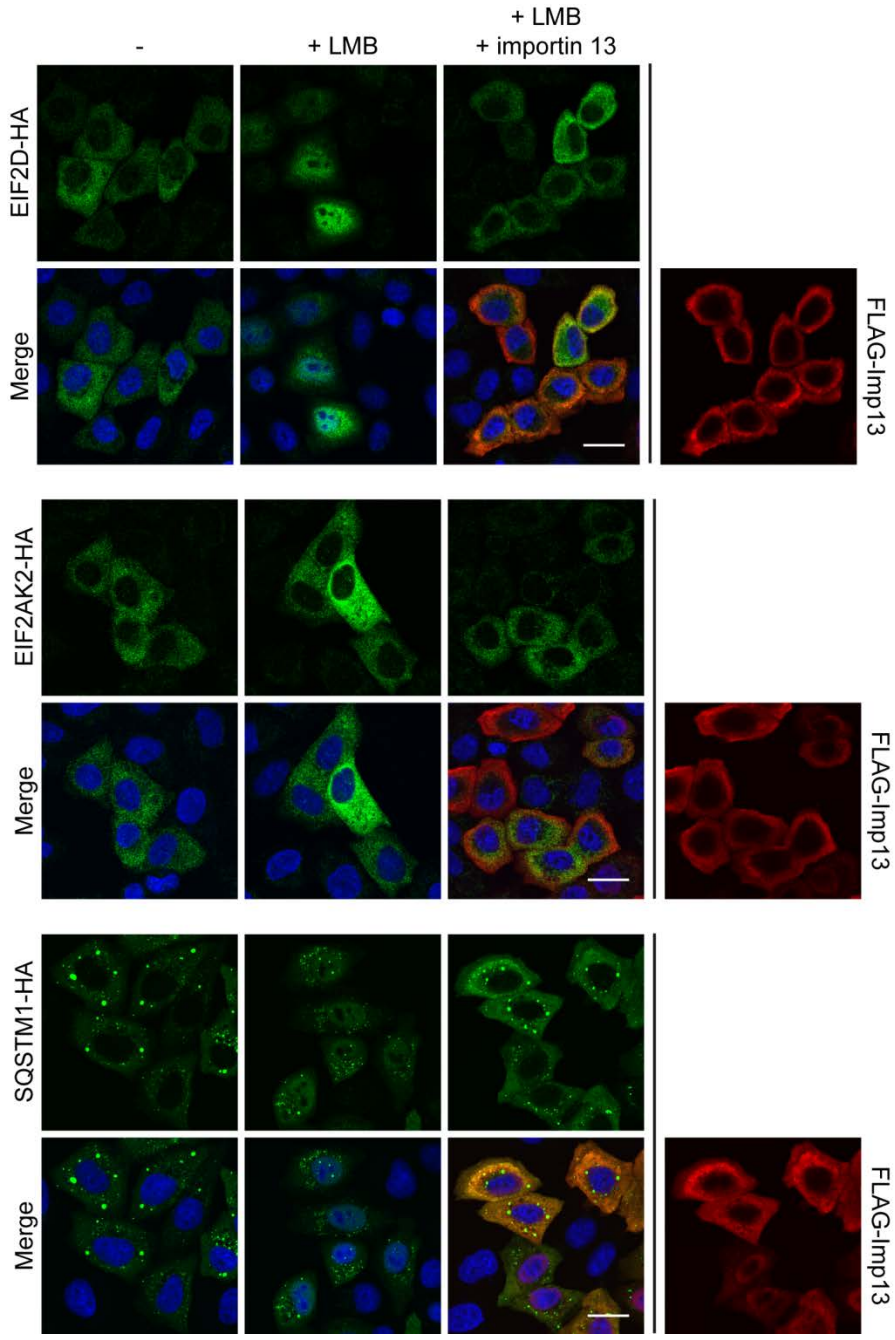

Figure 28: Effect of FLAG-importin 13 overexpression on subcellular localization of HA-tagged SILAC cargo candidates in leptomycin B treated cells. HeLa P4 cells were transiently cotransfected with plasmids coding for HA-tagged proteins from the SILAC screen and FLAG-importin 13 or an empty control vector (pcDNA3.1-HA) using the calcium phosphate method. Prior to fixation cells were treated with 10 nM leptomycin B, a Crm1 export inhibitor, for 2 hours. FLAG-importin 13 and HA-substrates were visualized by indirect immunofluorescence with an anti-FLAG and anti-HA antibody, respectively. The scale bars correspond to 20 µm.

3.3.3.4.4 Characterization of the Interaction of Importin 13 with Importin 13 Cargo Candidates

Similar to the experiments performed in section 3.2.2 and 3.2.3.2, cargo candidates affected by importin 13 overexpression were characterized for their interaction with importin 13. To test whether the cargo candidates NSUN2, HNRNPD, XRCC6, FEN1, PDCD4 and ERI1 bind importin 13 through the same key residues as the known export cargo eIF1A, subcellular localization of these proteins in the absence or presence of importin 13 wild type or mutant Glu436Arg/Asp481Arg, which is deficient in eIF1A export, was analyzed (Figure 29). With the exception of eIF1A, all proteins tested changed their localization upon coexpression of FLAG-importin 13-E436R/D481R. This demonstrates that the novel cargo candidates have a different binding site on importin 13 than eIF1A or that more residues need to be mutated to abolish the interaction.

To assess as to where these newly identified importin 13 cargo candidates might bind, the effect of an N-terminal (amino acids 1-669) and a C-terminal importin 13 fragment (amino acids 526-963) on the localization of these proteins was analyzed. The C-terminal fragment is a physiologically relevant, testis-specific form of importin 13 that lacks the N-terminal RanGTP binding site and has been suggested to function as a negative regulator of nuclear import. HeLa P4 cells were transfected with plasmids coding for cargo candidates and analyzed for any changes in subcellular localization in the presence or absence of the importin 13 fragments. The known export cargo eIF1A was relocalized to cytoplasm by full-length importin 13 but was not affected by the importin 13 fragments. This finding is in accordance with previous observations that eIF1A mainly binds to the middle region of importin 13. In contrast, the established import cargo Ubc9, that is known to bind to the N-terminus of importin 13, was indeed relocalized to the nucleus by the N-terminal fragment but not the C-terminal fragment. Similar to Ubc9, all cargo candidates tested, namely NSUN2, HNRNPD, XRCC6, FEN1 and PDCD4, with the exception of ERI1, were relocalized by both full-length importin 13 and the N-terminal fragment but not by the C-terminal fragment. ERI1, as eIF1A, changed its subcellular localization only in the presence of full-length importin 13. Note that the expression levels of the C-terminal fragment were generally lower than that of the N-terminal importin 13 fragment.

In summary, the novel cargo candidates tested bind importin 13 differently to eIF1A and the far C-terminus of importin 13 is dispensable for their interaction, with the exception of ERI1, whose subcellular localization was only affected by full-length importin 13.

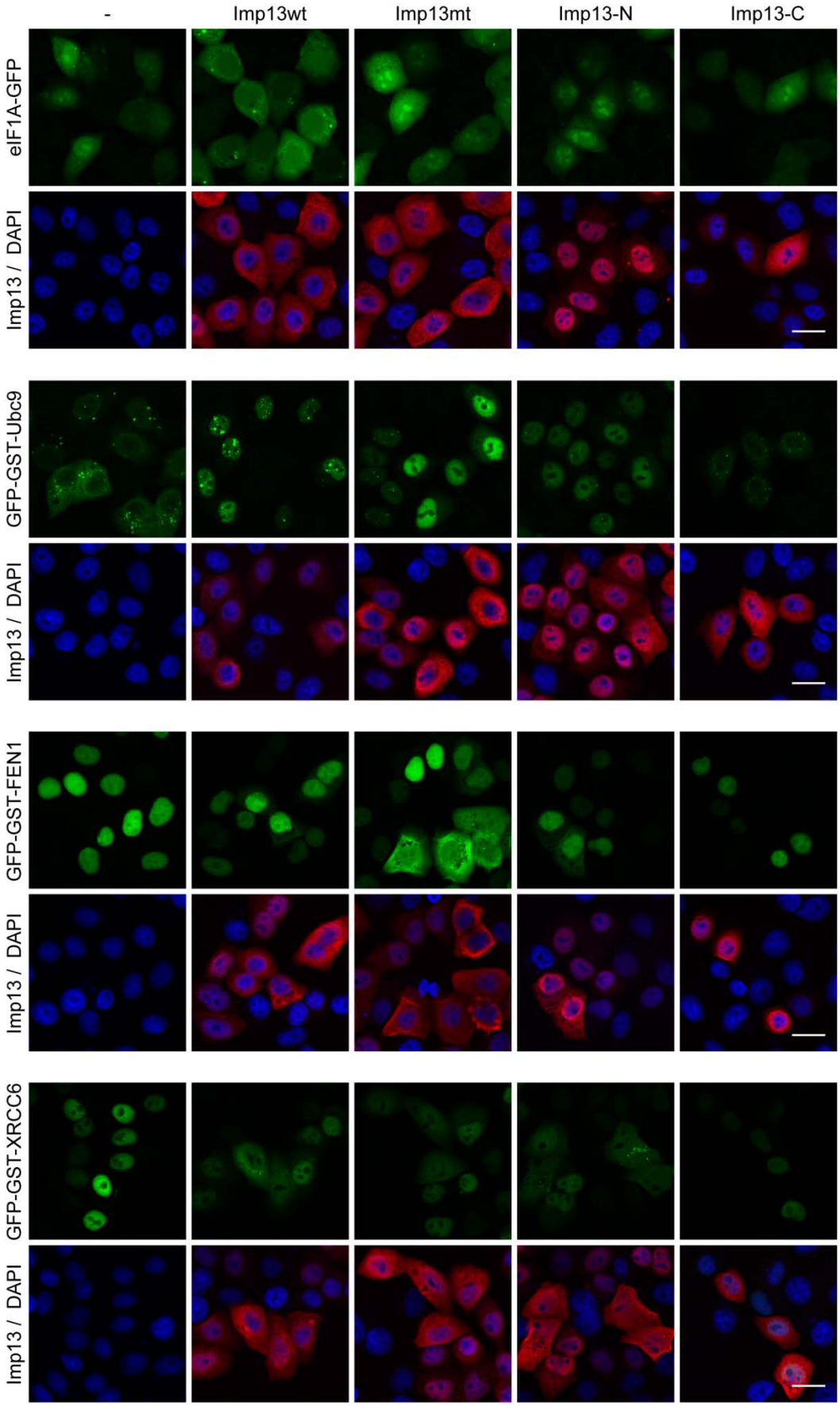
-
Imp13wt
Imp13mt
Imp13-N
Imp13-C
eIF1A-GFP
Imp13 / DAPI
GFP-GST-Ubc9
Imp13 / DAPI
GFP-GST-FEN1
Imp13 / DAPI
GFP-GST-XRCC6
Imp13 / DAPI

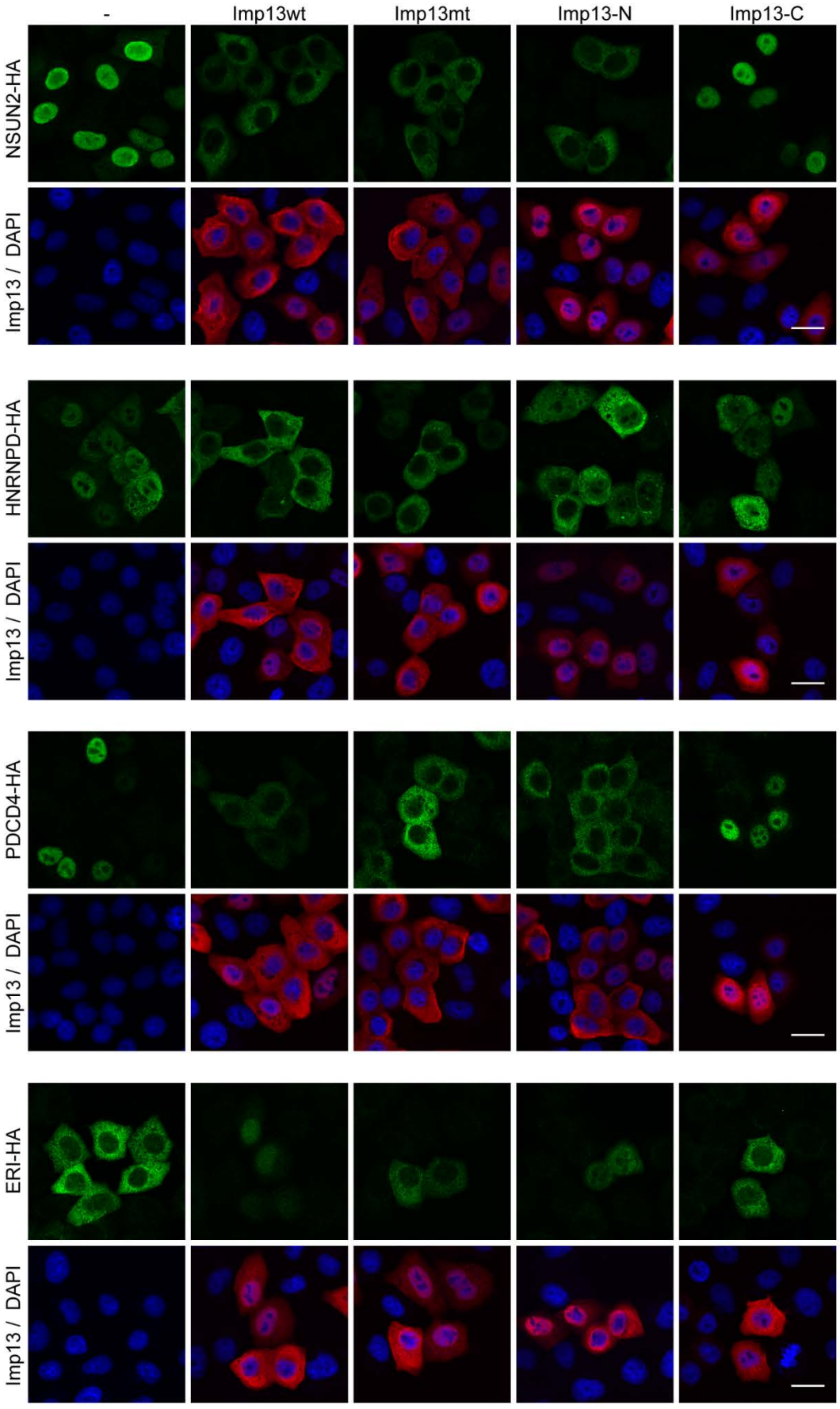
-
Imp13wt
Imp13mt
Imp13-N
Imp13-C
NSUN2-HA
Imp13 / DAPI
HNRNPD-HA
Imp13 / DAPI
PDCD4-HA
Imp13 / DAPI
ERI-HA
Imp13 / DAPI

Figure 29: SILAC cargo candidates bind importin 13 differently to eIF1A and the C-terminus of importin 13 is dispensable for their interaction. HeLa P4 cells were transiently cotransfected using the calcium phosphate method with plasmids coding for HA-or GFP-GST-tagged proteins from the SILAC screen and FLAG-importin 13 wild type (Imp13wt), FLAG-importin 13-E436R/D481R (Imp13mt, importin 13 mutant impaired in eIF1A export); FLAG-importin 13 (aa 1-669) (Imp13-N) and FLAG-importin 13 (aa 526-963) (Imp13-C) or an empty control vector. FLAG-importin 13 and HA-substrates were visualized by indirect immunofluorescence with an anti-FLAG and anti-HA antibody, respectively. The scale bars correspond to 20 µm.

3.3.3.4.5 Functional Roles of Novel Importin 13 Cargo Candidates

To gain insight into what cellular pathways importin 13 might regulate through transport of specific cargoes, a gene ontology enrichment analysis was done. In total 38 gene ontology clusters were identified if an enrichment score cut-off of 1.5 was applied. Table 17 shows a summary of the 10 most enriched clusters, with three representative enriched GO terms. The analysis suggests that importin 13 influences the subcellular distribution of proteins involved in processes such as translation, microtubule and cytoskeleton organization, mRNA processing and chromosome organization.

Table 17: Gene Ontology (GO) analysis of importin 13 cargo candidates [#]

GO Term	Count	p-value
Annotation Cluster 1, Enrichment Score: 13.26		
cellular component organization or biogenesis	143	4.60E-15
cellular component organization	139	3.00E-14
organelle organization	99	1.20E-12
Annotation Cluster 2, Enrichment Score: 11.33		
organonitrogen compound metabolic process	54	1.80E-05
cellular amide metabolic process	45	1.90E-12
translation	42	4.70E-17
Annotation Cluster 3, Enrichment Score: 11.19		
multi-organism process	60	8.50E-07
interspecies interaction between organisms	49	6.60E-15
viral process	47	3.90E-14
Annotation Cluster 4, Enrichment Score: 9.31		
cell adhesion	54	3.70E-09
biological adhesion	54	4.20E-09
cell-cell adhesion	48	7.40E-12
Annotation Cluster 5, Enrichment Score: 7.77		
cellular component biogenesis	81	4.40E-11
macromolecular complex subunit organization	73	3.70E-11
protein complex assembly	40	2.10E-05
Annotation Cluster 6, Enrichment Score: 6.58		
multi-organism metabolic process	14	6.80E-06
formation of translation preinitiation complex	11	2.70E-13
viral gene expression	11	2.80E-04

Annotation Cluster 7, Enrichment Score: 6.36		
cytoskeleton organization	36	4.10E-06
microtubule-based process	26	9.70E-07
microtubule cytoskeleton organization	21	1.40E-06
Annotation Cluster 8, Enrichment Score: 5.19		
cytoplasmic translational initiation	6	2.30E-06
IRES-dependent translational initiation	5	1.50E-05
cap-independent translational initiation	5	3.90E-05
Annotation Cluster 9, Enrichment Score: 5.08		
RNA processing	34	1.90E-07
mRNA metabolic process	31	7.90E-09
mRNA splicing, via spliceosome	16	1.40E-05
Annotation Cluster 10, Enrichment Score: 5		
chromosome organization	35	2.20E-05
DNA metabolic process	33	4.00E-06
telomere maintenance	15	3.50E-09

#: importin 13 cargo candidates listed in Table S6, Table S7 and Table S8 were subjected to gene ontology analysis with the DAVID software, only three representative GO terms per cluster are shown. Count: number of genes per GO term; p-value: EASE score (modified Fisher Exact P-Value).

4. Discussion

The mechanisms of nucleocytoplasmic transport are well understood. Rather little is known, however, about the biological significance of individual nuclear transport receptors. A major restriction here is the limited number of reported cargo proteins. Only recently, a large proteomics screen (76) identified multiple cargo proteins specific for the twelve species of human import receptors, including importin 13. The authors, however, did not screen for potential importin 13 export cargoes, which was a major goal of the work presented here. To expand the number of importin 13 substrates and specifically importin 13 export cargoes, three different approaches were used in this work, including an importin 13 overexpression screen using a library of nuclear proteins, an importin 13 binding experiment followed by mass spectrometry and an importin 13 binding experiment coupled to quantitative proteomics using SILAC.

4.1 Characterization of Known Importin 13 Cargoes

To allow for characterization of newly identified importin 13 substrates, various cellular and biochemical assays were established with the known importin 13 import cargo Ubc9 and the export cargo eIF1A. Overall, the performed assays confirmed previous findings. In addition, a few observations were made that have not been previously discussed.

Endogenous eIF1A has been shown to be primarily localized in nucleoli (107), whereas in this study a homogenous distribution of endogenous eIF1A between nucleoli and the nucleoplasm was observed. As different antibodies were used, it is possible that both antibodies recognize different epitopes on eIF1A that are partially occluded if eIF1A is complexed to other proteins, such as the 40S ribosomal subunit. The primarily nuclear localization of eIF1A is rather unique, as the vast majority of translation factors are thought to be restricted to the cytoplasm to prevent nuclear translation or interference with ribosome biogenesis by untimely interactions with pre-ribosomes (189). In turn, eIF1A has been suggested to have a yet unidentified nuclear function and that importin 13 mediated export is required to ensure efficient translation by maintaining sufficient cytoplasmic levels of eIF1A (189).

The primarily nuclear localization of endogenous eIF1A suggests that importin 13 mediated export of eIF1A is rate limiting in HeLa P4 cells. Indeed, overexpression of importin 13 resulted in a more cytoplasmic localization of endogenous eIF1A, confirming that importin 13 is rate limiting for its export. In contrast, overexpressed HA-Ubc9 already localized to the nucleus without importin 13 coexpression. This suggests that either

importin 13 is not rate limiting for Ubc9 nuclear import or Ubc9, as eIF1A, is small enough (18 kDa) to diffuse into the nucleus, where it gets sequestrated through interaction with nuclear components. Likely, both diffusion and importin 13 mediated transport play a role in Ubc9 nuclear localization, as GFP-GST-Ubc9, which should be above the diffusion limit of the NPC, requires importin 13 coexpression not only to enter the nucleus but also to maintain an exclusively nuclear localization. This shows that in contrast to HA-Ubc9, endogenous importin 13 is rate limiting for the nuclear localization of GFP-GST-Ubc9. Thus, an additional mechanism such as diffusion into the nucleus is essential to confine Ubc9 to the nucleus. Another indicator that importin 13 helps to confine Ubc9 to the nucleus is the result of proximity ligation assays, where the majority of importin 13/Ubc9 *in situ* interactions were detected in the nucleus. Less transient interactions in the nucleus might prevent immediate redistribution to the cytoplasm by diffusion. In this regard, an effect of importin 13 knock-down on the subcellular localization of Ubc9 should be analyzed, to determine if importin 13 is essential for the nuclear localization of Ubc9.

The notion that importin 13 is rate limiting for at least some of its cargoes in HeLa P4 cells is further supported by the observation that endogenous importin 13 levels in HeLa P4 cells as well as other cancer cell lines is very low with levels around 100-350 nM. In comparison, other nuclear transport receptors have a several fold higher cellular concentration of 1-4 µM (77, 185). It has previously been demonstrated that the transport efficiency of nuclear import receptors depends on their cellular concentration (83, 192). Similarly, cellular Crm1 concentrations were reported to be rate limiting for export of overexpressed cargo proteins in HeLa P4 cells (193).

In summary, importin 13 is rate limiting for nucleocytoplasmic transport of its cargoes Ubc9 and eIF1A. Importin 13 mediated export of eIF1A might be essential for efficient translation by ensuring sufficient cytoplasmic levels of eIF1A. Import of Ubc9 mediated by importin 13 could be required to confine Ubc9 to the nucleus and thus to prevent unspecific interactions in the cytoplasm. Indeed, many of the known Ubc9 SUMOylation targets are nuclear proteins (194) and importin 13 could function as a chaperone to prevent untimely SUMOylation.

4.2 Overexpression Experiments for the Identification of Importin 13 Cargoes

4.2.1 Are DBC-1, DMAP1, TERT, DDX43 and DDX59 Importin 13 Cargoes?

In an overexpression screen for potential importin 13 export cargoes, several nuclear proteins that were affected by importin 13 overexpression and showed an increased

cytoplasmic localization were identified. The observed effects appear to be specific, as two of the identified proteins, DBC-1 and c-Jun, have previously been shown to interact with importin 13 in binding experiments (49, 117). While the importin 13 effect was largely independent of the cell line and fusion tag used, cell to cell variation could be observed within one experiment. Possible explanations could be cell cycle specific effects or higher importin 13 expression levels in cells with strong cytoplasmic accumulation.

Several different mechanisms could account for the increased cytoplasmic localization of the identified proteins upon importin 13 coexpression, including direct or indirect stimulation of nuclear export as well as reduced or inhibited nuclear import. In this regard, a testis-specific form of importin 13 (amino acids 526-963) has been reported to function as a negative regulator of nuclear import (136), a mechanism that might also apply to full-length importin 13. Further, several transport cargoes have been reported to interact with various nuclear transport receptors *in vitro* but it has been suggested that *in vivo* a preference for a specific nuclear transport receptor might exist (195). Thus importin 13 might only bind to the identified proteins if overexpressed, thereby competing with the preferred nuclear transport receptor. Fos and c-Jun for example are proteins that have been reported to bind to several different karyopherins *in vitro* (117, 196).

To further investigate these options, transport assays, heterokaryon assays or fluorescence recovery after photobleaching (FRAP) experiments, similar to the ones performed for the importin 13 export cargoes HMG20A and EIF4G2 (136), could be performed. Another approach could be siRNA mediated knock-down of importin 13. However, RNA interference experiments with importin 13 so far had no effect on established importin 13 cargoes (data not shown), possibly due to the observed low endogenous importin 13 levels in HeLa P4 cells. If some or all of the identified proteins are indeed importin 13 export cargoes, they bind importin 13 differently to eIF1A, as the importin 13 mutant impaired in eIF1A export was still fully functional in mediating relocalization of DBC-1, DMAP1, DDX43, DDX59 and TERT. This, is not surprising, as importin 13 has been demonstrated to bind its cargoes through different binding sites and key residues (92, 93, 107).

At least DBC-1 and c-Jun appear not to be importin 13 export cargoes, as their interaction with importin 13 is reduced in the presence of $RanGTP_{Q69L}$ (49, 117). Further, DBC-1 came up as a potential importin 13 import cargo in the SILAC screen, but only in one of the replicate experiments. Import assays should be done to test whether importin 13 can import DBC-1 or the other identified proteins. Import assays in permeabilized cells with c-Jun have previously been performed, but no efficient import by importin 13 could be

detected (117). Still, silencing of importin 13 in pterygium epithelial cells has been reported to block the nuclear translocation of c-Jun (142). None of the other proteins identified in the overexpression screen were detected in the SILAC screen. This could be due to the cell extraction method using digitonin, which is known to selectively permeabilize the cell membrane but to leave the nuclear envelope largely intact (179, 180). Consequently, larger proteins such as TERT (127 kDa) as well as proteins tethered to nuclear structures or larger protein complexes might not be efficiently released from the nucleus with this extraction method. Further, the endogenous concentrations of these proteins in HeLa P4 cells might be too low, preventing their identification.

In summary, the overexpression screen seems to allow for the identification of importin 13 interaction partners but not for the specific identification of importin 13 export cargoes. Importin 13 could regulate the subcellular localization of the identified proteins either through facilitated transport or through negative regulation of nuclear transport. In the case of DBC-1, importin 13 seems to function rather as a negative regulator of nuclear import than as an exportin (see section 4.3.2.2 for alternative explanations). The advantage of the overexpression screen is that it requires little optimization and provides direct information on the subcellular localization of the proteins analyzed, but it is limited by the number of available plasmids.

4.2.2 Interaction of Importin 13 and DBC-1

One of the cargoes analyzed in more detail for its interaction with importin 13 was DBC-1. DBC-1 regulates several nuclear proteins, such as nuclear receptors (androgen receptor, estrogen receptor α and β, retinoic acid receptor, thyroid hormone receptor, heam receptor Rev-erbα), deacetylases (SIRT1, HDAC3) and the methyltransferase SUV39H1 (197). Previously, the coiled-coil domain of DBC-1 has been suggested to be involved in the translocation of DBC-1 through the NPC (198). Indeed, the coiled-coil domain of DBC-1 fused to a cNLS was relocalized to the cytoplasm upon importin 13 coexpression. To gain insights into which region of importin 13 is required for its interaction with DBC-1, different importin 13 fragments were coexpressed with DBC-1. Only N-terminal but not C-terminal importin 13 fragments promoted a cytoplasmic localization of DBC-1 similar to full-length importin 13. Nevertheless, as discussed above, this could be due to different mechanisms, like active export or negative regulation of import. Although, one might expect that importin 13 deletion constructs are impaired in shuttling through the NPC, an importin 13

N-terminal fragment has been shown to still be capable of shuttling, albeit at a slower rate than full-length importin 13 (162).

In conclusion, importin 13 interacts with the coiled-coil domain of DBC-1 and at least one binding site on the N-terminus of importin 13 is required for their interaction.

4.2.3 Functional Link Between Importin 13 and Nup358 Mediated Transport?

Interestingly, the proteins that were affected the strongest by importin 13 overexpression, DBC-1, DMAP1, DDX43 and DDX59, were also identified in a screen for Nup358-dependent proteins (49). In this study, Nup358 was shown to be required not only for the nuclear localization of these proteins but to also bind DBC-1 and DMAP1 directly. Consequently, Nup358 was proposed to function as an assembly platform for import complexes (49). The strong overlap of proteins affected by Nup358 depletion and importin 13 overexpression suggests a functional link between importin 13 and Nup358, with the latter possibly serving as an assembly or disassembly platform for importin 13 transport complexes. However, the observed overlap could also be due to a general involvement of Nup358 in nucleocytoplasmic transport, as Nup358 has been implicated in various transport pathways, including importin α/β, transportin 1, transportin 3, CAS, importin 7 and Crm1 (25). Previous binding experiments between importin 13 and a C-terminal Nup358 fragment present in a complex with Ubc9 and SUMOylated RanGAP showed no interaction (25). However, other regions of Nup358 might be involved. Binding assays should be done with importin 13 and the identified cargo candidates in the absence or presence of Nup358 wild type or deletion constructs. Importin 13 transport assays in Nup358 depleted and control cells could yield further information on a possible link.

The strong overlap of cargoes showing a dependency on both Nup358 and importin 13 suggests a functional link between the two proteins. Further experiments will be required to assess the nature of this overlap.

4.3 Mass Spectrometry Based Identification of Importin 13 Cargoes

4.3.1 Mass Spectrometry Based Methods for the Identification of β-karyopherin Cargoes

Different approaches have been used to identify nuclear transport receptor interaction partners, including the yeast-two hybrid system (136, 199) and mass spectrometry approaches (32, 135, 189, 200). Further, stable isotope labeling with amino acids in cell culture (SILAC), followed by quantitative mass spectrometry has been applied to identify importin α/β, transportin and Crm1 cargoes (76, 80–82, 201). Compared to the previous SILAC methods, the SILAC approach applied here is limited in the identification of transient interactions, but has the major advantage of specifically identifying both nuclear import and export cargoes. Of the importin 13 cargo candidates detected in this study, 11% were also identified in the SILAC-Tp study by Kimura *et al*., 2017 (76), showing that both approaches might effectively complement each other (Table S10). One of the major cargo candidates identified in the SILAC-Tp study, but not in this study, was the integral membrane protein LRRC59 (202). LCCR59 as well as other integral membrane proteins were not detected in the approach presented here, likely as integral membrane proteins are not extracted with digitonin. It remains unclear why an integral membrane protein should be a substrate for importin 13.

4.3.2 SILAC Based Importin 13 Binding Assays for the Identification of Importin 13 Import and Export Cargoes

The majority of the known importin 13 import and export cargoes were identified with the SILAC based pull-down assay, proving the utility of this approach in identifying novel importin 13 cargoes. Not all of the reported importin 13 substrates (Table 1) were identified in the SILAC screen. However, some of them, for instance the glucocorticoid receptor, CCCTC-binding factor (CTCF), and myopodin, have not been validated as cargoes in transport assays. Thus, interaction partners such as myopodin might not be transported by importin 13 and instead be involved in other cellular functions of importin 13. None of the paired homeodomain transcription factors that have been demonstrated to be imported by importin 13 in transport assays were identified in our SILAC screen. Perhaps they are tethered to other nuclear components such as proteins or chromatin, preventing their extraction with digitonin from HeLa P4 cells, a possibility that could also apply to other proteins. Many of the reported importin 13 cargoes were identified in other cell lines than HeLa P4 or were found to be developmentally regulated. Thus, HeLa P4 cells might not be

the ideal source to show an interaction of these proteins with importin 13. Since the endogenous levels of these proteins could be rather low in HeLa P4 cells, they possibly would not be detected by mass spectrometry. Certain substrates might also yield few or no ionizable tryptic peptides.

According to the SILAC screen, many importin 13 binding proteins were regulated neither by Ubc9 nor $RanGTP_{Q69L}$ in their binding to immobilized importin 13. These could be unspecific binding proteins that were not sufficiently removed by preincubation with Hzz-IgG-Sepharose or proteins that bind to other regions on importin 13 than Ubc9 and RanGTP. In total, 242 proteins were identified with the selected filtering criteria, whose binding to importin 13 was regulated by Ubc9 or $RanGTP_{Q69L}$, 131 of which were identified as potential import, 95 as export and 16 as ambiguous cargo candidates. The ambiguous proteins are considered to be export cargoes, as they were not only enriched in importin 13 binding reactions compared to binding reactions with excess Ubc9 (Imp13/Imp13+Ubc9), but also in importin 13 binding reactions with $RanGTP_{Q69L}$ compared to reactions without $RanGTP_{Q69L}$ (Imp13+Ran/Imp13 ratio). Indeed, eIF1A, a well-established importin 13 export cargo, was part of this group.

Several obligatory cytoplasmic proteins were identified as importin 13 cargo candidates. Mixing of nuclear and cytoplasmic content has been hypothesized to occur due to an imperfect NPC permeability barrier, leakage during NPC assembly, mechanical ruptures of the nuclear envelope and during open mitosis (32). Thus, importin 13 might be required to actively sort these proteins back to the cytoplasm.

4.3.2.1 Novel Importin 13 Export Cargoes

One of the first importin 13 cargoes to be identified was eIF1A (135) and thus it is probably one of the major importin 13 cargoes. It was therefore expected to be detected as a high scoring protein in the SILAC screen. Indeed, it was enriched 9-fold in the importin 13 pull-down reaction with RanGTP compared to the reaction without RanGTP (Imp13+Ran/Imp13) and even 28-fold compared to the reaction with Ubc9 (Imp13+Ran/Imp13+Ubc9). The higher enrichment for the Imp13+Ran/Imp13+Ubc9 ratio compared to the Imp13+Ran/Imp13 ratio illustrates that Ubc9 is an effective tool to prevent the formation of export complexes. Further, this shows that eIF1A can bind to importin 13 in the absence of RanGTP, as has previously been reported (135). Only export cargoes that bind to importin 13 in a non-cooperative manner, like eIF1A, are expected to be identified in the pull-down reaction with importin 13 alone. In contrast, export cargoes that

require cooperative binding with RanGTP are not expected to be identified in this reaction. This is based on the assumption that RanGTP is only present in its GDP-bound form in the cell extract due to the activity of cytoplasmic RanGAP. The other reported importin 13 export cargo HMG20A was not detected in the SILAC screen and EIF4G2 was identified as a low confidence export cargo. As these proteins were originally identified as interactors of the testis-specific form of importin 13 in a yeast-two hybrid screen using a human testis cDNA library, these proteins might be testis-specific importin 13 cargoes.

In total 12 out of 19 export cargo candidates tested in importin 13 overexpression experiments were relocalized to the cytoplasm in the presence of importin 13, validating them as novel export cargoes. While importin 13 overexpression did not affect all proteins tested, it does not necessarily mean that they are false positives. As demonstrated with the LMB treatment to inhibit Crm1 activity, other nuclear transport receptors can be involved in the subcellular localization of these proteins. While BTF3, EIF2D and SQSTM1 could be confirmed to be regulated by both Crm1 and importin 13 in their subcellular localization, TYW3, EIF2AK2 and PRMT5 remained cytoplasmic also after LMB treatment. These proteins might be exported by yet another exportin. Importin 13 mediated export could also be required exclusively after mitosis to sort the proteins back to their designated compartment. Knock-down of importin 13 could be a way to assess this latter possibility. Further, export cargo candidates with a nuclear localization that are not affected by importin 13 coexpression could also be part of a larger complex or require additional cofactors or post-translational modifications that are limiting in the overexpression conditions. Indeed, nuclear transport receptors have been shown to be functionally regulated by protein modifications, inhibitory factors and specific anchorings (reviewed in (88)). Thus, the effect of importin 13 overexpression or knock-down on the endogenous proteins should be analyzed. Furthermore, the observed interactions might have a regulatory function on importin 13 or be required for other cellular functions of importin 13. In this regard, nuclear transport receptors have been shown to be involved in cellular processes independent of transport such as mitosis and nuclear envelope assembly (71, 83–87).

4.3.2.2 Novel Importin 13 Import Cargoes

Apart from the known export cargo eIF1A, several of the well-established importin 13 import cargoes were identified in the SILAC screen, showing that this approach can effectively distinguish between import and export cargoes. All proteins reported to be imported as heterodimers by importin 13 showed similar enrichments for both subunits in

the SILAC experiment, further confirming that these proteins bind as heterodimers to importin 13. While the NFYB/NFYC heterodimer was enriched 1.4-fold for the binding reaction with importin 13 alone compared to binding reactions in the presence of excess Ubc9 (Imp13/Imp13+Ubc9), the CHRAC15/CHRAC17 heterodimer was enriched more than 30-fold. All of the known import cargoes were specifically enriched for the Imp13/Imp13+Ubc9 ratio, but not for the Imp13/Imp13+Ran ratio. This was surprising, as previous importin 13 pull-down experiments demonstrated that Ubc9 and Mago/Y14 can indeed be dissociated from importin 13 by $RanGTP_{Q69L}$ (135). Possibly, substantially different amounts of cell lysate were used for the binding experiments and/or the loading of Ran_{Q69L} with GTP was not 100% efficient. Consequently, limited amounts of Ran in its GTP-bound form might not be sufficient to prevent the binding of import cargoes to importin 13. However, as export cargoes were enriched in the binding reaction with $RanGTP_{Q69L}$ (Imp13+Ran/Imp13), loading of Ran_{Q69L} with GTP must have occurred to some extent.

Independent of the findings described above, proteins were selected that were enriched for either the Imp13/Imp13+Ubc9 ratio or the Imp13/Imp13+Ran ratio or both, to analyze whether import cargoes can also be identified using the Imp13/Imp13+Ran criterion. For the import cargo candidates tested, 9 out of 18 proteins were affected by importin 13 overexpression. As discussed for the export cargo candidates (4.3.2.1), proteins that could not be verified in overexpression experiments are not necessarily false positives. Additional factors or modifications that are limiting in the overexpression conditions could be required. In this regard, several known importin 13 cargoes have been shown to be imported only as heterodimers but not as individual subunits (135, 141, 146, 147). This could also apply to the subunits of the negative elongation factor (NELF) complex. While NELFA and NELFB were not affected by importin 13 overexpression, NELFCD did show a minor increase in nuclear localization. Thus, it is possible that not the individual subunits, but rather the whole NELF complex is imported by importin 13. Apart from NELFCD, other subunits of the NELF complex might also bind to importin 13, resulting in a stronger import than that of NELFCD alone. Coexpression experiments need be done for reported oligomeric proteins to test whether nuclear import is enhanced if more than one subunit is coexpressed with importin 13. In addition, binding experiments should be performed to test if binding of only the oligomer to importin 13 can be detected or also binding of the individual subunits.

PDCD4, RBM22 and NELFA fused to both an HA- and a GFP-GST-tag already showed a nuclear localization in the absence of importin 13, preventing an assessment of

importin 13 involvement in the nuclear localization of these proteins using overexpression assays. Similar to the experiments performed with LMB to inhibit Crm1-dependent export, one could test if import of these proteins is mediated by importin α/β or transportin using the inhibitors Bimax (203) and M9M (99), respectively. Proteins relocalized to the cytoplasm could then be analyzed for importin 13 effects. The import cargo candidates ERI1 and NELFCD could be shown to relocalize to the nucleus in the presence of importin 13 overexpression. In contrast, the other seven import cargo candidates that were affected by importin 13 overexpression were not relocalized to the nucleus, but against expectations to the cytoplasm. Two of these proteins, namely GTF2F2 and PPP1CA, could indeed be export cargoes, as they showed a minor enrichment for Imp13+Ran/Imp13 of 1.3- and 1.1-fold, respectively. All other proteins were specifically enriched for importin 13 and reduced in the presence of excess $RanGTP_{Q69L}$ or Ubc9, emphasizing them as potential import cargoes. Several reasons could account for this observation. The interaction could be transport independent, with coexpressed importin 13 trapping the protein in the cytoplasm and preventing its nuclear import through other transport receptors. Similarly, importin 13 could function as a negative regulator of import, as it has been reported for the testis-specific form of importin 13 (136, 172). Further, importin 13 might bind to the protein, but transport could depend on a heterodimer of transport receptors as has been shown for the H1 histone linker that is imported by the importin β/importin 7 heterodimer but not by the individual transport receptors (113, 114). The identification of importin 5 as a putative importin 13 import cargo in this work and the SILAC-Tp study (76) and the relatively high overlap of identified cargo candidates for importin 13 and importin 5 suggest that they might form a heterodimer. Finally, a protein could be both imported and exported by importin 13, depending on its interaction with other proteins or its post-translational modifications. If the export rate for one protein complex is faster than the import rate for the other complex, then the protein is expected to accumulate in the cytoplasm.

In conclusion, the SILAC screen is a more suitable approach than the importin 13 overexpression screen, allowing for the large-scale identification of both importin 13 import and export cargo candidates. Further analysis is required to show that the interaction is direct and that importin 13 mediates their nuclear transport. For this, binding assays with recombinant proteins or transport assays in permeabilized cells could be used.

4.3.3 Importin 13 a Bidirectional Nuclear Transport Receptor of Many Import and Export Cargoes

When this study was started, it was unclear whether the primary function of importin 13 is nuclear import or whether it also plays a significant role in nuclear export, as eIF1A was the only established importin 13 export cargo. The identification of many novel importin 13 cargo candidates in this study shows that importin 13 is indeed a bidirectional transport receptor. While bidirectional transport would be assumed to be more effective than unidirectional transport, as it can mediate transport of two cargoes with the hydrolysis of one RanGTP molecule, it does give rise to the question as to why this is not a general function of all nuclear transport receptors. As discussed by Mingot *et al*., 2001 (135), bidirectional transport could be limiting in the accumulation of cargoes against a chemical gradient due to the lesser expenditure of energy.

4.3.4 Importin 13 a Negative Regulator of Nucleocytoplasmic Transport?

Although the results obtained here demonstrate that importin 13 interacts with a large number of cellular proteins, they do not allow for differentiation of facilitated transport or inhibition of transport for all cargoes. This especially applies to the proteins identified as putative import cargoes that were relocalized to the cytoplasm and not to the nucleus upon coexpression of both full-length and an N-terminally truncated importin 13. The N-terminal fragment of importin 13 is expected to be functional, as FRAP experiments by Tao *et al*., 2004 (162) demonstrated that an N-terminal importin 13 fragment (amino acids 1-488) is still capable of shuttling, albeit at a reduced rate. Similarly, the N-terminus of importin β has been suggested to be sufficient for mediating the nuclear import of the parathyroid hormone-related protein (PTHrP) in a Ran-dependent manner (90). FRAP and FLIP experiments as well as transport assays could be performed to test if the cargo candidates are shuttled in the presence of importin 13. As discussed earlier, additional factors or modifications might be required to facilitate importin 13 mediated import of these proteins. In this regard, it has been suggested that import cargo release depends not only on RanGTP binding, but also requires the presence of an importin 13 export cargo. Thus, overexpression experiments in the presence of an export cargo could be performed to assess if they are required for import complex disassembly.

4.3.5 Importin 13 an Exportin for M9 Containing Proteins?

A curious finding of the overexpression screen was that importin 13 affected the subcellular distribution of the artificial import cargo dGFP-GST-M9. M9 is an import signal (PY-NLS) found in the heterogeneous nuclear ribonucleoproteins hnRNPA1 and hnRNPA2 that is recognized by transportin (204). hnRNPA1 functions in regulation of transcription, alternative splicing and mRNA nuclear export (205–207). The M9 sequence has been suggested to not only function as an import signal, but also as a signal sequence for nuclear export (208). Thus, importin 13 might function as an exportin for M9 containing substrates. This hypothesis is further supported by findings from the SILAC screen, where hnRNPA1 was identified as a high confidence export cargo candidate with a more than 9-fold enrichment for binding reactions in the presence of $RanGTP_{Q69L}$ compared to binding reactions without $RanGTP_{Q69L}$ (Imp13+Ran/Imp13) (Table 18). Apart from hnRNPA1, several other heterogeneous nuclear ribonucleoproteins were identified as potential importin 13 export cargoes, namely hnRNPH1, A2B1, AB and C in at least one of the SILAC replicates and HNRNPD, K, and U in all three biological replicates (Table 18). Of these, HNRNPD was analyzed in more detail and indeed it was relocalized to the cytoplasm in importin 13 overexpression experiments. For the validation of importin 13 as a potential exportin for M9 containing cargoes, overexpression experiments, binding assays, transport assays and mutational studies should be performed.

Table 18: Heterogeneous nuclear ribonucleoproteins (hnRNPs) identified in SILAC screen (see section 3.3.3 for experimental details)

Uniprot ID	Protein Name	Gene	log2(Imp13+Ran/ Imp13)	log2(Imp13+Ran/ Imp13+Ubc9)
detected in 3 SILAC replicates				
F8VZ49	Heterogeneous nuclear ribonucleoprotein A1	HNRNPA1	3.33691	3.12131
H0YA96	Heterogeneous nuclear ribonucleoprotein D0	HNRNPD	2.96732	2.53505
P61978	Heterogeneous nuclear ribonucleoprotein K	HNRNPK	1.19892	2.05797
Q00839	Heterogeneous nuclear ribonucleoprotein U	HNRNPU	0.939557	0.290223
detected in 2 SILAC replicates				
E9PCY7	Heterogeneous nuclear ribonucleoprotein H	HNRNPH1	0.430966	1.55829
detected in 1 SILAC replicates				
P22626	Heterogeneous nuclear ribonucleoproteins A2/B1	HNRNPA2B1	1.4814	1.94375
Q99729	Heterogeneous nuclear ribonucleoprotein A/B	HNRNPAB	1.32688	0.662844
G3V5X6	Heterogeneous nuclear ribonucleoproteins C1/C2	HNRNPC	0.542857	-0.026021

5. Outlook

Further validation of the identified importin 13 cargo candidates is required to confirm them as importin 13 transport cargoes. In a first step, binding experiments with recombinant proteins should be performed to show that the interaction between the identified proteins and importin 13 is direct. In a second step, these proteins should then be tested in transport assays in permeabilized cells to prove that they are indeed imported or exported in an importin 13-dependent manner. Confirmed importin 13 cargoes should then be analyzed for a possible common targeting signal that is recognized by importin 13. Furthermore, the binding regions on importin 13 for these proteins should be identified. In addition, it could be interesting to test if importin 13 can bind the novel export cargoes in a cooperative or non-cooperative manner with RanGTP, as has been suggested for eIF1A (107, 135).

As importin 13 is expressed only at low levels in HeLa P4 cells, the effect of importin 13 on the identified cargoes should also be analyzed in cells with higher endogenous importin 13 concentrations, such as cells derived from brain or from testis. Knock-down of importin 13 in such cells could help to verify additional importin 13 cargo candidates. Similarly, the cargo candidates could be analyzed in embryonic stem cells to determine if they are developmentally regulated.

The possible functional link between importin 13 and Nup358-dependent transport should be tested for the identified SILAC cargo candidates by knocking-down Nup358 in HeLa P4 cells or expressing inhibitory soluble Nup358 fragments (49). Complementary to this, a direct interaction between importin 13 and Nup358, Nup50 (135) or other nucleoporins should be analyzed, to gain insights into importin 13 translocation through the NPC. To this end binding assays, proximity ligation assays, RanGAP assays or siRNA mediated knock-down of specific nucleoporins could be performed.

Furthermore, the possible role of importin 13 in the export of M9 signal sequence containing proteins as well as the formation of a possible importin 13/importin 5 heterodimer should be tested using overexpression experiments, binding assays and transport assays.

Finally, it will be of interest to see how importin 13 mediated nucleocytoplasmic transport of specific cargoes affects certain cellular pathways and its possible involvement in diseases such as asthma and cancer.

Taken together, the larger spectrum of importin 13 cargoes will give new insights into importin 13 mediated nucleocytoplasmic transport.

References

1. Alberts, B. (2008) *Molecular Biology of the Cell,* 5th Ed., Garland Science
2. Watson ML. (1959) Further observations on the nuclear envelope of the animal cell. *The Journal of Biophysical and Biochemical Cytology* **6**, 147–156
3. Hoelz, A., Debler, E. W., and Blobel, G. (2011) The structure of the nuclear pore complex. *Annual Review of Biochemistry* **80**, 613–643
4. Lin, D. H., Stuwe, T., Schilbach, S., Rundlet, E. J., Perriches, T., Mobbs, G., Fan, Y., Thierbach, K., Huber, F. M., Collins, L. N., Davenport, A. M., Jeon, Y. E., and Hoelz, A. (2016) Architecture of the symmetric core of the nuclear pore. *Science* **352**, aaf1015
5. Kosinski, J., Mosalaganti, S., Appen, A. von, Teimer, R., DiGuilio, A. L., Wan, W., Bui, K. H., Hagen, W. J. H., Briggs, J. A. G., Glavy, J. S., Hurt, E., and Beck, M. (2016) Molecular architecture of the inner ring scaffold of the human nuclear pore complex. *Science* **352**, 363–365
6. Appen, A. von, Kosinski, J., Sparks, L., Ori, A., DiGuilio, A. L., Vollmer, B., Mackmull, M.-T., Banterle, N., Parca, L., Kastritis, P., Buczak, K., Mosalaganti, S., Hagen, W., Andres-Pons, A., Lemke, E. A., Bork, P., Antonin, W., Glavy, J. S., Bui, K. H., and Beck, M. (2015) In situ structural analysis of the human nuclear pore complex. *Nature* **526**, 140–143
7. Bui, K. H., Appen, A. von, DiGuilio, A. L., Ori, A., Sparks, L., Mackmull, M.-T., Bock, T., Hagen, W., Andres-Pons, A., Glavy, J. S., and Beck, M. (2013) Integrated structural analysis of the human nuclear pore complex scaffold. *Cell* **155**, 1233–1243
8. Beck, M., Forster, F., Ecke, M., Plitzko, J. M., Melchior, F., Gerisch, G., Baumeister, W., and Medalia, O. (2004) Nuclear pore complex structure and dynamics revealed by cryoelectron tomography. *Science* **306**, 1387–1390
9. Hinshaw, J. E., Carragher, B. O., and Milligan, R. A. (1992) Architecture and design of the nuclear pore complex. *Cell* **69**, 1133–1141
10. Maimon, T., Elad, N., Dahan, I., and Medalia, O. (2012) The human nuclear pore complex as revealed by cryo-electron tomography. *Structure* **20**, 998–1006
11. Ungricht, R., Klann, M., Horvath, P., and Kutay, U. (2015) Diffusion and retention are major determinants of protein targeting to the inner nuclear membrane. *The Journal of Cell Biology* **209**, 687–703
12. Schwartz, T. U. (2016) The Structure Inventory of the Nuclear Pore Complex. *Journal of Molecular Biology* **428**, 1986–2000

13. Dickmanns, A., Kehlenbach, R. H., and Fahrenkrog, B. (2015) Nuclear Pore Complexes and Nucleocytoplasmic Transport: From Structure to Function to Disease. *International Review of Cell and Molecular Biology* **320**, 171–233
14. Gall, J. G. (1967) Octagonal nuclear pores. *The Journal of Cell Biology* **32**, 391–399
15. Reichelt, R., Holzenburg, A., Buhle, E. L., JR, Jarnik, M., Engel, A., and Aebi, U. (1990) Correlation between structure and mass distribution of the nuclear pore complex and of distinct pore complex components. *The Journal of Cell Biology* **110**, 883–894
16. Schmidt, H. B., and Görlich, D. (2016) Transport Selectivity of Nuclear Pores, Phase Separation, and Membraneless Organelles. *Trends in Biochemical Sciences* **41**, 46–61
17. Rout, M. P., and Blobel, G. (1993) Isolation of the yeast nuclear pore complex. *The Journal of Cell Biology* **123**, 771–783
18. Asakawa, H., Yang, H.-J., Yamamoto, T. G., Ohtsuki, C., Chikashige, Y., Sakata-Sogawa, K., Tokunaga, M., Iwamoto, M., Hiraoka, Y., and Haraguchi, T. (2014) Characterization of nuclear pore complex components in fission yeast Schizosaccharomyces pombe. *Nucleus* **5**, 149–162
19. Grossman, E., Medalia, O., and Zwerger, M. (2012) Functional architecture of the nuclear pore complex. *Annual Review of Biophysics* **41**, 557–584
20. Ribbeck, K., and Görlich, D. (2001) Kinetic analysis of translocation through nuclear pore complexes. *The EMBO Journal* **20**, 1320–1330
21. Cronshaw, J. M., Krutchinsky, A. N., Zhang, W., Chait, B. T., and Matunis, M. J. (2002) Proteomic analysis of the mammalian nuclear pore complex. *The Journal of Cell Biology* **158**, 915–927
22. Rout, M. P., Aitchison, J. D., Suprapto, A., Hjertaas, K., Zhao, Y., and Chait, B. T. (2000) The yeast nuclear pore complex: Composition, architecture, and transport mechanism. *The Journal of Cell Biology* **148**, 635–651
23. Werner, A., Flotho, A., and Melchior, F. (2012) The RanBP2/RanGAP1*SUMO1/Ubc9 complex is a multisubunit SUMO E3 ligase. *Molecular Cell* **46**, 287–298
24. Yaseen, N. R., and Blobel, G. (1999) GTP hydrolysis links initiation and termination of nuclear import on the nucleoporin nup358. *The Journal of Biological Chemistry* **274**, 26493–26502
25. Ritterhoff, T., Das, H., Hofhaus, G., Schroder, R. R., Flotho, A., and Melchior, F. (2016) The RanBP2/RanGAP1*SUMO1/Ubc9 SUMO E3 ligase is a disassembly machine for Crm1-dependent nuclear export complexes. *Nature Communications* **7**, 11482
26. Patel, S. S., Belmont, B. J., Sante, J. M., and Rexach, M. F. (2007) Natively unfolded nucleoporins gate protein diffusion across the nuclear pore complex. *Cell* **129**, 83–96

27. Ribbeck, K., and Görlich, D. (2002) The permeability barrier of nuclear pore complexes appears to operate via hydrophobic exclusion. *The EMBO Journal* **21**, 2664–2671
28. Beck, M., and Hurt, E. (2017) The nuclear pore complex: Understanding its function through structural insight. *Nature Reviews. Molecular Cell Biology* **18**, 73–89
29. Strambio-De-Castillia, C., Niepel, M., and Rout, M. P. (2010) The nuclear pore complex: Bridging nuclear transport and gene regulation. *Nature Reviews. Molecular Cell Biology* **11**, 490–501
30. Hezwani, M., and Fahrenkrog, B. (2017) The Functional Versatility of The Nuclear Pore Complex Proteins. *Seminars in Cell & Developmental Biology*, (Epub ahead of print)
31. Sakuma, S., and D'Angelo, M. A. (2017) The roles of the nuclear pore complex in cellular dysfunction, aging and disease. *Seminars in Cell & Developmental Biology*, (Epub ahead of print)
32. Kirli, K., Karaca, S., Dehne, H. J., Samwer, M., Pan, K. T., Lenz, C., Urlaub, H., and Görlich, D. (2015) A deep proteomics perspective on CRM1-mediated nuclear export and nucleocytoplasmic partitioning. *eLife* **4**, e11466
33. Hülsmann, B. B., Labokha, A. A., and Görlich, D. (2012) The permeability of reconstituted nuclear pores provides direct evidence for the selective phase model. *Cell* **150**, 738–751
34. Frey, S., Richter, R. P., and Görlich, D. (2006) FG-rich repeats of nuclear pore proteins form a three-dimensional meshwork with hydrogel-like properties. *Science* **314**, 815–817
35. Frey, S., and Görlich, D. (2007) A saturated FG-repeat hydrogel can reproduce the permeability properties of nuclear pore complexes. *Cell* **130**, 512–523
36. Rout, M. P., Aitchison, J. D., Magnasco, M. O., and Chait, B. T. (2003) Virtual gating and nuclear transport: the hole picture. *Trends in Cell Biology* **13**, 622–628
37. Lim, R. Y. H., Fahrenkrog, B., Köser, J., Schwarz-Herion, K., Deng, J., and Aebi, U. (2007) Nanomechanical basis of selective gating by the nuclear pore complex. *Science* **318**, 640–643
38. Kapinos, L. E., Schoch, R. L., Wagner, R. S., Schleicher, K. D., and Lim, R. Y. H. (2014) Karyopherin-centric control of nuclear pores based on molecular occupancy and kinetic analysis of multivalent binding with FG nucleoporins. *Biophysical Journal* **106**, 1751–1762
39. Yamada, J., Phillips, J. L., Patel, S., Goldfien, G., Calestagne-Morelli, A., Huang, H., Reza, R., Acheson, J., Krishnan, V. V., Newsam, S., Gopinathan, A., Lau, E. Y., Colvin, M. E., Uversky, V. N., and Rexach, M. F. (2010) A bimodal distribution of two

distinct categories of intrinsically disordered structures with separate functions in FG nucleoporins. *Molecular & Cellular Proteomics* **9**, 2205–2224

40. Melcák, I., Hoelz, A., and Blobel, G. (2007) Structure of Nup58/45 suggests flexible nuclear pore diameter by intermolecular sliding. *Science* **315**, 1729–1732
41. Solmaz, S. R., Blobel, G., and Melcák, I. (2013) Ring cycle for dilating and constricting the nuclear pore. *Proceedings of the National Academy of Sciences of the United States of America* **110**, 5858–5863
42. Wälde, S., and Kehlenbach, R. H. (2010) The Part and the Whole: Functions of nucleoporins in nucleocytoplasmic transport. *Trends in Cell Biology* **20**, 461–469
43. Fried, H., and Kutay, U. (2003) Nucleocytoplasmic transport: taking an inventory. *Cellular and Molecular Life Sciences* **60**, 1659–1688
44. Kalab, P., Weis, K., and Heald, R. (2002) Visualization of a Ran-GTP gradient in interphase and mitotic Xenopus egg extracts. *Science* **295**, 2452–2456
45. Smith, A. E., Slepchenko, B. M., Schaff, J. C., Loew, L. M., and Macara, I. G. (2002) Systems analysis of Ran transport. *Science* **295**, 488–491
46. Ben-Efraim, I., and Gerace, L. (2001) Gradient of increasing affinity of importin beta for nucleoporins along the pathway of nuclear import. *The Journal of Cell Biology* **152**, 411–417
47. Hutten, S., Flotho, A., Melchior, F., and Kehlenbach, R. H. (2008) The Nup358-RanGAP complex is required for efficient importin alpha/beta-dependent nuclear import. *Molecular Biology of the Cell* **19**, 2300–2310
48. Hutten, S., Wälde, S., Spillner, C., Hauber, J., and Kehlenbach, R. H. (2009) The nuclear pore component Nup358 promotes transportin-dependent nuclear import. *Journal of Cell Science* **122**, 1100–1110
49. Wälde, S., Thakar, K., Hutten, S., Spillner, C., Nath, A., Rothbauer, U., Wiemann, S., and Kehlenbach, R. H. (2012) The nucleoporin Nup358/RanBP2 promotes nuclear import in a cargo- and transport receptor-specific manner. *Traffic* **13**, 218–233
50. Izaurralde, E., Kutay, U., Kobbe, C. von, Mattaj, I. W., and Görlich, D. (1997) The asymmetric distribution of the constituents of the Ran system is essential for transport into and out of the nucleus. *The EMBO Journal* **16**, 6535–6547
51. Richards, S. A., Carey, K. L., and Macara, I. G. (1997) Requirement of guanosine triphosphate-bound ran for signal-mediated nuclear protein export. *Science* **276**, 1842–1844
52. Bischoff, F. R., and Ponstingl, H. (1991) Catalysis of guanine nucleotide exchange on Ran by the mitotic regulator RCC1. *Nature* **354**, 80–82

53. Bischoff, F. R., Klebe, C., Kretschmer, J., Wittinghofer, A., and Ponstingl, H. (1994) RanGAP1 induces GTPase activity of nuclear Ras-related Ran. *Proceedings of the National Academy of Sciences of the United States of America* **91**, 2587–2591
54. Rexach, M., and Blobel, G. (1995) Protein import into nuclei: Association and dissociation reactions involving transport substrate, transport factors, and nucleoporins. *Cell* **83**, 683–692
55. Görlich, D., Panté, N., Kutay, U., Aebi, U., and Bischoff, F. R. (1996) Identification of different roles for RanGDP and RanGTP in nuclear protein import. *The EMBO Journal* **15**, 5584–5594
56. Askjaer, P., Jensen, T. H., Nilsson, J., Englmeier, L., and Kjems, J. (1998) The specificity of the CRM1-Rev nuclear export signal interaction is mediated by RanGTP. *The Journal of Biological Chemistry* **273**, 33414–33422
57. Monecke, T., Haselbach, D., Voss, B., Russek, A., Neumann, P., Thomson, E., Hurt, E., Zachariae, U., Stark, H., Grubmüller, H., Dickmanns, A., and Ficner, R. (2013) Structural basis for cooperativity of CRM1 export complex formation. *Proceedings of the National Academy of Sciences of the United States of America* **110**, 960–965
58. Kehlenbach, R. H., Dickmanns, A., Kehlenbach, A., Guan, T., and Gerace, L. (1999) A role for RanBP1 in the release of CRM1 from the nuclear pore complex in a terminal step of nuclear export. *The Journal of Cell Biology* **145**, 645–657
59. Bischoff, F. R., and Görlich, D. (1997) RanBP1 is crucial for the release of RanGTP from importin beta-related nuclear transport factors. *FEBS letters* **419**, 249–254
60. Moore, M. S., and Blobel, G. (1994) Purification of a Ran-interacting protein that is required for protein import into the nucleus. *Proceedings of the National Academy of Sciences of the United States of America* **91**, 10212–10216
61. Paschal, B. M., and Gerace, L. (1995) Identification of NTF2, a cytosolic factor for nuclear import that interacts with nuclear pore complex protein p62. *The Journal of Cell Biology* **129**, 925–937
62. Ribbeck, K., Lipowsky, G., Kent, H. M., Stewart, M., and Görlich, D. (1998) NTF2 mediates nuclear import of Ran. *The EMBO Journal* **17**, 6587–6598
63. Smith, A., Brownawell, A., and Macara, I. G. (1998) Nuclear import of Ran is mediated by the transport factor NTF2. *Current Biology* **8**, 1403–1406
64. Bischoff, F. R., and Ponstingl, H. (1991) Mitotic regulator protein RCC1 is complexed with a nuclear ras-related polypeptide. *Proceedings of the National Academy of Sciences of the United States of America* **88**, 10830–10834

65. Adam, S. A., Marr, R. S., and Gerace, L. (1990) Nuclear protein import in permeabilized mammalian cells requires soluble cytoplasmic factors. *The Journal of Cell Biology* **111**, 807–816
66. Adam, E. J., and Adam, S. A. (1994) Identification of cytosolic factors required for nuclear location sequence-mediated binding to the nuclear envelope. *The Journal of Cell Biology* **125**, 547–555
67. Melchior, F., Paschal, B., Evans, J., and Gerace, L. (1993) Inhibition of nuclear protein import by nonhydrolyzable analogues of GTP and identification of the small GTPase Ran/TC4 as an essential transport factor. *The Journal of Cell Biology* **123**, 1649–1659
68. Moore, M. S., and Blobel, G. (1993) The GTP-binding protein Ran/TC4 is required for protein import into the nucleus. *Nature* **365**, 661–663
69. Görlich, D., and Kutay, U. (1999) Transport between the cell nucleus and the cytoplasm. *Annual Review of Cell and Developmental Biology* **15**, 607–660
70. Port, S. A., Monecke, T., Dickmanns, A., Spillner, C., Hofele, R., Urlaub, H., Ficner, R., and Kehlenbach, R. H. (2015) Structural and Functional Characterization of CRM1-Nup214 Interactions Reveals Multiple FG-Binding Sites Involved in Nuclear Export. *Cell Reports* **13**, 690–702
71. Chook, Y. M., and Süel, K. E. (2011) Nuclear import by karyopherin-betas: recognition and inhibition. *Biochimica et Biophysica Acta* **1813**, 1593–1606
72. Cook, A., Bono, F., Jinek, M., and Conti, E. (2007) Structural biology of nucleocytoplasmic transport. *Annual Review of Biochemistry* **76**, 647–671
73. Andrade, M. A., and Bork, P. (1995) HEAT repeats in the Huntington's disease protein. *Nature Genetics* **11**, 115–116
74. Andrade, M. A., Perez-Iratxeta, C., and Ponting, C. P. (2001) Protein repeats: structures, functions, and evolution. *Journal of Structural Biology* **134**, 117–131
75. Pemberton, L. F., and Paschal, B. M. (2005) Mechanisms of receptor-mediated nuclear import and nuclear export. *Traffic* **6**, 187–198
76. Kimura, M., Morinaka, Y., Imai, K., Kose, S., Horton, P., and Imamoto, N. (2017) Extensive cargo identification reveals distinct biological roles of the 12 importin pathways. *eLife* **6**, e21184
77. Hahn, S., and Schlenstedt, G. (2011) Importin beta-type nuclear transport receptors have distinct binding affinities for Ran-GTP. *Biochemical and Biophysical Research Communications* **406**, 383–388

78. Kimura, M., Thakar, K., Karaca, S., Imamoto, N., and Kehlenbach, R. H. (2014) Novel approaches for the identification of nuclear transport receptor substrates. *Methods in Cell Biology* **122**, 353–378
79. Mann, M. (2006) Functional and quantitative proteomics using SILAC. *Nature Reviews. Molecular Cell Biology* **7**, 952–958
80. Kimura, M., Kose, S., Okumura, N., Imai, K., Furuta, M., Sakiyama, N., Tomii, K., Horton, P., Takao, T., and Imamoto, N. (2013) Identification of cargo proteins specific for the nucleocytoplasmic transport carrier transportin by combination of an in vitro transport system and stable isotope labeling by amino acids in cell culture (SILAC)-based quantitative proteomics. *Molecular & Cellular Proteomics* **12**, 145–157
81. Kimura, M., Okumura, N., Kose, S., Takao, T., and Imamoto, N. (2013) Identification of cargo proteins specific for importin-beta with importin-alpha applying a stable isotope labeling by amino acids in cell culture (SILAC)-based in vitro transport system. *The Journal of Biological Chemistry* **288**, 24540–24549
82. Thakar, K., Karaca, S., Port, S. A., Urlaub, H., and Kehlenbach, R. H. (2013) Identification of CRM1-dependent Nuclear Export Cargos Using Quantitative Mass Spectrometry. *Molecular & Cellular Proteomics* **12**, 664–678
83. Mosammaparast, N., and Pemberton, L. F. (2004) Karyopherins: from nuclear-transport mediators to nuclear-function regulators. *Trends in Cell Biology* **14**, 547–556
84. Arnaoutov, A., and Dasso, M. (2005) Ran-GTP regulates kinetochore attachment in somatic cells. *Cell Cycle* **4**, 1161–1165
85. Budhu, A. S., and Wang, X. W. (2005) Loading and unloading: orchestrating centrosome duplication and spindle assembly by Ran/Crm1. *Cell Cycle* **4**, 1510–1514
86. Lau, C. K., Delmar, V. A., Chan, R. C., Phung, Q., Bernis, C., Fichtman, B., Rasala, B. A., and Forbes, D. J. (2009) Transportin regulates major mitotic assembly events: from spindle to nuclear pore assembly. *Molecular Biology of the Cell* **20**, 4043–4058
87. Dishinger, J. F., Kee, H. L., Jenkins, P. M., Fan, S., Hurd, T. W., Hammond, J. W., Truong, Y. N.-T., Margolis, B., Martens, J. R., and Verhey, K. J. (2010) Ciliary entry of the kinesin-2 motor KIF17 is regulated by importin-beta2 and RanGTP. *Nature Cell Biology* **12**, 703–710
88. Kimura, M., and Imamoto, N. (2014) Biological significance of the importin-beta family-dependent nucleocytoplasmic transport pathways. *Traffic* **15**, 727–748
89. Imasaki, T., Shimizu, T., Hashimoto, H., Hidaka, Y., Kose, S., Imamoto, N., Yamada, M., and Sato, M. (2007) Structural basis for substrate recognition and dissociation by human transportin 1. *Molecular Cell* **28**, 57–67

90. Cingolani, G., Bednenko, J., Gillespie, M. T., and Gerace, L. (2002) Molecular basis for the recognition of a nonclassical nuclear localization signal by importin beta. *Molecular Cell* **10**, 1345–1353
91. Lee, B. J., Cansizoglu, A. E., Süel, K. E., Louis, T. H., Zhang, Z., and Chook, Y. M. (2006) Rules for nuclear localization sequence recognition by karyopherin beta 2. *Cell* **126**, 543–558
92. Bono, F., Cook, A. G., Grünwald, M., Ebert, J., and Conti, E. (2010) Nuclear import mechanism of the EJC component Mago-Y14 revealed by structural studies of importin 13. *Molecular Cell* **37**, 211–222
93. Grünwald, M., and Bono, F. (2011) Structure of Importin13-Ubc9 complex: nuclear import and release of a key regulator of sumoylation. *The EMBO Journal* **30**, 427–438
94. Jeong, S. A., Kim, K., Lee, J. H., Cha, J. S., Khadka, P., Cho, H.-S., and Chung, I. K. (2015) Akt-mediated phosphorylation increases the binding affinity of hTERT for importin alpha to promote nuclear translocation. *Journal of Cell Science* **128**, 2287–2301
95. Niu, C., Zhang, J., Gao, F., Yang, L., Jia, M., Zhu, H., and Gong, W. (2012) FUS-NLS/Transportin 1 complex structure provides insights into the nuclear targeting mechanism of FUS and the implications in ALS. *PloS One* **7**, e47056
96. Maertens, G. N., Cook, N. J., Wang, W., Hare, S., Gupta, S. S., Öztop, I., Lee, K., Pye, V. E., Cosnefroy, O., Snijders, A. P., KewalRamani, V. N., Fassati, A., Engelman, A., and Cherepanov, P. (2014) Structural basis for nuclear import of splicing factors by human Transportin 3. *Proceedings of the National Academy of Sciences of the United States of America* **111**, 2728–2733
97. Cingolani, G., Petosa, C., Weis, K., and Muller, C. W. (1999) Structure of importin-beta bound to the IBB domain of importin-alpha. *Nature* **399**, 221–229
98. Lee, S. J., Sekimoto, T., Yamashita, E., Nagoshi, E., Nakagawa, A., Imamoto, N., Yoshimura, M., Sakai, H., Chong, K. T., Tsukihara, T., and Yoneda, Y. (2003) The structure of importin-beta bound to SREBP-2: nuclear import of a transcription factor. *Science* **302**, 1571–1575
99. Cansizoglu, A. E., Lee, B. J., Zhang, Z. C., Fontoura, B. M. A., and Chook, Y. M. (2007) Structure-based design of a pathway-specific nuclear import inhibitor. *Nature Structural & Molecular Biology* **14**, 452–454
100. Huber, F. M., and Hoelz, A. (2017) Molecular basis for protection of ribosomal protein L4 from cellular degradation. *Nature Communications* **8**, 14354

101. Monecke, T., Güttler, T., Neumann, P., Dickmanns, A., Görlich, D., and Ficner, R. (2009) Crystal structure of the nuclear export receptor CRM1 in complex with Snurportin1 and RanGTP. *Science* **324**, 1087–1091

102. Güttler, T., Madl, T., Neumann, P., Deichsel, D., Corsini, L., Monecke, T., Ficner, R., Sattler, M., and Görlich, D. (2010) NES consensus redefined by structures of PKI-type and Rev-type nuclear export signals bound to CRM1. *Nature Structural & Molecular Biology* **17**, 1367–1376

103. Fung, H. Y. J., Fu, S.-C., and Chook, Y. M. (2017) Nuclear export receptor CRM1 recognizes diverse conformations in nuclear export signals. *eLife* **6**, e23961

104. Cook, A. G., and Conti, E. (2010) Nuclear export complexes in the frame. *Current Opinion in Structural Biology* **20**, 247–252

105. Okada, C., Yamashita, E., Lee, S. J., Shibata, S., Katahira, J., Nakagawa, A., Yoneda, Y., and Tsukihara, T. (2009) A high-resolution structure of the pre-microRNA nuclear export machinery. *Science* **326**, 1275–1279

106. Aksu, M., Trakhanov, S., and Görlich, D. (2016) Structure of the exportin Xpo4 in complex with RanGTP and the hypusine-containing translation factor eIF5A. *Nature Communications* **7**, 11952

107. Grünwald, M., Lazzaretti, D., and Bono, F. (2013) Structural basis for the nuclear export activity of Importin13. *The EMBO Journal* **32**, 899–913

108. Matsuura, Y., and Stewart, M. (2004) Structural basis for the assembly of a nuclear export complex. *Nature* **432**, 872–877

109. Görlich, D., Prehn, S., Laskey, R. A., and Hartmann, E. (1994) Isolation of a protein that is essential for the first step of nuclear protein import. *Cell* **79**, 767–778

110. Goldfarb, D. S., Corbett, A. H., Mason, D. A., Harreman, M. T., and Adam, S. A. (2004) Importin alpha: a multipurpose nuclear-transport receptor. *Trends in Cell Biology* **14**, 505–514

111. Huber, J., Cronshagen, U., Kadokura, M., Marshallsay, C., Wada, T., Sekine, M., and Lührmann, R. (1998) Snurportin1, an m3G-cap-specific nuclear import receptor with a novel domain structure. *The EMBO Journal* **17**, 4114–4126

112. Ström, A. C., and Weis, K. (2001) Importin-beta-like nuclear transport receptors. *Genome Biology* **2**, 3008

113. Görlich, D., Dabrowski, M., Bischoff, F. R., Kutay, U., Bork, P., Hartmann, E., Prehn, S., and Izaurralde, E. (1997) A novel class of RanGTP binding proteins. *The Journal of Cell Biology* **138**, 65–80

114. Jäkel, S., Albig, W., Kutay, U., Bischoff, F. R., Schwamborn, K., Doenecke, D., and Görlich, D. (1999) The importin beta/importin 7 heterodimer is a functional nuclear import receptor for histone H1. *The EMBO Journal* **18**, 2411–2423

115. Mühlhaüsser, P., Müller, E. C., Otto, A., and Kutay, U. (2001) Multiple pathways contribute to nuclear import of core histones. *EMBO Reports* **2**, 690–696

116. Arnold, M., Nath, A., Hauber, J., and Kehlenbach, R. H. (2006) Multiple importins function as nuclear transport receptors for the Rev protein of human immunodeficiency virus type 1. *The Journal of Biological Chemistry* **281**, 20883–20890

117. Waldmann, I., Wälde, S., and Kehlenbach, R. H. (2007) Nuclear import of c-Jun is mediated by multiple transport receptors. *The Journal of Biological Chemistry* **282**, 27685–27692

118. Jäkel, S., and Görlich, D. (1998) Importin beta, transportin, RanBP5 and RanBP7 mediate nuclear import of ribosomal proteins in mammalian cells. *The EMBO Journal* **17**, 4491–4502

119. Tu, L.-C., Fu, G., Zilman, A., and Musser, S. M. (2013) Large cargo transport by nuclear pores: implications for the spatial organization of FG-nucleoporins. *The EMBO Journal* **32**, 3220–3230

120. Xu, D., Farmer, A., and Chook, Y. M. (2010) Recognition of nuclear targeting signals by Karyopherin-beta proteins. *Current Opinion in Structural Biology* **20**, 782–790

121. Dingwall, C., Sharnick, S. V., and Laskey, R. A. (1982) A polypeptide domain that specifies migration of nucleoplasmin into the nucleus. *Cell* **30**, 449–458

122. Lanford, R. E., and Butel, J. S. (1984) Construction and characterization of an SV40 mutant defective in nuclear transport of T antigen. *Cell* **37**, 801–813

123. Kalderon, D., Richardson, W. D., Markham, A. F., and Smith, A. E. (1984) Sequence requirements for nuclear location of simian virus 40 large-T antigen. *Nature* **311**, 33–38

124. Görlich, D., Kostka, S., Kraft, R., Dingwall, C., Laskey, R. A., Hartmann, E., and Prehn, S. (1995) Two different subunits of importin cooperate to recognize nuclear localization signals and bind them to the nuclear envelope. *Current Biology* **5**, 383–392

125. Radu, A., Moore, M. S., and Blobel, G. (1995) The peptide repeat domain of nucleoporin Nup98 functions as a docking site in transport across the nuclear pore complex. *Cell* **81**, 215–222

126. Kataoka, N., Bachorik, J. L., and Dreyfuss, G. (1999) Transportin-SR, a nuclear import receptor for SR proteins. *The Journal of Cell Biology* **145**, 1145–1152

127. Fischer, U., Huber, J., Boelens, W. C., Mattaj, I. W., and Lührmann, R. (1995) The HIV-1 Rev activation domain is a nuclear export signal that accesses an export pathway used by specific cellular RNAs. *Cell* **82**, 475–483

128. Wen, W., Meinkoth, J. L., Tsien, R. Y., and Taylor, S. S. (1995) Identification of a signal for rapid export of proteins from the nucleus. *Cell* **82**, 463–473

129. Fornerod, M., Ohno, M., Yoshida, M., and Mattaj, I. W. (1997) CRM1 is an export receptor for leucine-rich nuclear export signals. *Cell* **90**, 1051–1060

130. Fukuda, M., Asano, S., Nakamura, T., Adachi, M., Yoshida, M., Yanagida, M., and Nishida, E. (1997) CRM1 is responsible for intracellular transport mediated by the nuclear export signal. *Nature* **390**, 308–311

131. Sorokin, A. V., Kim, E. R., and Ovchinnikov, L. P. (2007) Nucleocytoplasmic transport of proteins. *Biochemistry. Biokhimiia* **72**, 1439–1457

132. Poon, I. K. H., and Jans, D. A. (2005) Regulation of nuclear transport: central role in development and transformation? *Traffic* **6**, 173–186

133. Nagase, T., Ishikawa, K., Suyama, M., Kikuno, R., Miyajima, N., Tanaka, A., Kotani, H., Nomura, N., and Ohara, O. (1998) Prediction of the coding sequences of unidentified human genes. XI. The complete sequences of 100 new cDNA clones from brain which code for large proteins in vitro. *DNA Research* **5**, 277–286

134. Zhang, C., Sweezey, N. B., Gagnon, S., Muskat, B., Koehler, D., Post, M., and Kaplan, F. (2000) A novel karyopherin-beta homolog is developmentally and hormonally regulated in fetal lung. *American Journal of Respiratory Cell and Molecular Biology* **22**, 451–459

135. Mingot, J. M., Kostka, S., Kraft, R., Hartmann, E., and Görlich, D. (2001) Importin 13: A novel mediator of nuclear import and export. *The EMBO Journal* **20**, 3685–3694

136. Fatima, S., Wagstaff, K. M., Lieu, K. G., Davies, R. G., Tanaka, S. S., Yamaguchi, Y. L., Loveland, K. L., Tam, P. P. L., and Jans, D. A. (2017) Interactome of the inhibitory isoform of the nuclear transporter Importin 13. *Biochimica et Biophysica Acta* **1864**, 546–561

137. Ploski, J. E., Shamsher, M. K., and Radu, A. (2004) Paired-type homeodomain transcription factors are imported into the nucleus by karyopherin 13. *Molecular and Cellular Biology* **24**, 4824–4834

138. Lin, W., Ye, W., Cai, L., Meng, X., Ke, G., Huang, C., Peng, Z., Yu, Y., Golden, J. A., Tartakoff, A. M., and Tao, T. (2009) The roles of multiple importins for nuclear import of murine aristaless-related homeobox protein. *The Journal of Biological Chemistry* **284**, 20428–20439

139. Shoubridge, C., Cloosterman, D., Parkinson-Lawerence, E., Brooks, D., and Gécz, J. (2007) Molecular pathology of expanded polyalanine tract mutations in the Aristaless-related homeobox gene. *Genomics* **90**, 59–71

140. Lin, W., Xu, P., Guo, Y., Jia, Q., and Tao, T. (2017) Nuclear import of Nkx2-2 is mediated by multiple pathways. *Biochemical and Biophysical Research Communications* **482**, 1511–1516

141. Kahle, J., Baake, M., Doenecke, D., and Albig, W. (2005) Subunits of the heterotrimeric transcription factor NF-Y are imported into the nucleus by distinct pathways involving importin beta and importin 13. *Molecular and Cellular Biology* **25**, 5339–5354

142. Xu, K., Tao, T., Jie, J., Lu, X., Li, X., Mehmood, M. A., He, H., Liu, Z., Xiao, X., Yang, J., Ma, J.-x., Li, W., Zhou, Y., and Liu, Z. (2013) Increased importin 13 activity is associated with the pathogenesis of pterygium. *Molecular Vision* **19**, 604–613

143. Tao, T., Lan, J., Lukacs, G. L., Hache, R. J. G., and Kaplan, F. (2006) Importin 13 regulates nuclear import of the glucocorticoid receptor in airway epithelial cells. *American Journal of Respiratory Cell and Molecular Biology* **35**, 668–680

144. Kanno, Y., Miyazaki, Y., and Inouye, Y. (2010) The nuclear import of the constitutive androstane receptor by importin/Ran-GTP systems. *Biochimica et Biophysica Acta* **1803**, 968–974

145. Wang, R., Shen, J., Huang, P., and Zhu, X. (2013) CCCTC-binding factor controls its own nuclear transport via regulating the expression of importin 13. *Molecules and Cells* **35**, 388–395

146. Kahle, J., Piaia, E., Neimanis, S., Meisterernst, M., and Doenecke, D. (2009) Regulation of nuclear import and export of negative cofactor 2. *The Journal of Biological Chemistry* **284**, 9382–9393

147. Walker, P., Doenecke, D., and Kahle, J. (2009) Importin 13 mediates nuclear import of histone fold-containing chromatin accessibility complex heterodimers. *The Journal of Biological Chemistry* **284**, 11652–11662

148. Liang, J., Ke, G., You, W., Peng, Z., Lan, J., Kalesse, M., Tartakoff, A. M., Kaplan, F., and Tao, T. (2008) Interaction between importin 13 and myopodin suggests a nuclear import pathway for myopodin. *Molecular and Cellular Biochemistry* **307**, 93–100

149. Huang, S., Chang, I. S., Lin, W., Ye, W., Luo, R. Z., Lu, Z., Lu, Y., Zhang, K., Liao, W. S.-L., Tao, T., Bast, R. C., JR, Chen, X., and Yu, Y. (2009) ARHI (DIRAS3), an imprinted tumour suppressor gene, binds to importins and blocks nuclear import of cargo proteins. *Bioscience Reports* **30**, 159–168

150. Gontan, C., Güttler, T., Engelen, E., Demmers, J., Fornerod, M., Grosveld, F. G., Tibboel, D., Görlich, D., Poot, R. A., and Rottier, R. J. (2009) Exportin 4 mediates a novel nuclear import pathway for Sox family transcription factors. *The Journal of Cell Biology* **185**, 27–34

151. Yoshida, K., and Blobel, G. (2001) The karyopherin Kap142p/Msn5p mediates nuclear import and nuclear export of different cargo proteins. *The Journal of Cell Biology* **152**, 729–740

152. Blondel, M., Alepuz, P. M., Huang, L. S., Shaham, S., Ammerer, G., and Peter, M. (1999) Nuclear export of Far1p in response to pheromones requires the export receptor Msn5p/Ste21p. *Genes & Development* **13**, 2284–2300

153. Taberner, F. J., Quilis, I., Sendra, J., Banó, M. C., and Igual, J. C. (2012) Regulation of cell cycle transcription factor Swi5 by karyopherin Msn5. *Biochimica et Biophysica Acta* **1823**, 959–970

154. Queralt, E., and Igual, J. C. (2003) Cell cycle activation of the Swi6p transcription factor is linked to nucleocytoplasmic shuttling. *Molecular and Cellular Biology* **23**, 3126–3140

155. Görner, W., Durchschlag, E., Wolf, J., Brown, E. L., Ammerer, G., Ruis, H., and Schüller, C. (2002) Acute glucose starvation activates the nuclear localization signal of a stress-specific yeast transcription factor. *The EMBO Journal* **21**, 135–144

156. Kaffman, A., Rank, N. M., O'Neill, E. M., Huang, L. S., and O'Shea, E. K. (1998) The receptor Msn5 exports the phosphorylated transcription factor Pho4 out of the nucleus. *Nature* **396**, 482–486

157. Lipowsky, G., Bischoff, F. R., Schwarzmaier, P., Kraft, R., Kostka, S., Hartmann, E., Kutay, U., and Görlich, D. (2000) Exportin 4: a mediator of a novel nuclear export pathway in higher eukaryotes. *The EMBO Journal* **19**, 4362–4371

158. Kurisaki, A., Kurisaki, K., Kowanetz, M., Sugino, H., Yoneda, Y., Heldin, C.-H., and Moustakas, A. (2006) The mechanism of nuclear export of Smad3 involves exportin 4 and Ran. *Molecular and Cellular Biology* **26**, 1318–1332

159. Subramanian, K. S., Dziedzic, R. C., Nelson, H. N., Stern, M. E., Roggero, V. R., Bondzi, C., and Allison, L. A. (2015) Multiple exportins influence thyroid hormone receptor localization. *Molecular and Cellular Endocrinology* **411**, 86–96

160. Tsuchiya, M., Ogawa, H., Suzuki, T., Sugiyama, N., Haraguchi, T., and Hiraoka, Y. (2011) Exportin 4 interacts with Sox9 through the HMG Box and inhibits the DNA binding of Sox9. *PloS One* **6**, e25694

161. Shoubridge, C., Tan, M. H., Fullston, T., Cloosterman, D., Coman, D., McGillivray, G., Mancini, G. M., Kleefstra, T., and Gécz, J. (2010) Mutations in the nuclear localization sequence of the Aristaless related homeobox; sequestration of mutant ARX with IPO13 disrupts normal subcellular distribution of the transcription factor and retards cell division. *PathoGenetics* **3**, 1

162. Tao, T., Lan, J., Presley, J. F., Sweezey, N. B., and Kaplan, F. (2004) Nucleocytoplasmic shuttling of lgl2 is developmentally regulated in fetal lung. *American Journal of Respiratory Cell and Molecular Biology* **30**, 350–359

163. Raby, B. A., van Steen, K., Lasky-Su, J., Tantisira, K., Kaplan, F., and Weiss, S. T. (2009) Importin-13 genetic variation is associated with improved airway responsiveness in childhood asthma. *Respiratory Research* **10**, 67

164. Wang, H., Tao, T., Tang, J., Mao, Y.-H., Li, W., Peng, J., Tan, G., Zhou, Y.-P., Zhong, J.-X., Tseng, S. C. G., Kawakita, T., Zhao, Y.-X., and Liu, Z.-G. (2009) Importin 13 serves as a potential marker for corneal epithelial progenitor cells. *Stem Cells* **27**, 2516–2526

165. You, P., Peng, Z., Wang, Y., and Tao, T. (2013) Expression and subcellular distribution of imp13 are regulated in brain development. *In Vitro Cellular & Developmental Biology. Animal* **49**, 346–353

166. Giagtzoglou, N., Lin, Y. Q., Haueter, C., and Bellen, H. J. (2009) Importin 13 regulates neurotransmitter release at the Drosophila neuromuscular junction. *The Journal of Neuroscience* **29**, 5628–5639

167. Gehring, W. J. (1996) The master control gene for morphogenesis and evolution of the eye. *Genes to Cells* **1**, 11–15

168. Callaerts, P., Halder, G., and Gehring, W. J. (1997) PAX-6 in development and evolution. *Annual Review of Neuroscience* **20**, 483–532

169. Kitamura, K., Yanazawa, M., Sugiyama, N., Miura, H., Iizuka-Kogo, A., Kusaka, M., Omichi, K., Suzuki, R., Kato-Fukui, Y., Kamiirisa, K., Matsuo, M., Kamijo, S.-i., Kasahara, M., Yoshioka, H., Ogata, T., Fukuda, T., Kondo, I., Kato, M., Dobyns, W. B., Yokoyama, M., and Morohashi, K.-i. (2002) Mutation of ARX causes abnormal development of forebrain and testes in mice and X-linked lissencephaly with abnormal genitalia in humans. *Nature Genetics* **32**, 359–369

170. Friocourt, G., Poirier, K., Rakic, S., Parnavelas, J. G., and Chelly, J. (2006) The role of ARX in cortical development. *The European Journal of Neuroscience* **23**, 869–876

171. Quan, Y., Ji, Z.-L., Wang, X., Tartakoff, A. M., and Tao, T. (2008) Evolutionary and transcriptional analysis of karyopherin beta superfamily proteins. *Molecular & Cellular Proteomics* **7**, 1254–1269

172. Yamaguchi, Y. L., Tanaka, S. S., Yasuda, K., Matsui, Y., and Tam, P. P. L. (2006) Stage-specific Importin13 activity influences meiosis of germ cells in the mouse. *Developmental Biology* **297**, 350–360

173. Zeng, B., Hu, J., Yuan, R., Hu, L., Zhong, L., and Kang, K. (2012) Increased expression of importin13 in endometriosis and endometrial carcinoma. *Medical Science Monitor* **18**, CR361-7

174. Bannasch, D., Mehrle, A., Glatting, K.-H., Pepperkok, R., Poustka, A., and Wiemann, S. (2004) LIFEdb: a database for functional genomics experiments integrating information from external sources, and serving as a sample tracking system. *Nucleic Acids Research* **32**, D505-8

175. Wiemann, S., Arlt, D., Huber, W., Wellenreuther, R., Schleeger, S., Mehrle, A., Bechtel, S., Sauermann, M., Korf, U., Pepperkok, R., Sültmann, H., and Poustka, A. (2004) From ORFeome to biology: A functional genomics pipeline. *Genome Research* **14**, 2136–2144

176. Charneau, P., Mirambeau, G., Roux, P., Paulous, S., Buc, H., and Clavel, F. (1994) HIV-1 reverse transcription. A termination step at the center of the genome. *Journal of Molecular Biology* **241**, 651–662

177. Pichler, A., Gast, A., Seeler, J. S., Dejean, A., and Melchior, F. (2002) The nucleoporin RanBP2 has SUMO1 E3 ligase activity. *Cell* **108**, 109–120

178. Melchior, F., Sweet, D. J., and Gerace, L. (1995) Analysis of Ran/TC4 function in nuclear protein import. *Methods in Enzymology* **257**, 279–291

179. Holden, P., and Horton, W. A. (2009) Crude subcellular fractionation of cultured mammalian cell lines. *BMC Research Notes* **2**, 243

180. Tissera, H., Kodiha, M., and Stochaj, U. (2010) Nuclear envelopes show cell-type specific sensitivity for the permeabilization with digitonin. *Protocol Exchange*

181. Shevchenko, A., Wilm, M., Vorm, O., and Mann, M. (1996) Mass spectrometric sequencing of proteins silver-stained polyacrylamide gels. *Analytical Chemistry* **68**, 850–858

182. Huang, D. W., Sherman, B. T., and Lempicki, R. A. (2009) Bioinformatics enrichment tools: paths toward the comprehensive functional analysis of large gene lists. *Nucleic Acids Research* **37**, 1–13

183. Huang, D. W., Sherman, B. T., and Lempicki, R. A. (2009) Systematic and integrative analysis of large gene lists using DAVID bioinformatics resources. *Nature Protocols* **4**, 44–57

184. Moran, U., Phillips, R., and Milo, R. (2010) SnapShot: Key numbers in biology. *Cell* **141**, 1262-1262

185. Riddick, G., and Macara, I. G. (2005) A systems analysis of importin-{alpha}-{beta} mediated nuclear protein import. *The Journal of Cell Biology* **168**, 1027–1038

186. Klebe, C., Bischoff, F. R., Ponstingl, H., and Wittinghofer, A. (1995) Interaction of the nuclear GTP-binding protein Ran with its regulatory proteins RCC1 and RanGAP1. *Biochemistry* **34**, 639–647

187. Paraskeva, E., Izaurralde, E., Bischoff, F. R., Huber, J., Kutay, U., Hartmann, E., Luhrmann, R., and Görlich, D. (1999) CRM1-mediated recycling of snurportin 1 to the cytoplasm. *The Journal of Cell Biology* **145**, 255–264

188. Stüven, T., Hartmann, E., and Görlich, D. (2003) Exportin 6: a novel nuclear export receptor that is specific for profilin.actin complexes. *The EMBO Journal* **22**, 5928–5940

189. Bohnsack, M. T., Regener, K., Schwappach, B., Saffrich, R., Paraskeva, E., Hartmann, E., and Görlich, D. (2002) Exp5 exports eEF1A via tRNA from nuclei and synergizes with other transport pathways to confine translation to the cytoplasm. *The EMBO Journal* **21**, 6205–6215

190. Feng, W., Benko, A. L., Lee, J. H., Stanford, D. R., and Hopper, A. K. (1999) Antagonistic effects of NES and NLS motifs determine S. cerevisiae Rna1p subcellular distribution. *Journal of Cell Science* **112**, 339–347

191. Plafker, K., and Macara, I. G. (2000) Facilitated Nucleocytoplasmic Shuttling of the Ran Binding Protein RanBP1. *Molecular and Cellular Biology* **20**, 3510–3521

192. Yang, W., and Musser, S. M. (2006) Nuclear import time and transport efficiency depend on importin beta concentration. *The Journal of Cell Biology* **174**, 951–961

193. Waldmann, I., Spillner, C., and Kehlenbach, R. H. (2012) The nucleoporin-like protein NLP1 (hCG1) promotes CRM1-dependent nuclear protein export. *Journal of Cell Science* **125**, 144–154

194. Gill, G. (2004) SUMO and ubiquitin in the nucleus: different functions, similar mechanisms? *Genes & Development* **18**, 2046–2059

195. Kutay, U., Izaurralde, E., Bischoff, F. R., Mattaj, I. W., and Görlich, D. (1997) Dominant-negative mutants of importin-beta block multiple pathways of import and export through the nuclear pore complex. *The EMBO Journal* **16**, 1153–1163

196. Arnold, M., Nath, A., Wohlwend, D., and Kehlenbach, R. H. (2006) Transportin is a major nuclear import receptor for c-Fos: a novel mode of cargo interaction. *The Journal of Biological Chemistry* **281**, 5492–5499

197. Chini, E. N., Chini, C. C. S., Nin, V., and Escande, C. (2013) Deleted in breast cancer-1 (DBC-1) in the interface between metabolism, aging and cancer. *Bioscience Reports* **33**

198. Sundararajan, R., Chen, G., Mukherjee, C., and White, E. (2005) Caspase-dependent processing activates the proapoptotic activity of deleted in breast cancer-1 during tumor necrosis factor-alpha-mediated death signaling. *Oncogene* **24**, 4908–4920

199. Brownawell, A. M., and Macara, I. G. (2002) Exportin-5, a novel karyopherin, mediates nuclear export of double-stranded RNA binding proteins. *The Journal of Cell Biology* **156**, 53–64

200. Mingot, J.-M., Bohnsack, M. T., Jäkle, U., and Görlich, D. (2004) Exportin 7 defines a novel general nuclear export pathway. *The EMBO Journal* **23**, 3227–3236

201. Wang, C.-I., Chien, K.-Y., Wang, C.-L., Liu, H.-P., Cheng, C.-C., Chang, Y.-S., Yu, J.-S., and Yu, C.-J. (2012) Quantitative proteomics reveals regulation of karyopherin subunit alpha-2 (KPNA2) and its potential novel cargo proteins in nonsmall cell lung cancer. *Molecular & Cellular Proteomics* **11**, 1105–1122

202. Zhen, Y., Sørensen, V., Skjerpen, C. S., Haugsten, E. M., Jin, Y., Wälchli, S., Olsnes, S., and Wiedlocha, A. (2012) Nuclear import of exogenous FGF1 requires the ER-protein LRRC59 and the importins Kpnα1 and Kpnβ1. *Traffic* **13**, 650–664

203. Kosugi, S., Hasebe, M., Matsumura, N., Takashima, H., Miyamoto-Sato, E., Tomita, M., and Yanagawa, H. (2009) Six classes of nuclear localization signals specific to different binding grooves of importin alpha. *The Journal of Biological Chemistry* **284**, 478–485

204. Pollard, V. W., Michael, W. M., Nakielny, S., Siomi, M. C., Wang, F., and Dreyfuss, G. (1996) A novel receptor-mediated nuclear protein import pathway. *Cell* **86**, 985–994

205. Piñol-Roma, S., and Dreyfuss, G. (1992) Shuttling of pre-mRNA binding proteins between nucleus and cytoplasm. *Nature* **355**, 730–732

206. Izaurralde, E., Jarmolowski, A., Beisel, C., Mattaj, I. W., Dreyfuss, G., and Fischer, U. (1997) A role for the M9 transport signal of hnRNP A1 in mRNA nuclear export. *The Journal of Cell Biology* **137**, 27–35

207. Singh, R., and Valcárcel, J. (2005) Building specificity with nonspecific RNA-binding proteins. *Nature Structural & Molecular Biology* **12**, 645–653

208. Michael, W. M., Choi, M., and Dreyfuss, G. (1995) A nuclear export signal in hnRNP A1: A signal-mediated, temperature-dependent nuclear protein export pathway. *Cell* **83**, 415–422

List of Figures

List of Tables

Appendix

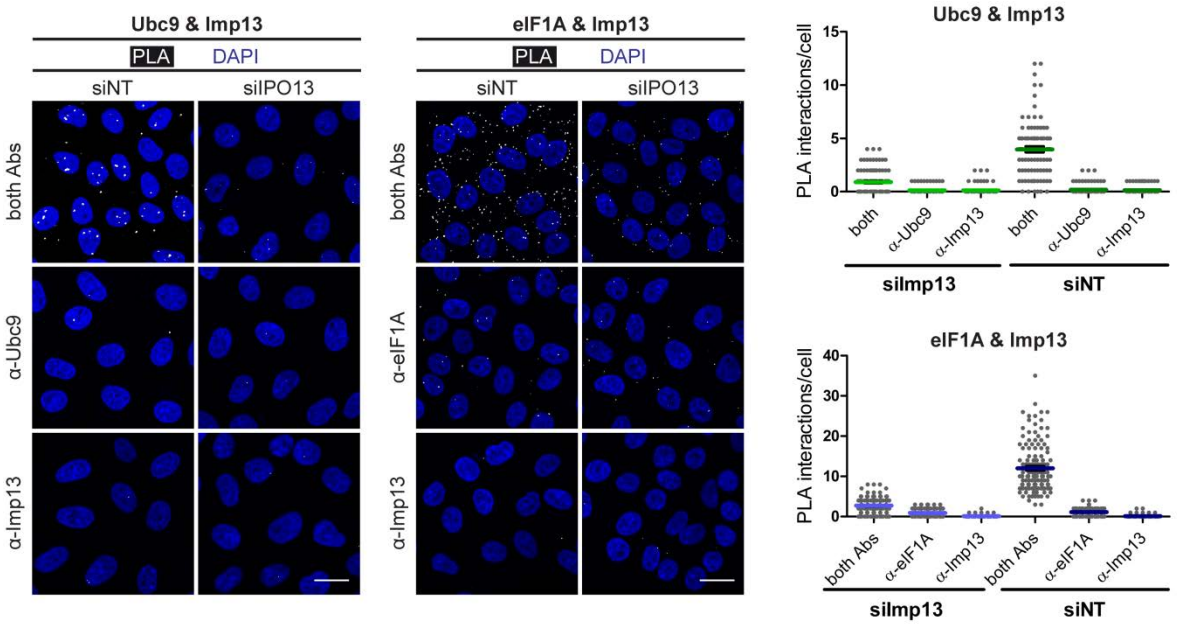

Figure S1: *In situ* proximity ligation assay (PLA) detection of importin 13 with Ubc9 and eIF1A. Fixed HeLa P4 cells were incubated with primary antibodies against the proteins of interest, followed by incubation with secondary PLA probes. Close proximity of the PLA probes allows for rolling circle amplification, and visualization by hybridization of a fluorescent probe. Each white dot represents a single protein-protein interaction. Specificity of the observed interaction was confirmed by siRNA mediated knock-down of importin 13. A minimum of 50 cells was analyzed and PLA dots were quantified with the CellProfiler software. See section 3.1.6 for more information.

Table S1: Proteins from overexpression screen (3.2.1) reanalyzed for changes in subcellular distribution upon importin 13 coexpression.

Protein	Protein Name	Importin 13 Effect
Proteins from overexpression screen		
GFP-DBC-1	Deleted in breast cancer gene 1	++
mCherry-DBC-1	Deleted in breast cancer gene 1	+
HA-DBC-1	Deleted in breast cancer gene 1	+
GFP-DMAP1	DNA methyltransferase 1-associated protein 1	++
HA-DMAP1	DNA methyltransferase 1-associated protein 1	+
GFP-TERT	Telomerase reverse transcriptase	++
TERT-HA	Telomerase reverse transcriptase	++
CFP-DDX43	Probable ATP-dependent RNA helicase DDX43	++
CFP-DDX59	Probable ATP-dependent RNA helicase DDX59	++

Protein	Protein Name	Importin 13 Effect
dGFP-cJun	Transcription factor AP-1	+
dGFP-Fos	Proto-oncogene c-Fos	+
Sirt1-GFP	NAD-dependent protein deacetylase sirtuin-1	+
Hsp22-YFP	Heat shock protein beta-8	-
CPF-YFP	Chondroitin polymerizing factor	-
Lim6-YFP	LIM homeobox 6	-
Tmp29-YFP	Transmembrane protein 29	-
Nip30-YFP	NEFA-interacting nuclear protein NIP30	-
Zinc313-YFP	Zinc finger protein 313	-
KIAA1826-YFP	KIAA1826 protein	-
DNAPTP6-YFP	DNA polymerase-transactivated protein 6	-
H3.3-YFP	H3 histone, family 3B	-
Known importin 13 cargoes		
eIF1A-GFP	Eukaryotic translation initiation factor 1A	++
eIF1A-R46E-GFP	Eukaryotic translation initiation factor 1A mutant impaired in its interaction with importin 13 (107)	-
HA-Ubc9	SUMO-conjugating enzyme UBC9	-
GFP-GST-Ubc9	SUMO-conjugating enzyme UBC9	++
Natural and artificial cargoes of other nuclear transport receptors		
dGFP-GST-cNLS	Classical nuclear localization sequence (imported by importin α/β)	-
GFP-M9	PY-NLS initially described for hnRNPA1 (imported by transportin)	+
dGFP-GST-RevNLS	Nuclear localization signal in HIV-1Rev (imported by different nuclear import receptors)	-
HA-SPN1	Snurportin 1	-
Randomly selected proteins		
HA-p53	Cellular tumor antigen p53	-
HA-ERα	Estrogen receptor alpha	-
HA-Hsp70	Heat shock protein 70	-

++: strong importin 13 effect, +: weak importin 13 effect; -: no importin 13 effect

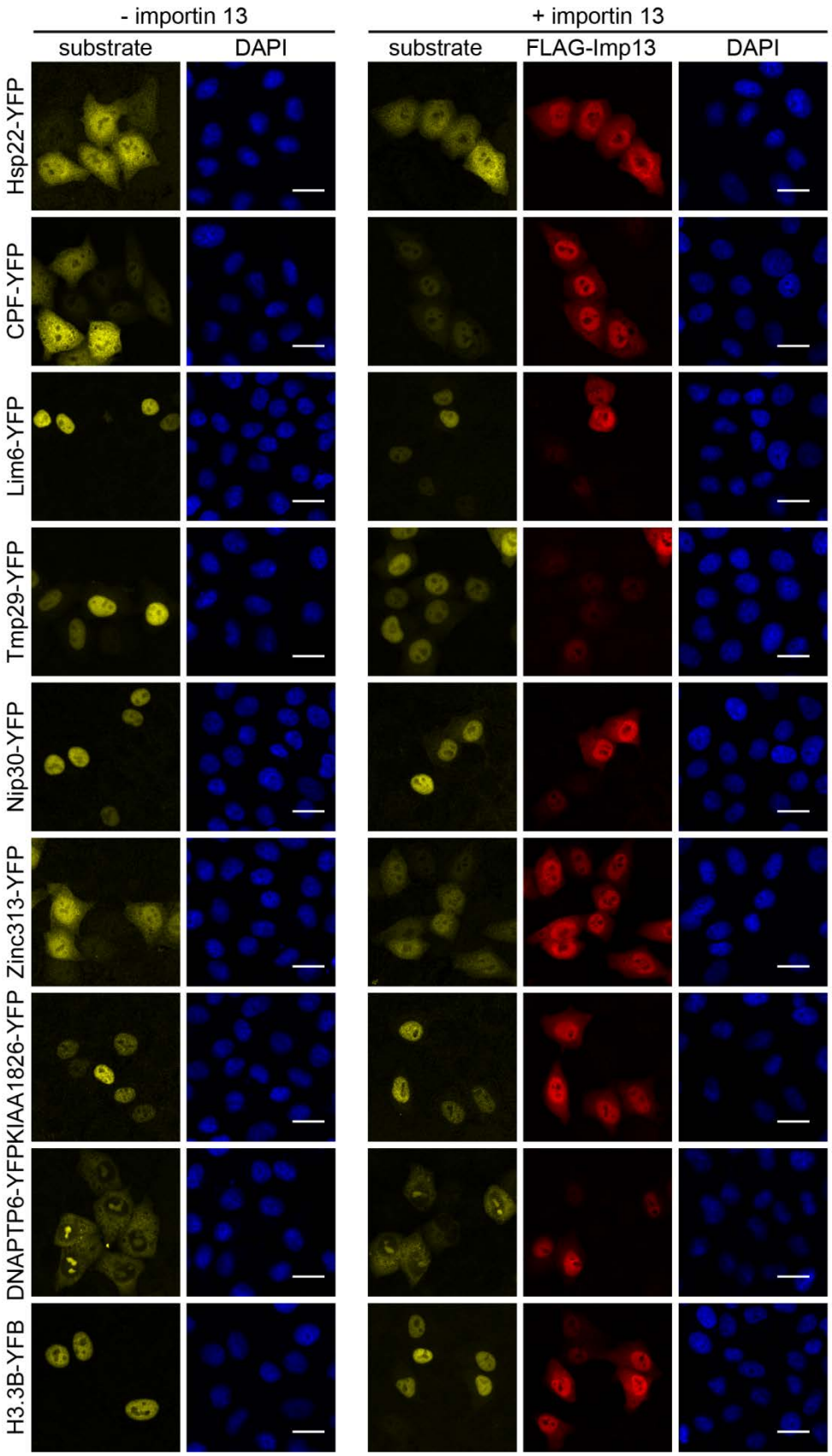
- importin 13
+ importin 13
substrate
DAPI
substrate
FLAG-Imp13
DAPI
Hsp22-YFP
CPF-YFP
Lim6-YFP
Tmp29-YFP
Nip30-YFP
Zinc313-YFP
KIAA1826-YFP
DNAPTP6-YFP
H3.3B-YFB

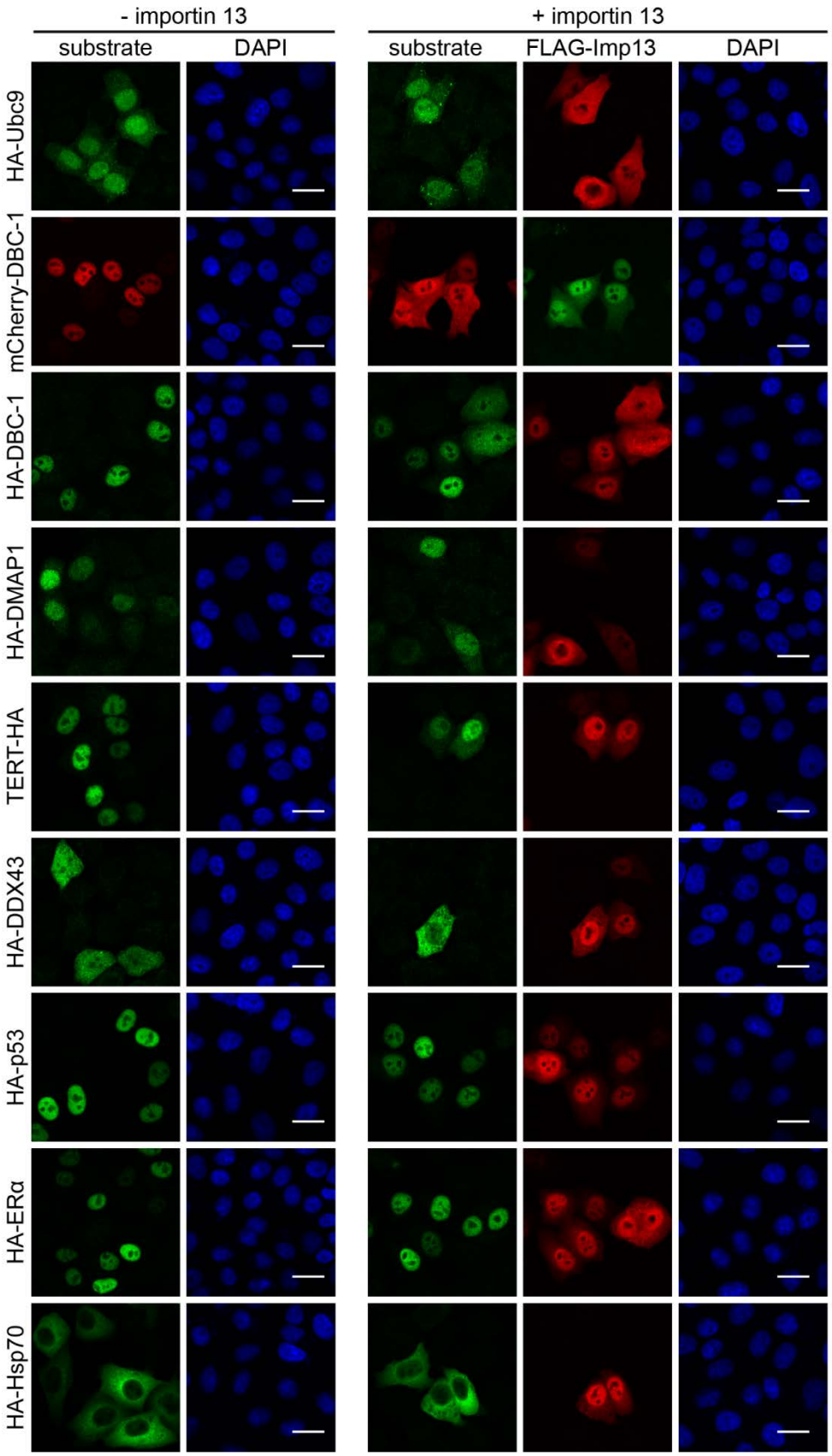
- importin 13
+ importin 13
substrate
DAPI
substrate
FLAG-Imp13
DAPI
HA-Ubc9
mCherry-DBC-1
HA-DBC-1
HA-DMAP1
TERT-HA
HA-DDX43
HA-p53
HA-ERα
HA-Hsp70

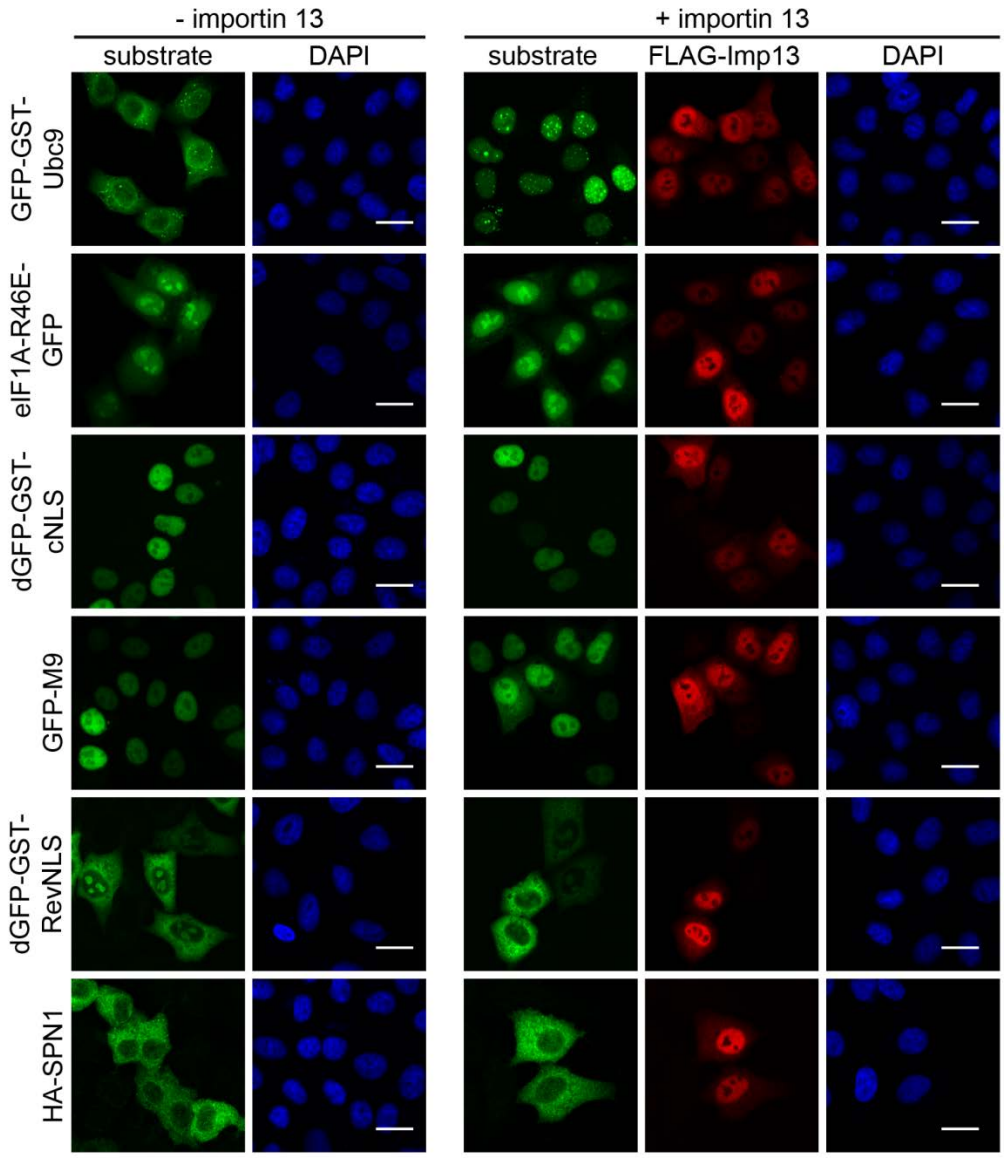

Figure S2: Proteins from the overexpression screen and other proteins analyzed for importin 13 effects. HeLa P4 cells were transiently transfected with plasmids coding for a tagged protein and an empty control vector or FLAG-importin 13 using the calcium phosphate method. The scale bars correspond to 20 µm. Proteins affected by importin 13 overexpression but tested with a different tag: DBC-1, DMAP1, TERT, DDX43 and DDX59. Other proteins tested from overexpression screen: Hsp22, CPF, Lim6, TMP29, Nip30, Zinc313, KIAA1826, DNAPTP6 and H3.3B. Randomly chosen proteins tested: p53, ERα and Hsp70. Artificial cargoes and proteins recognized by other nuclear transport receptors: cNLS, M9, RevNLS and SPN1. Known importin 13 cargoes: Ubc9 and eIF1A. For full protein names see Table S1. See section 3.2.1 for details and Figure 10 for further proteins tested.

Table S2: List of proteins that bound to Hzz-importin 13 from a digitonin but not a freeze/thaw HeLa P4 cell extract (see Table 10 and section 3.3.1 for details)[#]

Uniprot ID	Protein Name	Gene
Q60FE5	Filamin A	FLNA
P68032	Actin, alpha cardiac muscle 1	ACTC1
Q71U36	Tubulin alpha-1A chain	TUBA1A
P49327	Fatty acid synthase	FASN
P12268	Inosine-5'-monophosphate dehydrogenase 2	IMPDH2
P12814	Alpha-actinin-1	ACTN1
O75369	Filamin-B	FLNB
Q13509	Tubulin beta-3 chain	TUBB3
O15084	Serine/threonine-protein phosphatase 6 regulatory ankyrin repeat subunit A	ANKRD28
Q562R1	Beta-actin-like protein 2	ACTBL2
P63244	Receptor of activated protein C kinase 1	RACK1
Q8WX93	Palladin	PALLD
P37802	Transgelin-2	TAGLN2
P13798	Acylamino-acid-releasing enzyme	APEH
Q6PGP7	Tetratricopeptide repeat protein 37	TTC37
P58107	Epiplakin	EPPK1
A0A0D9SF54	Spectrin alpha chain, non-erythrocytic 1	SPTAN1
B7ZAR1	T-complex protein 1 subunit epsilon	CCT5
Q8IUD2	ELKS/Rab6-interacting/CAST family member 1	ERC1
P32969	60S ribosomal protein L9	RPL9
O00743	Serine/threonine-protein phosphatase 6 catalytic subunit	PPP6C
Q92974	Rho guanine nucleotide exchange factor 2	ARHGEF2
P08237	ATP-dependent 6-phosphofructokinase, muscle type	PFKM
P34932	Heat shock 70 kDa protein 4	HSPA4
C9JZR2	Catenin delta-1	CTNND1
P49588	Alanine--tRNA ligase, cytoplasmic	AARS
P52907	F-actin-capping protein subunit alpha-1	CAPZA1
P17812	CTP synthase 1	CTPS1
Q15477	Helicase SKI2W	SKIV2L
Q8N8S7	Protein enabled homolog	ENAH
P27708	CAD protein	CAD
P17987	T-complex protein 1 subunit alpha	TCP1
Q9UQ80	Proliferation-associated protein 2G4	PA2G4
Q5T4S7	E3 ubiquitin-protein ligase UBR4	UBR4
Q8NE71	ATP-binding cassette sub-family F member 1	ABCF1
P28074	Proteasome subunit beta type-5	PSMB5
Q96II8	Leucine-rich repeat and calponin homology domain-containing protein 3	LRCH3
Q01813	ATP-dependent 6-phosphofructokinase, platelet type	PFKP
Q7L2H7	Eukaryotic translation initiation factor 3 subunit M	EIF3M
Q96T76	MMS19 nucleotide excision repair protein homolog	MMS19
Q96RT1	Erbin	ERBIN
Q9Y281	Cofilin-2	CFL2
Q01082	Spectrin beta chain, non-erythrocytic 1	SPTBN1
P39023	60S ribosomal protein L3	RPL3
Q9GZS3	WD repeat-containing protein 61	WDR61
P35579	Myosin-9	MYH9
P55884	Eukaryotic translation initiation factor 3 subunit B	EIF3B
P14735	Insulin-degrading enzyme	IDE
Q15029	116 kDa U5 small nuclear ribonucleoprotein component	EFTUD2
P05198	Eukaryotic translation initiation factor 2 subunit 1	EIF2S1
Q16513	Serine/threonine-protein kinase N2	PKN2

Uniprot ID	Protein Name	Gene
Q01518	Adenylyl cyclase-associated protein 1	CAP1
O00151	PDZ and LIM domain protein 1	PDLIM1
Q9UIA9	Exportin-7	XPO7
Q92888	Rho guanine nucleotide exchange factor 1	ARHGEF1
Q96JG6	Syndetin	VPS50
P61160	Actin-related protein 2	ACTR2
Q9Y2T2	AP-3 complex subunit mu-1	AP3M1
P60981	Destrin	DSTN
Q9Y4E8	Ubiquitin carboxyl-terminal hydrolase 15	USP15
Q7Z2W4	Zinc finger CCCH-type antiviral protein 1	ZC3HAV1
Q96C19	EF-hand domain-containing protein D2	EFHD2
Q2NL82	Pre-rRNA-processing protein TSR1 homolog	TSR1
P46060	Ran GTPase-activating protein 1	RANGAP1
O15144	Actin-related protein 2/3 complex subunit 2	ARPC2
Q5VWV2	Partitioning defective 3 homolog	PARD3
Q12965	Unconventional myosin-Ie	MYO1E
Q99460	26S proteasome non-ATPase regulatory subunit 1	PSMD1
P60842	Eukaryotic initiation factor 4A-I	EIF4A1
P62081	40S ribosomal protein S7	RPS7
P47755	F-actin-capping protein subunit alpha-2	CAPZA2
Q9NYL9	Tropomodulin-3	TMOD3
Q9NZQ3	NCK-interacting protein with SH3 domain	NCKIPSD
P35268	60S ribosomal protein L22	RPL22
P47813	**Eukaryotic translation initiation factor 1A**	EIF1AX
P50570	Dynamin-2	DNM2
C9J381	Inosine-5'-monophosphate dehydrogenase	IMPDH1
C9J4M6	DNA-directed RNA polymerase subunit beta	POLR2B
A0A087WUT6	Eukaryotic translation initiation factor 5B	EIF5B
P61981	14-3-3 protein gamma	YWHAG
P11908	Ribose-phosphate pyrophosphokinase 2	PRPS2
Q9BVS4	Serine/threonine-protein kinase RIO2	RIOK2
P23258	Tubulin gamma-1 chain	TUBG1
E9PKZ0	60S ribosomal protein L8	RPL8
P84077	ADP-ribosylation factor 1	ARF1
Q96LD4	Tripartite motif-containing protein 47	TRIM47
Q9NR09	Baculoviral IAP repeat-containing protein 6	BIRC6
O15371	Eukaryotic translation initiation factor 3 subunit D	EIF3D
Q13200	26S proteasome non-ATPase regulatory subunit 2	PSMD2
Q9UBQ5	Eukaryotic translation initiation factor 3 subunit K	EIF3K
B1ALK7	Rho guanine nucleotide exchange factor 7	ARHGEF7
Q93100	Phosphorylase b kinase regulatory subunit beta	PHKB
A0A087WTT1	Polyadenylate-binding protein	PABPC1
Q9BTW9	Tubulin-specific chaperone D	TBCD
Q9BYX4	Interferon-induced helicase C domain-containing protein 1	IFIH1
Q00653	Nuclear factor NF-kappa-B p100 subunit	NFKB2
Q9NR33	**DNA polymerase epsilon subunit 4**	POLE4
Q13347	Eukaryotic translation initiation factor 3 subunit I	EIF3I
P53611	Geranylgeranyl transferase type-2 subunit beta	RABGGTB
Q9H6S3	Epidermal growth factor receptor kinase substrate 8-like protein 2	EPS8L2
P60228	Eukaryotic translation initiation factor 3 subunit E	EIF3E
P62906	60S ribosomal protein L10a	RPL10A
Q96IZ0	PRKC apoptosis WT1 regulator protein	PAWR
Q8N1F7	Nuclear pore complex protein Nup93	NUP93
Q14558	Phosphoribosyl pyrophosphate synthase-associated protein 1	PRPSAP1

Uniprot ID	Protein Name	Gene
Q86UU1	Pleckstrin homology-like domain family B member 1	PHLDB1
O76071	Probable cytosolic iron-sulfur protein assembly protein CIAO1	CIAO1
Q92598	Heat shock protein 105 kDa	HSPH1
Q5VIR6	Vacuolar protein sorting-associated protein 53 homolog	VPS53
Q9Y530	O-acetyl-ADP-ribose deacetylase 1	OARD1
B1AK87	Capping protein (Actin filament) muscle Z-line, beta	CAPZB
P63208	S-phase kinase-associated protein 1	SKP1
P07355	Annexin A2	ANXA2
Q9BQA1	Methylosome protein 50	WDR77
P22314	Ubiquitin-like modifier-activating enzyme 1	UBA1
Q96QK1	Vacuolar protein sorting-associated protein 35	VPS35
A0A087WZK9	Eukaryotic translation initiation factor 3 subunit H	EIF3H
Q01433	AMP deaminase 2	AMPD2
P62913	60S ribosomal protein L11	RPL11
P19474	E3 ubiquitin-protein ligase TRIM21	TRIM21
Q7Z6Z7	E3 ubiquitin-protein ligase HUWE1	HUWE1
Q9UDY8	Mucosa-associated lymphoid tissue lymphoma translocation protein 1	MALT1
P21291	Cysteine and glycine-rich protein 1	CSRP1
P62753	40S ribosomal protein S6	RPS6
Q6Y7W6	GRB10-interacting GYF protein 2	GIGYF2
Q9Y4B5	Microtubule cross-linking factor 1	MTCL1
Q5T6K7	**Nuclear transcription factor Y subunit gamma**	NFYC
P31946	14-3-3 protein beta/alpha	YWHAB
Q15942	Zyxin (Zyxin-2)	ZYX
P62241	40S ribosomal protein S8	RPS8
E9PDE8	Heat shock 70 kDa protein 4L	HSPA4L
O00487	26S proteasome non-ATPase regulatory subunit 14	PSMD14
Q9UPQ0	LIM and calponin homology domains-containing protein 1	LIMCH1
E7ERI8	CLIP-associating protein 2	CLASP2
P20618	Proteasome subunit beta type-1	PSMB1
A0A087X2G1	ATP-dependent RNA helicase DDX1	DDX1
Q96P70	Importin-9	IPO9
Q9Y262	Eukaryotic translation initiation factor 3 subunit L	EIF3L
Q9UNM6	26S proteasome non-ATPase regulatory subunit 13	PSMD13
P33176	Kinesin-1 heavy chain	KIF5B
P10155	60 kDa SS-A/Ro ribonucleoprotein	TROVE2
Q6IBS0	Twinfilin-2	TWF2
S4R3H3	Zinc finger SWIM domain-containing protein 8	ZSWIM8
Q14258	E3 ubiquitin/ISG15 ligase TRIM25	TRIM25
Q15366	Poly(rC)-binding protein 2	PCBP2
Q14847	LIM and SH3 domain protein 1	LASP1
Q14019	Coactosin-like protein	COTL1
Q15645	Pachytene checkpoint protein 2 homolog	TRIP13
E9PGZ1	Caldesmon	CALD1
P04075	Fructose-bisphosphate aldolase A	ALDOA
P62979	Ubiquitin-40S ribosomal protein S27a	RPS27A
Q86VP6	Cullin-associated NEDD8-dissociated protein 1	CAND1
P46778	60S ribosomal protein L21	RPL21
P25787	Proteasome subunit alpha type-2	PSMA2
Q12792	Twinfilin-1	TWF1
Q9HCN4	GPN-loop GTPase 1	GPN1
A0A024QZP7	Cell division cycle 2	CDC2
Q9NR31	GTP-binding protein SAR1a	SAR1A
Q02790	Peptidyl-prolyl cis-trans isomerase FKBP4	FKBP4

Uniprot ID	Protein Name	Gene
K7EL20	Eukaryotic translation initiation factor 3 subunit G	EIF3G
P63167	Dynein light chain 1, cytoplasmic	DYNLL1
P61158	Actin-related protein 3	ACTR3
Q99471	Prefoldin subunit 5	PFDN5
P19338	Nucleolin	NCL
O00178	GTP-binding protein 1	GTPBP1
Q6NZ67	Mitotic-spindle organizing protein 2B	MZT2B
F8VQE1	LIM domain and actin-binding protein 1	LIMA1
Q7KZF4	Staphylococcal nuclease domain-containing protein 1	SND1
O14818	Proteasome subunit alpha type-7	PSMA7
Q12800	Alpha-globin transcription factor CP2	TFCP2
H0YM23	Ankyrin repeat domain-containing protein 17	ANKRD17
P54619	5'-AMP-activated protein kinase subunit gamma-1	PRKAG1
P62487	DNA-directed RNA polymerase II subunit RPB7	POLR2G
P17858	ATP-dependent 6-phosphofructokinase, liver type	PFKL
Q86TC9	Myopalladin	MYPN
D6REY2	Colorectal mutant cancer protein	MCC
Q9Y3F4	Serine-threonine kinase receptor-associated protein	STRAP
Q5VZK9	F-actin-uncapping protein LRRC16A	CARMIL1
Q5VYK3	Proteasome-associated protein ECM29 homolog	ECM29
E5RHG8	Elongin-C	ELOC
O75340	Programmed cell death protein 6	PDCD6
Q9Y597	BTB/POZ domain-containing protein KCTD3	KCTD3
Q96CW5	Gamma-tubulin complex component 3	TUBGCP3
F5H018	GTP-binding nuclear protein Ran	RAN
Q9UDY4	DnaJ homolog subfamily B member 4	DNAJB4
Q9BV44	THUMP domain-containing protein 3	THUMPD3

#: Proteins are sorted according to the total number of identified peptide sequences for a protein. Proteins written in bold are known importin 13 cargoes. Identified proteins that corresponded to the same protein but had different Uniprot IDs were listed only once. Further keratin and immunoglobulin contaminants were removed.

Table S3: List of proteins that bound to Hzz-importin 13 from a freeze/thaw but not a digitonin HeLa P4 cell extract (see Table 10 and section 3.3.1 for details)[#]

Uniprot ID	Protein Name	Gene
A0A0U1RQF0	Fatty acid synthase	FASN
Q9BPW8	Protein NipSnap homolog 1	NIPSNAP1
O75323	Protein NipSnap homolog 2	NIPSNAP2
P39880	Homeobox protein cut-like 1	CUX1
C9JE98	Nuclear receptor corepressor 2	NCOR2
Q5HY54	Filamin-A	FLNA
O75376	Nuclear receptor corepressor 1	NCOR1
Q13952	**Nuclear transcription factor Y subunit gamma**	NFYC
P40424	Pre-B-cell leukemia transcription factor 1	PBX1
A0A087WZ13	Ribonucleoprotein PTB-binding 1	RAVER1
K7EKE6	Lon protease homolog, mitochondrial	LONP1
P25208	**Nuclear transcription factor Y subunit beta**	NFYB
Q14919	**Dr1-associated corepressor**	DRAP1
Q9Y6D9	Mitotic spindle assembly checkpoint protein MAD1	MAD1L1
Q01658	**Protein Dr1**	DR1

Uniprot ID	Protein Name	Gene
P62841	40S ribosomal protein S15	RPS15
P40425	Pre-B-cell leukemia transcription factor 2	PBX2
O75116	Rho-associated protein kinase 2	ROCK2
A0A0C4DFV9	Protein SET	SET
B1AKN7	Nuclear factor 1	NFIA
P49321	Nuclear autoantigenic sperm protein	NASP
Q8TEW0	Partitioning defective 3 homolog	PARD3
F5GYS8	Homeobox protein Meis1	MEIS1
O14770	Homeobox protein Meis2	MEIS2
O95425	Supervillin	SVIL
P08651	Nuclear factor 1 C-type	NFIC
Q92734	Protein TFG	TFG
P62854	40S ribosomal protein S26	RPS26
Q14444	Caprin-1	CAPRIN1
O60506	Heterogeneous nuclear ribonucleoprotein Q	SYNCRIP
Q5VTR2	E3 ubiquitin-protein ligase BRE1A	RNF20
Q15120	[Pyruvate dehydrogenase	PDK3
P35249	Replication factor C subunit 4	RFC4
Q8NHP8	Putative phospholipase B-like 2	PLBD2
H9KV28	Protein diaphanous homolog 1	DIAPH1
J3QL15	Ribosomal protein L19	RPL19
H0YNH8	Uveal autoantigen with coiled-coil domains and ankyrin repeats	UACA
P62750	60S ribosomal protein L23a	RPL23A
Q09666	Neuroblast differentiation-associated protein AHNAK	AHNAK
Q8TF72	Protein Shroom3	SHROOM3
Q13162	Peroxiredoxin-4	PRDX4
I3L2J8	Centrosomal protein of 131 kDa	CEP131
C9JXB8	60S ribosomal protein L24	RPL24
P26373	60S ribosomal protein L13	RPL13
Q99536	Synaptic vesicle membrane protein VAT-1 homolog	VAT1
P78337	Pituitary homeobox 1	PITX1
P48634	Protein PRRC2A	PRRC2A
P60953	Cell division control protein 42 homolog	CDC42
Q14678	KN motif and ankyrin repeat domain-containing protein 1	KANK1
Q96A19	Coiled-coil domain-containing protein 102A	CCDC102A
Q9H2J4	Phosducin-like protein 3	PDCL3
P62826	GTP-binding nuclear protein Ran	RAN
P85037	Forkhead box protein K1	FOXK1
R4GNB2	DENN domain-containing protein 4C	DENND4C
Q13136	Liprin-alpha-1	PPFIA1
Q9Y2R9	28S ribosomal protein S7, mitochondrial	MRPS7
H7C2W9	60S ribosomal protein L31	RPL31
A6NJA2	Ubiquitin carboxyl-terminal hydrolase 14	USP14

#: Proteins are sorted according to the total number of identified peptide sequences for a protein. Proteins written in bold are known importin 13 cargoes. Identified proteins that corresponded to the same protein but had different Uniprot IDs were listed only once. Further keratin and immunoglobulin contaminants were removed.

A

SILAC binding reactions:

1. Hzz-importin 13 + light HeLa P4 cell extract (l) + $RanGTP_{Q69L}$
2. Hzz-importin 13 + medium HeLa P4 cell extract (m)
3. Hzz-importin 13 + heavy HeLa P4 cell extract (h) + Ubc9

B

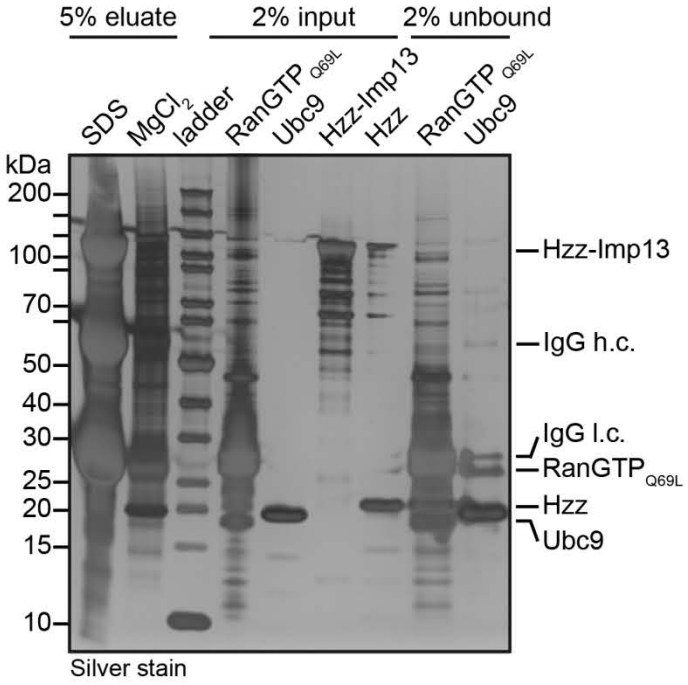

C

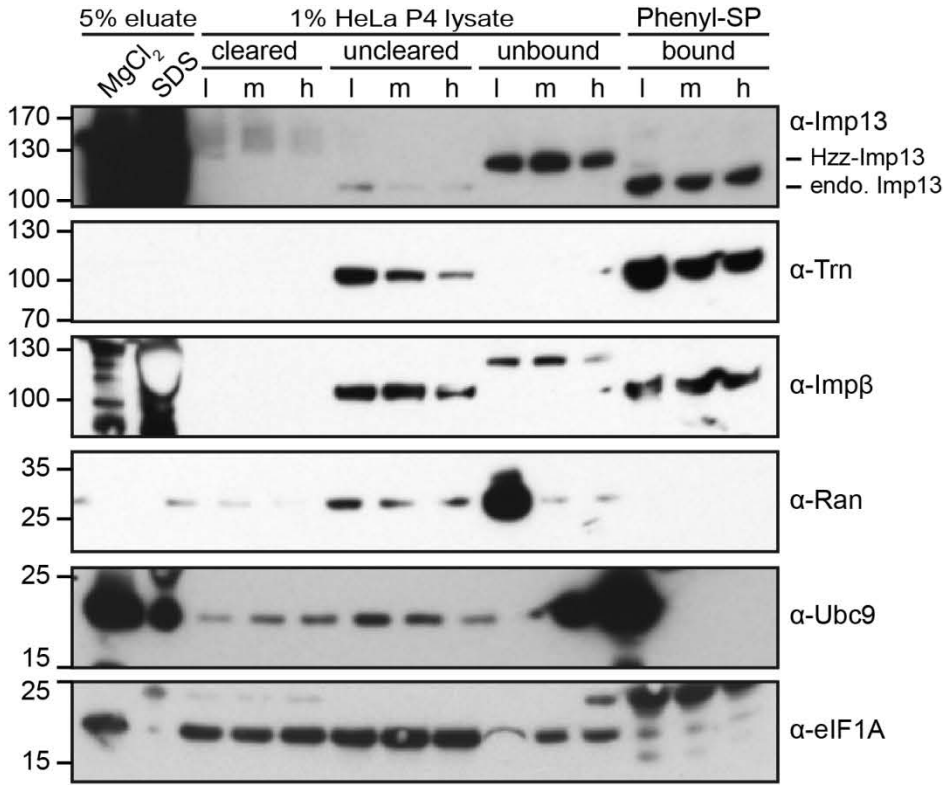

Figure S3: SILAC binding reactions and phenyl-Sepharose depletion of HeLa P4 cell extracts (experiment 2). (A) Schematic showing exemplary SILAC binding reactions. (B, C) Hzz-tagged importin 13 (0.5 nmol) was immobilized on IgG-Sepharose and incubated with cell extracts of HeLa P4 cells grown in DMEM medium containing light, medium or heavy amino acids in the absence or presence of 10 µM $RanGTP_{Q69L}$ or 5 µM Ubc9 in transport buffer. Cell extracts (uncleared) were precleared with Hzz/IgG-Sepharose and phenyl-Sepharose (cleared) to reduce unspecific interactions. Bound proteins were eluted in a first elution step with magnesium chloride, followed by a second elution step with 4x SDS sample buffer. Cell lysates and eluted proteins were separated by SDS-PAGE and analyzed by silver staining (B) or immunoblotting with an anti-importin 13, anti-transportin, anti-importin β, anti-Ran, anti-Ubc9 and anti-eIF1A antibody (C). Note that in the unbound cell lysate some free Hzz-importin 13 can be detected, as well as excess exogenous $RanGTP_{Q69L}$ and Ubc9 in the unbound light and heavy isotopically labeled cell lysate, respectively. See section 3.3.3 for details and Figure 18 and Figure S4 for replicates. ladder: PageRuler Unstained Protein Ladder; $MgCl_2$: magnesium chloride eluate; SDS: 4x SDS sample buffer eluate; l: light; m: medium; h: heavy; endog.: endogenous.

A

SILAC binding reactions:

1. Hzz-importin 13 + light HeLa P4 cell extract (l) + $RanGTP_{Q69L}$
2. Hzz-importin 13 + medium HeLa P4 cell extract (m)
3. Hzz-importin 13 + heavy HeLa P4 cell extract (h) + Ubc9

B

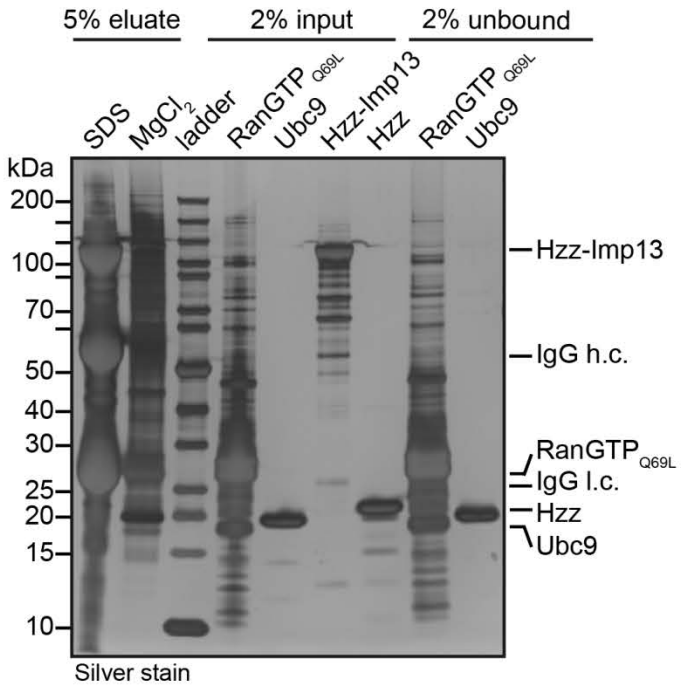

C

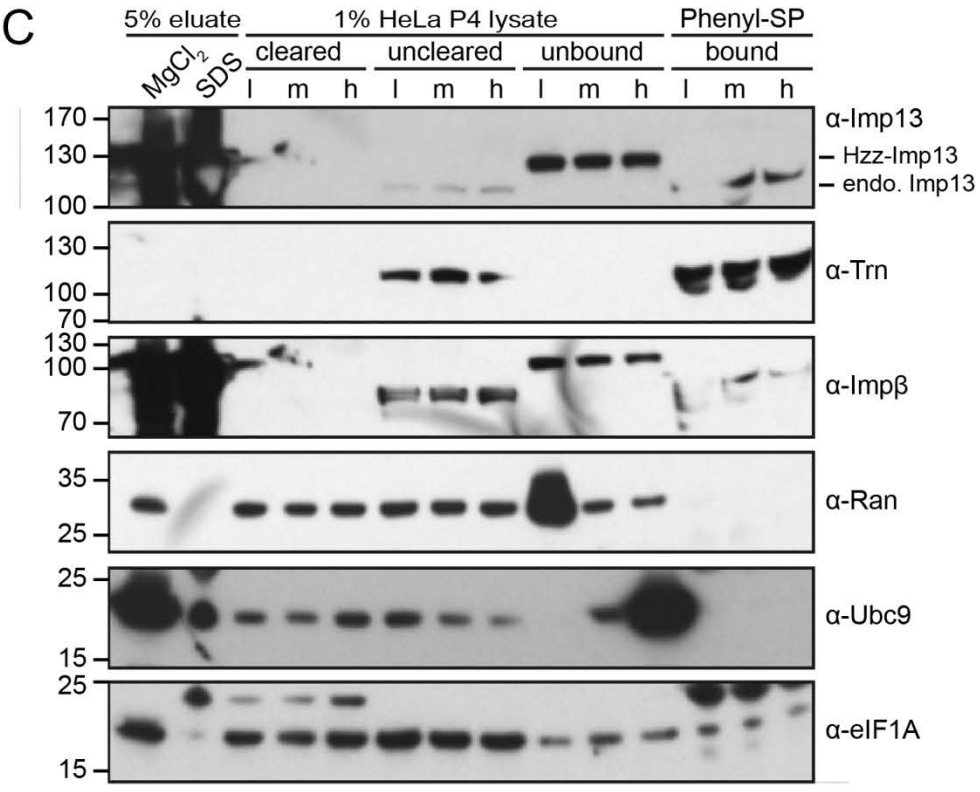

Figure S4: SILAC binding reactions and phenyl-Sepharose depletion of HeLa P4 cell extracts (experiment 3). (A) Schematic showing exemplary SILAC binding reactions. (B, C) Hzz-tagged importin 13 (0.5 nmol) was immobilized on IgG-Sepharose and incubated with cell extracts of HeLa P4 cells grown in DMEM medium containing light, medium or heavy amino acids in the absence or presence of 10 µM $RanGTP_{Q69L}$ or 5 µM Ubc9 in transport buffer. Cell extracts (uncleared) were precleared with Hzz/IgG-Sepharose and phenyl-Sepharose (cleared) to reduce unspecific interactions. Bound proteins were eluted in a first elution step with magnesium chloride, followed by a second elution step with 4x SDS sample buffer. Cell lysates and eluted proteins were separated by SDS-PAGE and analyzed by silver staining (B) or immunoblotting with an anti-importin 13, anti-transportin, anti-importin β, anti-Ran, anti-Ubc9 and anti-eIF1A antibody (C). Note that in the unbound cell lysate some free Hzz-importin 13 can be detected, as well as excess exogenous $RanGTP_{Q69L}$ and Ubc9 in the unbound light and heavy isotopically labeled cell lysate, respectively. See section 3.3.3 for details and Figure 18 and Figure S3 for replicates. ladder: PageRuler Unstained Protein Ladder; $MgCl_2$: magnesium chloride eluate; SDS: 4x SDS sample buffer eluate; l: light; m: medium; h: heavy; endog.: endogenous.

Table S4: Perseus workflow for the identification of importin 13 export cargoes (see section 3.3.3 for SILAC experiment)

Matrix	Processing	Settings	Description
Matrix 1	Generic matrix upload	**Expression**: Ratio M/L normalized SILAC4 Ratio H/L normalized SILAC4 Ratio H/M normalized SILAC4 Ratio M/L normalized SILAC5 Ratio H/L normalized SILAC5 Ratio H/M normalized SILAC5 Ratio M/L normalized SILAC6 Ratio H/L normalized SILAC6 Ratio H/M normalized SILAC6 **Numerical**: Ratio M/L variability [%] SILAC4 Ratio H/L variability [%] SILAC4 Ratio H/M variability [%] SILAC4 Ratio M/L variability [%] SILAC5 Ratio H/L variability [%] SILAC5 Ratio H/M variability [%] SILAC5 Ratio M/L variability [%] SILAC6 Ratio H/L variability [%] SILAC6 Ratio H/M variability [%] SILAC6 Ratio M/L count SILAC4 Ratio H/L count SILAC4 Ratio H/M count SILAC4 Ratio M/L count SILAC5 Ratio H/L count SILAC5 Ratio H/M count SILAC5 Ratio M/L count SILAC6 Ratio H/L count SILAC6 Ratio H/M count SILAC6 **Categorical**: Only identified by site Reverse Potential contaminants **Text**: Protein IDs	Load MaxQuant derived proteomics data from the tab-separated file proteinGroups.txt

Matrix	Processing	Settings	Description
		Majority protein IDs Protein names Gene names	
Matrix 2	Filter rows based on categorical column	**Column**: Only identified by site **Values**: + **Mode**: Remove matching rows **Filter mode**: Reduce matrix	Remove proteins only identified by peptides carrying a modified residue
Matrix 3	Filter rows based on categorical column	**Column**: Reverse **Values**: + **Mode**: Remove matching rows **Filter mode**: Reduce matrix	Remove hits that match against a nonsense database
Matrix 4	Filter rows based on categorical column	**Column**: Potential contaminants **Values**: + **Mode**: Remove matching rows **Filter mode**: Reduce matrix	Remove common contaminants
Matrix 5	Remove empty columns		Remove empty columns
Matrix 6	Select rows manually	Select immunoglobulin contaminants manually and remove selected rows	Remove immunoglobulin contaminants
Matrix 7	Transform	**Transformation**: 1/x **Columns**: Ratio M/L normalized SILAC4 Ratio H/L normalized SILAC4 Ratio H/M normalized SILAC4 Ratio M/L normalized SILAC5 Ratio H/L normalized SILAC5 Ratio H/M normalized SILAC5 Ratio M/L normalized SILAC6 Ratio H/L normalized SILAC6 Ratio H/M normalized SILAC6	Invert ratios by using the formula 1/x
Matrix 8	Matching rows by name	**Base matrix**: Matrix 6 **Other matrix**: Matrix 7 **Matching column 1**: Protein IDs **Matching column 2**: Protein IDs **Expression columns**: Ratio M/L normalized SILAC4 Ratio H/L normalized SILAC4 Ratio H/M normalized SILAC4 Ratio M/L normalized SILAC5 Ratio H/L normalized SILAC5 Ratio H/M normalized SILAC5 Ratio M/L normalized SILAC6 Ratio H/L normalized SILAC6 Ratio H/M normalized SILAC6	Combine columns of the existing protein ratios with the newly generated inverted ratios (rows of the other matrix are associated with rows of the base matrix via matching expressions in a textual column from each matrix)

Matrix	Processing	Settings	Description
Matrix 9	Transform	**Transformation**: log2(x) **Columns**: Ratio M/L normalized SILAC4 Ratio H/L normalized SILAC4 Ratio H/M normalized SILAC4 Ratio M/L normalized SILAC5 Ratio H/L normalized SILAC5 Ratio H/M normalized SILAC5 Ratio M/L normalized SILAC6 Ratio H/L normalized SILAC6 Ratio H/M normalized SILAC6 Ratio M/L normalized SILAC4_1 Ratio H/L normalized SILAC4_1 Ratio H/M normalized SILAC4_1 Ratio M/L normalized SILAC5_1 Ratio H/L normalized SILAC5_1 Ratio H/M normalized SILAC5_1 Ratio M/L normalized SILAC6_1 Ratio H/L normalized SILAC6_1 Ratio H/M normalized SILAC6_1	Log transformation of expression columns using the formula log2(x)
Matrix 10	Categorical annotation rows	**Action**: Create **Row name**: Group 1 Ratio H/M normalized SILAC4_1 Ratio M/L normalized SILAC5_1 Ratio M/L normalized SILAC6_1 → Imp13+Ran/Imp13 Ratio M/L normalized SILAC4 Ratio H/L normalized SILAC5_1 Ratio H/L normalized SILAC6_1 → Imp13+Ran/Imp13+Ubc9 Ratio H/M normalized SILAC4 Ratio M/L normalized SILAC5 Ratio M/L normalized SILAC6 → Imp13/Imp13+Ran Ratio H/L normalized SILAC4 Ratio H/M normalized SILAC5_1 Ratio H/M normalized SILAC6_1 → Imp13/Imp13+Ubc9 Ratio H/L normalized SILAC4_1 Ratio H/M normalized SILAC5 Ratio H/M normalized SILAC6 → Imp13+Ubc9/Imp13 Ratio M/L normalized SILAC4_1 Ratio H/L normalized SILAC5 Ratio H/L normalized SILAC6 → Imp13+Ubc9/Imp13+Ran	Define the following ratio groups: Imp13+Ran/Imp13 Imp13+Ran/Imp13+Ubc9 Imp13/Imp13+Ran Imp13/Imp13+Ubc9 Imp13+Ubc9/Imp13 Imp13+Ubc9/Imp13+Ran

Matrix	Processing	Settings	Description
Matrix 11	Reorder/remove columns	**Expression column**: Ratio H/M normalized SILAC4_1 Ratio M/L normalized SILAC5_1 Ratio M/L normalized SILAC6_1 Ratio M/L normalized SILAC4 Ratio H/L normalized SILAC5_1 Ratio H/L normalized SILAC6_1 **Numerical columns**: Ratio M/L variability [%] SILAC4 Ratio H/M variability [%] SILAC4 Ratio M/L variability [%] SILAC5 Ratio H/L variability [%] SILAC5 Ratio M/L variability [%] SILAC6 Ratio H/L variability [%] SILAC6 Ratio M/L count SILAC4 Ratio H/M count SILAC4 Ratio M/L count SILAC5 Ratio H/L count SILAC5 Ratio M/L count SILAC6 Ratio H/L count SILAC6	Selection of columns required for identification of Imp13 export candidates
Matrix 12	Categorical annotation row	**Action**: Create **Row name**: Imp13+Ran/Imp13 Ratio H/M normalized SILAC4_1 Ratio M/L normalized SILAC5_1 Ratio M/L normalized SILAC6_1	The following ratio group was defined: Imp13+Ran/Imp13
Matrix 13	Categorical annotation row	**Action**: Create **Row name**: Imp13+Ran/Imp13+Ubc9 Ratio M/L normalized SILAC4 Ratio H/L normalized SILAC5_1 Ratio H/L normalized SILAC6_1	The following ratio group was defined: Imp13+Ran/Imp13+Ubc9
Matrix 14	Filter rows based on valid values	**Min. number of values**: 3 **Mode**: In each group **Grouping**: Imp13+Ran/Imp13 **Values should be**: Greater or equal **Minimum**: 0.5 **Filter mode**: Add categorical row	Imp13+Ran/Imp13 ratios were filtered to be ≥0.5 for all three replicates.
Matrix 15	Filter rows based on valid values	**Min. number of values**: 3 **Mode**: In each group **Grouping**: Imp13+Ran/Imp13 **Values should be**: Greater or equal **Minimum**: 1.5 **Filter mode**: Add categorical row	Imp13+Ran/Imp13 ratios were filtered to be ≥1.5 for all three replicates.
Matrix 16	Filter rows based on valid values	**Min. number of values**: 3 **Mode**: In each group **Grouping**: Imp13+Ran/Imp13 **Values should be**: Greater or equal **Minimum**: 3.0 **Filter mode**: Add categorical row	Imp13+Ran/Imp13 ratios were filtered to be ≥3.0 for all three replicates.
Matrix 17	One-sample test	**Columns**: Ratio H/M normalized SILAC4_1 Ratio M/L normalized SILAC5_1 Ratio M/L normalized SILAC6_1 **Value**: 0 **Test**: t-test **Side**: Right **Use for truncation**: P value **Threshold p-value**: 0.05 **-Log10**: tick **Suffix**:	One sample-test for determining if the mean Imp13+Ran/Imp13 ratio is significantly different from 0 using a threshold p-value of 0.05

Matrix	Processing	Settings	Description
Matrix 18	One-sample test	**Columns**: Ratio H/M normalized SILAC4_1 Ratio M/L normalized SILAC5_1 Ratio M/L normalized SILAC6_1 **Value**: 0 **Test**: t-test **Side**: Right **Use for truncation**: P value **Threshold p-value**: 0.01 **-Log10**: tick **Suffix**:	One sample-test for determining if the mean Imp13+Ran/Imp13 ratio is significantly different from 0 using a threshold p-value of 0.01
Matrix 19	Rename columns	Filter → T(log2)=0.5 Filter_ → T(log2)=1.5 Filter__ → T(log2)=3.0 t-test Significant → t-test 0.05 t-test Significant_ → t-test 0.01	Give expression columns (filtering + t-test) a more explicit name
Matrix 20	Fill categorical columns	**Columns**: Filter → T(log2)=0.5 Filter_ → T(log2)=1.5 Filter__ → T(log2)=3.0 t-test Significant → t-test 0.05 t-test Significant_ → t-test 0.01 **Value**: -	Fill empty field in categorical columns with '-' to allow for later combining of categorical columns
Matrix 21	Combine categorical columns	**First column**: t-test 0.05 **Second column**: t-test 0.01	Combine categorical columns that were t-test significant for a threshold p-value of 0.05 and 0.01
Matrix 22	Combine categorical columns	**First column**: T(log2)=0.5 **Second column**: T(log2)=1.5	Combine categorical columns filtered for ratio thresholds of ≥0.5 and ≥1.5
Matrix 23	Combine categorical columns	**First column**: T(log2)=0.5_T(log2)=1.5 **Second column**: T(log2)=3	Combine categorical columns filtered for ratio thresholds of ≥0.5, ≥1.5 and ≥ 3
Matrix 24	Combine categorical columns	**First column**: T(log2)=0.5_T(log2)=1.5_ T(log2)=3 **Second column**: t-test 0.05_ t-test 0.01	Combine categorical columns filtered for ratio threshold of ≥0.5, ≥1.5 and ≥ 3 with t-test significant categorical column with a threshold p-value of 0.05 and 0.01. Required for data visualization
Matrix 25	Average groups	**Grouping**: Group1 **Average type**: mean **Min. valid values per group**: 1 **Keep original data**: tick **Add standard deviation**: tick	Average Imp13+Ran/Imp13 and Imp13+Ran/Imp13+Ubc9 ratios from all three replicates (Note: averaging is done for all ratios)
Matrix 26	Categorical annotation row	**Action**: Create **Row name**: Imp13+Ran/Imp13_fwd Ratio H/M normalized SILAC4_1	Distinguish between label-switch experiments for Imp13+Ran/Imp13 Ratios ('forward reaction')
Matrix 27	Categorical annotation row	**Action**: Create **Row name**: Imp13+Ran/Imp13_rev Ratio M/L normalized SILAC5_1 Ratio M/L normalized SILAC6_1	Distinguish between label-switch experiments for Imp13+Ran/Imp13 Ratios ('reverse reaction')
Matrix 28	Categorical annotation row	**Action**: Create **Row name**: Imp13+Ran/Imp13+Ubc9_fwd Ratio M/L normalized SILAC4	Distinguish between label-switch experiments for Imp13+Ran/Imp13+Ubc9 ratios ('forward reaction')
Matrix 29	Categorical annotation row	**Action**: Create **Row name**: Imp13+Ran/Imp13+Ubc9_rev Ratio H/L normalized SILAC5_1 Ratio H/L normalized SILAC6_1	Distinguish between label-switch experiments for Imp13+Ran/Imp13+Ubc9 ratios ('reverse reaction')

Matrix	Processing	Settings	Description
Matrix 30	Average groups	**Grouping**: Imp13+Ran/Imp13_fwd **Average type**: mean **Min. valid values per group**: 1 **Keep original data**: tick **Add standard deviation**: tick	Average Imp13+Ran/Imp13 ratios from forward label-switch experiment
Matrix 31	Average groups	**Grouping**: Imp13+Ran/Imp13_rev **Average type**: mean **Min. valid values per group**: 1 **Keep original data**: tick **Add standard deviation**: tick	Average Imp13+Ran/Imp13 ratios from reverse label-switch experiment
Matrix 32	Average groups	**Grouping**: Imp13+Ran/Imp13+Ubc9_fwd **Average type**: mean **Min. valid values per group**: 1 **Keep original data**: tick **Add standard deviation**: tick	Average Imp13+Ran/Imp13+Ubc9 ratios from forward label-switch experiment
Matrix 33	Average groups	**Grouping**: Imp13+Ran/Imp13+Ubc9_rev **Average type**: mean **Min. valid values per group**: 1 **Keep original data**: tick **Add standard deviation**: tick	Average Imp13+Ran/Imp13+Ubc9 ratios from reverse label-switch experiment
Matrix 34	Filter rows based on valid values	**Min. number of valid values**: 3 **Mode**: In each group **Grouping**: Group 1 **Values should be**: Valid **Filter mode**: Reduce matrix	To assign annotations all values need to be valid
Matrix 35	Add annotation	**Source**: MainPerseusAnnot.txt.gz **UniProt column**: Majority protein IDs **Annotations to be added**: GOBP name GOMF name GOCC name KEGG name **Additional sources**:	Annotation of: GOBP: Gene Ontology Biological Process GOMF: Gene Ontology Molecular Function GOCC: Gene Ontology Cellular Component KEGG: Kyoto Encyclopedia of Genes and Genomes

Table S5: Perseus workflow for the identification of importin 13 import cargoes (see section 3.3.3 for SILAC experiment)

Matrix	Processing	Settings	Description
Matrix 1-10	Processing steps Matrix 1-10 are identical to Matrix 1-10 in Table S4		

Matrix	Processing	Settings	Description
Matrix 11	Reorder/remove columns	**Expression column**: Ratio H/M normalized SILAC4 Ratio M/L normalized SILAC5 Ratio M/L normalized SILAC6 Ratio H/L normalized SILAC4 Ratio H/M normalized SILAC5_1 Ratio H/M normalized SILAC6_1 **Numerical columns**: Ratio H/L variability [%] SILAC4 Ratio H/M variability [%] SILAC4 Ratio M/L variability [%] SILAC5 Ratio H/M variability [%] SILAC5 Ratio M/L variability [%] SILAC6 Ratio H/M variability [%] SILAC6 Ratio H/L count SILAC4 Ratio H/M count SILAC4 Ratio M/L count SILAC5 Ratio H/M count SILAC5 Ratio M/L count SILAC6 Ratio H/M count SILAC6	Selection of columns required for identification of Imp13 import candidates
Matrix 12	Categorical annotation row	**Action**: Create **Row name**: Imp13/Imp13+Ran Ratio H/M normalized SILAC4 Ratio M/L normalized SILAC5 Ratio M/L normalized SILAC6	The following ratio group was defined: Imp13/Imp13+Ran
Matrix 13	Categorical annotation row	**Action**: Create **Row name**: Imp13/Imp13+Ubc9 Ratio H/L normalized SILAC4 Ratio H/M normalized SILAC5_1 Ratio H/M normalized SILAC6_1	The following ratio group was defined: Imp13/Imp13+Ubc9
Matrix 14	Filter rows based on valid values	**Min. number of values**: 3 **Mode**: In each group **Grouping**: Group1 **Values should be**: Greater or equal **Minimum**: 0.5 **Filter mode**: Add categorical row	Imp13/Imp13+Ran & Imp13/Imp13+Ubc9 ratios were filtered to be ≥0.5 for all three replicates.
Matrix 15	Filter rows based on valid values	**Min. number of values**: 3 **Mode**: In each group **Grouping**: Group1 **Values should be**: Greater or equal **Minimum**: 1.5 **Filter mode**: Add categorical row	Imp13/Imp13+Ran & Imp13/Imp13+Ubc9 ratios were filtered to be ≥1.5 for all three replicates.
Matrix 16	Filter rows based on valid values	**Min. number of values**:3 **Mode**: In each group **Grouping**: Group1 **Values should be**: Greater or equal **Minimum**: 3.0 **Filter mode**: Add categorical row	Imp13/Imp13+Ran & Imp13/Imp13+Ubc9 ratios were filtered to be ≥3.0 for all three replicates.
Matrix 17	One-sample test	**Columns**: Ratio H/M normalized SILAC4 Ratio M/L normalized SILAC5 Ratio M/L normalized SILAC6 Ratio H/L normalized SILAC4 Ratio H/M normalized SILAC5_1 Ratio H/M normalized SILAC6_1 **Value**: 0 **Test**: t-test **Side**: Right **Use for truncation**: P value **Threshold p-value**: 0.05 **-Log10**: tick **Suffix**:	One sample-test for determining if the mean Imp13/Imp13+Ran & Imp13/Imp13+Ubc9 ratios are significantly different from 0 using a threshold p-value of 0.05

Matrix	Processing	Settings	Description
Matrix 18	One-sample test	**Columns**: Ratio H/M normalized SILAC4 Ratio M/L normalized SILAC5 Ratio M/L normalized SILAC6 Ratio H/L normalized SILAC4 Ratio H/M normalized SILAC5_1 Ratio H/M normalized SILAC6_1 **Value**: 0 **Test**: t-test **Side**: Right **Use for truncation**: P value **Threshold p-value**: 0.01 **-Log10**: tick **Suffix**:	One sample-test for determining if the mean Imp13/Imp13+Ran & Imp13/Imp13+Ubc9 ratios are significantly different from 0 using a threshold p-value of 0.01
Matrix 19	Rename columns	Filter → T(log2)=0.5 Filter_ → T(log2)=1.5 Filter__ → T(log2)=3.0 t-test Significant → t-test 0.05 t-test Significant_ → t-test 0.01	Give expression columns (filtering + t-test) a more explicit name
Matrix 20	Fill categorical columns	**Columns**: Filter → T(log2)=0.5 Filter_ → T(log2)=1.5 Filter__ → T(log2)=3.0 t-test Significant → t-test 0.05 t-test Significant_ → t-test 0.01 **Value**: -	Fill empty field in categorical columns with '-' to allow for later combining of categorical columns
Matrix 21	Combine categorical columns	**First column**: t-test 0.05 **Second column**: t-test 0.01	Combine categorical columns that were t-test significant for a threshold p-value of 0.05 and 0.01
Matrix 22	Combine categorical columns	**First column**: T(log2)=0.5 **Second column**: T(log2)=1.5	Combine categorical columns filtered for ratio thresholds of ≥0.5 and ≥1.5
Matrix 23	Combine categorical columns	**First column**: T(log2)=0.5_T(log2)=1.5 **Second column**: T(log2)=3	Combine categorical columns filtered for ratio thresholds of ≥0.5, ≥1.5 and ≥ 3
Matrix 24	Combine categorical columns	**First column**: T(log2)=0.5_T(log2)=1.5_ T(log2)=3 **Second column**: t-test 0.05_ t-test 0.01	Combine categorical columns filtered for ratio threshold of ≥0.5, ≥1.5 and ≥ 3 with t-test significant categorical column with a threshold p-value of 0.05 and 0.01. Required for data visualization
Matrix 25	Average groups	**Grouping**: Group1 **Average type**: mean **Min. valid values per group**: 1 **Keep original data**: tick **Add standard deviation**: tick	Average Imp13/Imp13+Ran and Imp13/Imp13+Ubc9 ratios from all three replicates
Matrix 26	Categorical annotation row	**Action**: Create **Row name**: Imp13/Imp13+Ran _fwd Ratio H/M normalized SILAC4	Distinguish between label-switch experiments for Imp13/Imp13+Ran Ratios ('forward reaction')
Matrix 27	Categorical annotation row	**Action**: Create **Row name**: Imp13/Imp13+Ran _rev Ratio M/L normalized SILAC5 Ratio M/L normalized SILAC6	Distinguish between label-switch experiments for Imp13/Imp13+Ran Ratios ('reverse reaction')
Matrix 28	Categorical annotation row	**Action**: Create **Row name**: Imp13/Imp13+Ubc9_fwd Ratio H/L normalized SILAC4	Distinguish between label-switch experiments for Imp13/Imp13+Ubc9 ratios ('forward reaction')
Matrix 29	Categorical annotation row	**Action**: Create **Row name**: Imp13/Imp13+Ubc9_rev Ratio H/M normalized SILAC5_1 Ratio H/M normalized SILAC6_1	Distinguish between label-switch experiments for Imp13/Imp13+Ubc9 ratios ('reverse reaction')

Matrix	Processing	Settings	Description
Matrix 30	Average groups	**Grouping**: Imp13/Imp13+Ran _fwd **Average type**: mean **Min. valid values per group**: 1 **Keep original data**: tick **Add standard deviation**: tick	Average Imp13/Imp13+Ran ratios from forward label-switch experiment
Matrix 31	Average groups	**Grouping**: Imp13/Imp13+Ran _rev **Average type**: mean **Min. valid values per group**: 1 **Keep original data**: tick **Add standard deviation**: tick	Average Imp13/Imp13+Ran ratios from reverse label-switch experiment
Matrix 32	Average groups	**Grouping**: Imp13/Imp13+Ubc9_fwd **Average type**: mean **Min. valid values per group**: 1 **Keep original data**: tick **Add standard deviation**: tick	Average Imp13/Imp13+Ubc9 ratios from forward label-switch experiment
Matrix 33	Average groups	**Grouping**: Imp13/Imp13+Ubc9_rev **Average type**: mean **Min. valid values per group**: 1 **Keep original data**: tick **Add standard deviation**: tick	Average Imp13/Imp13+Ubc9 ratios from reverse label-switch experiment
Matrix 34	Filter rows based on valid values	**Min. number of valid values**: 3 **Mode**: In each group **Grouping**: Group 1 **Values should be**: Valid **Filter mode**: Reduce matrix	To assign annotations all values need to be valid
Matrix 35	Add annotation	**Source**: MainPerseusAnnot.txt.gz **UniProt column**: Majority protein IDs **Annotations to be added**: GOBP name GOMF name GOCC name KEGG name **Additional sources**:	Annotation of: GOBP: Gene Ontology Biological Process GOMF: Gene Ontology Molecular Function GOCC: Gene Ontology Cellular Component KEGG: Kyoto Encyclopedia of Genes and Genomes

Table S6: List of potential importin 13 import cargoes identified in SILAC screen (log2 SILAC ratio > 0.5 for all three experimental replicates, see section 3.3.3 for experimental details)[#]

Uniprot ID	Protein Name	Gene	log2(Imp13/ Imp13+Ran)	log2(Imp13/ Imp13+Ubc9)	-log (p value)*
Proteins identified for both Imp13/Imp13+Ran & Imp13/Imp13+Ubc9					
Q92538	Golgi-specific brefeldin A-resistance guanine nucleotide exchange factor 1	GBF1	0.813033	4.71873	1.86233
Q92888	Rho guanine nucleotide exchange factor 1	ARHGEF1	1.42738	3.78382	2.63594
Q6PGP7	Tetratricopeptide repeat protein 37	TTC37	0.939691	3.65913	2.11507
Q14247	Src substrate cortactin	CTTN	1.75313	3.62126	3.11061
O75815	Breast cancer anti-estrogen resistance protein 3	BCAR3	1.26153	3.23052	2.69767
Q12800	Alpha-globin transcription factor CP2	TFCP2	1.06516	2.75921	2.5538
Q14C86	GTPase-activating protein and VPS9 domain-containing protein 1	GAPVD1	1.4609	2.68049	3.40625
Q12774	Rho guanine nucleotide exchange factor 5	ARHGEF5	0.705027	2.41263	2.30914
Q15025	TNFAIP3-interacting protein 1	TNIP1	0.95981	2.24084	2.85848
O43896	Kinesin-like protein KIF1C	KIF1C	1.11685	2.10933	3.33456
Q13263	Transcription intermediary factor 1-beta	TRIM28	0.867331	1.90373	2.95866
Q3V6T2	Girdin	CCDC88A	0.981046	1.86711	2.40064
P23258	Tubulin gamma-1 chain	TUBG1	0.693187	1.63586	2.83976
Q8IV48	**3-5 exoribonuclease 1**	ERI1	0.93069	1.46739	3.46771
O15084	Serine/threonine-protein phosphatase 6 regulatory ankyrin repeat subunit A	ANKRD28	1.04204	0.864303	4.21767
Q92974	Rho guanine nucleotide exchange factor 2	ARHGEF2	1.0197	0.829202	4.22529
Proteins identified for Imp13/Imp13+Ran					
Q9BPX7	UPF0415 protein C7orf25	C7orf25	3.80688	0.642	3.00728

Uniprot ID	Protein Name	Gene	log2(Imp13/ Imp13+Ran)	log2(Imp13/ Imp13+Ubc9)	-log (p value)*
O00303	Eukaryotic translation initiation factor 3 subunit F	EIF3F	1.71919	-0.0768488	1.84627
O75821	Eukaryotic translation initiation factor 3 subunit G	EIF3G	1.63573	0.0269878	1.74379
Q14152	Eukaryotic translation initiation factor 3 subunit A	EIF3A	1.62644	-0.137368	1.75614
O15479	Melanoma-associated antigen B2	MAGEB2	1.53793	-0.195129	1.57917
Q7L2H7	Eukaryotic translation initiation factor 3 subunit M	EIF3M	1.50969	-0.00783382	1.74761
P05783	Keratin, type I cytoskeletal 18	KRT18	1.4847	2.92434	1.59389
P55884	Eukaryotic translation initiation factor 3 subunit B	EIF3B	1.47532	-0.140885	1.88281
P36578	60S ribosomal protein L4	RPL4	1.41764	-0.229922	1.52031
Q9NSD9	Phenylalanine--tRNA ligase beta subunit	FARSB	1.41105	-0.0168935	1.46055
Q53EL6	**Programmed cell death protein 4****	PDCD4	1.38179	-0.239508	1.9684
Q9P0J7	E3 ubiquitin-protein ligase KCMF1	KCMF1	1.38113	-0.366198	2.02826
P60228	Eukaryotic translation initiation factor 3 subunit E	EIF3E	1.37905	0.0827138	1.74038
C9J9K3	40S ribosomal protein SA	RPSA	1.35307	-0.143419	1.56352
Q99613	Eukaryotic translation initiation factor 3 subunit C	EIF3C	1.32125	-0.0816751	1.70334
P39023	60S ribosomal protein L3	RPL3	1.30222	-0.244874	1.51126
Q9Y262	Eukaryotic translation initiation factor 3 subunit L	EIF3L	1.28118	-0.0190674	1.77652
Q13347	Eukaryotic translation initiation factor 3 subunit I	EIF3I	1.20545	0.0620854	1.38953
Q5T4S7	E3 ubiquitin-protein ligase UBR4	UBR4	1.12458	-0.358052	1.77364
Q9Y285	Phenylalanine--tRNA ligase alpha subunit	FARSA	1.10485	0.273047	1.68737
Q99615	DnaJ homolog subfamily C member 7	DNAJC7	1.05021	-0.141127	2.01229
Q13895	Bystin	BYSL	0.812382	-0.246966	2.6437
H7BXH2	Serine/threonine-protein phosphatase 6 regulatory subunit 3	PPP6R3	0.63477	0.492251	2.99464
	Proteins identified for Imp13/Imp13+Ubc9				
Q9NRG0	**Chromatin accessibility complex protein 1**	CHRAC1	0.417418	5.31296	3.99816
Q9NRF9	**DNA polymerase epsilon subunit 3**	POLE3	0.168921	5.01915	2.80557
Q9Y530	O-acetyl-ADP-ribose deacetylase 1	OARD1	-0.00054066	4.49774	2.52061
Q9Y314	Nitric oxide synthase-interacting protein	NOSIP	0.364505	4.48227	3.23087
Q9NR33	**DNA polymerase epsilon subunit 4**	POLE4	-0.243075	3.91994	2.54084
P62380	TATA box-binding protein-like protein 1	TBPL1	-0.318334	3.90187	2.173
Q16513	Serine/threonine-protein kinase N2	PKN2	-0.2442	3.57229	4.13079
Q15477	Helicase SKI2W	SKIV2L	0.624186	3.46386	2.80251
Q9GZS3	WD repeat-containing protein 61	WDR61	0.269134	3.43407	2.461
P27540	Aryl hydrocarbon receptor nuclear translocator	ARNT	0.470754	3.28838	2.69279
Q96JG6	Coiled-coil domain-containing protein 132	CCDC132	0.120687	3.27985	2.09074
Q9NRF2	SH2B adapter protein 1	SH2B1	0.95146	3.15032	3.11739
Q5VIR6	Vacuolar protein sorting-associated protein 53 homolog	VPS53	0.229217	3.07472	2.87329
P23588	Eukaryotic translation initiation factor 4B	EIF4B	0.283411	3.01306	2.62681
Q9Y606	tRNA pseudouridine synthase A, mitochondrial	PUS1	-0.255249	2.97562	2.86354
P05783	Keratin, type I cytoskeletal 18	KRT18	1.4847	2.92434	2.4275
J3KNC0	Transcription initiation factor IIA subunit 1	GTF2A1	-0.232213	2.86042	2.21091
P52657	**Transcription initiation factor IIA subunit 2****	GTF2A2	-0.805258	2.83151	2.22288
P53999	Activated RNA polymerase II transcriptional coactivator p15	SUB1	-1.50329	2.80937	2.53168
Q9NQT8	Kinesin-like protein KIF13B	KIF13B	0.839283	2.64362	3.32859
Q8WUF5	RelA-associated inhibitor	PPP1R13L	0.646154	2.61013	2.93803
Q9P1Y5	Calmodulin-regulated spectrin-associated protein 3	CAMSAP3	-0.040654	2.58535	2.84022
Q9BYX4	Interferon-induced helicase C domain-containing protein 1	IFIH1	-0.0877257	2.54065	2.77674
E3W994	CLIP-associating protein 2	CLASP2	0.175809	2.52605	3.97909
O60343	TBC1 domain family member 4	TBC1D4	0.433131	2.4178	3.09736
Q9Y4H2	Insulin receptor substrate 2	IRS2	0.310145	2.35194	2.34747
Q14157	Ubiquitin-associated protein 2-like	UBAP2L	0.4474	2.19262	1.91864
C9JZR2	Catenin delta-1	CTNND1	-0.535033	2.16381	2.70911
P13984	General transcription factor IIF subunit 2	GTF2F2	-0.29533	2.1155	2.8392
Q9UGJ1	Gamma-tubulin complex component 4	TUBGCP4	0.444484	2.07017	2.982
P62136	Serine/threonine-protein phosphatase PP1-alpha catalytic subunit	PPP1CA	-0.0792858	2.05476	2.28248
Q16204	Coiled-coil domain-containing protein 6	CCDC6	0.484694	2.05259	2.49215
P61956	Small ubiquitin-related modifier	SUMO2,3,4	0.131713	2.04704	1.39415
C9JEL3	Eukaryotic translation initiation factor 4E type 2	EIF4E2	-0.31437	1.98722	4.11817
Q14693	Phosphatidate phosphatase LPIN1	LPIN1	0.468605	1.96606	2.188
P62140	Serine/threonine-protein phosphatase PP1-beta catalytic subunit	PPP1CB	0.168797	1.95883	1.34722
H7C170	Uncharacterized methyltransferase WBSCR22	WBSCR22	0.484091	1.89476	2.03673
Q9Y6R0	Numb-like protein	NUMBL	-0.260254	1.87456	2.35055
Q7Z460	CLIP-associating protein 1	CLASP1	0.538826	1.86087	2.3655
Q8TEW0	Partitioning defective 3 homolog	PARD3	-0.15918	1.85178	2.34429
Q86UU1	Pleckstrin homology-like domain family B member 1	PHLDB1	0.222936	1.80549	1.97365
Q8WX93	Palladin	PALLD	0.367969	1.74021	2.26034
Q96F86	**Enhancer of mRNA-decapping protein 3****	EDC3	0.867101	1.72773	2.35559
Q92620	Pre-mRNA-splicing factor ATP-dependent RNA helicase PRP16	DHX38	0.403327	1.71743	2.29087
Q3MHD2	Protein LSM12 homolog	LSM12	-0.180633	1.712	2.40183
Q14244	Ensconsin	MAP7	-0.300793	1.69568	1.81708
Q00403	Transcription initiation factor IIB	GTF2B	-1.80555	1.67293	1.43181

Uniprot ID	Protein Name	Gene	log2(Imp13/ Imp13+Ran)	log2(Imp13/ Imp13+Ubc9)	-log (p value)*
Q14919	**Dr1-associated corepressor**	DRAP1	-0.434796	1.6483	2.10521
Q9UI30	tRNA methyltransferase 112 homolog	TRMT112	-0.31314	1.63061	1.77601
P41743	Protein kinase C iota type	PRKCI	-0.36483	1.62035	2.48096
P15924	Desmoplakin	DSP	0.408405	1.61421	1.28908
Q8ND56	Protein LSM14 homolog A	LSM14A	-0.890691	1.6105	2.63839
P50548	ETS domain-containing transcription factor ERF	ERF	-0.875577	1.60979	2.9159
P49757	Protein numb homolog	NUMB	-0.429043	1.60483	2.4028
Q8WWI1	LIM domain only protein 7	LMO7	0.229279	1.59937	1.91315
Q8IUD2	ELKS/Rab6-interacting/CAST family member 1	ERC1	0.257515	1.59886	2.05536
O75420	PERQ amino acid-rich with GYF domain-containing protein 1	GIGYF1	-0.216063	1.59731	2.48073
Q8NEY1	Neuron navigator 1	NAV1	-0.465412	1.59462	1.97797
Q15427	Splicing factor 3B subunit 4	SF3B4	0.552802	1.57273	2.55564
Q01658	**Protein Dr1**	DR1	-0.480059	1.54603	2.12448
B7Z5N5	Mothers against decapentaplegic homolog 2	SMAD2	-0.961146	1.53707	2.66277
B1ALK7	Rho guanine nucleotide exchange factor 7	ARHGEF7	0.906418	1.52958	2.17687
Q08AD1	Calmodulin-regulated spectrin-associated protein 2	CAMSAP2	-0.240718	1.47753	2.89932
P47813	**Eukaryotic translation initiation factor 1A**	EIF1A	-3.25237	1.42849	2.37898
Q92900	Regulator of nonsense transcripts 1	UPF1	-1.15652	1.3723	2.60415
B1AKN7	Nuclear factor 1 A-type	NFIA	0.627497	1.36784	2.14935
Q13435	Splicing factor 3B subunit 2	SF3B2	0.318339	1.35689	2.11956
P61978	Heterogeneous nuclear ribonucleoprotein K	HNRNPK	-1.19892	1.3447	1.8493
P48729	Casein kinase I isoform alpha	CSNK1A1	-1.06365	1.31741	2.39073
Q04917	14-3-3 protein eta	YWHAH	-0.337327	1.3135	2.25234
P61981	14-3-3 protein gamma	YWHAG	-0.28702	1.31075	2.27926
E7EV99	Alpha-adducin	ADD1	-0.922004	1.30584	1.81035
Q684P5	Rap1 GTPase-activating protein 2	RAP1GAP2	0.541901	1.28222	1.71409
Q7Z3U7	Protein MON2 homolog	MON2	0.758447	1.27967	1.61195
Q13501	**Sequestosome-1****	SQSTM1	0.755231	1.26888	2.0583
F5GWN5	Phosphatidylinositol 4-phosphate 3-kinase C2 domain-containing subunit beta	PIK3C2B	-0.2512	1.26783	1.97628
P26196	Probable ATP-dependent RNA helicase DDX6	DDX6	-0.713644	1.21929	3.03261
Q9BXB4	Oxysterol-binding protein-related protein 11	OSBPL11	0.366041	1.19809	2.94503
P31946	14-3-3 protein beta/alpha	YWHAB	-0.686851	1.16229	2.04505
Q9P270	SLAIN motif-containing protein 2	SLAIN2	-1.01011	1.12969	1.70625
P62258	14-3-3 protein epsilon	YWHAE	-0.501352	1.11888	2.19164
Q96SU4	Oxysterol-binding protein-related protein 9	OSBPL9	0.370393	1.07767	2.34754
P78344	Eukaryotic translation initiation factor 4 gamma 2	EIF4G2	0.29085	1.01729	2.88712
Q14161	ARF GTPase-activating protein GIT2	GIT2	0.717892	1.00944	1.67464
O60825	6-phosphofructo-2-kinase/fructose-2,6-bisphosphatase 2	PFKFB2	-3.29633	1.00394	1.84653
P27348	14-3-3 protein theta	YWHAQ	-0.922545	0.961431	1.82235
P63104	14-3-3 protein zeta/delta	YWHAZ	-0.85652	0.961046	1.96388
Q96HC4	PDZ and LIM domain protein 5	PDLIM5	-2.97543	0.955176	2.8885
Q9BXB5	Oxysterol-binding protein-related protein 10	OSBPL10	0.238173	0.926031	2.18881
P05549	Transcription factor AP-2-alpha	TFAP2A	-0.638872	0.924126	2.26235
Q6ZSZ5	Rho guanine nucleotide exchange factor 18	ARHGEF18	-0.150335	0.919987	1.44517
Q86W92	Liprin-beta-1	PPFIBP1	0.340308	0.889209	2.54334
B7Z7P8	Eukaryotic peptide chain release factor subunit 1	ETF1	-1.00667	0.872366	1.67055
P12956	X-ray repair cross-complementing protein 6	XRCC6	-0.977419	0.841513	1.51525
P61326	**Protein mago nashi homolog**	MAGOH	-0.724602	0.814207	2.25492
Q7Z2W4	Zinc finger CCCH-type antiviral protein 1	ZC3HAV1	0.701945	0.791835	2.22414
O00571	ATP-dependent RNA helicase DDX3	DDX3	0.664858	0.780721	1.90872
H0YM23	Ankyrin repeat domain-containing protein 17	ANKRD17	-0.532403	0.780196	2.383
Q9UHR6	Zinc finger HIT domain-containing protein 2	ZNHIT2	0.501032	0.753856	2.71696
P49368	T-complex protein 1 subunit gamma	CCT3	-0.731554	0.739372	2.11106
P06493	Cyclin-dependent kinase 1	CDK1	-1.34662	0.738885	2.26621
O00743	Serine/threonine-protein phosphatase 6 catalytic subunit	PPP6C	0.261494	0.71037	2.52078
	Proteins analyzed that were identified for both Imp13/Imp13+Ran & Imp13/Imp13+Ubc9 for two out of three SILAC experiments				
F2Z2T2	**DNA repair protein complementing XP-A cells****	XPA	0.783184	3.01102	1.11602
Q9HCN4	GPN-loop GTPase 1	GPN1	0.535254	0.668491	1.38373
Q9NW64	**Pre-mRNA-splicing factor RBM22****	RBM22	1.15759	1.93592	1.47532
Q9H3P2	Negative elongation factor A	NELFA	1.54779	2.50404	2.02116
Q8WX92	Negative elongation factor B	NELFB	1.47736	2.75735	1.84038
Q8IXH7	**Negative elongation factor C/D**	NELFCD	1.54033	2.70383	1.18886

proteins highlighted with color were tested in importin 13 overexpression experiments with bold and underlined proteins changing their subcellular distribution upon importin 13 coexpression: red: proteins enriched for Imp13/Imp13+Ran and Imp13/Imp13+Ubc9.; blue: proteins enriched only for Imp13/Imp13+Ran; orange: proteins enriched only for Imp13/Imp13+Ubc9; green: proteins enriched for Imp13/Imp13+Ran and Imp13/Imp13+Ubc9 in two out of three SILAC replicates; proteins labeled bold and black are known importin 13 import cargoes and the known export cargo eIF1A

*right sided, one sample t-test ($p \leq 0.01$), which tested the hypothesis that the log2 SILAC ratios were not equal to the value zero

**proteins were localized to the cytoplasm and not the nucleus upon importin 13 coexpression

Table S7: List of proteins identified as ambiguous importin 13 cargoes in SILAC screen (see section 3.3.3 for experimental details)[#]

Uniprot ID	Protein Name	Gene	log2(Imp13+Ran/ Imp13)	log2(Imp13+Ran/ Imp13+Ubc9)	log2(Imp13/ Imp13+Ran)	log2(Imp13/ Imp13+Ubc9)
P47813	**Eukaryotic translation initiation factor 1A**	EIF1AX	3.25237	4.8423	-3.25237	1.42849
Q96HC4	PDZ and LIM domain protein 5	PDLIM5	2.97543	3.80419	-2.97543	0.955176
O60825	6-phosphofructo-2-kinase/fructose-2,6-bisphosphatase 2	PFKFB2	3.29633	3.83705	-3.29633	1.00394
E7EV99	Alpha-adducin	ADD1	0.922004	1.80595	-0.922004	1.30584
P26196	Probable ATP-dependent RNA helicase DDX6	DDX6	0.713644	1.66241	-0.713644	1.21929
P61978	Heterogeneous nuclear ribonucleoprotein K	HNRNPK	1.19892	2.05797	-1.19892	1.3447
Q8ND56	Protein LSM14 homolog A	LSM14A	0.890691	2.15422	-0.890691	1.6105
Q9P270	SLAIN motif-containing protein 2	SLAIN2	1.01011	1.95006	-1.01011	1.12969
P06493	Cyclin-dependent kinase 1	CDK1	1.34662	2.27739	-1.34662	0.738885
B7Z5N5	Mothers against decapentaplegic homolog	SMAD2	0.961146	2.27677	-0.961146	1.53707
B7Z7P8	Eukaryotic peptide chain release factor subunit 1	ETF1	1.00667	1.57229	-1.00667	0.872366
P12956	**X-ray repair cross-complementing protein 6**	XRCC6	0.977419	1.37652	-0.977419	0.841513
P50548	ETS domain-containing transcription factor ERF	ERF	0.875577	2.19828	-0.875577	1.60979
P53999	Activated RNA polymerase II transcriptional coactivator p15	SUB1	1.50329	4.967	-1.50329	2.80937
Q00403	Transcription initiation factor IIB	GTF2B	1.80555	3.2855	-1.80555	1.67293
Q92900	Regulator of nonsense transcripts 1	UPF1	1.15652	2.18872	-1.15652	1.3723

protein labeled bold and black is a known importin 13 export cargo; protein labeled in green and underlined was validated as an export cargo in importin 13 overexpression experiments

Table S8: List of potential importin 13 export cargoes identified in SILAC screen (log2(Imp13+Ran/Imp13) > 0.5 for all three experimental replicates, see section 3.3.3 for experimental details)[#]

Uniprot ID	Protein Name	Gene	log2(Imp13+Ran/ Imp13)	log2(Imp13+Ran/ Imp13+Ubc9)	-log (p value)*
	log2(Imp13+Ran/Imp13) ≥ 3.0				
P43487	Ran-specific GTPase-activating protein	RANBP1	5.38648	5.32265	1.81783
O00442	**RNA 3-terminal phosphate cyclase**	RTCA	4.57597	5.59694	2.50708
P39748	**Flap endonuclease 1**	FEN1	4.43566	3.9402	1.84603
Q6IPR3	tRNA wybutosine-synthesizing protein 3 homolog	TYW3	4.26835	4.34712	2.42506
P27695	**DNA-(apurinic or apyrimidinic site) lyase**	APEX1	4.12269	3.50792	2.09237
Q9H3H3	UPF0696 protein C11orf68	C11orf68	4.07843	3.406	1.75539
Q86W56	Poly(ADP-ribose) glycohydrolase	PARG	3.89607	2.94416	2.03045
P37108	Signal recognition particle 14 kDa protein	SRP14	3.77885	4.36023	3.05751
Q96PZ0	Pseudouridylate synthase 7 homolog	PUS7	3.7069	2.6616	1.93934
P35241	Radixin	RDX	3.61814	3.22884	2.60103
O94829	Importin-13	IPO13	3.56757	2.26277	1.28052
Q08J23	**tRNA (cytosine(34)-C(5))-methyltransferase**	NSUN2	3.56745	2.93758	2.29027
P54577	Tyrosine--tRNA ligase, cytoplasmic	YARS	3.56152	3.04854	2.04963
P84077	ADP-ribosylation factor 1	ARF1;ARF3	3.54006	3.5376	2.09902
Q32Q12	Nucleoside diphosphate kinase	NME1-NME2	3.46541	3.61361	2.03003
P08237	6-phosphofructokinase, muscle type	PFKM	3.44466	3.14856	1.96288
Q8WWH5	Probable tRNA pseudouridine synthase 1	TRUB1	3.41881	3.07742	2.07842
B5MCF9	Pescadillo homolog	PES1	3.37922	3.12792	1.77702
F8VZ49	Heterogeneous nuclear ribonucleoprotein A1	HNRNPA1	3.33691	3.12131	1.60299
O60825	6-phosphofructo-2-kinase/fructose-2,6-bisphosphatase 2	PFKFB2	3.29633	3.83705	1.98737
P47813	**Eukaryotic translation initiation factor 1A**	EIF1A	3.25237	4.8423	4.24736
	log2(Imp13+Ran/Imp13) ≥ 1.5				
Q96HC4	PDZ and LIM domain protein 5	PDLIM5	2.97543	3.80419	2.37063
H0YA96	**Heterogeneous nuclear ribonucleoprotein D0**	HNRNPD	2.96732	2.53505	2.24646

Uniprot ID	Protein Name	Gene	log2(Imp13+Ran/ Imp13)	log2(Imp13+Ran/ Imp13+Ubc9)	-log (p value)*
P26038	Moesin	MSN	2.95718	3.0089	1.27479
O95347	Structural maintenance of chromosomes protein 2	SMC2	2.93072	2.13327	2.17994
P13010	**X-ray repair cross-complementing protein 5**	XRCC5	2.82663	1.82907	2.72781
Q6VY07	Phosphofurin acidic cluster sorting protein 1	PACS1	2.82146	2.83474	2.62546
Q7Z4S6	Kinesin-like protein KIF21A	KIF21A	2.78632	2.54737	2.35845
O75116	Rho-associated protein kinase 2	ROCK2	2.78412	2.10553	2.80105
Q8TBB5	Kelch domain-containing protein 4	KLHDC4	2.77381	2.83467	1.84029
Q9NTK5	Obg-like ATPase 1	OLA1	2.76445	2.21738	3.92603
Q9UK59	Lariat debranching enzyme	DBR1	2.6774	2.10752	2.66408
Q9BQ52	Zinc phosphodiesterase ELAC protein 2	ELAC2	2.60043	1.21415	1.88731
O75534	Cold shock domain-containing protein E1	CSDE1	2.52311	2.63836	1.87994
P15311	Ezrin	EZR	2.48226	1.67527	1.48324
Q9Y3F4	Serine-threonine kinase receptor-associated protein	STRAP	2.40696	2.44099	1.68925
Q9BPX3	Condensin complex subunit 3	NCAPG	2.29883	2.17429	2.48105
Q5VTE0	Putative elongation factor 1-alpha-like 3	EEF1A1P5	2.29715	1.93896	1.87181
Q15631	Translin	TSN	2.2224	2.3705	2.27251
P09661	U2 small nuclear ribonucleoprotein A	SNRPA1	2.21552	2.5631	1.62974
P25205	DNA replication licensing factor MCM3	MCM3	2.2095	1.8214	2.44116
P36915	Guanine nucleotide-binding protein-like 1	GNL1	2.14833	2.18778	1.93622
P24534	Elongation factor 1-beta	EEF1B2	1.97594	1.76944	1.40369
Q96K76	Ubiquitin carboxyl-terminal hydrolase 47	USP47	1.95828	0.601034	2.78035
Q7KZF4	Staphylococcal nuclease domain-containing protein 1	SND1	1.93858	0.886815	2.02139
Q9NRF8	CTP synthase 2	CTPS2	1.91466	-0.496447	2.31617
Q66K74	Microtubule-associated protein 1S	MAP1S	1.89109	1.42357	2.27209
O00203	AP-3 complex subunit beta-1	AP3B1	1.86118	0.904195	1.35445
P20290	**Transcription factor BTF3**	BTF3	1.82755	1.8911	1.59095
Q00403	Transcription initiation factor IIB	GTF2B	1.80555	3.2855	1.75203
Q9UHD8	Septin-9	SEPT9	1.75664	1.8294	1.67951
H0YBP1	Focal adhesion kinase 1	PTK2	1.73248	1.95922	2.19702
Q9BV44	THUMP domain-containing protein 3	THUMPD3	1.70402	1.51059	2.36607
P41214	**Eukaryotic translation initiation factor 2D**	EIF2D	1.63737	1.46164	1.72077
P26639	Threonine--tRNA ligase, cytoplasmic	TARS	1.60822	1.18292	0.947564
E9PK01	Elongation factor 1-delta	EEF1D	1.54923	0.900679	1.62074
P53999	Activated RNA polymerase II transcriptional coactivator p15	SUB1	1.50329	4.967	1.49769
	log2(Imp13+Ran/Imp13) ≥ 0.5				
P26641	Elongation factor 1-gamma	EEF1G	1.49928	0.940673	1.63639
Q14008	Cytoskeleton-associated protein 5	CKAP5	1.48043	1.59961	1.7579
Q01813	6-phosphofructokinase type C	PFKP	1.47333	1.66786	1.54622
P19338	Nucleolin	NCL	1.4483	0.362352	2.02784
P40227	T-complex protein 1 subunit zeta	CCT6A	1.43843	1.00277	1.8217
Q92499	ATP-dependent RNA helicase DDX1	DDX1	1.42124	0.879824	2.54251
Q96CX2	BTB/POZ domain-containing protein KCTD12	KCTD12	1.39005	-1.47452	2.00427
P27448	MAP/microtubule affinity-regulating kinase 3	MARK3	1.38863	1.12089	1.75108
P17987	T-complex protein 1 subunit alpha	TCP1	1.3804	0.963823	1.74164
E9PC69	Serine/threonine-protein kinase MARK2	MARK2	1.37177	1.51294	1.69682
P06493	Cyclin-dependent kinase 1	CDK1	1.34662	2.27739	1.64412
P28482	Mitogen-activated protein kinase 1	MAPK1	1.345	1.27727	1.42906
Q9HB71	Calcyclin-binding protein	CACYBP	1.33717	1.79655	1.60171
Q9UDY4	DnaJ homolog subfamily B member 4	DNAJB4	1.32143	0.922722	1.44451
P34932	Heat shock 70 kDa protein 4	HSPA4	1.30134	0.723749	2.41801
F8VZJ2	Nascent polypeptide-associated complex subunit alpha	NACA	1.29685	0.884699	1.20009
P62937	Peptidyl-prolyl cis-trans isomerase A	PPIA	1.27194	2.3087	1.63458
P27816	Microtubule-associated protein 4;Microtubule-associated protein	MAP4	1.23621	0.871172	1.73817
F8VPF3	Myosin light polypeptide 6	MYL6	1.22701	1.53608	1.13832
Q3KQU3	MAP7 domain-containing protein 1	MAP7D1	1.22021	1.0111	1.40087
Q06830	Peroxiredoxin-1	PRDX1	1.19912	1.609	1.87588
P50990	T-complex protein 1 subunit theta	CCT8	1.19894	0.809329	1.73926

Uniprot ID	Protein Name	Gene	log2(Imp13+Ran/ Imp13)	log2(Imp13+Ran/ Imp13+Ubc9)	-log (p value)*
P61978	Heterogeneous nuclear ribonucleoprotein K	HNRNPK	1.19892	2.05797	3.26672
B4E1C5	Histidine--tRNA ligase, cytoplasmic	HARS	1.18682	0.84494	1.13876
P46940	Ras GTPase-activating-like protein IQGAP1	IQGAP1	1.17839	0.84498	1.75069
Q15366	Poly(rC)-binding protein 2	PCBP2	1.16694	0.795609	1.33161
Q92900	Regulator of nonsense transcripts 1	UPF1	1.15652	2.18872	1.49077
P17812	CTP synthase 1	CTPS1	1.1524	-0.202184	2.33023
P50991	T-complex protein 1 subunit delta	CCT4	1.12879	0.681773	1.73994
P78371	T-complex protein 1 subunit beta	CCT2	1.09746	0.654692	1.60643
P48643	T-complex protein 1 subunit epsilon	CCT5	1.08008	0.74469	1.64779
P49327	Fatty acid synthase	FASN	1.06924	0.653674	1.33252
Q92598	Heat shock protein 105 kDa	HSPH1	1.06503	0.487717	2.35444
Q9P270	SLAIN motif-containing protein 2	SLAIN2	1.01011	1.95006	2.64552
B7Z7P8	Eukaryotic peptide chain release factor subunit 1	ETF1	1.00667	1.57229	1.97514
Q9Y4E8	Ubiquitin carboxyl-terminal hydrolase 15	USP15	0.979349	0.217313	2.22068
P12956	**X-ray repair cross-complementing protein 6**	XRCC6	0.977419	1.37652	1.40745
P19525	Interferon-induced, double-stranded RNA-activated protein kinase	EIF2AK2	0.97668	0.410077	2.54683
O14744	Protein arginine N-methyltransferase 5	PRMT5	0.967085	0.708434	1.96941
Q15365	Poly(rC)-binding protein 1	PCBP1	0.964946	0.634472	2.96652
B7Z5N5	Mothers against decapentaplegic homolog 2	SMAD2	0.961146	2.27677	1.96035
E7EV99	Alpha-adducin	ADD1	0.922004	1.80595	3.00514
Q8ND56	Protein LSM14 homolog A	LSM14A	0.890691	2.15422	3.56774
O60506	Heterogeneous nuclear ribonucleoprotein Q	SYNCRIP	0.883583	0.40863	1.48999
P50548	ETS domain-containing transcription factor ERF	ERF	0.875577	2.19828	1.38588
P16989	Y-box-binding protein 3	YBX3	0.825159	0.469257	2.04904
Q01105	**Protein SET**	SET	0.81555	0.0277848	2.56819
Q9BRS2	Serine/threonine-protein kinase RIO1	RIOK1	0.802329	1.13405	2.09427
P78527	DNA-dependent protein kinase catalytic subunit	PRKDC	0.724773	0.91282	1.92342
O60524	Nuclear export mediator factor NEMF	NEMF	0.721399	0.0807594	2.1625
P26196	Probable ATP-dependent RNA helicase DDX6	DDX6	0.713644	1.66241	2.0097
O00178	GTP-binding protein 1	GTPBP1	0.694846	1.07533	1.90228
K7EN82	Glycylpeptide N-tetradecanoyltransferase 1	NMT1	0.651957	-0.137875	2.2303
	log2(Imp13+Ran/Imp13) ≥ 0.5 for only 2 out of 3 replicates				
Q9BQA1	Methylosome protein 50	WDR77	0.946335	0.381559	1.04849

proteins highlighted with color were tested in importin 13 overexpression experiments with bold and underlined proteins changing their subcellular distribution upon importin 13 coexpression: blue: proteins with an average log2(Imp13+Ran/Imp13) ≥ 3.0; orange: proteins with an average log2(Imp13+Ran/Imp13) ≥ 1.5; green: proteins with an average log2(Imp13+Ran/Imp13) ≥ 0.5.; proteins labeled bold and black are known importin 13 export cargoes

*right sided, one sample t-test (p≤0.01), which tested the hypothesis that the log2 SILAC ratios were not equal to the value zero

Table S9: Importin 13 cargo candidates identified in SILAC screen and by mass spectrometry in section 3.3.1 (see section 3.3.1 and 3.3.3 for experimental details)[#]

Uniprot ID	Protein Name	Gene
	Identified as export cargoes	
P49327	Fatty acid synthase	FASN
P08237	ATP-dependent 6-phosphofructokinase, muscle type	PFKM
P34932	Heat shock 70 kDa protein 4	HSPA4
P17812	CTP synthase 1	CTPS1
P17987	T-complex protein 1 subunit alpha	TCP1
Q01813	ATP-dependent 6-phosphofructokinase, platelet type	PFKP
Q9Y4E8	Ubiquitin carboxyl-terminal hydrolase 15	USP15
P47813	**Eukaryotic translation initiation factor 1A**	EIF1AX
P84077	ADP-ribosylation factor 1	ARF1
Q92598	Heat shock protein 105 kDa	HSPH1
Q15366	Poly(rC)-binding protein 2	PCBP2

Uniprot ID	Protein Name	Gene
P19338	Nucleolin	NCL
O00178	GTP-binding protein 1	GTPBP1
Q7KZF4	Staphylococcal nuclease domain-containing protein 1	SND1
Q9Y3F4	Serine-threonine kinase receptor-associated protein	STRAP
Q9UDY4	DnaJ homolog subfamily B member 4	DNAJB4
Q9BV44	THUMP domain-containing protein 3	THUMPD3
O75116	Rho-associated protein kinase 2	ROCK2
O60506	Heterogeneous nuclear ribonucleoprotein Q	SYNCRIP
	Identified as import cargoes	
Q92538	Golgi-specific brefeldin A-resistance guanine nucleotide exchange factor 1	GBF1
Q7Z3U7	Protein MON2 homolog	MON2
Q9NRF9	**DNA polymerase epsilon subunit 3**	POLE3
P61326	**Protein mago nashi homolog**	MAGOH
O75420	GRB10-interacting GYF protein 1	GIGYF1
Q9NRG0	**Chromatin accessibility complex protein 1**	CHRAC1
Q9Y4H2	Insulin receptor substrate 2	IRS2
Q8WUF5	RelA-associated inhibitor	PPP1R13L
P27540	Aryl hydrocarbon receptor nuclear translocator	ARNT
Q7Z460	CLIP-associating protein 1	CLASP1
Q16204	Coiled-coil domain-containing protein 6	CCDC6
Q9P1Y5	Calmodulin-regulated spectrin-associated protein 3	CAMSAP3
O15084	Serine/threonine-protein phosphatase 6 regulatory ankyrin repeat subunit A	ANKRD28
Q8WX93	Palladin	PALLD
Q6PGP7	Tetratricopeptide repeat protein 37	TTC37
Q8IUD2	ELKS/Rab6-interacting/CAST family member 1	ERC1
O00743	Serine/threonine-protein phosphatase 6 catalytic subunit	PPP6C
Q92974	Rho guanine nucleotide exchange factor 2	ARHGEF2
C9JZR2	Catenin delta-1	CTNND1
Q15477	Helicase SKI2W	SKIV2L
Q5T4S7	E3 ubiquitin-protein ligase UBR4	UBR4
Q7L2H7	Eukaryotic translation initiation factor 3 subunit M	EIF3M
P39023	60S ribosomal protein L3	RPL3
Q9GZS3	WD repeat-containing protein 61	WDR61
P55884	Eukaryotic translation initiation factor 3 subunit B	EIF3B
Q16513	Serine/threonine-protein kinase N2	PKN2
Q92888	Rho guanine nucleotide exchange factor 1	ARHGEF1
Q96JG6	Syndetin	VPS50
Q7Z2W4	Zinc finger CCCH-type antiviral protein 1	ZC3HAV1
P61981	14-3-3 protein gamma	YWHAG
P23258	Tubulin gamma-1 chain	TUBG1
B1ALK7	Rho guanine nucleotide exchange factor 7	ARHGEF7
Q9BYX4	Interferon-induced helicase C domain-containing protein 1	IFIH1
Q9NR33	**DNA polymerase epsilon subunit 4**	POLE4
Q13347	Eukaryotic translation initiation factor 3 subunit I	EIF3I
P60228	Eukaryotic translation initiation factor 3 subunit E	EIF3E
Q86UU1	Pleckstrin homology-like domain family B member 1	PHLDB1
Q5VIR6	Vacuolar protein sorting-associated protein 53 homolog	VPS53
Q9Y530	O-acetyl-ADP-ribose deacetylase 1	OARD1
P31946	14-3-3 protein beta/alpha	YWHAB
Q9Y262	Eukaryotic translation initiation factor 3 subunit L	EIF3L
Q12800	Alpha-globin transcription factor CP2	TFCP2
H0YM23	Ankyrin repeat domain-containing protein 17	ANKRD17
Q14919	**Dr1-associated corepressor**	DRAP1
Q01658	**Protein Dr1**	DR1
B1AKN7	Nuclear factor 1	NFIA
Q8TEW0	Partitioning defective 3 homolog	PARD3

#: Bold and black: known importin 13 cargoes; orange: proteins tested but not affected in importin 13 overexpression assays

Table S10: Importin 13 cargo candidates identified in SILAC screen and the Kimura *et al.*, 2017 study (76) (see section 3.3.3 for experimental details)[#]

Uniprot ID	Protein Name	Gene
	Identified as ambiguous importin 13 cargoes	
Q96HC4	PDZ and LIM domain protein 5	PDLIM5
P47813	**Eukaryotic translation initiation factor 1A**	EIF1AX
P26196	Probable ATP-dependent RNA helicase DDX6	DDX6
P06493	Cyclin-dependent kinase 1	CDK1
	Identified as importin 13 export cargoes	
Q9Y3F4	Serine-threonine kinase receptor-associated protein	STRAP
Q9NTK5	Obg-like ATPase 1	OLA1
P16989	Y-box-binding protein 3	YBX3
P62937	Peptidyl-prolyl cis-trans isomerase A	PPIA
P24534	Elongation factor 1-beta	EEF1B2
Q15366	Poly(rC)-binding protein 2	PCBP2
P26641	Elongation factor 1-gamma	EEF1G
P20290	**Transcription factor BTF3**	BTF3
Q9Y4E8	Ubiquitin carboxyl-terminal hydrolase 15	USP15
P27816	Microtubule-associated protein 4	MAP4
P49327	Fatty acid synthase	FASN
	Identified as importin 13 import cargoes	
P52657	**Transcription initiation factor IIA subunit 2**	GTF2A2
P61326	**Protein mago nashi homolog**	MAGOH
Q9NRG0	**Chromatin accessibility complex protein 1**	CHRAC1
Q9NRF9	**DNA polymerase epsilon subunit 3**	POLE3
Q14247	Src substrate cortactin	CTTN
P61956	Small ubiquitin-related modifier 2	SUMO2
Q14157	Ubiquitin-associated protein 2-like	UBAP2L
Q9Y262	Eukaryotic translation initiation factor 3 subunit L	EIF3L
Q99613	Eukaryotic translation initiation factor 3 subunit C	EIF3C
Q14244	Ensconsin	MAP7
P23588	Eukaryotic translation initiation factor 4B	EIF4B
P78344	**Eukaryotic translation initiation factor 4 gamma 2**	EIF4G2
Q7Z2W4	Zinc finger CCCH-type antiviral protein 1	ZC3HAV1

#: Bold and black: known importin 13 cargoes; bold and blue: proteins validated in this study as importin 13 cargo candidates using importin 13 overexpression assays; orange: proteins tested but not affected in importin 13 overexpression assays

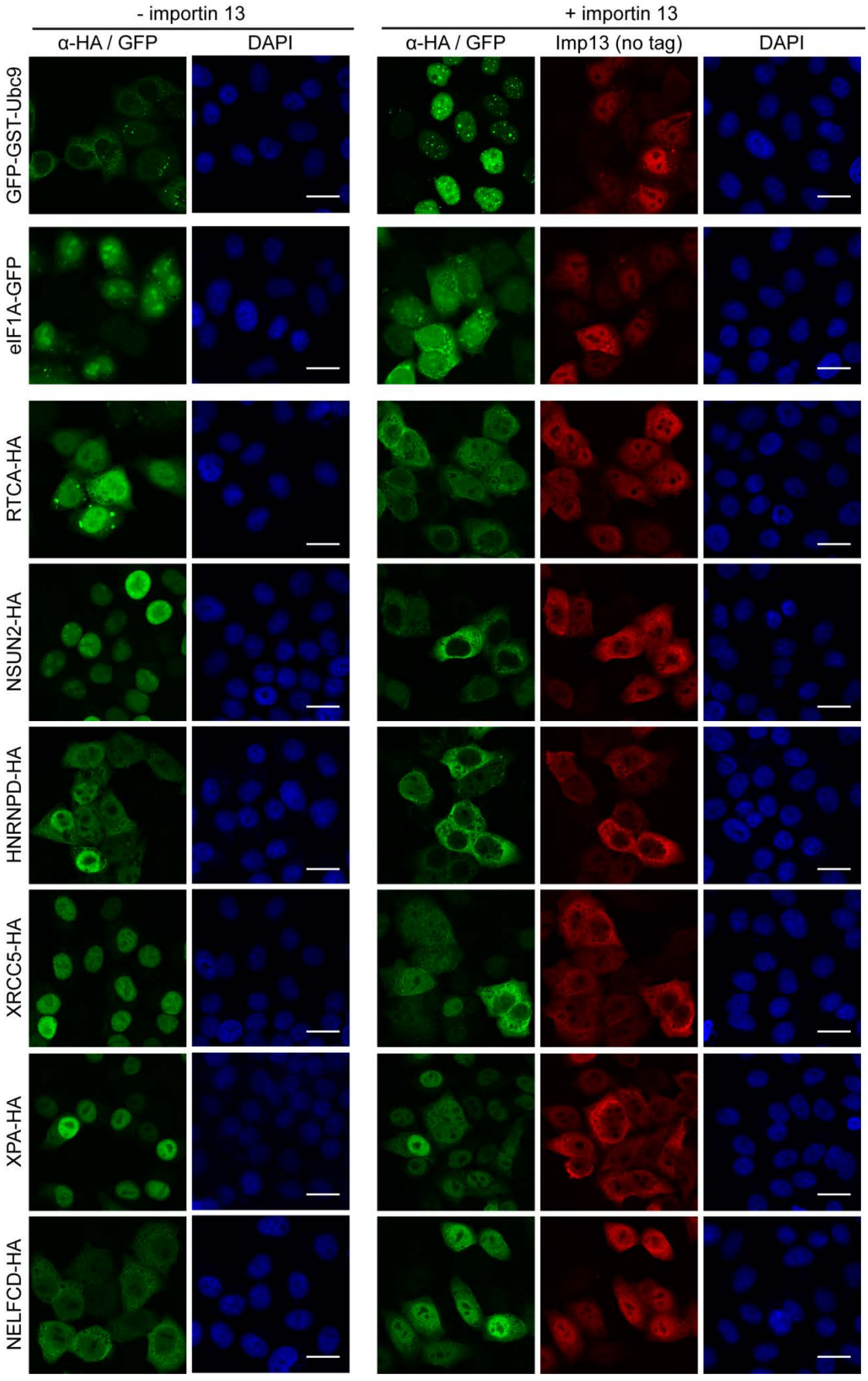
- importin 13
+ importin 13
α-HA / GFP
DAPI
α-HA / GFP
Imp13 (no tag)
DAPI
GFP-GST-Ubc9
eIF1A-GFP
RTCA-HA
NSUN2-HA
HNRNPD-HA
XRCC5-HA
XPA-HA
NELFCD-HA

Figure S5: Effect of untagged importin 13 overexpression on the subcellular distribution of HA-tagged SILAC cargo candidates. HeLa P4 cells were transiently cotransfected with plasmids coding for HA-tagged proteins form the SILAC screen, GFP-GST-Ubc9 or eIF1A-GFP and untagged importin 13 or an empty control vector (pcDNA3.1) using the calcium phosphate method. HA-tagged substrates and untagged importin 13 were visualized by indirect immunofluorescence with an anti-HA and anti-importin 13 antibody, respectively. Note that the endogenous importin 13 levels are not high enough to be detected by the importin 13 antibody. See section 3.3.3.4.3 for details. The scale bars correspond to 20 µm.

Table S11: Overlap of importin 13 and Crm1 cargo candidates[#] (see section 3.3.3.4.3 for details)

Uniprot ID	Protein Name	Gene
	Identified as ambiguous importin 13 cargoes	
P50548	ETS domain-containing transcription factor ERF	ERF
P26196	Probable ATP-dependent RNA helicase DDX6	DDX6
Q8ND56	Protein LSM14 homolog A	LSM14A
Q96HC4	PDZ and LIM domain protein 5	PDLIM5
Q9P270	SLAIN motif-containing protein 2	SLAIN2
Q92900	Regulator of nonsense transcripts 1	UPF1
	Identified as importin 13 export cargoes	
Q9UHD8	Septin-9	SEPT9
O00203	AP-3 complex subunit beta-1	AP3B1
O75534	Cold shock domain-containing protein E1	CSDE1
Q9UK59	Lariat debranching enzyme	DBR1
Q9NRF8	CTP synthase 2	CTPS2
P09661	U2 small nuclear ribonucleoprotein A'	SNRPA1
Q8WWH5	Probable tRNA pseudouridine synthase 1	TRUB1
Q9Y3F4	Serine-threonine kinase receptor-associated protein	STRAP
Q96K76	Ubiquitin carboxyl-terminal hydrolase 47	USP47
Q9BRS2	Serine/threonine-protein kinase RIO1	RIOK1
	Identified as importin 13 import cargoes	
Q12800	Alpha-globin transcription factor CP2	TFCP2
Q7Z2W4	Zinc finger CCCH-type antiviral protein 1	ZC3HAV1
Q13895	Bystin	BYSL
P49757	Protein numb homolog	NUMB
Q9Y6R0	Numb-like protein	NUMBL
Q9P0J7	E3 ubiquitin-protein ligase KCMF1	KCMF1
Q9UHR6	Zinc finger HIT domain-containing protein 2	ZNHIT2
Q14693	Phosphatidate phosphatase LPIN1	LPIN1
Q96F86	Enhancer of mRNA-decapping protein 3	EDC3
Q13501	**Sequestosome-1****	SQSTM1
P60228	Eukaryotic translation initiation factor 3 subunit E	EIF3E
P78344	**Eukaryotic translation initiation factor 4 gamma 2**	EIF4G2
Q9Y4H2	Insulin receptor substrate 2	IRS2
P48729	Casein kinase I isoform alpha	CSNK1A1
P23588	Eukaryotic translation initiation factor 4B	EIF4B
Q3V6T2	Girdin	CCDC88A
Q15025	TNFAIP3-interacting protein 1	TNIP1
Q16204	Coiled-coil domain-containing protein 6	CCDC6
Q9Y262	Eukaryotic translation initiation factor 3 subunit L	EIF3L
Q53EL6	**Programmed cell death protein 4****	PDCD4
P13984	**General transcription factor IIF subunit 2****	GTF2F2
Q99613	Eukaryotic translation initiation factor 3 subunit C	EIF3C
O00743	Serine/threonine-protein phosphatase 6 catalytic subunit	PPP6C
Q14157	Ubiquitin-associated protein 2-like	UBAP2L

Uniprot ID	Protein Name	Gene
Q684P5	Rap1 GTPase-activating protein 2	RAP1GAP2
Q8WUF5	RelA-associated inhibitor	PPP1R13L
O75420	GRB10-interacting GYF protein 1	GIGYF1
Q7Z460	CLIP-associating protein 1	CLASP1
Q08AD1	Calmodulin-regulated spectrin-associated protein 2	CAMSAP2
P23258	Tubulin gamma-1 chain	TUBG1
Q9GZS3	WD repeat-containing protein 61	WDR61
Q14C86	GTPase-activating protein and VPS9 domain-containing protein 1	GAPVD1
P41743	Protein kinase C iota type	PRKCI
Q92888	Rho guanine nucleotide exchange factor 1	ARHGEF1
P61981	14-3-3 protein gamma	YWHAG
Q5T4S7	E3 ubiquitin-protein ligase UBR4	UBR4
O00571	ATP-dependent RNA helicase DDX3X	DDX3X
P36578	60S ribosomal protein L4	RPL4
Q8IV48	**3'-5' exoribonuclease 1**	ERI1
Q86UU1	Pleckstrin homology-like domain family B member 1	PHLDB1

proteins labeled bold and black are known importin 13 cargoes; proteins highlighted with color were tested in importin 13 overexpression experiments with bold and underlined proteins changing their subcellular distribution upon importin 13 coexpression. Export candidates: orange: proteins with an average log2(Imp13+Ran/Imp13) ≥ 1.5. Import candidates: red: proteins enriched for Imp13/Imp13+Ran and Imp13/Imp13+Ubc9.; blue: proteins enriched only for Imp13/Imp13+Ran; orange: proteins enriched only for Imp13/Imp13+Ubc9; green: proteins enriched for Imp13/Imp13+Ran and Imp13/Imp13+Ubc9 in two out of three SILAC replicates.

**proteins were localized to the cytoplasm and not the nucleus upon importin 13 coexpression

Table S12: Overlap importin 13 and importin 5 cargo candidates[#] (see section 3.3.3.4.3 for details)

Uniprot ID	Protein Name	Gene
	Identified as ambiguous importin 13 cargoes	
Q8ND56	Protein LSM14 homolog A	LSM14A
P47813	**Eukaryotic translation initiation factor 1A**	EIF1AX
Q96HC4	PDZ and LIM domain protein 5	PDLIM5
P06493	Cyclin-dependent kinase 1	CDK1
P26196	Probable ATP-dependent RNA helicase DDX6	DDX6
Q92900	Regulator of nonsense transcripts 1	UPF1
	Identified as importin 13 export cargoes	
Q14008	Cytoskeleton-associated protein 5	CKAP5
Q9Y3F4	Serine-threonine kinase receptor-associated protein	STRAP
P24534	Elongation factor 1-beta	EEF1B2
P20290	**Transcription factor BTF3**	BTF3
P26641	Elongation factor 1-gamma	EEF1G
P43487	Ran-specific GTPase-activating protein	RANBP1
Q3KQU3	MAP7 domain-containing protein 1	MAP7D1
P16989	Y-box-binding protein 3	YBX3
O00442	**RNA 3'-terminal phosphate cyclase**	RTCA
Q9NTK5	Obg-like ATPase 1	OLA1
Q15366	Poly(rC)-binding protein 2	PCBP2
P27816	Microtubule-associated protein 4	MAP4
Q8TBB5	Kelch domain-containing protein 4	KLHDC4
Q7KZF4	Staphylococcal nuclease domain-containing protein 1	SND1
	Identified as importin 13 import cargoes	
P78344	**Eukaryotic translation initiation factor 4 gamma 2**	EIF4G2
Q8WWI1	LIM domain only protein 7	LMO7
Q96SU4	Oxysterol-binding protein-related protein 9	OSBPL9
Q14157	Ubiquitin-associated protein 2-like	UBAP2L
P23588	Eukaryotic translation initiation factor 4B	EIF4B
Q14247	Src substrate cortactin	CTTN
O00571	ATP-dependent RNA helicase DDX3X	DDX3X
Q9NSD9	Phenylalanine--tRNA ligase beta subunit	FARSB

Uniprot ID	Protein Name	Gene
Q5T4S7	E3 ubiquitin-protein ligase UBR4	UBR4
P60228	Eukaryotic translation initiation factor 3 subunit E	EIF3E
Q99613	Eukaryotic translation initiation factor 3 subunit C	EIF3C
Q9Y262	Eukaryotic translation initiation factor 3 subunit L	EIF3L

proteins labeled bold and black are known importin 13 cargoes; proteins highlighted with color were tested in importin 13 overexpression experiments with bold and underlined proteins changing their subcellular distribution upon importin 13 coexpression. Export candidates: blue: proteins with an average log2(Imp13+Ran/Imp13) ≥ 3.0; orange: proteins with an average log2(Imp13+Ran/Imp13) ≥ 1.5. Import candidates: orange: proteins enriched only for Imp13/Imp13+Ubc9.

Abbreviations

A549	transformed adenocarcinoma cell line
aa	amino acid
AP	aprotinin
APS	ammonium persulfate
Arg	arginine
Arg-6:HCl	$^{13}C_6$-L-arginine HCl
Arg-10:HCl	$^{13}C_6{}^{15}N_4$-L-arginine HCl
Asp	aspartic acid
ATP	adenosine-5-triphosphate
bp	base pair
BSA	bovine serum albumin
cDNA	complementary DNA
Crm1	chromosome region maintenance 1
C-terminus	carboxy-terminus
D	aspartic acid
DAPI	4’,6-diamidino-2-phenylindole
DNA	desoxyribonucleic acid
DMEM	Dulbecco’s modified eagles medium
DMSO	dimethyl sulfoxide
dNTPs	2’-desoxynucleoside-5’-triphosphate
DTT	dithiothreitol
E	glutamic acid
E. coli	*Escherichia coli*
EDTA	ethylenediaminetetraacetic acid
ESI	electrospray ionization
EtOH	ethanol
FG	phenylalanine glycine
FLAG	polypeptide protein tag with the sequence DYKDDDDK
FRAP	fluorescence recovery after photobleaching
GAP	GTPase-activating protein
GDP	guanosine-5’-diphosphate
GFP	green fluorescent protein
Glu	glutamic acid
GO	Gene Ontology
GST	glutathione S-transferase
GTP	guanosine-5’-triphosphate
h	heavy (SILAC)
HA	hemagglutinin
HCl	hydrochloric acid
HEAT	Huntingtin Elongation Factor A Subunit Tor
HEPES	2-[4-(2-hydroxyethyl)piperazin-1-yl]ethanesulfonic acid
His	histidine tag
HIV-1	human immunodeficiency virus type 1

hnRNP	heterogeneous nuclear ribonucleoproteins
HRP	horseradish peroxidase
IF	immunofluorescence
Imp13	importin 13
IPO13	importin 13 gene
IPTG	isopropyl-beta-D-thiogalactopyranoside
kDa	kilo dalton
l	light (SILAC)
LB	Luria-Bertani
LC	liquid chromatography
LMB	Leptomycin B
m	medium (SILAC)
M9	PY-NLS initially described for hnRNPA1
MCS	multiple cloning site
mock	control treated sample
MS	mass spectrometry
MW	molecular weight
MWCO	molecular weight cut-off
m/z	mass-to-charge ratio
LC	liquid chromatography
LC-MS	liquid chromatography – mass spectrometry
LP	leupeptin, pepstatin
Lys-4D:2HCl	4,4,5,5-D4-L-Lysine 2HCl
Lys-8:HCl	$^{13}C_6{}^{15}N_2$-L-lysine HCl
NA	numerical aperture
NE	nuclear envelope
NES	nuclear export signal
NFAT	nuclear factor of activated T-cells
NLS	nuclear localization signal
NPC	nuclear pore complex
NT	non targeting
N-terminus	amino terminus
NTF2	nuclear transport factor 2
Nup	nucleoporin
PAGE	polyacrylamide gel electrophoresis
PBS	phosphate buffered saline
PCR	polymerase chain reaction
PMSF	phenylmethylsulphonyl fluoride
PLA	proximity ligation assay
PY-NLS	NLS with $RX_{2\text{-}5}PY$ motif at its C-terminus and either a hydrophobic or basic motif at its N-terminus
R	arginine
Ran	Ras-related nuclear protein
RCC1	regulator of chromatin condensation 1
RFP	red fluorescent protein

RNA	ribonucleic acid
RNAi	RNA interference
RP	reversed phase
rpm	rotations per minute
S. cerevisiae	Saccharomyces cerevisiae
SDS	sodium dodecyl sulphate
SILAC	stable isotope labeling with amino acids in cell culture
siRNA	small interfering RNA
SPN1	snurportin 1
SUMO	small ubiquitin-like modifier
SV40	simian virus 40
tev	TEV-protease cleavage site
TAE	Tris/ Acetate/ EDTA
TAP	Tip-associated protein
TPB	transport buffer
Triton X-100	4-octylphenol polyethoxylate
Tween 20	polyoxyethylene (20) sorbitan monolaurate
UV	ultraviolet
v/v	volume per volume
w/o	without
w/v	weight per volume
WB	western blot
WGA	wheat germ agglutinin
WT	wild type
ZZ	protein tag (*S. aureus* protein A IgG-binding domain)

Acknowledgments

I want to thank Prof. Ralph Kehlenbach for giving me the opportunity to work on this project, his continuous support and giving me the possibility to go on conferences.

The members of my thesis committee Prof. Heike Krebber and Prof. Jörg Großhans I thank for helpful discussions and inputs to my project.

Special thanks go to Christiane Spillner for taking care of general things in the lab, creating a positive working atmosphere and her experimental support during the last months of my PhD. Further, I am very grateful to Annegret Nath for doing the initial overexpression screen for potential importin 13 cargoes.

All current (Marina Blenski, Mohamed Hamed, Christina James, Floriane Lagadec, Marret Müller, Christiane Spillner) and former members (Cara Jamieson, Annegret Nath, Janine Pfaff, Sarah Port, Kalpana Rajanala, Janssel Reyes del Castillo) of the lab, I thank for the good working atmosphere and also the nice times outside of the lab. Special thanks to Dr. Janine Pfaff, Dr. Marret Müller, Christina James, Kirstin Runge and Anne Clancy for proof-reading parts of the thesis.

I thank the whole Department of Molecular Biology for the supportive and positive working environment.

A big thank you goes to my collaborators Dr. Oliver Valerius und Dr. Kerstin Schmitt for the quick analysis of my MS-samples, showing me how to prepare my samples for mass spectrometry, introducing me to the Proteome Discoverer, MaxQuant and Perseus software, doing the Proteome Discoverer analysis and answering all of my questions.

The Göttingen Graduate School for Neurosciences, Biophysics, and Molecular Biosciences (GGNB) I thank for the opportunity to participate in method courses, go to retreats and providing funding to go on a conference.

Finally, I would like to thank all the people, who supported and influenced me in some way or another during the years of my PhD.

Publications

Halder K, Dölker N, Van Q, Gregor I, Dickmanns A, Baade I, Kehlenbach RH, Ficner R, Enderlein J, Grubmüller H, Neumann H. (2015) MD simulations and FRET reveal an environment-sensitive conformational plasticity of importin-β. *Biophys J.* **109**, 277-86.

Parts of this thesis were published in Molecular & Cellular Proteomics on 17th April 2018:

Baade I, Spillner C, Schmitt K, Valerius O, Kehlenbach RH. (2018) Extensive identification and in-depth validation of importin 13 cargoes. *Mol Cell Proteomics.* doi: 10.1074/mcp.RA118.000623.